Detection of Small Buried Objects: Asymptotic Factorization and MUSIC

Dissertation zur Erlangung des Grades
"Doktor der Naturwissenschaften"

am Fachbereich Physik, Mathematik und Informatik
der Johannes Gutenberg–Universität Mainz

Roland Griesmaier

geboren in Innsbruck

Mainz 2008

D77 Mainzer Dissertation

Abstract

We are concerned with the analysis and numerical solution of the inverse scattering problem to reconstruct the number and the positions of a collection of finitely many small perfectly conducting scatterers buried within the lower halfspace of an unbounded three–dimensional two–layered background medium from near field measurements of time–harmonic electromagnetic waves.

For this purpose, we first study the corresponding direct scattering problem in detail and derive an asymptotic expansion of the scattered field as the size of the scatterers tends to zero. Integral equation methods and a factorization of the corresponding near field measurement operator are applied to prove this result.

Then, we use the asymptotic expansion of the scattered field to justify a noniterative MUSIC–type reconstruction method for the solution of the inverse scattering problem. We propose a numerical implementation of this reconstruction method and provide a series of numerical experiments that confirm our theoretical results.

Because our proof of the asymptotic expansion for the scattering problem in the two–layered background medium is quite technical, we discuss a reduced model problem in advance to explain the basic ideas of our approach to verify asymptotic expansions of this type more clearly. We study the electrostatic potential in a conductor consisting of finitely many small insulating inclusions embedded within a bounded homogeneous background medium, corresponding to an electric current applied at the boundary of the conductor, and prove an asymptotic expansion of this scalar potential at the boundary of the conductor, as the size of the inclusions tends to zero.

Contents

Chapter 1

Introduction

In this work, we consider a simple model problem for the electromagnetic exploration of perfectly conducting objects buried within the lower halfspace of an unbounded two–layered background medium. In possible applications, such as, e.g., humanitarian demining, or more generally the exploration of the grounds subsurface to detect and identify buried objects, the two layers would correspond to air and soil. Moving a set of electric devices parallel to the surface of ground to generate a time–harmonic field, the induced field is measured within the same devices. The goal is to retrieve information about the position and the shape of buried scatterers from these data.

This problem originated in the project "HuMin/MD — Metal detectors for humanitarian demining — Development potentials in data analysis methodology and measurement" [61], supported by the German Federal Ministry of Education and Research. The aim of this project has been to reduce the number of false alarms produced by metal detectors used for humanitarian demining. For this purpose mathematical methods for analyzing data obtained from devices, which are idealizations of devices made up of standard off–the–shelf metal detectors, have been developed. The construction and investigation of such a method is also the main objective of the present thesis.

In mathematical terms, we consider an inverse obstacle scattering problem for time–harmonic electromagnetic waves in a two–layered background medium. Before we start to investigate this specific problem, we give a very brief introduction to inverse obstacle scattering for time–harmonic electromagnetic waves and summarize some numerical approaches for solving such problems.

Broadly speaking, *inverse obstacle scattering* for time–harmonic electromagnetic waves seeks to recover the position and the shape of inhomo-

geneities in a known background medium from measurements of electromagnetic fields at a single frequency. These fields can be described by time–harmonic Maxwell's equations, which form a system of vector valued linear partial differential equations, together with appropriate boundary and radiation conditions. Writing the total field as the sum of the incident field and the scattered field, the *direct (scattering) problem* in this context is to determine the scattered field from a knowledge of the incident field and the properties of the scatterers, i.e., to solve the partial differential equation. On the other hand, the corresponding *inverse (scattering) problem* consists in recovering information about the scatterers from a knowledge of (one or many) scattered fields on a surface near or far away from the scatterers, i.e., in reconstructing the differential equation and/or its domain of definition from the behavior of (one or many of) its solutions [39]. We are mainly interested in the latter problem, which is well known to be *nonlinear* and *ill–posed* in the sense that the solution of the problem, i.e., the shape and the position of the scatterers, does not depend continuously on the scattered fields in any reasonable norm.

Over the past thirty years a considerable amount of work has been dedicated to the development of the mathematical theory and numerical algorithms for this inverse problem. For a survey on the state of the art we refer the reader to the monograph by Colton and Kress [39] and their recent review article [40]; see also Colton, Coyle, and Monk [36], Isakov [66], Kirsch [71], and Pike and Sabatier [93].

A classical attempt to solve this problem is to formulate it as a nonlinear (ill–posed) operator equation and to use *regularized nonlinear optimization techniques* such as e.g. regularized Newton–type methods; cf. e.g. [39] and Engl, Hanke, and Neubauer [48]. The advantage of these methods is that they require as data only the scattered field for one incident field. But this approach has two major drawbacks. First, nonlinear optimization techniques typically need a priori information about the obstacles, like for instance their number or their approximate position, which is in general not available, and second, such methods usually solve the forward problem in each iteration step, which is computationally very expensive.

So–called *decomposition methods*, as e.g. the *Dual Space Method* due to Colton and Monk [41, 42] or the method due to Kirsch and Kress [77], overcome the latter disadvantage by breaking up the inverse problem into two parts. First the scattered field is reconstructed from the known data by analytic continuation, which is linear but ill–posed, and then the boundaries of the scatterers are reconstructed as the location where the boundary condition for the total field is satisfied, which is a nonlinear process. We refer to [39, 40] for details and additional references.

Influenced by decomposition methods a new class of solution methods has been developed during the last ten years. These methods are noniterative and use no or at least less a priori information on the unknown

scatterers, but only seek to recover limited (qualitative) information about the scattering objects. They have been termed *qualitative methods* and examples are the *Linear Sampling Method* introduced first by Colton and Kirsch [37], the *Factorization Method* by Kirsch [72], Ikahata's *Probe Method* [64], and the *Method of Singular Sources* developed by Potthast [94]. A common feature of these methods is that they use criteria on the known data to decide whether a point (or a curve or a set) in the search domain belongs to a scatterer or not. These criteria can be implemented by sampling the search domain, using an appropriate collection of points (or curves or sets). A drawback of most qualitative methods is that they require the knowledge of much more measurement data than iterative methods or decomposition methods. But recently also qualitative methods, which use only scattering data for one incident field, have been developed by Kusiak and Sylvester [84], by Potthast, Kusiak, and Sylvester [96], and by Luke and Potthast [85]. As a starting point to qualitative methods we refer the reader to the recent review articles by Colton and Kress [40] and by Potthast [95] and to the monographs by Cakoni and Colton [24] and by Kirsch and Grinberg [76].

Also the study of two–layered background media has over the past years been the subject of extensive research. In this work, we develop a reconstruction method for two–layered background media that is particularly adapted to the mine detection application mentioned above. In the course of the project [61] several reconstruction methods for this problem have been proposed: Reformulating the inverse scattering problem as a least squares optimization problem and applying a direct search method, Delbary et al. [46] developed an iterative reconstruction method. Among qualitative methods, the Linear Sampling Method was studied by Gebauer et al. [52] and by Cakoni, Fares, and Haddar [25]. Moreover, the Factorization Method was applied by Kirsch [75] and in combination with low frequency approximations by Gebauer, Hanke, and Schneider [53]; see also Gebauer [51].

Although these methods give good reconstructions of the position and shape of buried scatterers in case of sufficiently accurate data, they turn out to be quite sensitive to noise contained in these data. This is of course due to the ill–posedness of the inverse problem. For the mine detection application it would be useful to have a method at hand that can handle bigger amounts of noise, even if it reconstructs only the approximate positions of the scatterers. Knowing these positions, for instance a decomposition method can be used to reconstruct the shapes of the scatterers in a post processing step. Of course, information on the shape of buried objects is necessary to identify mines.

In order to handle the ill–posedness of the inverse problem we incorporate a priori knowledge on the measurement device and the scatterers available from our application. Standard off–the–shelf metal detectors used for humanitarian demining work at very low frequencies around 20 kHz;

cf. e.g. Guelle et al. [57]. Depending on the medium, this corresponds to wavelengths of several kilometers. Thus, the typical size of the objects of interest, i.e., mines or even only the metal parts contained in mines, which is only a few centimeters, is very small with respect to the wavelength of the incident field. We use this information to construct a noniterative reconstruction method that is more robust against noise in the data. This method is a generalization of a method, which was originally developed for electrical impedance tomography by Brühl, Hanke, and Vogelius [22]. It belongs to the class of *MUSIC–type reconstruction methods*, applied first to inverse scattering problems by Devaney [47]. The method is based on an asymptotic expansion of the scattered field as the size of the scatterers tends to zero. Similar reconstruction methods for inverse electromagnetic obstacle scattering were recently investigated by Ammari et al. [4] and Iakovleva et al. [62].

Asymptotic expansions of the scattered field in case of small scatterers have already been studied in the context of *low frequency scattering* more than 100 years ago. In 1897 Lord Rayleigh [97] observed that a small perfectly conducting obstacle illuminated by an electromagnetic wave gives rise to a scattered field that can be ascribed to equivalent electric and magnetic dipoles. The corresponding dipole moments are given as integrals of certain electric and magnetic potentials over the surface of the scatterer. Keller, Kleinman, and Senior [69] pointed out that these dipole moments can be written in terms of the electric and magnetic field at the obstacle, multiplied by a matrix, called the electric and magnetic polarizability tensor, respectively. The elements of these matrices depend only on the geometry of the scatterers.

The asymptotic expansion we are going to prove is essentially of the same structure. But there is a fundamental difference between low frequency expansions and asymptotic expansions for small obstacles: In low frequency expansions the wavenumber, i.e., a parameter in the differential equation governing the wave motion, is supposed to be small, while in expansions of the scattered field in case of small scatterers the size of the inhomogeneities is assumed to be small, which is information on the domain of definition of the differential equation. For a comprehensive presentation of classical low frequency scattering we refer to Dassios and Kleinman [44]. Asymptotic expansions for small inhomogeneities were first studied by Friedman and Vogelius in their work [49] on inverse conductivity problems. Since then expansions of this type have been derived for a variety of different problems. For an introduction to this topic we refer the interested reader to the monographs [7, 8] by Ammari and Kang. Asymptotic expansions of electromagnetic fields in case of small scatterers were studied by Ammari et al. in [10, 12, 14] for boundary value problems in bounded domains and in [4, 15] for scattering problems in unbounded homogeneous background media. But no rigorous analysis for layered background media has been available so far.

We investigate the direct scattering problem in unbounded two–layered background media in detail and end up with an asymptotic expansion of the scattered field as the size of the scatterers tends to zero, which is uniform with respect to the incident field. Considering only the leading order term in this expansion, we construct a characterization of the scatterers in terms of the given data. Implementing this criterion numerically in a sampling method, we obtain a noniterative visualization method for the approximate positions of the unknown scatterers.

Outline:

In Chapter 2, we start with a reduced model problem. We study the electrostatic potential in a conductor consisting of finitely many insulating inclusions of small diameter embedded in a homogeneous background medium, corresponding to a current applied at the boundary of the conductor. We derive an asymptotic expansion of this scalar potential at the boundary of the conductor as the size of the inclusions tends to zero. This result is of interest on its own and has previously been investigated in [49], by Ammari and Kang [5], and by Capdeboscq and Vogelius [26] using different methods. Because this problem is less technical than the full electromagnetic scattering problem in the two–layered medium, it allows for a simpler presentation of our approach to prove this kind of asymptotic expansions.

In Chapter 3, we consider the direct scattering problem for small perfectly conducting scatterers buried within the lower halfspace of an unbounded two–layered background medium. We describe our model for the measurement process and derive an asymptotic expansion of the scattered field corresponding to some dipole excitation on the measurement device as the size of the scatterers tends to zero.

In Chapter 4, we use this asymptotic expansion to construct a characterization of the positions of the scatterers in terms of the corresponding scattered fields. This characterization is implemented numerically in a MUSIC–type reconstruction method. At the end of this chapter we present numerical results.

In Appendix A, we recall the definitions and some important properties of electric and magnetic polarizability tensors. Appendix B is devoted to a representation theorem for electromagnetic fields in two–layered media, and we study reciprocity relations for the corresponding dyadic Green's functions. In Appendix C, we comment on the uniqueness of solutions to a boundary value problem and a transmission problem for Maxwell's equations in two–layered background media.

Remarks:

The results of Chapter 2, which have been obtained jointly with Habib Ammari and Martin Hanke, have already been published [3]. Some of the developments of Chapter 3 and Chapter 4 have been published in [56].

Chapter 2

Asymptotic Factorization for the Laplace Equation

In this chapter, we consider a reduced model problem. We study the electrostatic potential in a conductor consisting of finitely many insulating inclusions of small diameter embedded in a homogeneous reference medium corresponding to an electric current applied at the boundary of the conductor. The electrostatic potential in the conductor is harmonic outside the inclusions and satisfies homogeneous Neumann boundary conditions on their boundaries. The normal derivative of the voltage potential on the boundary of the conductor is proportional to the applied current. For a derivation of this model from Maxwell's equations we refer the reader to Cheney, Isaacson, and Newell [33].

Here, the *direct problem* is to calculate the voltage potential in the conductor, given the position and the shape of the inclusions and the boundary current. The corresponding *inverse problem* is to recover the position and the shape of the inclusions from a knowledge of the electrostatic potential on the boundary of the conductor corresponding to (one or many) boundary currents. More precisely, we suppose in this chapter that the Neumann–to–Dirichlet operators, which map currents on the boundary of the conductor to the corresponding boundary voltages, are given, both with and without inclusions. This latter problem is a special case of the *inverse conductivity problem*, a classical inverse boundary value problem. We refer the reader to [33] and to Borcea [18, 19] for review articles on that topic.

Uniqueness of solutions to inverse problems of this type is known, cf. e.g. Isakov [65] and Kohn and Vogelius [78]. But the problem has also been shown to be nonlinear and ill–posed; see Alessandrini [2].

Among other qualitative methods for solving this inverse problem, the Factorization Method has shown to be quite successful in recent years. For inverse conductivity problems this reconstruction method was developed by Brühl [21], Hähner [58], Kress [79], and Kress and Kühn [82]. It

has been extended to the halfspace geometry by Hanke and Schappel [60], and Gebauer [50] succeeded in generalizing the method to a large class of real elliptic problems; cf. also Kirsch [74] and Nachman, Päivärinta, and Teirilä [90].

According to our general strategy, we assume that the inclusions are of small diameter and incorporate this a priori information to handle the ill–posedness of the inverse problem. For this purpose, we examine the corresponding direct problem in detail and derive an asymptotic expansion of the *measurement operator*, which is the difference of the Neumann–to–Dirichlet operators with and without inclusions, as the size of the inclusions tends to zero. Our proof of this expansion is based on a factorization of the measurement operator developed in [21]. We use layer potential techniques to describe the three operators occurring in this factorization, expand them separately as the size of the inclusions tends to zero and use these expansions to calculate the leading order term in the asymptotic expansion of the measurement operator.

Over the past twenty years asymptotic expansions for the electrostatic potential in presence of low volume fraction inhomogeneities have been studied intensively. In [49] Friedman and Vogelius deduced the leading order term in this asymptotic expansion for insulating and perfectly conducting inclusions using variational methods. Cedio–Fengya, Moskow, and Vogelius [29] proved similar formulas for penetrable inhomogeneities. Using layer potential techniques Ammari and Kang [5] extended these asymptotic expansions including higher order terms. Capdeboscq and Vogelius [26] generalized the formula for the leading order term to the case of inclusions that are just measurable with small Lebesgue measure. This generalization encompasses also the formulas for inhomogeneities of small thickness derived by Beretta et al. [16, 17].

Reconstruction methods for the inverse problem under consideration, which make use of these asymptotic expansions of the solution of the corresponding direct problem have, e.g., been developed by Ammari, Moskow, and Vogelius [12], by Ammari and Seo [13], by Brühl, Hanke, and Vogelius [22], in [29], and by Kang and Lee [67]. Among those, MUSIC–type algorithms seem to be very stable and therefore particularly useful for noisy data; cf. [22] and Hanke and Brühl [59] for details and numerical results. As pointed out by Cheney [34], in [59], and by Kirsch [73], there is a strong relation between MUSIC–type methods and Linear Sampling Methods or Factorization Methods. Our way of proving the asymptotic formula enables us to clarify the connection between these methods completely.

For surveys on imaging of low volume fraction inhomogeneities in the context of inverse boundary value problems we refer the reader to the monographs [7, 8] by Ammari and Kang and to Capdeboscq and Vogelius [28].

The outline of this chapter is as follows. After a short presentation of our notation in the next section and recalling two results from functional analysis, which we apply frequently in this work, we study surface potentials for the Laplace equation in Section 2.2. In Section 2.3, we set up the model, we are going to use, and in Section 2.4, we review the factorization of the measurement operator, i.e., of the difference of the two Neumann–to–Dirichlet operators mentioned above. Here and in the following two sections, we restrict our derivations to the case of a single inclusion. In order to establish the asymptotic expansion, we require some technical estimates; these are found in Section 2.5. Then, in Section 2.6, we derive the main result of this chapter, the asymptotic expansion of the measurement operator. Multiple inclusions are treated in Section 2.7. Finally, we comment on how the asymptotic formula can be used to solve the inverse problem numerically in Section 2.8, and we explain the connection between Factorization Methods and MUSIC–type methods in detail.

2.1 Preliminaries

First a word about notation: Vectors are distinguished from scalars by the use of bold typeface (but this convention does not, in general, carry over to operators). By $\boldsymbol{x} = (x_1, x_2, \ldots, x_n)^\top$ we denote a generic point in $\mathbb{R}^n$, $n \geq 2$, where $(\cdot)^\top$ denotes the transpose of a vector or matrix. Throughout let $\boldsymbol{x} \cdot \boldsymbol{y}$ be the standard scalar product of $\boldsymbol{x}, \boldsymbol{y} \in \mathbb{R}^n$ and let $|\boldsymbol{x}|$ denote the Euclidean norm of $\boldsymbol{x}$.

Suppose $D \subset \mathbb{R}^n$ is a bounded open set of class $C^{2,\alpha}$, $0 < \alpha < 1$. The standard *real valued* Sobolev spaces $H^r(D)$, $H^r_{\mathrm{loc}}(\mathbb{R}^n)$, and $H^r_{\mathrm{loc}}(\mathbb{R}^n \setminus \overline{D})$, $r \in \mathbb{R}$, and $H^s(\partial D)$, $s \in [-2, 2]$, are defined on D, $\mathbb{R}^n$, $\mathbb{R}^n \setminus \overline{D}$, and on the boundary ∂D, respectively. For $1/2 < r \leq 2$ let $\gamma_0 : H^r(D) \to H^{r-1/2}(\partial D)$ be the corresponding trace operator. We refer the reader to McLean [86, pp. 57–107] for details. For any regular vector field $\boldsymbol{u} \in C^\infty(\overline{D})^3$, we define the normal trace $\gamma_n(\boldsymbol{u}) := \boldsymbol{\nu} \cdot \boldsymbol{u}|_{\partial D}$. Then, γ_n can be extended to a continuous linear map γ_n from $\boldsymbol{H}(\mathrm{div}, D; \mathbb{R}^3) := \left\{ \boldsymbol{u} \in L^2(D)^3 \;\middle|\; \mathrm{div}\, \boldsymbol{u} \in L^2(D) \right\}$ to $H^{-1/2}(\partial D)$; see Monk [88, Theorem 3.24].

For Banach spaces X and Y we denote by $\mathcal{L}(X, Y)$ the set of all bounded linear operators on X to Y. Together with the usual operator norm $\|\cdot\|$ this is also a Banach space. We write $\mathcal{L}(X)$ for $\mathcal{L}(X, X)$, and by $I : X \to X$ we denote the identity operator. Throughout we let scalar operators operate on vectors component–wise and vector operators on matrices column by column. Moreover, in our estimates we shall use a generic positive constant C everywhere different.

In the next two lemmas, we recall the *Fredholm alternative* and a simple but useful result from functional analysis in the form we will apply them later.

Theorem 2.1. *Let $A : X \to X$, $B : Y \to Y$ be compact adjoint operators in a dual system $\langle X, Y\rangle$. Then, either $I - A$ and $I - B$ are bijective or $I - A$ and $I - B$ have nontrivial nullspaces.*

Proof. This result is a part of the Fredholm alternative. For a proof we refer the reader to Kress [79, Theorem 4.15]. □

Lemma 2.2. *Let $A, B \in \mathcal{L}(X)$ be bounded linear operators on a Banach space X. Assume that A^{-1} and B^{-1} exist. Then,*

$$\|A^{-1} - B^{-1}\| \leq \|A^{-1}\|\|B^{-1}\|\|A - B\|.$$

Proof. Noting that

$$B^{-1} - A^{-1} = B^{-1}(A - B)A^{-1},$$

the assertion follows directly from the definition of the operator norm. □

2.2 Neumann Function and Surface Potentials

In this section, we collect some results concerning fundamental solutions and boundary integral operators occurring in potential theory.

The function

$$\Phi_0(\boldsymbol{x} - \boldsymbol{y}) := \begin{cases} -\dfrac{1}{2\pi}\log|\boldsymbol{x} - \boldsymbol{y}|, & \boldsymbol{x}, \boldsymbol{y} \in \mathbb{R}^n,\ \boldsymbol{x} \neq \boldsymbol{y},\ n = 2, \\ \dfrac{1}{(n-2)\omega_n}|\boldsymbol{x} - \boldsymbol{y}|^{2-n}, & \boldsymbol{x}, \boldsymbol{y} \in \mathbb{R}^n,\ \boldsymbol{x} \neq \boldsymbol{y},\ n \geq 3, \end{cases} \tag{2.1}$$

where ω_n denotes the area of the $(n-1)$–dimensional unit sphere, is called *fundamental solution* for the Laplace equation. It satisfies

$$\Delta_x \Phi_0(\boldsymbol{x} - \boldsymbol{y}) = -\delta(\boldsymbol{x} - \boldsymbol{y}), \qquad \boldsymbol{x}, \boldsymbol{y} \in \mathbb{R}^3,$$

where δ denotes the Dirac–delta distribution.

Suppose $\Omega \subset \mathbb{R}^n$, $n \geq 2$, is a bounded domain of class $C^{2,\alpha}$, $0 < \alpha < 1$, and denote by $\boldsymbol{\nu}$ the unit outward normal to $\partial\Omega$ relative to Ω. We denote by N the *Neumann function* for Δ in Ω, i.e., for all $\boldsymbol{y} \in \Omega$, $N(\cdot, \boldsymbol{y})$ is the unique distributional solution of

$$\Delta_x N(\boldsymbol{x}, \boldsymbol{y}) = -\delta(\boldsymbol{x} - \boldsymbol{y}), \qquad \boldsymbol{x} \in \Omega, \tag{2.2a}$$

$$\frac{\partial N}{\partial \boldsymbol{\nu}(\boldsymbol{x})}(\boldsymbol{x}, \boldsymbol{y}) = -\frac{1}{|\partial\Omega|}, \qquad \boldsymbol{x} \in \partial\Omega, \tag{2.2b}$$

together with the normalization condition $\int_{\partial\Omega} N(\boldsymbol{x}, \boldsymbol{y})\, \mathrm{d}s(\boldsymbol{x}) = 0$. Here, $|\partial\Omega|$ denotes the area of $\partial\Omega$. Then, N is symmetric in its arguments on $(\Omega \times \Omega) \setminus \operatorname{diag}(\Omega \times \Omega)$, i.e.,

$$N(\boldsymbol{x}, \boldsymbol{y}) = N(\boldsymbol{y}, \boldsymbol{x}), \qquad (\boldsymbol{x}, \boldsymbol{y}) \in (\Omega \times \Omega) \setminus \operatorname{diag}(\Omega \times \Omega),$$

(cf. [7, p. 30]), and for each $\boldsymbol{y} \in \Omega$ it is of the form

$$N(\boldsymbol{x}, \boldsymbol{y}) = \Phi_0(\boldsymbol{x} - \boldsymbol{y}) + p_N(\boldsymbol{x}, \boldsymbol{y}), \tag{2.3}$$

where $p_N(\cdot, \boldsymbol{y})$ solves the boundary value problem

$$\begin{aligned} &\Delta_x p_N(\boldsymbol{x}, \boldsymbol{y}) = 0, && \boldsymbol{x} \in \Omega, \\ &\frac{\partial p_N}{\partial \boldsymbol{\nu}(\boldsymbol{x})}(\boldsymbol{x}, \boldsymbol{y}) = -\frac{1}{|\partial\Omega|} + \frac{1}{\omega_n} \frac{(\boldsymbol{x} - \boldsymbol{y}) \cdot \boldsymbol{\nu}(\boldsymbol{x})}{|\boldsymbol{x} - \boldsymbol{y}|^n}, && \boldsymbol{x} \in \partial\Omega, \end{aligned}$$

with $\int_{\partial\Omega} p_N(\boldsymbol{x}, \boldsymbol{y}) \, \mathrm{d}s(\boldsymbol{x}) = -\int_{\partial\Omega} \Phi_0(\boldsymbol{x} - \boldsymbol{y}) \, \mathrm{d}s(\boldsymbol{x})$. Note that $\frac{\partial p_N}{\partial \boldsymbol{\nu}}\big|_{\partial\Omega}(\cdot, \boldsymbol{y})$ is continuous and therefore this problem has a unique classical solution; cf. [79, Theorem 6.28]. Because Φ_0 is symmetric, it follows that also p_N is symmetric in its arguments in $\Omega \times \Omega$. As a consequence, $p_N(\boldsymbol{x}, \cdot)$ is a harmonic function on Ω for all $\boldsymbol{x} \in \Omega$.

Let $D \subset \mathbb{R}^n$ be a bounded open set of class $C^{2,\alpha}$, $0 < \alpha < 1$, consisting of finitely many domains such that the boundary of every component of D is connected. We denote the unit outward normal to ∂D relative to D by $\boldsymbol{\nu}$, too. Given a function $\phi \in C(\partial D)$, the *single layer potential* and *double layer potential* with density ϕ are defined by

$$(\mathcal{S}_D^0 \phi)(\boldsymbol{x}) := \int_{\partial D} \Phi_0(\boldsymbol{x} - \boldsymbol{y}) \phi(\boldsymbol{y}) \, \mathrm{d}s(\boldsymbol{y}), \qquad \boldsymbol{x} \in \mathbb{R}^n \setminus \partial D,$$

and

$$(\mathcal{D}_D^0 \phi)(\boldsymbol{x}) := \int_{\partial D} \frac{\partial \Phi_0(\boldsymbol{x} - \boldsymbol{y})}{\partial \boldsymbol{\nu}(\boldsymbol{y})} \phi(\boldsymbol{y}) \, \mathrm{d}s(\boldsymbol{y}), \qquad \boldsymbol{x} \in \mathbb{R}^n \setminus \partial D.$$

Then, $\mathcal{S}_D^0 \phi$ is continuous throughout $\mathbb{R}^n$ and the following trace formulas hold (cf. [79, p. 78–82]):

$$\frac{\partial \mathcal{S}_D^0 \phi}{\partial \boldsymbol{\nu}}\Big|_{\partial D}^{\pm}(\boldsymbol{x}) = \Big(\Big(\mp \frac{1}{2} I + {K_D^0}^{\top} \Big) \phi \Big)(\boldsymbol{x}), \qquad \boldsymbol{x} \in \partial D, \tag{2.4a}$$

$$\mathcal{D}_D^0 \phi\Big|_{\partial D}^{\pm}(\boldsymbol{x}) = \Big(\Big(\pm \frac{1}{2} I + K_D^0 \Big) \phi \Big)(\boldsymbol{x}), \qquad \boldsymbol{x} \in \partial D, \tag{2.4b}$$

where K_D^0 is defined by

$$(K_D^0 \phi)(\boldsymbol{x}) := \int_{\partial D} \frac{\partial \Phi_0(\boldsymbol{x} - \boldsymbol{y})}{\partial \boldsymbol{\nu}(\boldsymbol{y})} \phi(\boldsymbol{y}) \, \mathrm{d}s(\boldsymbol{y}), \qquad \boldsymbol{x} \in \partial D,$$

and ${K_D^0}^{\top}$ is the transpose of K_D^0, i.e.,

$$\big({K_D^0}^{\top} \phi\big)(\boldsymbol{x}) = \int_{\partial D} \frac{\partial \Phi_0(\boldsymbol{x} - \boldsymbol{y})}{\partial \boldsymbol{\nu}(\boldsymbol{x})} \phi(\boldsymbol{y}) \, \mathrm{d}s(\boldsymbol{y}), \qquad \boldsymbol{x} \in \partial D.$$

Furthermore, the normal derivative of the double layer potential $\mathcal{D}_D^0\phi$ is continuous across ∂D.

The expressions $\mathcal{S}_D^0$, $\mathcal{D}_D^0$, K_D^0, and ${K_D^0}^\top$ can be extended such that they define bounded linear operators

$$\mathcal{S}_D^0 : H^{-1/2}(\partial D) \to H^1_{\mathrm{loc}}(\mathbb{R}^n), \tag{2.5a}$$

$$\mathcal{D}_D^0\big|_D : H^{1/2}(\partial D) \to H^1(D), \tag{2.5b}$$

$$\mathcal{D}_D^0\big|_{\mathbb{R}^n\setminus\overline{D}} : H^{1/2}(\partial D) \to H^1_{\mathrm{loc}}(\mathbb{R}^n \setminus \overline{D}), \tag{2.5c}$$

$$K_D^0 : H^{1/2}(\partial D) \to H^{1/2}(\partial D), \tag{2.5d}$$

$${K_D^0}^\top : H^{-1/2}(\partial D) \to H^{-1/2}(\partial D), \tag{2.5e}$$

and the jump conditions remain valid for these operators; cf. [86, Theorem 6.11]. Moreover, K_D^0 as well as ${K_D^0}^\top$ is compact (cf. Nédélec [91, Theorem 4.4.1]) and $-\frac{1}{2}I + K_D^0$ has trivial nullspace in $H^{1/2}(\partial D)$ (see [7, Lemma 2.5]). Hence, by Theorem 2.1, $-\frac{1}{2}I + K_D^0$ and $-\frac{1}{2}I + {K_D^0}^\top$ are invertible on $H^{1/2}(\partial D)$ and $H^{-1/2}(\partial D)$, respectively.

Because $K_D^0 1 = -\frac{1}{2}$ (cf. [79, p. 79]), we get for each $\phi \in H^{-1/2}(\partial D)$ that

$$\int_{\partial D}\Big(-\frac{1}{2}I + {K_D^0}^\top\Big)\phi \,\mathrm{d}s = -\int_{\partial D}\phi \,\mathrm{d}s.$$

Thus, $-\frac{1}{2}I + {K_D^0}^\top$ maps

$$H_\diamond^{-1/2}(\partial D) := \Big\{\phi \in H^{-1/2}(\partial D) \;\Big|\; \int_{\partial D}\phi \,\mathrm{d}s = 0\Big\}$$

to $H_\diamond^{-1/2}(\partial D)$. In the same way, we find that $\frac{1}{2}I + {K_D^0}^\top$ maps $H^{-1/2}(\partial D)$ to $H_\diamond^{-1/2}(\partial D)$, and from [7, Lemma 2.5] we get that $\frac{1}{2}I + {K_D^0}^\top$ is one to one on $H_\diamond^{-1/2}(\partial D)$. Hence, by Theorem 2.1, $\frac{1}{2}I + {K_D^0}^\top$ is invertible on $H_\diamond^{-1/2}(\partial D)$.

Next, we consider *modified surface potentials*. Let now D be a bounded open set of class $C^{2,\alpha}$ that is compactly contained in Ω such that the boundaries of all components of D are connected. For $\phi \in C(\partial D)$ we define

$$(\mathcal{S}_D^N\phi)(\boldsymbol{x}) := \int_{\partial D} N(\boldsymbol{x},\boldsymbol{y})\phi(\boldsymbol{y}) \,\mathrm{d}s(\boldsymbol{y}), \qquad \boldsymbol{x} \in \Omega \setminus \partial D,$$

$$(\mathcal{D}_D^N\phi)(\boldsymbol{x}) := \int_{\partial D} \frac{\partial N(\boldsymbol{x},\boldsymbol{y})}{\partial \boldsymbol{\nu}(\boldsymbol{y})}\phi(\boldsymbol{y}) \,\mathrm{d}s(\boldsymbol{y}), \qquad \boldsymbol{x} \in \Omega \setminus \partial D.$$

According to (2.3), and because $p_N(\cdot,\boldsymbol{y})$ is C^2 (with respect to both variables) for $\boldsymbol{y}$ in any compact subset of Ω, we find that $\mathcal{S}_D^N\phi$ is continuous in

Ω and obtain the following trace formulas:

$$\frac{\partial \mathcal{S}_D^N \phi}{\partial \boldsymbol{\nu}}\Big|_{\partial D}^{\pm}(\boldsymbol{x}) = \Big(\Big(\mp \frac{1}{2} I + {K_D^0}^\top \Big)\phi\Big)(\boldsymbol{x}) + \int_{\partial D} \frac{\partial p_N(\boldsymbol{x},\boldsymbol{y})}{\partial \boldsymbol{\nu}(\boldsymbol{x})} \phi(\boldsymbol{y})\, \mathrm{d}s(\boldsymbol{y}), \tag{2.6a}$$

$$\mathcal{D}_D^N \phi\Big|_{\partial D}^{\pm}(\boldsymbol{x}) = \Big(\Big(\pm \frac{1}{2} I + K_D^0 \Big)\phi\Big)(\boldsymbol{x}) + \int_{\partial D} \frac{\partial p_N(\boldsymbol{x},\boldsymbol{y})}{\partial \boldsymbol{\nu}(\boldsymbol{y})} \phi(\boldsymbol{y})\, \mathrm{d}s(\boldsymbol{y}) \tag{2.6b}$$

for $\boldsymbol{x} \in \partial D$. Define

$$(P_D^N \phi)(\boldsymbol{x}) := \int_{\partial D} \frac{\partial p_N(\boldsymbol{x},\boldsymbol{y})}{\partial \boldsymbol{\nu}(\boldsymbol{y})} \phi(\boldsymbol{y})\, \mathrm{d}s(\boldsymbol{y}), \qquad \boldsymbol{x} \in \partial D, \tag{2.7}$$

and let

$$K_D^N \phi := K_D^0 \phi + P_D^N \phi. \tag{2.8}$$

Then, we can write (2.6) as follows:

$$\frac{\partial \mathcal{S}_D^N \phi}{\partial \boldsymbol{\nu}}\Big|_{\partial D}^{\pm}(\boldsymbol{x}) = \Big(\Big(\mp \frac{1}{2} I + {K_D^N}^\top \Big)\phi\Big)(\boldsymbol{x}), \qquad \boldsymbol{x} \in \partial D, \tag{2.9a}$$

$$\mathcal{D}_D^N \phi\Big|_{\partial D}^{\pm}(\boldsymbol{x}) = \Big(\Big(\pm \frac{1}{2} I + K_D^N \Big)\phi\Big)(\boldsymbol{x}), \qquad \boldsymbol{x} \in \partial D, \tag{2.9b}$$

where ${K_D^N}^\top$ is the transpose of K_D^N.

Recalling (2.3), the mapping properties of the boundary integral operators from (2.5) and that $p_N(\cdot, \boldsymbol{y})$ is C^2 (with respect to both variables) for $\boldsymbol{y}$ in any compact subset of Ω, we find that the expressions $\mathcal{S}_D^N$, $\mathcal{D}_D^N$, K_D^N, and ${K_D^N}^\top$ can be extended such that they define bounded linear operators

$$\begin{aligned}
\mathcal{S}_D^N &: H^{-1/2}(\partial D) \to H^1(\Omega), \\
\mathcal{D}_D^N\big|_D &: H^{1/2}(\partial D) \to H^1(D), \\
\mathcal{D}_D^N\big|_{\Omega\setminus\overline{D}} &: H^{1/2}(\partial D) \to H^1(\Omega \setminus \overline{D}), \\
K_D^N &: H^{1/2}(\partial D) \to H^{1/2}(\partial D), \\
{K_D^N}^\top &: H^{-1/2}(\partial D) \to H^{-1/2}(\partial D).
\end{aligned}$$

The jump relations (2.9) remain valid for these operators. Moreover, P_D^N gives rice to a compact operator

$$P_D^N : H^{1/2}(\partial D) \to H^{1/2}(\partial D),$$

and so the corresponding dual operator

$${P_D^N}^\top : H^{-1/2}(\partial D) \to H^{-1/2}(\partial D)$$

and the operators K_D^N and ${K_D^N}^\top$ are compact, too.

Lemma 2.3. *The operators* $-\frac{1}{2}I + K_D^N$ *and* $-\frac{1}{2}I + K_D^{N^\top}$ *have trivial nullspace in* $H^{1/2}(\partial D)$ *and* $H^{-1/2}(\partial D)$*, respectively.*

Proof. Let $\phi \in H^{-1/2}(\partial D)$ be a solution of the homogeneous equation $\big(-\frac{1}{2}I + K_D^{N^\top}\big)\phi = 0$ and define $v := \mathcal{S}_D^N \phi$. Then, by (2.9a),

$$\frac{\partial v}{\partial \boldsymbol{\nu}}\Big|_{\partial D}^{+} = \Big(-\frac{1}{2}I + K_D^{N^\top}\Big)\phi = 0,$$

and v solves the Neumann problem

$$\Delta v = 0 \quad \text{in } \Omega \setminus \overline{D}, \qquad \frac{\partial v}{\partial \boldsymbol{\nu}}\Big|_{\partial\Omega} = c, \qquad \frac{\partial v}{\partial \boldsymbol{\nu}}\Big|_{\partial D} = 0,$$

where $c := -\frac{1}{|\partial\Omega|}\int_{\partial D} \phi \, \mathrm{d}s$ is constant. From the Divergence Theorem (cf. [88, Theorem 3.19]), we obtain $c = 0$. Thus, we find that v is constant in $\Omega \setminus \overline{D}$ and therefore also on ∂D. Because $\Delta v = 0$ in D, this yields that v is constant in D. From (2.9a), we see that $\phi = -\frac{\partial v}{\partial \boldsymbol{\nu}}\Big|_{\partial D}^{+} + \frac{\partial v}{\partial \boldsymbol{\nu}}\Big|_{\partial D}^{-} = 0$. Hence, $\mathcal{N}\big(-\frac{1}{2}I + K_D^{N^\top}\big) = \{0\}$.

By Theorem 2.1, also $\mathcal{N}\big(-\frac{1}{2}I + K_D^N\big) = \{0\}$ in $H^{1/2}(\partial D)$. □

So, by Lemma 2.3 and Theorem 2.1, $-\frac{1}{2}I + K_D^N$ and $-\frac{1}{2}I + K_D^{N^\top}$ are invertible on $H^{1/2}(\partial D)$ and $H^{-1/2}(\partial D)$, respectively.

Because $p_N(\boldsymbol{x}, \cdot)$ is harmonic in D for all $\boldsymbol{x} \in \partial D$, we find that

$$K_D^N 1 = K_D^0 1 + P_D^N 1 = -\frac{1}{2} + \int_{\partial D} \frac{\partial p_N(\cdot, \boldsymbol{y})}{\partial \boldsymbol{\nu}(\boldsymbol{y})} \, \mathrm{d}s(\boldsymbol{y}) = -\frac{1}{2}.$$

Thus, we get as above that $-\frac{1}{2}I + K_D^{N^\top}$ maps $H_\diamond^{-1/2}(\partial D)$ to $H_\diamond^{-1/2}(\partial D)$. Also as a consequence of this harmonicity, we find that the subspace of constant functions in $H^{1/2}(\partial D)$ is contained in the nullspace of P_D^N. Moreover, applying the harmonicity of $p_N(\cdot, \boldsymbol{y})$ in D for all $\boldsymbol{y} \in \partial D$, we see that $P_D^{N^\top}$ maps $H^{-1/2}(\partial D)$ to $H_\diamond^{-1/2}(\partial D)$. Therefore, we may in the following consider P_D^N and $P_D^{N^\top}$ as dual operators from

$$H_\diamond^{1/2}(\partial D) := \Big\{\phi \in H^{1/2}(\partial D) \;\Big|\; \int_{\partial D} \phi \, \mathrm{d}s = 0\Big\}$$

to $H^{1/2}(\partial D)$ and $H^{-1/2}(\partial D)$ to $H_\diamond^{-1/2}(\partial D)$, respectively.

2.3 Mathematical Setting

In this section, we set up the mathematical model we are going to use. Let $\Omega \subset \mathbb{R}^n$, $n \geq 2$, denote a bounded domain of class $C^{2,\alpha}$, $0 < \alpha < 1$, and assume that Ω is filled with a homogeneous material with constant

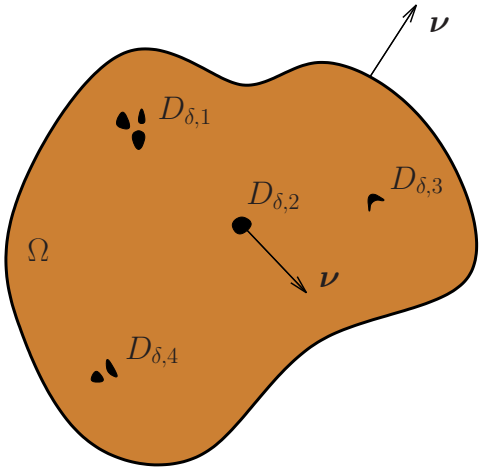

Figure 2.1: Sketch of the geometrical setup.

conductivity $\sigma_0 := 1$. Suppose that Ω contains a finite number of *well separated* small insulating inclusions, each of the form $D_{\delta,l} := \boldsymbol{z}_l + \delta B_l$, $1 \leq l \leq m$, where $B_l \subset \mathbb{R}^n$ is a bounded open set of class $C^{2,\alpha}$, $0 < \alpha < 1$, containing the origin that consists of finitely many domains such that the boundary of every component of B_l is connected. The points $\boldsymbol{z}_l \in \Omega$, $1 \leq l \leq m$, that determine the *position of the inclusions* are assumed to satisfy

$$|\boldsymbol{z}_j - \boldsymbol{z}_l| \geq d_0 \quad \text{for } j \neq l \quad \text{and} \quad \operatorname{dist}(\boldsymbol{z}_l, \partial\Omega) := \inf_{\boldsymbol{x}\in\partial\Omega} |\boldsymbol{z}_l - \boldsymbol{x}| \geq d_0$$

for some constant $d_0 > 0$, $1 \leq j, l \leq m$. The value of $0 < \delta \leq 1$, the common order of magnitude of the *size of the inclusions*, is assumed to be small enough such that the inclusions are disjoint and compactly contained in Ω. So, the total collection of inclusions takes the form $D_\delta := \bigcup_{l=1}^m (\boldsymbol{z}_l + \delta B_l)$. Throughout we denote by $\boldsymbol{\nu}$ the unit outward normal to $\partial\Omega$, $\partial D_{\delta,l}$, and ∂B_l relative to Ω, $D_{\delta,l}$, and B_l, $1 \leq l \leq m$, respectively. Later we will also consider the special case of a single inclusion. Then, we omit the subscripts l to simplify the notation.

Given the piecewise constant *conductivity distribution*

$$\sigma_\delta(x) := \begin{cases} 0, & \boldsymbol{x} \in D_\delta, \\ 1, & \boldsymbol{x} \in \Omega \setminus \overline{D_\delta}, \end{cases}$$

and prescribing a *boundary current* $f \in H_\diamond^{-1/2}(\partial\Omega)$ on $\partial\Omega$, let u_δ denote the corresponding *electrostatic potential* in presence of the inclusions D_δ, i.e., the unique weak solution

$$u_\delta \in H^1_{\diamond,\partial\Omega}(\Omega \setminus \overline{D_\delta}) := \left\{ u \in H^1(\Omega \setminus \overline{D_\delta}) \;\middle|\; \int_{\partial\Omega} u|_{\partial\Omega} \, \mathrm{d}s = 0 \right\}$$

to

$$\Delta u_\delta = 0 \qquad \text{in } \Omega \setminus \overline{D_\delta}, \tag{2.10a}$$

$$\frac{\partial u_\delta}{\partial \boldsymbol{\nu}} = f \qquad \text{on } \partial\Omega, \tag{2.10b}$$

$$\frac{\partial u_\delta}{\partial \boldsymbol{\nu}} = 0 \qquad \text{on } \partial D_\delta. \tag{2.10c}$$

On the other hand, the so–called *background potential* u_0 is the electrostatic potential for the same input current f but without inclusions. That is, u_0 denotes the unique weak solution

$$u_0 \in H^1_\diamond(\Omega) := \left\{ u \in H^1(\Omega) \;\middle|\; \int_{\partial\Omega} u|_{\partial\Omega} \, \mathrm{d}s = 0 \right\}$$

to

$$\Delta u_0 = 0 \qquad \text{in } \Omega, \tag{2.11a}$$

$$\frac{\partial u_0}{\partial \boldsymbol{\nu}} = f \qquad \text{on } \partial\Omega. \tag{2.11b}$$

The relations between the applied boundary current f and the boundary voltages $u_\delta|_{\partial\Omega}$ and $u_0|_{\partial\Omega}$ define bounded linear operators

$$\Lambda_\delta : H^{-1/2}_\diamond(\partial\Omega) \to H^{1/2}_\diamond(\partial\Omega), \quad f \mapsto u_\delta|_{\partial\Omega}$$

and

$$\Lambda_0 : H^{-1/2}_\diamond(\partial\Omega) \to H^{1/2}_\diamond(\partial\Omega), \quad f \mapsto u_0|_{\partial\Omega},$$

called the *Neumann–to–Dirichlet operators* associated with the boundary value problems (2.10) and (2.11), respectively. These mappings are in fact isomorphisms between these spaces. This follows from the existence and uniqueness of solutions of the corresponding Dirichlet boundary value problems, the continuous dependence of these solutions on their boundary values and from the continuity of normal trace operator γ_n.

2.4 Factorization of $\Lambda_\delta - \Lambda_0$

In this section, we recall a factorization of the difference of the Neumann–to–Dirichlet operators $\Lambda_\delta - \Lambda_0$, which was developed in [21]; cf. also [59]. Here and in the following two sections, we restrict ourselves to the case of a single inclusion, i.e., $D_\delta = \boldsymbol{z} + \delta B$.

In order to explain this factorization, we need to study two additional boundary value problems and a diffraction problem. First, we consider the

boundary value problem

$$\Delta v_\delta = 0 \qquad \text{in } \Omega \setminus \overline{D_\delta}, \tag{2.12a}$$

$$\frac{\partial v_\delta}{\partial \boldsymbol{\nu}} = 0 \qquad \text{on } \partial\Omega, \tag{2.12b}$$

$$\frac{\partial v_\delta}{\partial \boldsymbol{\nu}} = \phi \qquad \text{on } \partial D_\delta, \tag{2.12c}$$

which for $\phi \in H_\diamond^{-1/2}(\partial D_\delta)$ has a unique weak solution $v_\delta \in H^1_{\diamond,\partial\Omega}(\Omega \setminus \overline{D_\delta})$. Thus, we may define

$$L_\delta : H_\diamond^{-1/2}(\partial D_\delta) \to H_\diamond^{1/2}(\partial\Omega), \quad \phi \mapsto v_\delta|_{\partial\Omega}, \tag{2.13}$$

which is a bounded linear operator that takes Neumann data on ∂D_δ and maps them onto the associated Dirichlet values on $\partial\Omega$. Recalling (2.10) and (2.11) we find that $L_\delta(-\frac{\partial u_0}{\partial \boldsymbol{\nu}}\big|_{\partial D_\delta}) = L_\delta(\frac{\partial u_\delta}{\partial \boldsymbol{\nu}}\big|_{\partial D_\delta} - \frac{\partial u_0}{\partial \boldsymbol{\nu}}\big|_{\partial D_\delta}) = (u_\delta - u_0)|_{\partial\Omega}$.

A short computation reveals that the dual operator $L_\delta^\top$ of L_δ is given in terms of the problem

$$\Delta v'_\delta = 0 \qquad \text{in } \Omega \setminus \overline{D_\delta}, \tag{2.14a}$$

$$\frac{\partial v'_\delta}{\partial \boldsymbol{\nu}} = -\psi \qquad \text{on } \partial\Omega, \tag{2.14b}$$

$$\frac{\partial v'_\delta}{\partial \boldsymbol{\nu}} = 0 \qquad \text{on } \partial D_\delta, \tag{2.14c}$$

which for $\psi \in H_\diamond^{-1/2}(\partial\Omega)$ has a unique weak solution

$$v'_\delta \in H^1_{\diamond,\partial D_\delta}(\Omega \setminus \overline{D_\delta}) := \Big\{ u \in H^1(\Omega \setminus \overline{D_\delta}) \;\Big|\; \int_{\partial D_\delta} u|_{\partial D_\delta} \, \mathrm{d}s = 0 \Big\},$$

through

$$L_\delta^\top : H_\diamond^{-1/2}(\partial\Omega) \to H_\diamond^{1/2}(\partial D_\delta), \quad \psi \mapsto v'_\delta|_{\partial D_\delta}. \tag{2.15}$$

Note that apart from the normalization condition (2.14) coincides with the boundary value problem (2.10) and hence $L_\delta^\top f = -u_\delta|_{\partial D_\delta} + c_\delta$ with

$$c_\delta := \frac{1}{|\partial D_\delta|} \int_{\partial D_\delta} u_\delta|_{\partial D_\delta} \, \mathrm{d}s,$$

where $|\partial D_\delta|$ denotes the surface measure of ∂D_δ.

Next, we consider a diffraction problem with inhomogeneous jump condition. For any $\chi \in H_\diamond^{1/2}(\partial D_\delta)$, the system of equations

$$\Delta w_\delta = 0 \qquad \text{in } \Omega \setminus \partial D_\delta, \tag{2.16a}$$

$$\frac{\partial w_\delta}{\partial \boldsymbol{\nu}} = 0 \qquad \text{on } \partial\Omega, \tag{2.16b}$$

$$[w_\delta]_{\partial D_\delta} = \chi, \tag{2.16c}$$

$$\left[\frac{\partial w_\delta}{\partial \boldsymbol{\nu}}\right]_{\partial D_\delta} = 0, \tag{2.16d}$$

possesses a unique weak solution w_δ with $w_\delta|_{\Omega\setminus\overline{D_\delta}} \in H^1_{\diamond,\partial\Omega}(\Omega\setminus\overline{D_\delta})$ and $w_\delta|_{D_\delta} \in H^1(D_\delta)$. Here, $[\,\cdot\,]_{\partial D_\delta}$ denotes the difference between the respective traces from outside and inside the boundary ∂D_δ. Because of (2.16d),

$$F_\delta : H^{1/2}_\diamond(\partial D_\delta) \to H^{-1/2}_\diamond(\partial D_\delta), \quad \chi \mapsto -\frac{\partial w_\delta}{\partial \boldsymbol{\nu}}\Big|_{\partial D_\delta}, \tag{2.17}$$

is a well–defined bounded linear operator. Especially for $\chi := -u_\delta|_{\partial D_\delta} + c_\delta$, the function

$$w_\delta := \begin{cases} -u_\delta + u_0 & \text{in } \Omega\setminus\overline{D_\delta}, \\ -c_\delta + u_0 & \text{in } D_\delta, \end{cases}$$

is the solution to (2.16). Thus, $F_\delta(-u_\delta|_{\partial D_\delta} + c_\delta) = -\frac{\partial u_0}{\partial \boldsymbol{\nu}}\big|_{\partial D_\delta}$.

In sum, we have shown that the following diagram is commutative:

$$\begin{array}{ccc} H^{-1/2}_\diamond(\partial\Omega) & \xrightarrow{\Lambda_\delta-\Lambda_0} & H^{1/2}_\diamond(\partial\Omega) \\ \big\downarrow{\scriptstyle L_\delta^\top} & & {\scriptstyle L_\delta}\big\uparrow \\ H^{1/2}_\diamond(\partial D_\delta) & \xrightarrow{F_\delta} & H^{-1/2}_\diamond(\partial D_\delta) \end{array} \qquad \begin{array}{ccc} f & \longmapsto & (u_\delta - u_0)|_{\partial\Omega} \\ \big\downarrow & & \big\uparrow \\ -u_\delta|_{\partial D_\delta} + c_\delta & \longmapsto & -\frac{\partial u_0}{\partial \boldsymbol{\nu}}\big|_{\partial D_\delta} \end{array}$$

This yields the following lemma; cf. [21, p. 1338]:

Lemma 2.4. *With L_δ, $L_\delta^\top$, and F_δ defined by* (2.13), (2.15), *and* (2.17), *respectively, the difference of the Neumann–to–Dirichlet $\Lambda_\delta - \Lambda_0$ maps can be factorized as*

$$\Lambda_\delta - \Lambda_0 = L_\delta F_\delta L_\delta^\top. \tag{2.18}$$

2.5 First Estimates

In the following, we often have to deal with changes of coordinates. Therefore, we introduce some notation. Given $\phi \in C(\partial D_\delta)$ and $\psi \in C(\partial B)$, we define $\hat\phi, (\phi)^\wedge \in C(\partial B)$ and $\check\psi, (\psi)^\vee \in C(\partial D_\delta)$ by

$$(\phi)^\wedge(\boldsymbol{\xi}) := \hat\phi(\boldsymbol{\xi}) := \phi(\delta\boldsymbol{\xi} + \boldsymbol{z}), \qquad \boldsymbol{\xi} \in \partial B, \tag{2.19a}$$

$$(\psi)^\vee(\boldsymbol{x}) := \check\psi(\boldsymbol{x}) := \psi\Big(\frac{\boldsymbol{x}-\boldsymbol{z}}{\delta}\Big), \qquad \boldsymbol{x} \in \partial D_\delta, \tag{2.19b}$$

respectively. The same notation will also be used for functions in $H^{1/2}(\partial D_\delta)$ or $H^{-1/2}(\partial D_\delta)$ and $H^{1/2}(\partial B)$ or $H^{-1/2}(\partial B)$, respectively. This makes sense, because the corresponding Sobolev spaces on $\mathbb{R}^{n-1}$ are invariant under such regular changes of coordinates; cf. [86, Theorem 3.23]. Moreover, we apply this notation to functions in $H^1(D_\delta)$ and $H^1(B)$ in the same way.

For bounded open sets $D \subset \mathbb{R}^n$ of class $C^{2,\alpha}$, $0 < \alpha < 1$, we use the following norm on $H^{1/2}(\partial D)$ (cf. Girault and Raviart [54, p. 8]):

$$\|\phi\|_{H^{1/2}(\partial D)} := \inf_{\substack{u \in H^1(D) \\ u|_{\partial D} = \phi}} \|u\|_{H^1(D)}, \qquad \phi \in H^{1/2}(\partial D).$$

The dual space $H^{-1/2}(\partial D)$ shall be equipped with the corresponding dual norm

$$\|\psi\|_{H^{-1/2}(\partial D)} := \sup_{\substack{\phi \in H^{1/2}(\partial D) \\ \phi \neq 0}} \frac{|\langle \psi, \phi \rangle_{\partial D}|}{\|\phi\|_{H^{1/2}(\partial D)}}, \qquad \psi \in H^{-1/2}(\partial D),$$

where $\langle \cdot, \cdot \rangle_{\partial D}$ denotes the dual pairing between $H^{1/2}(\partial D)$ and $H^{-1/2}(\partial D)$.

The following lemma examines the scaling properties of these norms under changes of coordinates as in (2.19).

Lemma 2.5. *Suppose $0 < \delta \leq 1$. There exist constants $c > 0$ and $C > 0$ independent of δ such that for each $\phi \in H^{1/2}_\diamond(\partial D_\delta)$ and $\psi \in H^{-1/2}_\diamond(\partial D_\delta)$,*

$$\delta^{\frac{n-2}{2}} c \|\hat{\phi}\|_{H^{1/2}(\partial B)} \leq \|\phi\|_{H^{1/2}(\partial D_\delta)} \leq \delta^{\frac{n-2}{2}} \|\hat{\phi}\|_{H^{1/2}(\partial B)}, \tag{2.20a}$$

$$\delta^{\frac{n}{2}} \|\hat{\psi}\|_{H^{-1/2}(\partial B)} \leq \|\psi\|_{H^{-1/2}(\partial D_\delta)} \leq \delta^{\frac{n}{2}} C \|\hat{\psi}\|_{H^{-1/2}(\partial B)}. \tag{2.20b}$$

Proof. Let $\phi \in H^{1/2}_\diamond(\partial D_\delta)$ and $\psi \in H^{-1/2}_\diamond(\partial D_\delta)$. By a change of coordinates, $\boldsymbol{\xi} := \frac{\boldsymbol{x} - \boldsymbol{z}}{\delta}$, we observe that for all $u \in H^1_\diamond(D_\delta)$,

$$\begin{aligned}
\|u\|^2_{H^1(D_\delta)} &= \int_{D_\delta} \left(|u(\boldsymbol{x})|^2 + |\nabla_x u(\boldsymbol{x})|^2 \right) \mathrm{d}\boldsymbol{x} \\
&= \delta^n \int_B \left(|u(\delta\boldsymbol{\xi} + \boldsymbol{z})|^2 + \frac{1}{\delta^2} |\nabla_\xi u(\delta\boldsymbol{\xi} + \boldsymbol{z})|^2 \right) \mathrm{d}\boldsymbol{\xi} \\
&= \delta^n \int_B \left(|\hat{u}(\boldsymbol{\xi})|^2 + \frac{1}{\delta^2} |\nabla_\xi \hat{u}(\boldsymbol{\xi})|^2 \right) \mathrm{d}\boldsymbol{\xi}.
\end{aligned}$$

Thus,

$$\|u\|^2_{H^1(D_\delta)} \leq \delta^{n-2} \|\hat{u}\|^2_{H^1(B)},$$

because we have assumed that $0 < \delta \leq 1$, and therefore

$$\|\phi\|_{H^{1/2}(\partial D_\delta)} \leq \delta^{\frac{n-2}{2}} \|\hat{\phi}\|_{H^{1/2}(\partial B)}.$$

On the other hand, the Poincaré inequality (cf. [88, Lemma 3.13]) implies that there exists a constant $c > 0$ independent of δ such that for all $u \in H^1_\diamond(D_\delta)$,

$$\delta^{n-2} c \|\hat{u}\|^2_{H^1(B)} \leq \delta^{n-2} \|\nabla_\xi \hat{u}\|^2_{L^2(B)} = \|\nabla_x u\|^2_{L^2(D_\delta)} \leq \|u\|^2_{H^1(D_\delta)}.$$

Hence,

$$\delta^{\frac{n-2}{2}} c\|\hat{\phi}\|_{H^{1/2}(\partial B)} \leq \|\phi\|_{H^{1/2}(\partial D_\delta)},$$

and we have shown (2.20a).

For the dual norm we obtain by a change of coordinates and by applying (2.20a) that

$$\begin{aligned}\|\psi\|_{H^{-1/2}(\partial D_\delta)} &= \sup_{\substack{\phi\in H^{1/2}(\partial D_\delta)\\ \phi\neq 0}} \frac{|\langle\psi,\phi\rangle_{\partial D_\delta}|}{\|\phi\|_{H^{1/2}(\partial D_\delta)}} \geq \sup_{\substack{\phi\in H^{1/2}(\partial D_\delta)\\ \phi\neq 0}} \frac{\delta^{n-1}|\langle\hat{\psi},\hat{\phi}\rangle_{\partial B}|}{\delta^{\frac{n-2}{2}}\|\hat{\phi}\|_{H^{1/2}(\partial B)}} \\ &= \delta^{\frac{n}{2}} \sup_{\substack{\hat{\phi}\in H^{1/2}(\partial B)\\ \hat{\phi}\neq 0}} \frac{|\langle\hat{\psi},\hat{\phi}\rangle_{\partial B}|}{\|\hat{\phi}\|_{H^{1/2}(\partial B)}} = \delta^{\frac{n}{2}}\|\hat{\psi}\|_{H^{-1/2}(\partial B)}\end{aligned}$$

and in the same way

$$\begin{aligned}\|\psi\|_{H^{-1/2}(\partial D_\delta)} &\leq \sup_{\substack{\phi\in H^{1/2}(\partial D_\delta)\\ \phi\neq 0}} \frac{\delta^{n-1}|\langle\hat{\psi},\hat{\phi}\rangle_{\partial B}|}{\delta^{\frac{n-2}{2}} c\|\hat{\phi}\|_{H^{1/2}(\partial B)}} \\ &= c^{-1}\delta^{\frac{n}{2}} \sup_{\substack{\hat{\phi}\in H^{1/2}(\partial B)\\ \hat{\phi}\neq 0}} \frac{|\langle\hat{\psi},\hat{\phi}\rangle_{\partial B}|}{\|\hat{\phi}\|_{H^{1/2}(\partial B)}} = \delta^{\frac{n}{2}} C\|\hat{\psi}\|_{H^{-1/2}(\partial B)}.\end{aligned}$$

Here, we put $C := c^{-1}$. □

In the next lemma, we investigate the scaling properties of the integral operators $K^N_{D_\delta}$ and ${K^N_{D_\delta}}^\top$ under changes of coordinates as in (2.19).

Lemma 2.6. *Let $\phi \in H^{1/2}_\diamond(\partial D_\delta)$ and $\psi \in H^{-1/2}(\partial D_\delta)$. Then,*

$$K^N_{D_\delta}\phi = (K^0_B\hat{\phi})^\vee + (E_K\hat{\phi})^\vee, \tag{2.21a}$$

$${K^N_{D_\delta}}^\top\psi = ({K^0_B}^\top\hat{\psi})^\vee + (E_K^\top\hat{\psi})^\vee, \tag{2.21b}$$

where E_K is a bounded linear operator, independent of ϕ, which is $\mathcal{O}(\delta^n)$ in $\mathcal{L}(H^{1/2}_\diamond(\partial B), H^{1/2}(\partial B))$ as $\delta\to 0$, and $E_K^\top$ is the transpose of E_K, which is $\mathcal{O}(\delta^n)$ in $\mathcal{L}(H^{-1/2}(\partial B), H^{-1/2}_\diamond(\partial B))$ as $\delta\to 0$.

Proof. Let $\phi \in H^{1/2}_\diamond(\partial D_\delta)$. By a change of variables, $\boldsymbol{\xi} := \frac{\boldsymbol{x}-\boldsymbol{z}}{\delta}$ and $\boldsymbol{\eta} := \frac{\boldsymbol{y}-\boldsymbol{z}}{\delta}$, we see that for a.e. $\boldsymbol{x}\in\partial D_\delta$,

$$\begin{aligned}(K^0_{D_\delta}\phi)(\boldsymbol{x}) &= \frac{1}{\omega_n}\int_{\partial D_\delta} \frac{(\boldsymbol{x}-\boldsymbol{y})\cdot\boldsymbol{\nu}(\boldsymbol{y})}{|\boldsymbol{x}-\boldsymbol{y}|^n}\phi(\boldsymbol{y})\,\mathrm{d}s(\boldsymbol{y}) \\ &= \frac{1}{\omega_n}\int_{\partial B} \frac{(\delta\boldsymbol{\xi}-\delta\boldsymbol{\eta})\cdot\boldsymbol{\nu}(\boldsymbol{\eta})}{|\delta\boldsymbol{\xi}-\delta\boldsymbol{\eta}|^n}\phi(\delta\boldsymbol{\eta}+\boldsymbol{z})\delta^{n-1}\,\mathrm{d}s(\boldsymbol{\eta}) \\ &= \frac{1}{\omega_n}\int_{\partial B} \frac{(\boldsymbol{\xi}-\boldsymbol{\eta})\cdot\boldsymbol{\nu}(\boldsymbol{\eta})}{|\boldsymbol{\xi}-\boldsymbol{\eta}|^n}\hat{\phi}(\boldsymbol{\eta})\,\mathrm{d}s(\boldsymbol{\eta}) = (K^0_B\hat{\phi})(\boldsymbol{\xi}).\end{aligned}$$

Recalling (2.8), it remains to estimate the norm of $P^N_{D_\delta}\phi$. For this purpose, we denote by $\tilde{P}^N_{D_\delta}\phi$ the extension of $P^N_{D_\delta}\phi$ to $H^1(D_\delta)$, which is obtained canonically from (2.7) via

$$(\tilde{P}^N_{D_\delta}\phi)(\boldsymbol{x}) := \int_{\partial D_\delta} \frac{\partial p_N(\boldsymbol{x},\boldsymbol{y})}{\partial \boldsymbol{\nu}(\boldsymbol{y})}\phi(\boldsymbol{y})\,\mathrm{d}s(\boldsymbol{y}), \qquad \boldsymbol{x}\in D_\delta.$$

Then, because p_N and $\nabla_x p_N$ are uniformly bounded near the inclusion D_δ,

$$\begin{aligned}
\|P^N_{D_\delta}\phi\|^2_{H^{1/2}(\partial D_\delta)} &= \Big(\inf_{\substack{u\in H^1(D_\delta)\\ u|_{\partial D_\delta}=P^N_{D_\delta}\phi}} \|u\|_{H^1(D_\delta)}\Big)^2 \le \|\tilde{P}^N_{D_\delta}\phi\|^2_{H^1(D_\delta)}\\
&= \int_{D_\delta}\Big|\int_{\partial D_\delta}\frac{\partial p_N(\boldsymbol{x},\boldsymbol{y})}{\partial\boldsymbol{\nu}(\boldsymbol{y})}\phi(\boldsymbol{y})\,\mathrm{d}s(\boldsymbol{y})\Big|^2\,\mathrm{d}\boldsymbol{x}\\
&\quad+\int_{D_\delta}\Big|\nabla_x\int_{\partial D_\delta}\frac{\partial p_N(\boldsymbol{x},\boldsymbol{y})}{\partial\boldsymbol{\nu}(\boldsymbol{y})}\phi(\boldsymbol{y})\,\mathrm{d}s(\boldsymbol{y})\Big|^2\,\mathrm{d}\boldsymbol{x}\\
&\le \int_{D_\delta}\Big(\int_{\partial D_\delta}\Big(\Big|\frac{\partial p_N(\boldsymbol{x},\boldsymbol{y})}{\partial\boldsymbol{\nu}(\boldsymbol{y})}\Big|^2\\
&\qquad\qquad+\Big|\nabla_x\frac{\partial p_N(\boldsymbol{x},\boldsymbol{y})}{\partial\boldsymbol{\nu}(\boldsymbol{y})}\Big|^2\Big)\,\mathrm{d}s(\boldsymbol{y})\int_{\partial D_\delta}|\phi(\boldsymbol{y})|^2\,\mathrm{d}s(\boldsymbol{y})\Big)\,\mathrm{d}\boldsymbol{x}\\
&\le C\delta^{n-1}\|\phi\|^2_{L^2(\partial D_\delta)}\int_{D_\delta}1\,\mathrm{d}\boldsymbol{x} \le C\delta^{2n-1}\|\phi\|^2_{L^2(\partial D_\delta)}
\end{aligned}$$

for a positive constant C that is independent of δ. Moreover, applying the Sobolev Embedding Theorem (see [86, Theorem 3.27]), we find that

$$\|\phi\|^2_{L^2(\partial D_\delta)} = \delta^{n-1}\|\hat{\phi}\|^2_{L^2(\partial B)} \le C\delta^{n-1}\|\hat{\phi}\|^2_{H^{1/2}(\partial B)}$$

with a positive constant C that is independent of δ. Combining these two estimates and (2.20a) yields that

$$\begin{aligned}
\|(P^N_{D_\delta}\phi)^\wedge\|^2_{H^{1/2}(\partial B)} &\le C\delta^{2-n}\|P^N_{D_\delta}\phi\|^2_{H^{1/2}(\partial D_\delta)} \le C\delta^{n+1}\|\phi\|^2_{L^2(\partial D_\delta)}\\
&\le C\delta^{2n}\|\hat{\phi}\|^2_{H^{1/2}(\partial B)}.
\end{aligned} \tag{2.22}$$

Thus, we define

$$E_K\varphi := (P^N_{D_\delta}\check{\varphi})^\wedge, \qquad \varphi\in H^{1/2}_\diamond(\partial B),$$

and obtain the first part of the desired result. The second part follows by duality. □

In the following, according to our remarks at the end of Section 2.2, we consider $-\frac{1}{2}I + {K^0_{D_\delta}}^\top$ and $-\frac{1}{2}I + {K^N_{D_\delta}}^\top$ as operators in $\mathcal{L}(H^{-1/2}_\diamond(\partial D_\delta))$. From Lemma 2.6, we get for all $\phi\in H^{-1/2}_\diamond(\partial D_\delta)$ that

$$\Big(-\frac{1}{2}I + {K^N_{D_\delta}}^\top\Big)\phi = \Big(\Big(-\frac{1}{2}I + {K^0_B}^\top + E^\top_K\Big)\hat{\phi}\Big)^\vee$$

and thus,

$$\Big(-\frac{1}{2}I + {K_{D_\delta}^N}^\top\Big)^{-1}\phi = \Big(\Big(-\frac{1}{2}I + {K_B^0}^\top + E_K^\top\Big)^{-1}\hat{\phi}\Big)^\vee.$$

So, we obtain from Lemma 2.2 that

$$\Big(-\frac{1}{2}I + {K_{D_\delta}^N}^\top\Big)^{-1}\phi = \Big(\Big(-\frac{1}{2}I + {K_B^0}^\top\Big)^{-1}\hat{\phi}\Big)^\vee + (\tilde{E}_K^\top\hat{\phi})^\vee, \tag{2.23}$$

where $\tilde{E}_K^\top$ is a bounded linear operator, independent of ϕ, which is $\mathcal{O}(\delta^n)$ in $\mathcal{L}(H_\diamond^{-1/2}(\partial B))$ as $\delta \to 0$.

2.6 Asymptotic Expansion

In this section, we first expand the three operators L_δ, $L_\delta^\top$, and F_δ occurring in the factorization (2.18) of the difference of the Neumann–to–Dirichlet operators $\Lambda_\delta - \Lambda_0$ separately as the inhomogeneity size δ tends to zero. Then, we use these expansions to calculate the leading order term in the asymptotic expansion of $\Lambda_\delta - \Lambda_0$.

We first consider the boundary value problem (2.12) and the operator L_δ from (2.13). For $\phi \in H_\diamond^{-1/2}(\partial D_\delta)$ we define $v_\delta \in H^1_{\diamond,\partial\Omega}(\Omega \setminus \overline{D_\delta})$ by

$$v_\delta := \mathcal{S}_{D_\delta}^N\Big(-\frac{1}{2}I + {K_{D_\delta}^N}^\top\Big)^{-1}\phi.$$

Then, v_δ is a solution to (2.12), and by a change of coordinates and by applying (2.23) we have

$$\begin{aligned}
v_\delta|_{\partial\Omega} &= \int_{\partial D_\delta} N(\cdot,\boldsymbol{y})\Big(\Big(-\frac{1}{2}I + {K_{D_\delta}^N}^\top\Big)^{-1}\phi\Big)(\boldsymbol{y})\,\mathrm{d}s(\boldsymbol{y}) \\
&= \int_{\partial B} N(\cdot,\delta\boldsymbol{\eta}+\boldsymbol{z})\Big(\Big(-\frac{1}{2}I + {K_{D_\delta}^N}^\top\Big)^{-1}\phi\Big)(\delta\boldsymbol{\eta}+\boldsymbol{z})\delta^{n-1}\,\mathrm{d}s(\boldsymbol{\eta}) \\
&= \delta^{n-1}\int_{\partial B} N(\cdot,\delta\boldsymbol{\eta}+\boldsymbol{z})\Big(\Big(-\frac{1}{2}I + {K_B^0}^\top\Big)^{-1}\hat{\phi}\Big)(\boldsymbol{\eta})\,\mathrm{d}s(\boldsymbol{\eta}) \\
&\quad + \delta^{n-1}\int_{\partial B} N(\cdot,\delta\boldsymbol{\eta}+\boldsymbol{z})(\tilde{E}_K^\top\hat{\phi}))(\boldsymbol{\eta})\,\mathrm{d}s(\boldsymbol{\eta}).
\end{aligned}$$

By Taylor expansion, we obtain for $\boldsymbol{x} \in \partial\Omega$ and $\boldsymbol{\eta} \in \partial B$ as $\delta \to 0$ that

$$N(\boldsymbol{x},\delta\boldsymbol{\eta}+\boldsymbol{z}) = N(\boldsymbol{x},\boldsymbol{z}) + \delta\nabla_y N(\boldsymbol{x},\boldsymbol{z})\cdot\boldsymbol{\eta} + \mathcal{O}(\delta^2).$$

Recalling that $-\frac{1}{2}I + {K_B^0}^\top$ and $\tilde{E}_K^\top$ map $H_\diamond^{-1/2}(\partial D_\delta)$ to $H_\diamond^{-1/2}(\partial D_\delta)$, this gives

$$\begin{aligned}
v_\delta|_{\partial\Omega} &= \delta^n\nabla_y N(\cdot,\boldsymbol{z})\cdot\int_{\partial B}\boldsymbol{\eta}\Big(\Big(-\frac{1}{2}I + {K_B^0}^\top\Big)^{-1}\hat{\phi}\Big)(\boldsymbol{\eta})\,\mathrm{d}s(\boldsymbol{\eta}) \\
&\quad + \delta^n\nabla_y N(\cdot,\boldsymbol{z})\cdot\int_{\partial B}\boldsymbol{\eta}(\tilde{E}_K^\top\hat{\phi})(\boldsymbol{\eta})\,\mathrm{d}s(\boldsymbol{\eta}) + \mathcal{O}(\delta^{n+1}).
\end{aligned}$$

Because $\tilde{E}_K^\top$ is $\mathcal{O}(\delta^n)$ in $\mathcal{L}(H_\diamond^{-1/2}(\partial B))$, we find that

$$\begin{aligned}\Big\|\nabla_y N(\cdot,\boldsymbol{z})\cdot\int_{\partial B}\boldsymbol{\eta}(\tilde{E}_K^\top\hat{\phi})(\boldsymbol{\eta})\,\mathrm{d}s(\boldsymbol{\eta})\Big\|_{H^{1/2}(\partial\Omega)}&\\ \le C\max_{1\le j\le 3}\Big|\int_{\partial B}\eta_j(\tilde{E}_K^\top\hat{\phi})(\boldsymbol{\eta})\,\mathrm{d}s(\boldsymbol{\eta})\Big|&\\ \le C\|\tilde{E}_K^\top\hat{\phi}\|_{H^{-1/2}(\partial B)}\max_{1\le j\le 3}\|\eta_j\|_{H^{1/2}(\partial B)}&\\ \le C\delta^n\|\hat{\phi}\|_{H^{-1/2}(\partial B)}&\end{aligned}$$

So, as $\delta\to 0$,

$$v_\delta|_{\partial\Omega}=\delta^n\nabla_y N(\cdot,\boldsymbol{z})\cdot\int_{\partial B}\boldsymbol{\eta}\Big(\Big(-\frac{1}{2}I+{K_B^0}^\top\Big)^{-1}\hat{\phi}\Big)(\boldsymbol{\eta})\,\mathrm{d}s(\boldsymbol{\eta})+\mathcal{O}(\delta^{n+1}).$$

The last term on the right–hand side is bounded by $C\delta^{n+1}\|\hat{\phi}\|_{H^{-1/2}(\partial B)}$ in $H_\diamond^{1/2}(\partial\Omega)$, where the constant $C>0$ is independent of δ and ϕ. We define

$$\begin{aligned}&L:H_\diamond^{-1/2}(\partial B)\to H_\diamond^{1/2}(\partial\Omega),\\ &\qquad L\varphi:=\nabla_y N(\cdot,\boldsymbol{z})\cdot\int_{\partial B}\boldsymbol{\eta}\Big(\Big(-\frac{1}{2}I+{K_B^0}^\top\Big)^{-1}\varphi\Big)(\boldsymbol{\eta})\,\mathrm{d}s(\boldsymbol{\eta}).\end{aligned}\tag{2.24}$$

Then, L is a bounded linear operator, and we have shown the following asymptotic formula.

Proposition 2.7. *For all $\phi\in H_\diamond^{-1/2}(\partial D_\delta)$,*

$$L_\delta\phi=\delta^n L\hat{\phi}+E_L\hat{\phi},\tag{2.25}$$

where E_L is a bounded linear operator, independent of ϕ, which is $\mathcal{O}(\delta^{n+1})$ in $\mathcal{L}(H_\diamond^{-1/2}(\partial B),H_\diamond^{1/2}(\partial\Omega))$ as $\delta\to 0$.

Remark 2.8. Note that by duality the transpose $E_L^\top$ of E_L is $\mathcal{O}(\delta^{n+1})$ in $\mathcal{L}(H_\diamond^{-1/2}(\partial\Omega),H_\diamond^{1/2}(\partial B))$, too.

Next, we consider the asymptotic behavior of the operator $L_\delta^\top$ from (2.15). Let $\phi\in H_\diamond^{-1/2}(\partial D_\delta)$ and $\psi\in H_\diamond^{-1/2}(\partial\Omega)$. For $X\in\{\Omega,B,D_\delta\}$ we denote by $\langle\cdot,\cdot\rangle_{\partial X}$ the dual pairing between $H_\diamond^{1/2}(\partial X)$ and $H_\diamond^{-1/2}(\partial X)$ and use (2.25) to calculate

$$\begin{aligned}\big\langle\phi,L_\delta^\top\psi\big\rangle_{\partial D_\delta}&=\big\langle L_\delta\phi,\psi\big\rangle_{\partial\Omega}=\big\langle\delta^n L\hat{\phi}+E_L\hat{\phi},\psi\big\rangle_{\partial\Omega}\\ &=\big\langle\hat{\phi},\delta^n L^\top\psi+E_L^\top\psi\big\rangle_{\partial B}=\big\langle\phi,\delta(L^\top\psi)^\vee+\delta^{1-d}(E_L^\top\psi)^\vee\big\rangle_{\partial D_\delta},\end{aligned}$$

where $L^\top:H_\diamond^{-1/2}(\partial\Omega)\to H_\diamond^{1/2}(\partial B)$ is the transpose of L. Recalling Remark 2.8, we obtain the following asymptotic formula.

Proposition 2.9. *For all* $\psi \in H_\diamond^{-1/2}(\partial\Omega)$,

$$L_\delta^\top \psi = \delta (L^\top \psi)^\vee + \delta^{1-d} (E_L^\top \psi)^\vee,$$

where $E_L^\top$ *is a bounded linear operator, independent of* ψ, *which is* $\mathcal{O}(\delta^{n+1})$ *in* $\mathcal{L}(H_\diamond^{-1/2}(\partial\Omega), H_\diamond^{1/2}(\partial B))$ *as* $\delta \to 0$.

We now derive the operator $L^\top$ explicitly. Let $\phi \in H_\diamond^{-1/2}(\partial B)$ and $\psi \in H_\diamond^{-1/2}(\partial\Omega)$. Recalling the definition of the operator L from (2.24), we find that

$$\begin{aligned}
&\big\langle L\phi, \psi \big\rangle_{\partial\Omega} \\
&\quad = \int_{\partial\Omega} \nabla_y N(\boldsymbol{x}, \boldsymbol{z}) \cdot \bigg(\int_{\partial B} \boldsymbol{\eta} \Big(\Big(-\frac{1}{2} I + {K_B^0}^\top \Big)^{-1} \phi \Big)(\boldsymbol{\eta}) \, \mathrm{d}s(\boldsymbol{\eta}) \bigg) \psi(\boldsymbol{x}) \, \mathrm{d}s(\boldsymbol{x}) \\
&\quad = \bigg(\int_{\partial\Omega} \nabla_y N(\boldsymbol{x}, \boldsymbol{z}) \psi(\boldsymbol{x}) \, \mathrm{d}s(\boldsymbol{x}) \bigg) \cdot \int_{\partial B} \boldsymbol{\eta} \Big(\Big(-\frac{1}{2} I + {K_B^0}^\top \Big)^{-1} \phi \Big)(\boldsymbol{\eta}) \, \mathrm{d}s(\boldsymbol{\eta}) \\
&\quad = \bigg(\int_{\partial\Omega} \nabla_y N(\boldsymbol{x}, \boldsymbol{z}) \psi(\boldsymbol{x}) \, \mathrm{d}s(\boldsymbol{x}) \bigg) \cdot \int_{\partial B} \phi(\boldsymbol{\xi}) \Big(\Big(-\frac{1}{2} I + K_B^0 \Big)^{-1} \boldsymbol{\eta} \Big)(\boldsymbol{\xi}) \, \mathrm{d}s(\boldsymbol{\xi}).
\end{aligned}$$

Note that in the last line of this computation $\boldsymbol{\eta}$ is the surface variable on ∂B and therefore $(-\frac{1}{2} I + K_B^0)^{-1} \boldsymbol{\eta}$ is defined component–wise for this vector valued function. Because N solves (2.2) together with its normalization condition, we find that

$$v := \int_{\partial\Omega} N(\boldsymbol{x}, \boldsymbol{z}) \psi(\boldsymbol{x}) \, \mathrm{d}s(\boldsymbol{x})$$

solves

$$\Delta v = 0 \quad \text{in } \Omega, \qquad \frac{\partial v}{\partial \boldsymbol{\nu}} = \psi \quad \text{on } \partial\Omega, \tag{2.26}$$

together with the normalization $\int_{\partial\Omega} v \, \mathrm{d}s = 0$. Thus,

$$\int_{\partial\Omega} \nabla_y N(\boldsymbol{x}, \boldsymbol{z}) \psi(\boldsymbol{x}) \, \mathrm{d}s(\boldsymbol{x}) = \nabla v(\boldsymbol{z}),$$

which means that

$$L^\top \psi = \nabla v(\boldsymbol{z}) \cdot \Big(\Big(-\frac{1}{2} I + K_B^0 \Big)^{-1} \boldsymbol{\eta} \Big), \tag{2.27}$$

where v is the solution of (2.26).

We return to the diffraction problem (2.16) and to the operator F_δ from (2.17). Given $\chi \in H_\diamond^{1/2}(\partial D_\delta)$, we define w_δ with $w_\delta|_{\Omega \setminus \overline{D_\delta}} \in H^1_{\diamond, \partial\Omega}(\Omega \setminus \overline{D_\delta})$ and $w_\delta|_{D_\delta} \in H^1(D_\delta)$ by

$$w_\delta := \mathcal{D}_{D_\delta}^N \chi.$$

Then, w_δ is a solution to (2.16), and from (2.9b), we obtain that

$$w_\delta|^-_{\partial D_\delta} = \Big(-\frac{1}{2}I + K^N_{D_\delta}\Big)\chi.$$

Now, we consider the interior Dirichlet problem

$$\Delta w = 0 \quad \text{in } D_\delta, \qquad w = \varphi \quad \text{on } \partial D_\delta, \tag{2.28}$$

where $\varphi \in H^{1/2}(\partial D_\delta)$, and introduce the corresponding interior Dirichlet–to–Neumann operator

$$\Upsilon_\delta : H^{1/2}(\partial D_\delta) \to H_\diamond^{-1/2}(\partial D_\delta), \quad \Upsilon_\delta\varphi := \frac{\partial w}{\partial \boldsymbol{\nu}}\Big|_{\partial D_\delta}.$$

Because w_δ solves the diffraction problem (2.16), we can write

$$\frac{\partial w_\delta}{\partial \boldsymbol{\nu}}\Big|_{\partial D_\delta} = \Upsilon_\delta\Big(-\frac{1}{2}I + K^N_{D_\delta}\Big)\chi.$$

The interior Dirichlet–to–Neumann operator $\Upsilon : H^{1/2}(\partial B) \to H_\diamond^{-1/2}(\partial B)$ on ∂B is defined in the same way as Υ_δ. Note that these Dirichlet–to–Neumann maps are bounded linear operators. This follows from the existence and uniqueness of solutions of the corresponding Dirichlet boundary value problems, the continuous dependence of these solutions on their boundary values and from the continuity of normal trace operator γ_n. In order to investigate the asymptotic behavior of $\frac{\partial w_\delta}{\partial \boldsymbol{\nu}}\big|_{\partial D_\delta}$ as $\delta \to 0$, we take a closer look at the scaling properties of Υ_δ.

Lemma 2.10. *Let $\varphi \in H^{1/2}(\partial D_\delta)$. Then,*

$$\Upsilon_\delta\varphi = \delta^{-1}(\Upsilon\hat{\varphi})^\vee.$$

Proof. Suppose $w \in H^1(D_\delta)$ is a solution to (2.28). By a change of variables, $\boldsymbol{\xi} := \frac{\boldsymbol{x}-\boldsymbol{z}}{\delta}$, we find that $\hat{w}$ satisfies

$$\begin{aligned}
\Delta_\xi\hat{w} = \delta^2(\Delta_x w)^\wedge = 0 \qquad & \text{in } B,\\
\frac{\partial\hat{w}}{\partial\boldsymbol{\nu}}\Big|_{\partial B} = \delta\Big(\frac{\partial w}{\partial\boldsymbol{\nu}}\Big|_{\partial D_\delta}\Big)^\wedge \qquad & \text{on } \partial B,\\
\hat{w}|_{\partial B} = \big(w|_{\partial D_\delta}\big)^\wedge \qquad & \text{on } \partial B.
\end{aligned}$$

Hence,

$$\big(\Upsilon(\hat{w}|_{\partial B})\big)^\vee = \Big(\frac{\partial\hat{w}}{\partial\boldsymbol{\nu}}\Big|_{\partial B}\Big)^\vee = \delta\frac{\partial w}{\partial\boldsymbol{\nu}}\Big|_{\partial D_\delta} = \delta\Upsilon_\delta(w|_{\partial D_\delta}).$$

□

Therefore, applying Lemma 2.10 and Lemma 2.6, we can calculate

$$\begin{aligned}\frac{\partial w_\delta}{\partial \boldsymbol{\nu}}\Big|_{\partial D_\delta} &= \Upsilon_\delta\Big(-\frac{1}{2}I + K_{D_\delta}^N\Big)\chi \\ &= \delta^{-1}\bigg(\Upsilon\Big(\Big(-\frac{1}{2}I + K_{D_\delta}^N\Big)\chi\Big)^\wedge\bigg)^\vee \\ &= \delta^{-1}\Big(\Upsilon\Big(-\frac{1}{2}I + K_B^0\Big)\hat{\chi}\Big)^\vee + \delta^{-1}\Big(\Upsilon E_K\hat{\chi}\Big)^\vee.\end{aligned}$$

Note that according to Lemma 2.6 the operator $E_F := \delta^{-1}\Upsilon E_K$ is $\mathcal{O}(\delta^{n-1})$ in $\mathcal{L}(H_\diamond^{1/2}(\partial D_\delta), H_\diamond^{-1/2}(\partial D_\delta))$ as $\delta \to 0$. We define

$$F : H_\diamond^{1/2}(\partial B) \to H_\diamond^{-1/2}(\partial B), \qquad F\varphi := -\Upsilon\Big(-\frac{1}{2}I + K_B^0\Big)\varphi. \tag{2.29}$$

Then, F is a bounded linear operator, and we have shown the following asymptotic formula.

Proposition 2.11. *For all $\chi \in H_\diamond^{1/2}(\partial D_\delta)$,*

$$F_\delta\chi = \delta^{-1}(F\hat{\chi})^\vee + (E_F\hat{\chi})^\vee,$$

where E_F is a bounded linear operator, independent of χ, which is $\mathcal{O}(\delta^{n-1})$ in $\mathcal{L}(H_\diamond^{1/2}(\partial B), H_\diamond^{-1/2}(\partial B))$ as $\delta \to 0$.

We now put our results together and obtain the following asymptotic expansion of the factorization of the difference of the Neumann–to–Dirichlet operators $\Lambda_\delta - \Lambda_0$ from Lemma 2.4.

Theorem 2.12. *Let $f \in H_\diamond^{-1/2}(\partial\Omega)$. Then,*

$$(\Lambda_\delta - \Lambda_0)\, f = \delta^n LFL^\top f + \mathcal{O}(\delta^{n+1}) \tag{2.30}$$

in $H_\diamond^{1/2}(\partial\Omega)$ as $\delta \to 0$. More precisely, the last term on the right–hand side is bounded by $C\delta^{n+1}\|f\|_{H^{-1/2}(\partial\Omega)}$, where the constant $C > 0$ is independent of δ and f.

Proof. From Proposition 2.9, we obtain that

$$L_\delta^\top f = \delta(L^\top f)^\vee + \delta^{1-n}(E_L^\top f)^\vee.$$

So, by Proposition 2.11,

$$F_\delta L_\delta^\top f = (FL^\top f)^\vee + \delta^{-n}(FE_L^\top f)^\vee + \delta(E_F L^\top f)^\vee + \delta^{1-n}(E_F E_L^\top f)^\vee.$$

With the help of Proposition 2.7 we find that

$$\begin{aligned}(\Lambda_\delta - \Lambda_0)f = L_\delta F_\delta L_\delta^\top f &= \delta^n LFL^\top f + \delta^{n+1}LE_F L^\top f + LFE_L^\top f \\ &+ \delta LE_F E_L^\top f + E_L FL^\top f + \delta E_L E_F L^\top f + \delta^{-d}E_L FE_L^\top f + \delta^{1-d}E_L E_F E_L^\top f.\end{aligned}$$

Now, the assertion follows from the estimates given in Proposition 2.7, Proposition 2.11, and Proposition 2.9 and from the continuity of the operators L, F, and $L^\top$. □

The following diagrams illustrate the factorization $\Lambda_\delta - \Lambda_0 = L_\delta F_\delta L_\delta^\top$ from Lemma 2.4 and the leading order term $LFL^\top$ of the corresponding *asymptotic factorization* $\Lambda_\delta - \Lambda_0 = \delta^n LFL^\top + \mathcal{O}(\delta^{n+1})$ from Theorem 2.12:

$$\begin{array}{ccc} H_\diamond^{-1/2}(\partial\Omega) & \xrightarrow{\Lambda_\delta - \Lambda_0} & H_\diamond^{1/2}(\partial\Omega) \\ \big\downarrow{\scriptstyle L_\delta^\top} & & {\scriptstyle L_\delta}\big\uparrow \\ H_\diamond^{1/2}(\partial D_\delta) & \xrightarrow{F_\delta} & H_\diamond^{-1/2}(\partial D_\delta) \end{array} \qquad \begin{array}{ccc} H_\diamond^{-1/2}(\partial\Omega) & & H_\diamond^{1/2}(\partial\Omega) \\ \big\downarrow{\scriptstyle L^\top} & & {\scriptstyle L}\big\uparrow \\ H_\diamond^{1/2}(\partial B) & \xrightarrow{F} & H_\diamond^{-1/2}(\partial B) \end{array}$$

Finally, let $f \in H_\diamond^{-1/2}(\partial\Omega)$ and let u_0 be the solution to (2.11). We calculate $LFL^\top f$ explicitely. As (2.11) and (2.26) coincide for $\psi = f$, we obtain from (2.27) that

$$L^\top f = \nabla u_0(\boldsymbol{z}) \cdot \Big(\Big(-\frac{1}{2} I + K_B^0 \Big)^{-1} \boldsymbol{\eta} \Big).$$

Thus, by (2.29),

$$FL^\top f = -\nabla u_0(\boldsymbol{z}) \cdot \Upsilon \boldsymbol{\eta} = -\nabla u_0(\boldsymbol{z}) \cdot \boldsymbol{\nu}(\boldsymbol{\eta}),$$

where $\boldsymbol{\nu}$ denotes the unit outward normal to ∂B relative to B, because η_l is the unique harmonic function on B with Dirichlet data $\eta_l|_{\partial B}$, $1 \le l \le n$. So, by (2.24),

$$\begin{aligned} &LFL^\top f \\ &\quad = -\nabla_y N(\cdot, \boldsymbol{z}) \cdot \int_{\partial B} \boldsymbol{\eta} \left(\Big(-\frac{1}{2} I + {K_B^0}^\top \Big)^{-1} \big(\boldsymbol{\nu} \cdot \nabla u_0(\boldsymbol{z}) \big) \right) (\boldsymbol{\eta}) \, \mathrm{d}s(\boldsymbol{\eta}) \\ &\quad = \nabla_y N(\cdot, \boldsymbol{z}) \cdot \mathbb{M}_B^0 \nabla u_0(\boldsymbol{z}), \end{aligned} \tag{2.31}$$

where the matrix $\mathbb{M}_B^0 \in \mathbb{R}^{n \times n}$ is the magnetic polarizability tensor corresponding to B; cf. Definition A.1. Altogether, we obtain the following corollary.

Corollary 2.13. *Let $f \in H_\diamond^{-1/2}(\partial\Omega)$ and let u_0 be the corresponding solution of* (2.11)*. Then,*

$$(\Lambda_\delta - \Lambda_0) f = \delta^n \nabla_y N(\cdot, \boldsymbol{z}) \cdot \mathbb{M}_B^0 \nabla u_0(\boldsymbol{z}) + \mathcal{O}(\delta^{n+1})$$

in $H_\diamond^{1/2}(\partial\Omega)$ as $\delta \to 0$. More precisely, the last term on the right–hand side is bounded by $C\delta^{n+1} \|f\|_{H^{-1/2}(\partial\Omega)}$, where the constant $C > 0$ is independent of δ and f.

2.7 Multiple Inclusions

In this section, we extend the results obtained so far to the practically important case of finitely many well separated small inclusions as introduced in Section 2.3. Basically, the results and their proofs for a single inclusion from the previous sections can be adopted with few minor modifications, which we will comment on now.

The factorization of the Neumann–to–Dirichlet operator from Lemma 2.4 can be generalized as described in [21]. For this purpose, it is convenient to set $\partial D_\delta = \partial D_{\delta,1} \times \cdots \times \partial D_{\delta,m}$ and to interpret the relevant Sobolev spaces accordingly as product spaces, e.g.

$$H_\diamond^{\pm 1/2}(\partial D_\delta) = H_\diamond^{\pm 1/2}(\partial D_{\delta,1}) \times \cdots \times H_\diamond^{\pm 1/2}(\partial D_{\delta,m}).$$

The operator L_δ is again defined by (2.12) and (2.13), where the inner Neumann boundary condition should be understood component–wise, i.e., $\frac{\partial v_\delta}{\partial \boldsymbol{\nu}} = \phi_l$ on $\partial D_{\delta,l}$, $1 \le l \le m$, for $\boldsymbol{\phi} = (\phi_1, \ldots, \phi_m)^\top \in H_\diamond^{-1/2}(\partial D_\delta)$. For the definition of the corresponding dual operator $L_\delta^\top$ we consider again the boundary value problem (2.14), whose solution v'_δ is unique up to an additive constant. If we fix an arbitrary solution v'_δ of (2.14) and define $c_l := \big(\int_{\partial D_{\delta,l}} v'_\delta|_{\partial D_{\delta,l}}\, \mathrm{d}s\big)/|\partial D_{\delta,l}|$, $1 \le l \le m$, then the transpose of L_δ is given by

$$L_\delta^\top : H_\diamond^{-1/2}(\partial\Omega) \to H_\diamond^{1/2}(\partial D_\delta), \quad \psi \mapsto (v'_\delta|_{\partial D_{\delta,1}} - c_1, \ldots, v'_\delta|_{\partial D_{\delta,m}} - c_m).$$

The definition of the operator F_δ remains unchanged, if the boundary conditions on ∂D_δ are interpreted component–wise. With these definitions the factorization of $\Lambda_\delta - \Lambda_0$ stated in Lemma 2.4 holds true in the case of multiple inclusions as well.

Next, we generalize the asymptotic expansions derived in the previous section to the case of multiple inclusions. First, we reconsider the operator L_δ from (2.13). For $\boldsymbol{\phi} = (\phi_1, \ldots, \phi_m)^\top \in H_\diamond^{-1/2}(\partial D_\delta)$ we define $v_\delta \in H^1_{\diamond,\partial\Omega}(\Omega \setminus \overline{D_\delta})$ by

$$v_\delta := \sum_{l=1}^m \mathcal{S}^N_{D_{\delta,l}} a_l,$$

where $\boldsymbol{a} := (a_1, \ldots, a_m)^\top \in H_\diamond^{-1/2}(\partial D_\delta)$ solves the system of integral equations

$$\mathbb{A}\boldsymbol{a} = \boldsymbol{\phi},$$

with

$$\mathbb{A} := \begin{pmatrix} -\frac{1}{2}I + {K^N_{D_{\delta,1}}}^\top & \frac{\partial \mathcal{S}^N_{D_{\delta,2}}}{\partial \boldsymbol{\nu}}\Big|_{\partial D_{\delta,1}} & \dots & \frac{\partial \mathcal{S}^N_{D_{\delta,m}}}{\partial \boldsymbol{\nu}}\Big|_{\partial D_{\delta,1}} \\ \frac{\partial \mathcal{S}^N_{D_{\delta,1}}}{\partial \boldsymbol{\nu}}\Big|_{\partial D_{\delta,2}} & -\frac{1}{2}I + {K^N_{D_{\delta,2}}}^\top & \dots & \frac{\partial \mathcal{S}^N_{D_{\delta,m}}}{\partial \boldsymbol{\nu}}\Big|_{\partial D_{\delta,2}} \\ \dots & \dots & \dots & \dots \\ \frac{\partial \mathcal{S}^N_{D_{\delta,1}}}{\partial \boldsymbol{\nu}}\Big|_{\partial D_{\delta,m}} & \frac{\partial \mathcal{S}^N_{D_{\delta,2}}}{\partial \boldsymbol{\nu}}\Big|_{\partial D_{\delta,m}} & \dots & -\frac{1}{2}I + {K^N_{D_{\delta,m}}}^\top \end{pmatrix}.$$

As the small inclusions are assumed to be well separated from each other and from the boundary $\partial\Omega$, we can estimate the nondiagonal entries of the matrix $\mathbb{A}$, using the regularity of $\mathcal{S}^N_{D_{\delta,l}}\varphi_l$, $\varphi_l \in H_\diamond^{-1/2}(\partial D_{\delta,l})$, away from $\partial D_{\delta,l}$, $1 \le l \le m$. Set

$$\mathbb{B} := \begin{pmatrix} -\frac{1}{2}I + {K^N_{B_1}}^\top & 0 & \dots & 0 \\ 0 & -\frac{1}{2}I + {K^N_{B_2}}^\top & \dots & 0 \\ \dots & \dots & \dots & \dots \\ 0 & 0 & \dots & -\frac{1}{2}I + {K^N_{B_m}}^\top \end{pmatrix}$$

and note that $\mathbb{B}$ is invertible by Lemma 2.3 and Theorem 2.1. In the same way as in the proof of Lemma 2.3, we obtain that the nullspace of $\mathbb{A}$ is trivial, too. Because $\mathbb{A}$ is just a compact perturbation of $-\frac{1}{2}\mathbb{I}$, where $\mathbb{I}$ denotes the identity operator on $H^{-1/2}(\partial D_\delta)$, Theorem 2.1 yields that $\mathbb{A}$ is invertible. Similarly to Lemma 2.6 we get the following result, where we use the maximum row sum of $\mathcal{L}(H_\diamond^{-1/2}(\partial B_j), H_\diamond^{-1/2}(\partial B_l))$ norms, $1 \le j, l \le m$, as norm on $\mathcal{L}(H_\diamond^{-1/2}(\partial B))$.

Lemma 2.14. *Let $\boldsymbol{\varphi} \in H_\diamond^{-1/2}(\partial D_\delta)$. Then,*

$$\mathbb{A}\boldsymbol{\varphi} = (\,\mathbb{B}\hat{\boldsymbol{\varphi}})^\vee + (\,\mathbb{E}_A\hat{\boldsymbol{\varphi}})^\vee,$$

where $\mathbb{E}_A$ is a bounded linear operator, independent of $\boldsymbol{\varphi}$, which is $\mathcal{O}(\delta^n)$ in $\mathcal{L}(H_\diamond^{-1/2}(\partial B))$ as $\delta \to 0$.

Proof. Let $\boldsymbol{\varphi} = (\varphi_1, \dots, \varphi_m) \in H_\diamond^{-1/2}(\partial D_\delta)$ and $1 \le j \ne l \le m$. Using the regularity of $N(\boldsymbol{x}, \boldsymbol{y})$ in a neighborhood of $(\boldsymbol{x}, \boldsymbol{y}) \in \Omega \times \Omega$ with $\boldsymbol{x} \ne \boldsymbol{y}$ and

applying (2.20b), we obtain

$$\begin{aligned}
\Big\|\Big(\frac{\partial \mathcal{S}^N_{D_{\delta,j}}\varphi_j}{\partial \boldsymbol{\nu}}\Big|_{\partial D_{\delta,l}}\Big)^{\wedge_l}\Big\|^2_{H^{-1/2}(\partial B_l)} &\le C\Big\|\Big(\frac{\partial \mathcal{S}^N_{D_{\delta,j}}\varphi_j}{\partial \boldsymbol{\nu}}\Big|_{\partial D_{\delta,l}}\Big)^{\wedge_l}\Big\|^2_{L^2(\partial B_l)}\\
&= C\delta^{1-n}\Big\|\frac{\partial \mathcal{S}^N_{D_{\delta,j}}\varphi_j}{\partial \boldsymbol{\nu}}\Big|_{\partial D_{\delta,l}}\Big\|^2_{L^2(\partial D_{\delta,l})}\\
&= C\delta^{1-n}\int_{\partial D_{\delta,l}}\Big|\int_{\partial D_{\delta,j}}\frac{\partial N(\boldsymbol{x},\boldsymbol{y})}{\partial \boldsymbol{\nu}(\boldsymbol{x})}\varphi_j(\boldsymbol{y})\,\mathrm{d}s(\boldsymbol{y})\Big|^2\,\mathrm{d}s(\boldsymbol{x})\\
&\le C\delta^{1-n}\int_{\partial D_{\delta,l}}\Big\|\frac{\partial N(\boldsymbol{x},\cdot)}{\partial \boldsymbol{\nu}(\boldsymbol{x})}\Big\|^2_{H^{1/2}(\partial D_{\delta,j})}\|\varphi_j\|^2_{H^{-1/2}(\partial D_{\delta,j})}\,\mathrm{d}s(\boldsymbol{x})\\
&\le C\delta\|\varphi_j\|^2_{H^{-1/2}(\partial D_{\delta,j})}\int_{\partial D_{\delta,l}}1\,\mathrm{d}s \le C\delta^{2n}\|(\varphi_j)^{\wedge_j}\|^2_{H^{-1/2}(\partial B_j)}.
\end{aligned}$$

Here, $(\cdot)^{\wedge_l}$ denotes the transformation from (2.19), applied to the lth inhomogeneity $D_{\delta,l}$, $1 \le l \le m$. □

So, we find from Lemma 2.2 that for any $\boldsymbol{\varphi} \in H^{-1/2}_\diamond(\partial D_\delta)$,

$$\mathbb{A}^{-1}\boldsymbol{\varphi} = (\,\mathbb{B}^{-1}\hat{\boldsymbol{\varphi}})^\vee + (\,\tilde{\mathbb{E}}_A\hat{\boldsymbol{\varphi}})^\vee,$$

where $\tilde{\mathbb{E}}_A$ is a bounded linear operator, independent of $\boldsymbol{\varphi}$, which is $\mathcal{O}(\delta^n)$ in $\mathcal{L}(\boldsymbol{H}^{-1/2}_\diamond(\partial B))$ as $\delta \to 0$. Calculating along the lines of Section 2.6, we obtain the following asymptotic formula:

$$v_\delta\big|_{\partial\Omega} = \delta^n\sum_{l=1}^m \nabla_y N(\cdot,\boldsymbol{z}_l)\cdot\int_{\partial B_l}\boldsymbol{\eta}\Big(\Big(-\frac{1}{2}I + {K^0_{B_l}}^\top\Big)^{-1}\phi_l^{\wedge_l}\Big)(\boldsymbol{\eta})\,\mathrm{d}s(\boldsymbol{\eta}) + \mathcal{O}(\delta^{n+1})$$

as $\delta \to 0$, where $(\cdot)^{\wedge_l}$ again denotes the transformation from (2.19), applied to the lth inclusion $D_{\delta,l}$. The last term on the right–hand side is bounded by

$$C\delta^{n+1}\max_{1\le l\le m}\|\phi_l^{\wedge_l}\|_{H^{-1/2}(\partial B_l)}$$

in $H^{1/2}_\diamond(\partial\Omega)$, where the constant $C > 0$ is independent of δ and $\boldsymbol{\phi}$. Therefore, if we define

$$\begin{aligned}
&L : H^{-1/2}_\diamond(\partial B_1)\times\cdots\times H^{-1/2}_\diamond(\partial B_m) \to H^{1/2}_\diamond(\partial\Omega),\\
&\quad L\boldsymbol{\varphi} := \sum_{l=1}^m \nabla_y N(\cdot,\boldsymbol{z}_l)\cdot\int_{\partial B_l}\boldsymbol{\eta}\Big(\Big(-\frac{1}{2}I + {K^0_{B_l}}^\top\Big)^{-1}\varphi_l\Big)(\boldsymbol{\eta})\,\mathrm{d}s(\boldsymbol{\eta}), \quad (2.32)
\end{aligned}$$

Proposition 2.7 remains valid in the case of finitely many well separated small inclusions.

As in Section 2.6, we find by duality that Proposition 2.9 remains valid in case of finitely many well separated small inclusions too and that the adjoint operator

$$L^\top : H_\diamond^{-1/2}(\partial\Omega) \to H_\diamond^{1/2}(\partial B_1) \times \cdots \times H_\diamond^{1/2}(\partial B_m)$$

of L is given by

$$L^\top\psi = \Big(\nabla v(\boldsymbol{z}_1) \cdot \Big(\Big(-\frac{1}{2} I + K_{B_1}^0 \Big)^{-1} \boldsymbol{\eta} \Big), \ldots, \nabla v(\boldsymbol{z}_m) \cdot \Big(\Big(-\frac{1}{2} I + K_{B_m}^0 \Big)^{-1} \boldsymbol{\eta} \Big) \Big), \tag{2.33}$$

where v is the corresponding solution of (2.26).

We return to the diffraction problem (2.16) and the operator F_δ from (2.17). For $\boldsymbol{\chi} = (\chi_1, \ldots, \chi_m) \in H_\diamond^{1/2}(\partial D_\delta)$ we define $w_\delta := \sum_{l=1}^m \mathcal{D}_{D_{\delta,l}}^N \chi_l$. Then, for $1 \le j \le m$,

$$\frac{\partial w_\delta}{\partial \boldsymbol{\nu}}\Big|_{\partial D_{\delta,j}} = \Upsilon_{\delta,j} \Big(-\frac{1}{2} I + K_{D_{\delta,j}}^N \Big) \chi_j + \Upsilon_{\delta,j} \sum_{\substack{l=1 \\ l \ne j}}^m \big(\mathcal{D}_{D_{\delta,l}}^N \chi_l \big)\big|_{\partial D_{\delta,j}},$$

where $\Upsilon_{\delta,j}$ is the interior Dirichlet–to–Neumann operator on $\partial D_{\delta,j}$. Using Lemma 2.10 and the continuity of the interior Dirichlet–to–Neumann operator Υ_l on ∂B_l, $1 \le l \le m$, we can estimate as in the proof of Lemma 2.6 that

$$\begin{aligned}
&\Big\| \Big(\Upsilon_{\delta,j} \sum_{\substack{l=1 \\ l \ne j}}^m \big(\mathcal{D}_{D_{\delta,l}}^N \chi_l \big)\big|_{\partial D_{\delta,j}} \Big)^{\wedge_j} \Big\|_{H^{-1/2}(\partial B_j)} \\
&\qquad = C\delta^{-1} \Big\| \Upsilon_j \Big(\sum_{\substack{l=1 \\ l \ne j}}^m \big(\mathcal{D}_{D_{\delta,l}}^N \chi_l \big)\big|_{\partial D_{\delta,j}} \Big)^{\wedge_j} \Big\|_{H^{-1/2}(\partial B_j)} \\
&\qquad \le C\delta^{-1} \max_{\substack{1 \le l \le m \\ l \ne j}} \Big\| \Big(\big(\mathcal{D}_{D_{\delta,l}}^N \chi_l \big)\big|_{\partial D_{\delta,j}} \Big)^{\wedge_j} \Big\|_{H^{1/2}(\partial B_j)} \\
&\qquad \le C\delta^{n-1} \max_{1 \le l \le m} \|\chi_l^{\wedge_l}\|_{H^{1/2}(\partial B_l)},
\end{aligned} \tag{2.34}$$

where the constant $C > 0$ is independent of δ and $\boldsymbol{\chi}$. We define

$$\begin{aligned}
F : H_\diamond^{1/2}(\partial B_1) \times \cdots \times H_\diamond^{1/2}(\partial B_m) &\to H_\diamond^{-1/2}(\partial B_1) \times \cdots \times H_\diamond^{-1/2}(\partial B_m), \\
F\boldsymbol{\varphi} &:= \Big(-\Upsilon_1 \Big(-\frac{1}{2} I + K_{B_1}^0 \Big) \varphi_1, \ldots, -\Upsilon_m \Big(-\frac{1}{2} I + K_{B_m}^0 \Big) \varphi_m \Big).
\end{aligned} \tag{2.35}$$

Combining (2.34) with the Lemmas 2.6 and 2.10, we find that Proposition 2.11 remains valid in the case of finitely many well separated small inclusions.

Proposition 2.15. *Theorem 2.12 holds true in the case of finitely many well separated small inclusions, if L, F, and $L^\top$ are given as in* (2.32), (2.35), *and* (2.33), *respectively.*

Finally, let $\mathbb{M}^0_{B_1}, \dots, \mathbb{M}^0_{B_m}$ denote the magnetic polarizability tensors corresponding to $B_1, \dots, B_m$, respectively. In case of finitely many well separated small inclusions, Corollary 2.13 reads as follows.

Corollary 2.16. *Let $f \in H_\diamond^{-1/2}(\partial\Omega)$ and let u_0 be the corresponding solution of* (2.11). *Then,*

$$(\Lambda_\delta - \Lambda_0)\, f = \delta^n \sum_{l=1}^{m} \nabla_y N(\cdot, \boldsymbol{z}_l) \cdot \mathbb{M}^0_{B_l} \nabla u_0(\boldsymbol{z}_l) + \mathcal{O}(\delta^{n+1})$$

in $H_\diamond^{1/2}(\partial\Omega)$ as $\delta \to 0$. More precisely, the last term on the right–hand side is bounded by $C\delta^{n+1}\|f\|_{H^{-1/2}(\partial\Omega)}$, where the constant $C > 0$ is independent of δ and f.

2.8 Determining the Position of the Inclusions

In this section, we restrict ourselves again to the case of a single inhomogeneity $D_\delta = \boldsymbol{z} + \delta B$, although we mention that the whole theory also works for multiple inclusions.

We consider the problem of locating the inclusion D_δ from the boundary measurements $\Lambda_\delta - \Lambda_0$. In particular we want to compare the Factorization Method as developed in [21, 59] and the MUSIC–type method considered in [22, 59]. The fact that there is a relation between Factorization Methods and MUSIC–type methods has already been pointed out earlier by Cheney [34], Kirsch [73], and by Hanke and Brühl [59]. Using the asymptotic analysis from the previous sections, we can clarify the connection between these methods completely.

The Factorization Method got its name from the factorization of the difference of the Neumann–to–Dirichlet operators $\Lambda_\delta - \Lambda_0$ given in (2.18). The first observation to be made is that the range of the operator L_δ fully determines the inclusion D_δ. To see this, let $\boldsymbol{y} \in \Omega$ and define a *test function*

$$u_{y,d} := \boldsymbol{d} \cdot \nabla_y N(\cdot, \boldsymbol{y}), \qquad \boldsymbol{d} \in \mathbb{R}^n.$$

Then, $u_{y,d}$ solves

$$\Delta u_{y,d} = 0 \quad \text{in } \Omega \setminus \{\boldsymbol{y}\}, \qquad \frac{\partial u_{y,d}}{\partial \boldsymbol{\nu}} = 0 \quad \text{on } \partial\Omega. \tag{2.36}$$

Therefore, $\boldsymbol{y} \in D_\delta$ implies $g_{y,d} := u_{y,d}|_{\partial\Omega} \in \mathcal{R}(L_\delta)$, because $u_{y,d}|_{\Omega\setminus\overline{D_\delta}}$ solves (2.12) for $\phi = \frac{\partial u_{y,d}}{\partial \boldsymbol{\nu}}\big|_{\partial D_\delta}$. Moreover, as solutions to (2.36) are uniquely determined by their Cauchy data on $\partial\Omega$ (see Dautray and Lions [45, Corollary

11, p. 262]), also the converse is true, because of the singularity of $u_{y,d}$ in $\boldsymbol{y}$. Hence,

$$\boldsymbol{y} \in D_\delta \qquad \text{if and only if} \qquad g_{y,d} \in \mathcal{R}(L_\delta). \tag{2.37}$$

Now, the key result of the Factorization Method is that the range of L_δ can be computed from Λ_δ and Λ_0 by

$$\mathcal{R}\big((\Lambda_\delta - \Lambda_0)^{1/2}\big) = \mathcal{R}(L_\delta). \tag{2.38}$$

Thus, the inclusion D_δ is found by calculating $g_{y,d}$ for every *test point* $\boldsymbol{y} \in \Omega$ and checking whether $g_{y,d} \in \mathcal{R}((\Lambda_\delta - \Lambda_0)^{1/2})$, which is an infinite dimensional space. This *range criterion* can be implemented numerically by applying the Picard criterion; cf. [79, Theorem 15.18]. In practical computations this means that an infinite dimensional series has to be checked for convergence from finitely many data. We refer the reader to [20, 59] for details and numerical results.

On the other hand, it follows from the asymptotic expansion (2.30) that for small values of δ the operator $\Lambda_\delta - \Lambda_0$ is well approximated by $\delta^n L F L^\top$. The derivation of the MUSIC–type method starts by considering only this leading order term. Defining the linear operators

$$\begin{aligned} &R : \mathbb{R}^n \to H_\diamond^{1/2}(\partial\Omega), \quad R\boldsymbol{a} := \boldsymbol{a} \cdot \nabla_y N(\cdot, \boldsymbol{z})|_{\partial\Omega}, \\ &S : H_\diamond^{-1/2}(\partial B) \to \mathbb{R}^n, \quad S\varphi := \int_{\partial B} \boldsymbol{\eta}\Big(\Big(-\frac{1}{2}I + {K_B^0}^\top\Big)^{-1}\varphi\Big)(\boldsymbol{\eta})\, \mathrm{d}s(\boldsymbol{\eta}), \end{aligned}$$

an easy computation shows that their dual operators are

$$\begin{aligned} &R^\top : H_\diamond^{-1/2}(\partial\Omega) \to \mathbb{R}^n, \quad R^\top\psi = \nabla v(\boldsymbol{z}), \\ &S^\top : \mathbb{R}^n \to H_\diamond^{1/2}(\partial B), \quad S^\top\boldsymbol{a} = \boldsymbol{a} \cdot \Big(-\frac{1}{2}I + K_B^0\Big)^{-1}\boldsymbol{\eta}, \end{aligned}$$

respectively, where v is the corresponding solution of (2.26) and $\boldsymbol{\eta}$ denotes the surface variable on ∂B. From (2.24), we find that

$$L = RS, \qquad L^\top = S^\top R^\top, \qquad \text{and} \qquad LFL^\top = RSFS^\top R^\top.$$

Recalling (2.29) and Definition A.1, we see that

$$SFS^\top = \mathbb{M}_B^0,$$

where we identify the matrix $\mathbb{M}_B^0$ with the corresponding linear operator on $\mathbb{R}^n$. Hence,

$$LFL^\top = R\mathbb{M}_B^0 R^\top;$$

cf. (2.31).

It is clear from the definition of R that $g_{y,d} \in \mathcal{R}(R)$ if $\boldsymbol{y} = \boldsymbol{z}$. The converse can again be proven by using that solutions to (2.36) are uniquely determined by their Cauchy data on $\partial\Omega$. Thus,

$$\boldsymbol{y} = \boldsymbol{z} \qquad \text{if and only if} \qquad g_{y,d} \in \mathcal{R}(R). \tag{2.39}$$

It has been shown in [22] that

$$\mathcal{R}(R\,\mathbb{M}_B^0 R^\top) = \mathcal{R}(R). \tag{2.40}$$

Thus, the position $\boldsymbol{z}$ of the inclusion D_δ can be determined by calculating $g_{y,d}$ for every test point $\boldsymbol{y} \in \Omega$ and checking whether $g_{y,d} \in \mathcal{R}(R\,\mathbb{M}_B^0 R^\top)$, which is a finite dimensional space. This range criterion can be implemented very simply by calculating the angle $\beta(\boldsymbol{y})$ between $g_{y,d}$ and $\mathcal{R}(R\,\mathbb{M}_B^0 R^\top)$. Unfortunately, $R\,\mathbb{M}_B^0 R^\top$ is not known in practise. But, as already mentioned, $R\,\mathbb{M}_B^0 R^\top \approx \delta^{-n}(\Lambda_\delta - \Lambda_0)$ is a good approximation for small values of δ. Thus, it can be shown that

$$\mathcal{R}(R\,\mathbb{M}_B^0 R^\top) \approx \mathcal{R}(\Lambda_\delta - \Lambda_0),$$

and so approximations $\beta^\delta(\boldsymbol{y})$ of $\beta(\boldsymbol{y})$ can be computed by using $\mathcal{R}(\Lambda_\delta - \Lambda_0)$ instead of $\mathcal{R}(R\,\mathbb{M}_B^0 R^\top)$ in the definition of these angles. Plotting the values of $\cot\beta^\delta(\boldsymbol{y})$ for an appropriate collection of sampling points $\boldsymbol{y} \in \Omega$ we expect to see large values for points $\boldsymbol{y}$ which are close to the position of the inclusion $\boldsymbol{z}$. For details and numerical results we refer the reader to [22, 59]. Note that this MUSIC–type method does not reconstruct the shape of the inclusion, as the Factorization Method does. It gives just an idea of the position $\boldsymbol{z}$ of the small inclusion.

Now, we come to our conclusion. We have seen that the theoretical foundations of the Factorization Method and the MUSIC–type method are the range criteria (2.37) and (2.39) together with the range identities (2.38) and (2.40). As for $\boldsymbol{a} \in \mathbb{R}^n$,

$$0 = \boldsymbol{a} \cdot \left(-\frac{1}{2}I + {K_B^0}^\top\right)^{-1} \boldsymbol{\eta} = \left(-\frac{1}{2}I + {K_B^0}^\top\right)^{-1} (\boldsymbol{a} \cdot \boldsymbol{\eta}),$$

where $\boldsymbol{\eta}$ is again the surface variable on ∂B, is equivalent to $\boldsymbol{a} \cdot \boldsymbol{\eta} = 0$, which is equivalent to $\boldsymbol{a} = 0$, we find that the operator $S^\top$ is injective with finite dimensional range. Hence, $\mathcal{R}(S) = \mathcal{N}(S^\top)^a = \mathbb{R}^n$, i.e., S is surjective. Here, $\mathcal{N}(S^\top)^a$ denotes the annihilator of $\mathcal{N}(S^\top)$ in $\mathbb{R}^n$. So we find that $\mathcal{R}(L) = \mathcal{R}(RS) = \mathcal{R}(R)$, and thus (2.39) is equivalent to

$$\boldsymbol{y} = \boldsymbol{z} \qquad \text{if and only if} \qquad g_{y,d} \in \mathcal{R}(L).$$

This shows that the characterization of the inclusion used in the MUSIC–type reconstruction method is exactly the asymptotic version of the characterization of inclusion from the Factorization Method as the size of the inclusion tends to zero.

Chapter 3

Asymptotic Factorization for Maxwell's Equations

In this chapter, we consider the direct scattering problem in two–layered background media outlined in the introduction. We study the scattered electromagnetic field due to a collection of finitely many small perfectly conducting scatterers buried within the lower halfspace of an unbounded two–layered background medium. Excitations of incident fields and measurements of scattered fields are restricted to the measurement device, which is supposed to be contained in a bounded sheet parallel to the surface of ground in the upper halfspace. The *incident fields*, we are going to use, are superpositions of electromagnetic fields due to so–called magnetic dipoles on the measurement device. Note that by Biot–Savart's law electromagnetic fields generated by time–harmonic currents in any wire loop contained in the measurement device can be ascribed to such a magnetic dipole distribution on the measurement device; cf., e.g., Delbary et al. [46] for details.

We introduce the *near field measurement operator* that maps magnetic dipole distributions on the measurement device, which generate the incident fields, to the corresponding scattered fields on the same device. Then, we derive an asymptotic expansion of this operator as the size of the scatterers tends to zero, which, of course, also yields an asymptotic expansion of the scattered field corresponding to any dipole excitation on the measurement device.

Our proof of this asymptotic formula is based on a factorization of the measurement operator in terms of three appropriate boundary integral operators. A similar factorization has previously been studied by Gebauer et al. [52] to justify a Linear Sampling Method for the corresponding inverse scattering problem; see also Gebauer, Hanke, and Schneider [53]. We apply layer potential techniques to describe the three operators occurring in this factorization separately as the size of the scatterers tends to zero and use these expansions to compute the leading order term in the asymptotic ex-

pansion of the full measurement operator. This generalizes the approach we used in Chapter 2 for a boundary value problem in electrostatics.

In contrast to our work, Ammari et al. used variational methods to prove similar formulas for boundary value problems in bounded domains [10, 14] and (in combination with representation formulas) for scattering problems in unbounded homogeneous background media [15]. For unbounded two–layered background media the leading order term of the asymptotic expansion of the scattered field has been mentioned without proof by Iakovleva et al. [62]; see Ammari et al. [4] for a related formal derivation for homogeneous background media. However, no rigorous analysis for near field measurements in two–layered background media has been available so far.

The outline of this chapter is as follows. After introducing some additional notation in Section 3.1, we study dyadic Green's functions, surface potentials, and boundary integral operators arising in electromagnetic scattering theory for two–layered background media in Section 3.2 and Section 3.3. Then, in Section 3.4, we describe the mathematical model we are going to use and introduce the near field measurement operator that describes our measurement process. In Section 3.5, we derive a factorization of this operator, and Section 3.6 and Section 3.7 are devoted to the main result of this chapter, the asymptotic expansion of the measurement operator as the size of the scatterers tends to zero. Here, we restrict ourselves to the case of a single scatterer. Multiple scatterers are treated in Section 3.8.

3.1 Preliminaries

First, we introduce additional notation and recall some facts concerning function spaces used in the context of Maxwell's equations. Some results are stated without proofs. For details we refer the reader to Buffa, Costabel, and Sheen [23] and to Monk [88].

In this and the following chapter, we always work in $\mathbb{R}^3$. We denote by $(\boldsymbol{e}_1, \boldsymbol{e}_2, \boldsymbol{e}_3)$ the usual Cartesian basis of $\mathbb{R}^3$, by $\boldsymbol{x} = (x_1, x_2, x_3)^\top$ a generic point in $\mathbb{R}^3$, and by $B_r(\boldsymbol{x})$ the ball of radius $r > 0$ centered at $\boldsymbol{x}$. Throughout, let $\boldsymbol{x} \cdot \boldsymbol{y}$ and $\boldsymbol{x} \times \boldsymbol{y}$ be the standard scalar product and the vector product of $\boldsymbol{x}, \boldsymbol{y} \in \mathbb{R}^3$.

Suppose $D \subset \mathbb{R}^3$ is a bounded open set of class $C^{2,\alpha}$, $0 < \alpha < 1$, and denote by $\boldsymbol{\nu}$ the unit outward normal to ∂D relative to D. In the following, we consider the *complex valued* Sobolev spaces $H^r(D; \mathbb{C})$, $H^r_{\mathrm{loc}}(\mathbb{R}^3; \mathbb{C})$, and $H^r_{\mathrm{loc}}(\mathbb{R}^3 \setminus \overline{D}; \mathbb{C})$, $r \in \mathbb{R}$, and $H^s(\partial D; \mathbb{C})$, $s \in [-2, 2]$, which are defined on D, $\mathbb{R}^3$, $\mathbb{R}^3 \setminus \overline{D}$, and on the boundary ∂D, respectively. For $1/2 < r \leq 2$, let $\gamma_0 : H^r(D; \mathbb{C}) \to H^{r-1/2}(\partial D; \mathbb{C})$ be the corresponding standard trace operator.

We define

$$\begin{aligned}
\boldsymbol{L}_t^2(\partial D) &:= \big\{\boldsymbol{a} \in L^2(\partial D;\,\mathbb{C}\,)^3 \;\big|\; \boldsymbol{\nu}\cdot\boldsymbol{a} = 0 \text{ on } \partial D\big\},\\
\boldsymbol{H}_t^s(\partial D) &:= \big\{\boldsymbol{a} \in H^s(\partial D;\,\mathbb{C}\,)^3 \;\big|\; \boldsymbol{a} \in \boldsymbol{L}_t^2(\partial D)\big\}, \quad s \in [0,2],\\
\boldsymbol{H}(\mathrm{div}, D) &:= \big\{\boldsymbol{u} \in L^2(D;\,\mathbb{C}\,)^3 \;\big|\; \mathrm{div}\,\boldsymbol{u} \in L^2(D;\,\mathbb{C}\,)\big\},\\
\boldsymbol{H}(\mathbf{curl}, D) &:= \big\{\boldsymbol{u} \in L^2(D;\,\mathbb{C}\,)^3 \;\big|\; \mathbf{curl}\boldsymbol{u} \in L^2(D;\,\mathbb{C}\,)^3\big\},
\end{aligned}$$

and denote by $\boldsymbol{H}_{\mathrm{loc}}(\mathrm{div}, \mathbb{R}^3 \setminus \overline{D})$ and $\boldsymbol{H}_{\mathrm{loc}}(\mathbf{curl}, \mathbb{R}^3 \setminus \overline{D})$ the space of functions $\boldsymbol{u} \in L^2_{\mathrm{loc}}(\mathbb{R}^3 \setminus \overline{D};\,\mathbb{C}\,)^3$ so that $\boldsymbol{u}|_O \in \boldsymbol{H}(\mathbf{curl}, O)$ and $\boldsymbol{u}|_O \in \boldsymbol{H}(\mathrm{div}, O)$ for every bounded open subset $O \subset \mathbb{R}^3 \setminus \overline{D}$, respectively. Moreover, let $\boldsymbol{H}_t^{-s}(\partial D)$ be the dual space of $\boldsymbol{H}_t^s(\partial D)$ for $s \in [0,2]$.

The *surface gradient* $\nabla_{\partial D}$ and the *surface vector curl* $\mathbf{curl}_{\partial D}$ are defined on ∂D in the usual way by a localization argument, and they can be extended to continuous linear operators

$$\nabla_{\partial D} : H^{3/2}(\partial D;\,\mathbb{C}\,) \to \boldsymbol{H}_t^{1/2}(\partial D), \quad \mathbf{curl}_{\partial D} : H^{3/2}(\partial D;\,\mathbb{C}\,) \to \boldsymbol{H}_t^{1/2}(\partial D).$$

The dual operators of $-\nabla_{\partial D}$ and $\mathbf{curl}_{\partial D}$ are the *surface divergence* $\mathrm{div}_{\partial D}$ and the *surface scalar curl* $\mathrm{curl}_{\partial D}$, respectively. So, we can introduce the Hilbert spaces

$$\begin{aligned}
\boldsymbol{H}_{\mathrm{div}}^{-1/2}(\partial D) &:= \big\{\boldsymbol{a} \in \boldsymbol{H}_t^{-1/2}(\partial D) \;\big|\; \mathrm{div}_{\partial D}\,\boldsymbol{a} \in H^{-1/2}(\partial D;\,\mathbb{C}\,)\big\},\\
\boldsymbol{H}_{\mathrm{curl}}^{-1/2}(\partial D) &:= \big\{\boldsymbol{a} \in \boldsymbol{H}_t^{-1/2}(\partial D) \;\big|\; \mathrm{curl}_{\partial D}\,\boldsymbol{a} \in H^{-1/2}(\partial D;\,\mathbb{C}\,)\big\}.
\end{aligned}$$

For any regular vector field $\boldsymbol{u} \in C^\infty(\overline{D};\,\mathbb{C}\,)^3$, we define the *normal trace* $\gamma_n(\boldsymbol{u}) := \boldsymbol{\nu}\cdot\boldsymbol{u}|_{\partial D}$, the *tangential trace* $\gamma_t(\boldsymbol{u}) := \boldsymbol{\nu}\times\boldsymbol{u}|_{\partial D}$, and the *projection on the tangent plane* $\pi_t(\boldsymbol{u}) := (\boldsymbol{\nu}\times\boldsymbol{u}|_{\partial D})\times\boldsymbol{\nu}$. Moreover, let $n(\boldsymbol{a}) := \boldsymbol{\nu}\cdot\boldsymbol{a}$ and $r(\boldsymbol{a}) := \boldsymbol{\nu}\times\boldsymbol{a}$ for any regular vector field $\boldsymbol{a} \in C^\infty(\partial D;\,\mathbb{C}\,)^3$ on ∂D. Then, γ_n, γ_t, π_t, n, and r can be extended to continuous linear surjective operators

$$\begin{aligned}
\gamma_n &: \boldsymbol{H}(\mathrm{div}, D) \to H^{-1/2}(\partial D),\\
\gamma_t &: \boldsymbol{H}(\mathbf{curl}, D) \to \boldsymbol{H}_{\mathrm{div}}^{-1/2}(\partial D), \quad \pi_t : \boldsymbol{H}(\mathbf{curl}, D) \to \boldsymbol{H}_{\mathrm{curl}}^{-1/2}(\partial D)
\end{aligned}$$

and

$$n : H^s(\partial D;\,\mathbb{C}\,)^3 \to H^s(\partial D;\,\mathbb{C}\,), \quad r : \boldsymbol{H}_t^s(\partial D) \to \boldsymbol{H}_t^s(\partial D), \quad s \in [-1,1].$$

The extension of r is an isomorphism with $r^{-1} = -r = r^\top$ (with slight abuse of notation), which maps $\boldsymbol{H}_{\mathrm{div}}^{-1/2}(\partial D)$ to $\boldsymbol{H}_{\mathrm{curl}}^{-1/2}(\partial D)$ and vice versa. For $\boldsymbol{u} \in \boldsymbol{H}(\mathbf{curl}, D)$ we have $\gamma_t(\boldsymbol{u}) = r(\pi_t(\boldsymbol{u}))$ and $\pi_t(\boldsymbol{u}) = -r(\gamma_t(\boldsymbol{u}))$. The trace operators for $\boldsymbol{H}_{\mathrm{loc}}(\mathrm{div}, \mathbb{R}^3 \setminus \overline{D})$ and $\boldsymbol{H}_{\mathrm{loc}}(\mathbf{curl}, \mathbb{R}^3 \setminus \overline{D})$, also denoted by γ_n, γ_t, and π_t, respectively, are defined analogously and fulfill the same properties. For the matter of readability, we will often use the classical

notation for the trace operators and for the operators n and r on Sobolev spaces also.

The space $\boldsymbol{H}_{\mathrm{curl}}^{-1/2}(\partial D)$ can be naturally identified with the dual space of $\boldsymbol{H}_{\mathrm{div}}^{-1/2}(\partial D)$, and we have the following integration by parts formula. For any $\boldsymbol{u} \in \boldsymbol{H}(\mathbf{curl}, D)$ and $\boldsymbol{v} \in \boldsymbol{H}(\mathbf{curl}, D)$ it holds that

$$\int_D \mathbf{curl}\boldsymbol{u} \cdot \boldsymbol{v} \, \mathrm{d}\boldsymbol{x} - \int_D \boldsymbol{u} \cdot \mathbf{curl}\boldsymbol{v} \, \mathrm{d}\boldsymbol{x} = \langle \gamma_t(\boldsymbol{u}), \pi_t(\boldsymbol{v}) \rangle_{\partial D}, \tag{3.1}$$

where $\langle \cdot, \cdot \rangle_{\partial D}$ denotes the dual pairing between $\boldsymbol{H}_{\mathrm{curl}}^{-1/2}(\partial D)$ and $\boldsymbol{H}_{\mathrm{div}}^{-1/2}(\partial D)$. We note that for any $\boldsymbol{a} \in \boldsymbol{H}_t^{-1/2}(\partial D)$,

$$\mathrm{div}_{\partial D}\, \boldsymbol{a} = \mathrm{curl}_{\partial D}\, r(\boldsymbol{a}) \quad \text{and} \quad \mathrm{curl}_{\partial D}\, \boldsymbol{a} = -\,\mathrm{div}_{\partial D}\, r(\boldsymbol{a}). \tag{3.2}$$

Furthermore, for any $f \in H^1(D)$ (or $f \in H^1_{\mathrm{loc}}(\mathbb{R}^3 \setminus \overline{D})$),

$$\nabla_{\partial D}\gamma_0(f) = \pi_t(\nabla f), \tag{3.3}$$

$$\mathbf{curl}_{\partial D}\gamma_0(f) = -r(\nabla_{\partial D}\gamma_0(f)) = -\gamma_t(\nabla f), \tag{3.4}$$

and finally, for $\boldsymbol{u} \in \boldsymbol{H}(\mathbf{curl}, D)$ (or $\boldsymbol{u} \in \boldsymbol{H}_{\mathrm{loc}}(\mathbf{curl}, \mathbb{R}^3 \setminus \overline{D})$), it holds that

$$-\,\mathrm{div}_{\partial D}\, \gamma_t(\boldsymbol{u}) = \mathrm{curl}_{\partial D}\, \pi_t(\boldsymbol{u}) = \gamma_n(\mathbf{curl}\boldsymbol{u}). \tag{3.5}$$

3.2 Fundamental Solutions and Green's Functions

3.2.1 Homogeneous Medium

We assume that $\mathbb{R}^3$ is filled with a homogeneous material with constant *electric permittivity* ε and constant *magnetic permeability* μ, where μ is positive, whereas ε may be complex with positive real and nonnegative imaginary part. The associated *wavenumber* is $k := \omega\sqrt{\varepsilon\mu}$, where we assume that $\omega > 0$. If $\varepsilon \notin \mathbb{R}$, then k is taken to have positive imaginary part.

First, we recall the fundamental solution of the scalar Helmholtz equation, given by

$$\Phi_k(\boldsymbol{x} - \boldsymbol{y}) := \frac{1}{4\pi} \frac{e^{\mathrm{i}\, k|\boldsymbol{x}-\boldsymbol{y}|}}{|\boldsymbol{x} - \boldsymbol{y}|}, \qquad \boldsymbol{x}, \boldsymbol{y} \in \mathbb{R}^3,\ \boldsymbol{x} \neq \boldsymbol{y}. \tag{3.6}$$

It satisfies

$$\Delta_x \Phi_k(\boldsymbol{x} - \boldsymbol{y}) + k^2 \Phi_k(\boldsymbol{x} - \boldsymbol{y}) = -\delta(\boldsymbol{x} - \boldsymbol{y}), \qquad \boldsymbol{x}, \boldsymbol{y} \in \mathbb{R}^3,$$

where δ denotes the Dirac–delta distribution. Note that for $k = 0$ the function Φ_k reduces to the fundamental solution of the Laplace equation as defined in (2.1).

Next, we define the (matrix valued) *dyadic Green's function* $\mathbb{G}$ for time–harmonic Maxwell's equations in homogeneous medium as the (distributional) solution of

$$\mathbf{curl}_x\,\mathbf{curl}_x\,\mathbb{G}(\boldsymbol{x},\boldsymbol{y}) - k^2\,\mathbb{G}(\boldsymbol{x},\boldsymbol{y}) = \delta(\boldsymbol{x}-\boldsymbol{y})\,\mathbb{I}_3, \qquad \boldsymbol{x},\boldsymbol{y}\in\mathbb{R}^3,$$

together with the Silver–Müller radiation conditions

$$\int_{\partial B_R(0)} \Big|\frac{\boldsymbol{x}}{R}\times\,\mathbb{G}(\boldsymbol{x},\boldsymbol{y}) + \frac{\mathrm{i}}{k}\mathbf{curl}_x\,\mathbb{G}(\boldsymbol{x},\boldsymbol{y})\Big|^2\,\mathrm{d}s(\boldsymbol{x}) = o(1),$$
$$\int_{\partial B_R(0)} \Big|\frac{\boldsymbol{x}}{R}\times\mathbf{curl}_x\,\mathbb{G}(\boldsymbol{x},\boldsymbol{y}) + \mathrm{i}\,k\,\mathbb{G}(\boldsymbol{x},\boldsymbol{y})\Big|^2\,\mathrm{d}s(\boldsymbol{x}) = o(1),$$

as $R\to\infty$. Here, $\mathbb{I}_3$ denotes the 3×3 identity matrix. The dyadic Green's function $\mathbb{G}$ has the following representation, cf. Nédélec [91, Theorem 5.2.1],

$$\mathbb{G}(\boldsymbol{x},\boldsymbol{y}) = \Phi_k(\boldsymbol{x}-\boldsymbol{y})\,\mathbb{I}_3 + \frac{1}{k^2}\nabla_x\,\mathrm{div}_x\big(\Phi_k(\boldsymbol{x}-\boldsymbol{y})\,\mathbb{I}_3\big), \qquad \boldsymbol{x},\boldsymbol{y}\in\mathbb{R}^3, \boldsymbol{x}\neq\boldsymbol{y}. \tag{3.7}$$

3.2.2 Two–Layered Medium

We decompose the space $\mathbb{R}^3 = \mathbb{R}^3_+ \cup \Sigma_0 \cup \mathbb{R}^3_-$ in a hyperplane

$$\Sigma_0 := \{\boldsymbol{x}\in\mathbb{R}^3 \mid x_3 = 0\}$$

and the two halfspaces

$$\mathbb{R}^3_+ := \{\boldsymbol{x}\in\mathbb{R}^3 \mid x_3 > 0\} \quad\text{and}\quad \mathbb{R}^3_- := \{\boldsymbol{x}\in\mathbb{R}^3 \mid x_3 < 0\}$$

above and below Σ_0. For convenience, we set $\mathbb{R}^3_0 := \mathbb{R}^3\setminus\Sigma_0$. We assume that both halfspaces are filled with homogeneous materials with electric permittivity ε and magnetic permeability μ given by

$$\varepsilon(\boldsymbol{x}) := \begin{cases}\varepsilon_+, & \boldsymbol{x}\in\mathbb{R}^3_+,\\ \varepsilon_-, & \boldsymbol{x}\in\mathbb{R}^3_-,\end{cases} \qquad \mu(\boldsymbol{x}) := \begin{cases}\mu_+, & \boldsymbol{x}\in\mathbb{R}^3_+,\\ \mu_-, & \boldsymbol{x}\in\mathbb{R}^3_-,\end{cases} \tag{3.8}$$

and we require that ε_+ as well as $\mu_\pm$ are positive numbers, whereas ε_- may be complex with positive real and nonnegative imaginary part. The associated (discontinuous) wavenumber is $k := \omega\sqrt{\varepsilon\mu}$, where we assume $\omega > 0$. If $\varepsilon_-\notin\mathbb{R}$, then k is taken to have positive imaginary part.

For this two–layered background medium we have to distinguish between the electric and the magnetic dyadic Green's functions. The *electric dyadic Green's function* $\mathbb{G}^e$ is the (distributional) solution of

$$\mathbf{curl}_x\frac{1}{\mu(\boldsymbol{x})}\mathbf{curl}_x\,\mathbb{G}^e(\boldsymbol{x},\boldsymbol{y}) - \omega^2\varepsilon(\boldsymbol{x})\,\mathbb{G}^e(\boldsymbol{x},\boldsymbol{y}) = \frac{1}{\mu(\boldsymbol{x})}\delta(\boldsymbol{x}-\boldsymbol{y})\,\mathbb{I}_3, \tag{3.9}$$

$\boldsymbol{x}, \boldsymbol{y} \in \mathbb{R}^3$, together with the Silver–Müller radiation conditions

$$\int_{\partial B_R(0)} \Big| \frac{\boldsymbol{x}}{R} \times \mathbb{G}^e(\boldsymbol{x}, \boldsymbol{y}) + \frac{\mathrm{i}}{k(\boldsymbol{x})} \mathbf{curl}_x \mathbb{G}^e(\boldsymbol{x}, \boldsymbol{y}) \Big|^2 \, \mathrm{d}s(\boldsymbol{x}) = o(1), \tag{3.10a}$$

$$\int_{\partial B_R(0)} \Big| \frac{\boldsymbol{x}}{R} \times \mathbf{curl}_x \mathbb{G}^e(\boldsymbol{x}, \boldsymbol{y}) + \mathrm{i}\, k(\boldsymbol{x}) \mathbb{G}^e(\boldsymbol{x}, \boldsymbol{y}) \Big|^2 \, \mathrm{d}s(\boldsymbol{x}) = o(1) \tag{3.10b}$$

as $R \to \infty$. On the other hand, the *magnetic dyadic Green's function* $\mathbb{G}^m$ is the (distributional) solution of

$$\mathbf{curl}_x \frac{1}{\varepsilon(\boldsymbol{x})} \mathbf{curl}_x \, \mathbb{G}^m(\boldsymbol{x}, \boldsymbol{y}) - \omega^2 \mu(\boldsymbol{x}) \, \mathbb{G}^m(\boldsymbol{x}, \boldsymbol{y}) = \frac{1}{\varepsilon(\boldsymbol{x})} \delta(\boldsymbol{x} - \boldsymbol{y}) \, \mathbb{I}_3, \tag{3.11}$$

$\boldsymbol{x}, \boldsymbol{y} \in \mathbb{R}^3$, together with the Silver–Müller radiation conditions

$$\int_{\partial B_R(0)} \Big| \frac{\boldsymbol{x}}{R} \times \mathbb{G}^m(\boldsymbol{x}, \boldsymbol{y}) + \frac{\mathrm{i}}{k(\boldsymbol{x})} \mathbf{curl}_x \mathbb{G}^m(\boldsymbol{x}, \boldsymbol{y}) \Big|^2 \, \mathrm{d}s(\boldsymbol{x}) = o(1), \tag{3.12a}$$

$$\int_{\partial B_R(0)} \Big| \frac{\boldsymbol{x}}{R} \times \mathbf{curl}\, \mathbb{G}^m(\boldsymbol{x}, \boldsymbol{y}) + \mathrm{i}\, k(\boldsymbol{x}) \mathbb{G}^m(\boldsymbol{x}, \boldsymbol{y}) \Big|^2 \, \mathrm{d}s(\boldsymbol{x}) = o(1) \tag{3.12b}$$

as $R \to \infty$. Note that we are using $\boldsymbol{x}$ as an independent variable and $\boldsymbol{y}$ denotes the position of the source.

For derivations of these Green's functions we refer to Delbary et al. [46] and to [88, pp. 318–327]; see also Petry [92], Cutzach and Hazard [43], Muniz [89], and Sommerfeld [99]. From [88, 89] we find that $\mathbb{G}^e$ and $\mathbb{G}^m$ can be written as

$$\mathbb{G}^{e/m}(\boldsymbol{x}, \boldsymbol{y}) = \Pi^{e/m}(\boldsymbol{x}, \boldsymbol{y}) + \frac{1}{k(\boldsymbol{x})^2} \nabla_x \operatorname{div}_x \Pi^{e/m}(\boldsymbol{x}, \boldsymbol{y}), \tag{3.13}$$

$\boldsymbol{x}, \boldsymbol{y} \in \mathbb{R}^3_0$, $\boldsymbol{x} \neq \boldsymbol{y}$. Here, the (matrix valued) functions Π^e and Π^m are of the form

$$\Pi^{e/m}(\boldsymbol{x}, \boldsymbol{y}) = \Phi_{k(\boldsymbol{x})}(\boldsymbol{x} - \boldsymbol{y}) \, \mathbb{I}_3 + F^{e/m}(\boldsymbol{x}, \boldsymbol{y}), \qquad \boldsymbol{x}, \boldsymbol{y} \in \mathbb{R}^3_0, \, \boldsymbol{x} \neq \boldsymbol{y}, \tag{3.14}$$

and they solve

$$(\Delta_x + k(\boldsymbol{x})^2) \Pi^{e/m}(\boldsymbol{x}, \boldsymbol{y}) = -\delta(\boldsymbol{x} - \boldsymbol{y}) \, \mathbb{I}_3, \qquad \boldsymbol{x}, \boldsymbol{y} \in \mathbb{R}^3_0,$$

together with jump conditions on Σ_0, which can be derived using the continuity of the tangential components of $\mathbb{G}^{e/m}(\cdot, \boldsymbol{y})$, $(1/\mu) \operatorname{curl}_x \mathbb{G}^e(\cdot, \boldsymbol{y})$, and $(1/\varepsilon) \operatorname{curl}_x \mathbb{G}^m(\cdot, \boldsymbol{y})$ across Σ_0. The (matrix valued) functions F^e and F^m solve

$$(\Delta_x + k(\boldsymbol{x})^2) F^{e/m}(\boldsymbol{x}, \boldsymbol{y}) = 0, \qquad \boldsymbol{x}, \boldsymbol{y} \in \mathbb{R}^3_0,$$

and $F^e(\cdot, \boldsymbol{y})$ and $F^m(\cdot, \boldsymbol{y})$ are smooth functions (with resp. to both variables) in $\mathbb{R}^3_0$ for $\boldsymbol{y}$ in any compact subset of $\mathbb{R}^3_0$.

3.3 Surface Potentials for Maxwell's Equations

In this section, we collect some results concerning boundary integral operators arising in electromagnetic scattering theory. Although well known to experts, some of these results where not available to us in citable form.

3.3.1 Homogeneous Medium

We start with a homogeneous medium with (constant) wavenumber k as introduced in Section 3.2.1.

Let $D \subset \mathbb{R}^3$ be a bounded open set of class $C^{2,\alpha}$, $0 < \alpha < 1$, and denote by $\boldsymbol{\nu}$ the unit outward normal to ∂D relative to D. Given a continuous scalar function $f \in C(\partial D; \mathbb{C})$, the *single layer potential* with density f is given by

$$(\mathcal{S}_D^k f)(\boldsymbol{x}) := \int_{\partial D} \Phi_k(\boldsymbol{x} - \boldsymbol{y}) f(\boldsymbol{y}) \, \mathrm{d}s(\boldsymbol{y}), \qquad \boldsymbol{x} \in \mathbb{R}^3 \setminus \partial D.$$

Then, $\mathcal{S}_D^k f$ is continuous throughout $\mathbb{R}^3$ (cf. Colton and Kress [38, Theorem 2.12]), and if $f \in C^{0,\alpha}(\partial D; \mathbb{C})$, the following continuity result holds for the tangential trace of first derivative of $\mathcal{S}_D^k f$:

$$\boldsymbol{\nu}(\boldsymbol{x}) \times \nabla \mathcal{S}_D^k f\big|_{\partial D}^{\pm}(\boldsymbol{x}) = \boldsymbol{\nu}(\boldsymbol{x}) \times \int_{\partial D} \nabla_{\boldsymbol{x}} \Phi_k(\boldsymbol{x} - \boldsymbol{y}) f(\boldsymbol{y}) \, \mathrm{d}s(\boldsymbol{y}), \qquad \boldsymbol{x} \in \partial D, \tag{3.15}$$

where the integral exists as a Cauchy principal value, i.e., $\boldsymbol{\nu} \times \nabla \mathcal{S}_D^k f$ is continuous across ∂D, too; cf. [38, Theorem 2.17]. The expression $\mathcal{S}_D^k$ can be extended to a bounded linear operator

$$\mathcal{S}_D^k : H^{-1/2}(\partial D; \mathbb{C}) \to H^1_{\mathrm{loc}}(\mathbb{R}^3; \mathbb{C}); \tag{3.16}$$

cf. [86, Theorem 6.11].

Lemma 3.1. *The right–hand side of* (3.15) *can be extended to a bounded linear operator from* $H^{-1/2}(\partial D; \mathbb{C})$ *to* $\boldsymbol{H}_{\mathrm{div}}^{-1/2}(\partial D)$ *such that* (3.15) *remains valid for densities* $f \in H^{-1/2}(\partial D; \mathbb{C})$.

Proof. From (3.16), we find that

$$\nabla \mathcal{S}_D^k : H^{-1/2}(\partial D; \mathbb{C}) \to L^2_{\mathrm{loc}}(\mathbb{R}^3; \mathbb{C})^3$$

is bounded. Because $\mathbf{curl} \nabla \mathcal{S}_D^k f = 0$ for any $f \in H^{-1/2}(\partial D; \mathbb{C})$, we obtain that

$$\nabla \mathcal{S}_D^k : H^{-1/2}(\partial D; \mathbb{C}) \to \boldsymbol{H}_{\mathrm{loc}}(\mathbf{curl}, \mathbb{R}^3) \tag{3.17}$$

is bounded too. Hence, the tangential traces of $\nabla \mathcal{S}_D^k f$ from outside and inside the boundary ∂D are well defined and equal. Recalling the boundedness of the trace operator γ_t from $\boldsymbol{H}_{\mathrm{loc}}(\mathbf{curl}, \mathbb{R}^3 \setminus \overline{D})$ (resp. $\boldsymbol{H}(\mathbf{curl}, D)$) to $\boldsymbol{H}_{\mathrm{div}}^{-1/2}(\partial D)$, we find that the right–hand side of (3.15) can be extended to a bounded linear operator from $H^{-1/2}(\partial D; \mathbb{C})$ to $\boldsymbol{H}_{\mathrm{div}}^{-1/2}(\partial D)$. □

Given a continuous tangential vector field

$$\boldsymbol{a} \in \boldsymbol{T}(\partial D) := \big\{ \boldsymbol{b} \in C(\partial D;\, \mathbb{C})^3 \;\big|\; \boldsymbol{\nu} \cdot \boldsymbol{b} = 0 \text{ on } \partial D \big\},$$

the *vector potential* with density $\boldsymbol{a}$ is given by

$$(\mathcal{A}_D^k \boldsymbol{a})(\boldsymbol{x}) := \int_{\partial D} \Phi_k(\boldsymbol{x} - \boldsymbol{y}) \boldsymbol{a}(\boldsymbol{y})\, \mathrm{d}s(\boldsymbol{y}), \qquad \boldsymbol{x} \in \mathbb{R}^3 \setminus \partial D.$$

Then, $\mathcal{A}_D^k \boldsymbol{a}$ is continuous throughout $\mathbb{R}^3$. On the boundary, we have

$$\boldsymbol{\nu}(\boldsymbol{x}) \times \mathbf{curl} \mathcal{A}_D^k \boldsymbol{a}\big|_{\partial D}^{\pm}(\boldsymbol{x}) = \int_{\partial D} \boldsymbol{\nu}(\boldsymbol{x}) \times \mathbf{curl}_x \big(\Phi_k(\boldsymbol{x} - \boldsymbol{y}) \boldsymbol{a}(\boldsymbol{y}) \big)\, \mathrm{d}s(\boldsymbol{y}) \pm \frac{1}{2} \boldsymbol{a}(\boldsymbol{x}) \tag{3.18}$$

for $\boldsymbol{x} \in \partial D$ and

$$\boldsymbol{\nu} \times \mathbf{curl}\, \mathbf{curl} \mathcal{A}_D^k \boldsymbol{a}\big|_{\partial D}^{+} = \boldsymbol{\nu} \times \mathbf{curl}\, \mathbf{curl} \mathcal{A}_D^k \boldsymbol{a}\big|_{\partial D}^{-}; \tag{3.19}$$

cf. [39, Theorem 6.11]. Furthermore, for

$$\boldsymbol{a} \in \boldsymbol{T}^{0,\alpha}(\partial D) := \big\{ \boldsymbol{b} \in C^{0,\alpha}(\partial D;\, \mathbb{C})^3 \;\big|\; \boldsymbol{\nu} \cdot \boldsymbol{b} = 0 \text{ on } \partial D \big\},$$

$0 < \alpha < 1$, it holds that

$$\boldsymbol{\nu} \cdot \mathbf{curl} \mathcal{A}_D^k \boldsymbol{a}\big|_{\partial D}^{+} = \boldsymbol{\nu} \cdot \mathbf{curl} \mathcal{A}_D^k \boldsymbol{a}\big|_{\partial D}^{-}; \tag{3.20}$$

cf. [38, Theorem 2.24]. Next, for $0 < \alpha < 1$, we introduce the spaces

$$\begin{aligned}
\boldsymbol{T}_{\mathrm{div}}(\partial D) &:= \big\{ \boldsymbol{b} \in \boldsymbol{T}(\partial D) \;\big|\; \mathrm{div}_{\partial D}\, \boldsymbol{b} \in C(\partial D;\, \mathbb{C}) \big\}, \\
\boldsymbol{T}_{\mathrm{div}}^{0,\alpha}(\partial D) &:= \big\{ \boldsymbol{b} \in \boldsymbol{T}^{0,\alpha}(\partial D) \;\big|\; \mathrm{div}_{\partial D}\, \boldsymbol{b} \in C^{0,\alpha}(\partial D;\, \mathbb{C}) \big\}, \\
\boldsymbol{T}_{\mathrm{curl}}^{0,\alpha}(\partial D) &:= \big\{ \boldsymbol{b} \in \boldsymbol{T}^{0,\alpha}(\partial D) \;\big|\; \mathrm{curl}_{\partial D}\, \boldsymbol{b} \in C^{0,\alpha}(\partial D;\, \mathbb{C}) \big\}.
\end{aligned}$$

Given $\boldsymbol{a} \in \boldsymbol{T}(\partial D)$ and $\boldsymbol{b} \in \boldsymbol{T}_{\mathrm{curl}}^{0,\alpha}(\partial D)$, we define

$$\begin{aligned}
(M_D^k \boldsymbol{a})(\boldsymbol{x}) &:= \int_{\partial D} \boldsymbol{\nu}(\boldsymbol{x}) \times \mathbf{curl}_{\boldsymbol{x}} \big(\Phi_k(\boldsymbol{x} - \boldsymbol{y}) \boldsymbol{a}(\boldsymbol{y}) \big)\, \mathrm{d}s(\boldsymbol{y}), \\
(N_D^k \boldsymbol{b})(\boldsymbol{x}) &:= \boldsymbol{\nu}(\boldsymbol{x}) \times \mathbf{curl}\, \mathbf{curl} \int_{\partial D} \Phi_k(\boldsymbol{x} - \boldsymbol{y}) \boldsymbol{\nu}(\boldsymbol{y}) \times \boldsymbol{b}(\boldsymbol{y})\, \mathrm{d}s(\boldsymbol{y}) \\
&= -\boldsymbol{\nu}(\boldsymbol{x}) \times \int_{\partial D} \nabla_x \Phi_k(\boldsymbol{x} - \boldsymbol{y}) (\mathrm{curl}_{\partial D}\, \boldsymbol{b})(\boldsymbol{y})\, \mathrm{d}s(\boldsymbol{y}) \\
&\quad + k^2 \boldsymbol{\nu}(\boldsymbol{x}) \times \int_{\partial D} \Phi_k(\boldsymbol{x} - \boldsymbol{y}) \boldsymbol{\nu}(\boldsymbol{y}) \times \boldsymbol{b}(\boldsymbol{y})\, \mathrm{d}s(\boldsymbol{y})
\end{aligned}$$

for $\boldsymbol{x} \in \partial D$. Then, M_D^k is a bounded linear operator from $\boldsymbol{T}_{\mathrm{div}}(\partial D)$ to $\boldsymbol{T}_{\mathrm{div}}^{0,\alpha}(\partial D)$, and N_D^k is a bounded linear operator from $\boldsymbol{T}_{\mathrm{curl}}^{0,\alpha}(\partial D)$ to $\boldsymbol{T}_{\mathrm{div}}^{0,\alpha}(\partial D)$; cf. [39, Theorems 6.16 and 6.17]. By interchanging the order

of integration, it can be seen that the transpose ${M_D^k}^\top$ of M_D^k with respect to the bilinear form $\langle \boldsymbol{a}, \boldsymbol{b} \rangle := \int_{\partial D} \boldsymbol{a} \cdot \boldsymbol{b} \, \mathrm{d}s$, $\boldsymbol{a}, \boldsymbol{b} \in \boldsymbol{T}(\partial D)$, is given by

$$ {M_D^k}^\top \boldsymbol{a} = \boldsymbol{\nu} \times M_D^k(\boldsymbol{\nu} \times \boldsymbol{a}), \qquad \boldsymbol{a} \in \boldsymbol{T}(\partial D). $$

The operator N_D^k is symmetric; cf. [39, p. 171].

Lemma 3.2. (i) *The expression $\mathcal{A}_D^k$ can be extended to a bounded linear operator*

$$ \mathcal{A}_D^k : \boldsymbol{H}_{\mathrm{div}}^{-1/2}(\partial D) \to \boldsymbol{H}_{\mathrm{loc}}(\mathbf{curl}, \mathbb{R}^3). $$

(ii) *The operators M_D^k and ${M_D^k}^\top$ have compact extensions*

$$ M_D^k : \boldsymbol{H}_{\mathrm{div}}^{-1/2}(\partial D) \to \boldsymbol{H}_{\mathrm{div}}^{-1/2}(\partial D), \qquad {M_D^k}^\top : \boldsymbol{H}_{\mathrm{curl}}^{-1/2}(\partial D) \to \boldsymbol{H}_{\mathrm{curl}}^{-1/2}(\partial D). $$

(iii) *The operator N_D^k has a bounded extension*

$$ N_D^k : \boldsymbol{H}_{\mathrm{curl}}^{-1/2}(\partial D) \to \boldsymbol{H}_{\mathrm{div}}^{-1/2}(\partial D). $$

Proof. (i) From [86, Theorem 6.11], we obtain a continuous extension

$$ \mathcal{A}_D^k : H^{-1/2}(\partial D; \mathbb{C})^3 \to H^1_{\mathrm{loc}}(\mathbb{R}^3; \mathbb{C})^3. \tag{3.21} $$

This implies the desired result.

(ii) From Kirsch [70, Theorem 4.2], we obtain continuous extensions

$$ M_D^k, {M_D^k}^\top : \boldsymbol{L}_t^2(\partial D) \to \boldsymbol{H}_t^1(\partial D). $$

Thus, by duality, we get another bounded extension

$$ M_D^k : \boldsymbol{H}_t^{-1}(\partial D) \to \boldsymbol{L}_t^2(\partial D), $$

and recalling the interpolation property of Sobolev spaces (cf. [86, Theorem B.2]), we find that

$$ M_D^k : \boldsymbol{H}_t^{-3/4}(\partial D) \to \boldsymbol{H}_t^{1/4}(\partial D) $$

is bounded, too.

Given a continuous function $f \in C(\partial D; \mathbb{C})$, we define

$$ \big({K_D^k}^\top f\big)(\boldsymbol{x}) := \int_{\partial D} \frac{\partial \Phi_k(\boldsymbol{x} - \boldsymbol{y})}{\partial \boldsymbol{\nu}(\boldsymbol{x})} f(\boldsymbol{y}) \, \mathrm{d}s(\boldsymbol{y}), \qquad \boldsymbol{x} \in \partial D. $$

Then,

$$ {K_D^k}^\top : H^{-3/4}(\partial D; \mathbb{C}) \to H^{1/4}(\partial D; \mathbb{C}) $$

is bounded; cf. [91, Theorem 4.4.1]. Using (3.1), (3.3), and (3.4), the operators $\nabla_{\partial D}$ and $\mathbf{curl}_{\partial D}$ can be extended to continuous operators from $H^r(\partial D;\mathbb{C})$ to $\boldsymbol{H}_t^{r-1}(\partial D)$ for $1/2 \le r \le 2$. Accordingly, $\operatorname{div}_{\partial D}$ and $\operatorname{curl}_{\partial D}$ are continuous from $\boldsymbol{H}_t^{1-r}(\partial D)$ to $H^{-r}(\partial D;\mathbb{C})$. So we can define

$$\boldsymbol{H}^s_{\mathrm{div}}(\partial D) := \left\{ \boldsymbol{a} \in \boldsymbol{H}_t^s(\partial D) \;\middle|\; \operatorname{div}_{\partial D} \boldsymbol{a} \in H^s(\partial D;\mathbb{C}) \right\}, \qquad s \in [-1, 1/2].$$

Because the operators $\mathcal{S}_D^k$ and $\mathcal{A}_D^k$ have continuous extensions

$$\begin{aligned} \mathcal{S}_D^k &: H^{-3/4}(\partial D;\mathbb{C}) \to H^{3/4}_{\mathrm{loc}}(\mathbb{R}^3;\mathbb{C}), \\ \mathcal{A}_D^k &: \boldsymbol{H}_t^{-3/4}(\partial D) \to H^{3/4}_{\mathrm{loc}}(\mathbb{R}^3;\mathbb{C})^3 \end{aligned}$$

(cf. [86, Theorem 6.12]), we can extend a result for continuous tangential vector fields, proven in [39, p. 170], by a density argument (as, e.g., done by Mitrea, Mitrea, and Pipher in the proof of [87, Lemma. 4.2]) to obtain the identity

$$\operatorname{div} \mathcal{A}_D^k \boldsymbol{a} = \mathcal{S}_D^k \operatorname{div}_{\partial D} \boldsymbol{a}, \qquad \boldsymbol{a} \in \boldsymbol{H}^{-3/4}_{\mathrm{div}}(\partial D). \tag{3.22}$$

Hence, $\mathcal{A}_D$ is bounded from $\boldsymbol{H}^{-3/4}_{\mathrm{div}}(\partial D)$ to $\boldsymbol{H}^{3/4}_{\mathrm{loc}}(\mathrm{div}, \mathbb{R}^3)$, and so its normal trace on ∂D is well defined, and

$$\boldsymbol{\nu} \cdot \mathcal{A}_D^k\big|_{\partial D} : \boldsymbol{H}^{-3/4}_{\mathrm{div}}(\partial D) \to H^{1/4}(\partial D;\mathbb{C})$$

is bounded, too. Generalizing a formula from [39, p. 169] by a density argument, we find that

$$\operatorname{div}_{\partial D} M_D^k \boldsymbol{a} = -k^2 \boldsymbol{\nu} \cdot \mathcal{A}_D^k \boldsymbol{a}\big|_{\partial D} - {K_D^k}^{\top} \operatorname{div}_{\partial D} \boldsymbol{a}, \qquad \boldsymbol{a} \in \boldsymbol{H}^{-3/4}_{\mathrm{div}}(\partial D). \tag{3.23}$$

Thus, combining these results, we obtain that

$$M_D^k : \boldsymbol{H}^{-3/4}_{\mathrm{div}}(\partial D) \to \boldsymbol{H}^{1/4}_{\mathrm{div}}(\partial D)$$

is bounded. The embedding operator

$$I^{t,s} : \boldsymbol{H}^t_{\mathrm{div}}(\partial D) \to \boldsymbol{H}^s_{\mathrm{div}}(\partial D)$$

is compact for $-1 \le s < t \le 1/2$. This follows from the embedding theorem for standard Sobolev spaces $H^s(\partial D)$, $-1 \le s \le 1/2$ (cf. [86, Theorem 3.27]) in the same way as in the proof of a corresponding result for Hölder spaces in [39, Theorem 6.15]. So, we find that

$$M_D^k : \boldsymbol{H}^{-1/2}_{\mathrm{div}}(\partial D) \to \boldsymbol{H}^{-1/2}_{\mathrm{div}}(\partial D)$$

and the corresponding dual operator

$${M_D^k}^{\top} = r M_D^k r : \boldsymbol{H}^{-1/2}_{\mathrm{curl}}(\partial D) \to \boldsymbol{H}^{-1/2}_{\mathrm{curl}}(\partial D) \tag{3.24}$$

are compact.

(iii) Combining (3.17) and (3.21), we find that

$$\nabla \mathcal{S}_D^k \operatorname{curl}_{\partial D} + k^2 \mathcal{A}_D^k r : \boldsymbol{H}_{\mathrm{curl}}^{-1/2}(\partial D) \to \boldsymbol{H}_{\mathrm{loc}}(\mathbf{curl}, \mathbb{R}^3)$$

is bounded. Thus, recalling the boundedness of the trace operator γ_t from $\boldsymbol{H}_{\mathrm{loc}}(\mathbf{curl}, \mathbb{R}^3 \setminus \overline{D})$ (resp. $\boldsymbol{H}(\mathbf{curl}, D)$) to $\boldsymbol{H}_{\mathrm{div}}^{-1/2}(\partial D)$ and Lemma 3.1, we find that the operator N_D^k can be extended to a continuous linear operator from $\boldsymbol{H}_{\mathrm{curl}}^{-1/2}(\partial D)$ to $\boldsymbol{H}_{\mathrm{div}}^{-1/2}(\partial D)$.

□

It can be seen straightforwardly that the formulas (3.18), (3.19), and (3.20) remain valid for densities $\boldsymbol{a} \in \boldsymbol{H}_{\mathrm{div}}^{-1/2}(\partial D)$.

3.3.2 The Potential Theoretic Limit $k = 0$

Substituting Φ_k by Φ_0 in the definitions above, we obtain integral operators

$$\begin{aligned} &\mathcal{A}_D^0 : \boldsymbol{H}_{\mathrm{div}}^{-1/2}(\partial D) \to \boldsymbol{H}_{\mathrm{loc}}(\mathbf{curl}, \mathbb{R}^3), \quad M_D^0 : \boldsymbol{H}_{\mathrm{div}}^{-1/2}(\partial D) \to \boldsymbol{H}_{\mathrm{div}}^{-1/2}(\partial D), \\ &{M_D^0}^\top : \boldsymbol{H}_{\mathrm{curl}}^{-1/2}(\partial D) \to \boldsymbol{H}_{\mathrm{curl}}^{-1/2}(\partial D), \qquad N_D^0 : \boldsymbol{H}_{\mathrm{curl}}^{-1/2}(\partial D) \to \boldsymbol{H}_{\mathrm{div}}^{-1/2}(\partial D). \end{aligned}$$

The mapping properties and jump relations mentioned in the previous section remain valid for $k = 0$ (cf. [38, 86]). Furthermore, the integral operators $\mathcal{S}_D^0$, $\mathcal{D}_D^0$, and K_D^0 introduced in Section 2.2 on real–valued Sobolev spaces will in the following be considered as operators on the corresponding complex–valued Sobolev spaces.

Next, we study the invertibility of $\pm\frac{1}{2}I + M_D^0$ and $\pm\frac{1}{2}I + {M_D^0}^\top$. The proof of the following lemma is essentially the same as the proof of [38, Theorem 5.5] for continuous densities.

Lemma 3.3. *Assume that all components of D are simply connected and that the complement of D is connected. Then, the operators $\frac{1}{2}I + M_D^0$ and $\frac{1}{2}I + {M_D^0}^\top$ have trivial nullspace in $\boldsymbol{H}_{\mathrm{div}}^{-1/2}(\partial D)$ and $\boldsymbol{H}_{\mathrm{curl}}^{-1/2}(\partial D)$, respectively.*

Proof. Let $\boldsymbol{a} \in \mathcal{N}\big(\frac{1}{2}I + M_D^0\big)$ and set

$$\boldsymbol{E} := \mathbf{curl} \mathcal{A}_D^0 \boldsymbol{a} \qquad \text{in } \mathbb{R}^3 \setminus \overline{D}.$$

From (3.18), we find that $\boldsymbol{\nu} \times \boldsymbol{E}|_{\partial D}^+ = 0$. The potential theoretic form of the representation theorem [38, Theorem 4.13] for the vector Helmholtz equation can be generalized to Sobolev spaces in the same way as done in [88, Theorems 9.2 and 9.4] for a similar representation formula for Maxwell's equations. Applying this formula to the vector potential $\mathcal{A}_D^0 \boldsymbol{a}$ and taking the divergence, we get

$$\operatorname{div} \mathcal{A}_D^0 \boldsymbol{a} = \int_{\partial D} \frac{\partial \Phi_0(\boldsymbol{x} - \boldsymbol{y})}{\boldsymbol{\nu}(\boldsymbol{y})} (\operatorname{div} \mathcal{A}_D^0 \boldsymbol{a})(\boldsymbol{y}) \, \mathrm{d}s(\boldsymbol{y}) = \mathcal{D}_D^0 (\operatorname{div} \mathcal{A}_D^0 \boldsymbol{a})$$

in $\mathbb{R}^3 \setminus \overline{D}$. Recalling (3.22), we find that $\operatorname{div} \mathcal{A}_D^0 \boldsymbol{a} \in H^1_{\mathrm{loc}}(\mathbb{R}^3 \setminus \overline{D}; \mathbb{C})$. Taking the trace on ∂D from outside, using (2.4b), shows that

$$\operatorname{div} \mathcal{A}_D^0 \boldsymbol{a}|_{\partial D}^+ \in \mathcal{N}\Big(-\frac{1}{2}I + K_D^0\Big).$$

Hence (cf. Ammari and Kang [7, Lemma 2.5]), we have that $\operatorname{div} \mathcal{A}_D^0 \boldsymbol{a} = 0$ on ∂D, and from the uniqueness property for the Dirichlet problem for harmonic functions, it follows that $\operatorname{div} \mathcal{A}_D^0 \boldsymbol{a} = 0$ in D and in $\mathbb{R}^3 \setminus \overline{D}$. Thus,

$$\mathbf{curl} \boldsymbol{E} = -\Delta \mathcal{A}_D^0 \boldsymbol{a} + \nabla \operatorname{div} \mathcal{A}_D^0 \boldsymbol{a} = 0 \qquad \text{and} \qquad \operatorname{div} \boldsymbol{E} = \operatorname{div} \mathbf{curl} \mathcal{A}_D^0 \boldsymbol{a} = 0$$

in $\mathbb{R}^3 \setminus \overline{D}$. This means that $\boldsymbol{E}$ is a harmonic vector field in D and $\mathbb{R}^3 \setminus \overline{D}$.

Using integration by parts (3.1), we find that

$$\begin{aligned} \int_{\mathbb{R}^3 \setminus \overline{D}} \boldsymbol{E} \cdot \overline{\boldsymbol{E}} \, \mathrm{d}\boldsymbol{x} &= \int_{\mathbb{R}^3 \setminus \overline{D}} \mathbf{curl} \mathcal{A}_D^0 \boldsymbol{a} \cdot \overline{\boldsymbol{E}} \, \mathrm{d}\boldsymbol{x} \\ &= -\int_{\partial D} (\boldsymbol{\nu} \times \mathcal{A}_D^0 \boldsymbol{a}) \cdot \big((\boldsymbol{\nu} \times \overline{\boldsymbol{E}}) \times \boldsymbol{\nu}\big) \, \mathrm{d}s = 0, \end{aligned}$$

from which we conclude that $\boldsymbol{E} = 0$ in $\mathbb{R}^3 \setminus \overline{D}$.

From the jump relations (3.18) and (3.20), we find that $\boldsymbol{a} = -\boldsymbol{\nu} \times \boldsymbol{E}|_{\partial D}^-$ and $\boldsymbol{\nu} \cdot \boldsymbol{E}|_{\partial D}^- = 0$ on ∂D. Because all components of D are simply connected, there exists a harmonic scalar potential $q \in H^1(D)$ such that $\boldsymbol{E} = \nabla q$; cf. [88, Theorem 3.37]. From $\boldsymbol{\nu} \cdot \boldsymbol{E}|_{\partial D}^- = 0$ we obtain that $\frac{\partial q}{\partial \boldsymbol{\nu}} = 0$ on ∂D. Hence, $\boldsymbol{E} = \nabla q = 0$ in D and $\boldsymbol{a} = 0$. So, $\mathcal{N}\big(\frac{1}{2}I + M_D^0\big) = \{0\}$ in $\boldsymbol{H}_{\mathrm{div}}^{-1/2}(\partial D)$.

By Theorem 2.1, $\mathcal{N}\big(\frac{1}{2}I + {M_D^0}^\top\big) = \{0\}$ in $\boldsymbol{H}_{\mathrm{curl}}^{-1/2}(\partial D)$ also. □

So, if all components of D are simply connected and the complement of D is connected, we find from Lemma 3.3 and Theorem 2.1 that $\frac{1}{2}I + M_D^0$ and $\frac{1}{2}I + {M_D^0}^\top$ are invertible on $\boldsymbol{H}_{\mathrm{div}}^{-1/2}(\partial D)$ and $\boldsymbol{H}_{\mathrm{curl}}^{-1/2}(\partial D)$, respectively. Recalling (3.24), which remains true in the potential theoretic limit, we observe that for any $\boldsymbol{a} \in \boldsymbol{H}_{\mathrm{div}}^{-1/2}(\partial D)$

$$\Big(\frac{1}{2}I \pm {M_D^0}^\top\Big)(\boldsymbol{\nu} \times \boldsymbol{a}) = \boldsymbol{\nu} \times \Big(\frac{1}{2}I \mp M_D^0\Big)\boldsymbol{a}. \tag{3.25}$$

Thus, if all components of D are simply connected and the complement of D is connected, $-\frac{1}{2}I + M_D^0$ and $-\frac{1}{2}I + {M_D^0}^\top$ are invertible on $\boldsymbol{H}_{\mathrm{div}}^{-1/2}(\partial D)$ and $\boldsymbol{H}_{\mathrm{curl}}^{-1/2}(\partial D)$, respectively, too.

Lemma 3.4. (i) *The operators* $\pm\frac{1}{2}I + M_D^0$ *are isomorphisms on*

$$\boldsymbol{H}_{\mathrm{div},0}^{-1/2}(\partial D) := \big\{ \boldsymbol{a} \in \boldsymbol{H}_{\mathrm{div}}^{-1/2}(\partial D) \;\big|\; \operatorname{div}_{\partial D} \boldsymbol{a} = 0 \big\}.$$

(ii) *For any* $f \in H^{1/2}(\partial D;\, \mathbb{C}\,)$,

$$\Big(\pm\frac{1}{2}I + {M_D^0}^{\top}\Big)^{-1}\nabla_{\partial D} f = -\nabla_{\partial D}\Big(\mp\frac{1}{2}I + K_D^0\Big)^{-1} f. \tag{3.26}$$

Proof. Part (i) follows at once, because for $k = 0$ the identity (3.23) reduces to

$$\operatorname{div}_{\partial D} M_D^0 \boldsymbol{a} = -{K_D^0}^{\top} \operatorname{div}_{\partial D} \boldsymbol{a}, \qquad \boldsymbol{a} \in \boldsymbol{H}_{\rm div}^{-1/2}(\partial D). \tag{3.27}$$

By duality, we obtain from (3.27) for any $f \in H^{1/2}(\partial D;\, \mathbb{C}\,)$ that

$${M_D^0}^{\top}\nabla_{\partial D} f = -\nabla_{\partial D} K_D^0 f.$$

Thus,

$$\Big(\pm\frac{1}{2}I + {M_D^0}^{\top}\Big)\nabla_{\partial D} f = -\nabla_{\partial D}\Big(\mp\frac{1}{2}I + K_D^0\Big) f,$$

which yields (3.26). □

3.3.3 Two–Layered Medium

Let $D \subset \mathbb{R}^{\,3}_{-}$ be a bounded open set of class $C^{2,\alpha}$, $0 < \alpha < 1$, such that $\operatorname{dist}(D, \Sigma_0) \geq d_0$ for some constant $d_0 > 0$. Given a continuous tangential vector field $\boldsymbol{a} \in \boldsymbol{T}(\partial D)$, we define the *modified vector potential* with density $\boldsymbol{a}$ by

$$\begin{aligned}(\mathcal{A}_D^{e/m}\boldsymbol{a})(\boldsymbol{x}) &:= \int_{\partial D} \Pi^{e/m}(\boldsymbol{x},\boldsymbol{y})\boldsymbol{a}(\boldsymbol{y})\, \mathrm{d}s(\boldsymbol{y}) \\ &= (\mathcal{A}_D^{k_-}\boldsymbol{a})(\boldsymbol{x}) + \int_{\partial D} F^{e/m}(\boldsymbol{x},\boldsymbol{y})\boldsymbol{a}(\boldsymbol{y})\, \mathrm{d}s(\boldsymbol{y}), \qquad \boldsymbol{x} \in \mathbb{R}^{\,3} \setminus \partial D,\end{aligned}$$

and boundary integrals

$$(R_D^{e/m}\boldsymbol{a})(\boldsymbol{x}) := \int_{\partial D} \boldsymbol{\nu}(\boldsymbol{x}) \times \mathbf{curl}_x\big(F^{e/m}(\boldsymbol{x},\boldsymbol{y})\boldsymbol{a}(\boldsymbol{y})\big)\, \mathrm{d}s(\boldsymbol{y}), \quad \boldsymbol{x} \in \partial D, \tag{3.28}$$

$$\begin{aligned}(M_D^{e/m}\boldsymbol{a})(\boldsymbol{x}) &:= \int_{\partial D} \boldsymbol{\nu}(\boldsymbol{x}) \times \mathbf{curl}_x\big(\Pi^{e/m}(\boldsymbol{x},\boldsymbol{y})\boldsymbol{a}(\boldsymbol{y})\big)\, \mathrm{d}s(\boldsymbol{y}) \qquad (3.29)\\ &= (M_D^{k_-}\boldsymbol{a})(\boldsymbol{x}) + (R_D^{e/m}\boldsymbol{a})(\boldsymbol{x}), \qquad \boldsymbol{x} \in \partial D.\end{aligned}$$

Because $F^{e/m}(\cdot, \boldsymbol{y})$ is smooth (with resp. to both variables) in $\mathbb{R}^{\,3}_0$ for $\boldsymbol{y}$ in any compact subset of $\mathbb{R}^{\,3}_0$, $\mathcal{A}_D^{e/m}$ can be extended to a bounded linear operator

$$\mathcal{A}_D^{e/m} : \boldsymbol{H}_{\rm div}^{-1/2}(\partial D) \to \boldsymbol{H}_{\rm loc}(\mathbf{curl}, \mathbb{R}^{\,3}_0),$$

and $R_D^{e/m}$ and $M_D^{e/m}$ define compact operators

$$R_D^{e/m} : \boldsymbol{H}_{\rm div}^{-1/2}(\partial D) \to \boldsymbol{H}_{\rm div}^{-1/2}(\partial D), \qquad M_D^{e/m} : \boldsymbol{H}_{\rm div}^{-1/2}(\partial D) \to \boldsymbol{H}_{\rm div}^{-1/2}(\partial D).$$

Moreover, $\mathcal{A}_D^{e/m}\boldsymbol{a}$ is continuous across ∂D,

$$\boldsymbol{\nu}\times\mathbf{curl}\mathcal{A}_D^{e/m}\boldsymbol{a}\big|_{\partial D}^{\pm}=\Big(\pm\frac{1}{2}I+M_D^{e/m}\Big)\boldsymbol{a}\,, \tag{3.30}$$

and

$$\boldsymbol{\nu}\times\mathbf{curl}\,\mathbf{curl}\mathcal{A}_D^{e/m}\boldsymbol{a}\big|_{\partial D}^{+}=\boldsymbol{\nu}\times\mathbf{curl}\,\mathbf{curl}\mathcal{A}_D^{e/m}\boldsymbol{a}\big|_{\partial D}^{-}\,. \tag{3.31}$$

Finally, we want to study the invertibility of the operators $\frac{1}{2}I+M_D^m$ and $\frac{1}{2}I+M_D^{m\top}$. The proof of the following lemma is essentially the same as the proof of [38, Theorem 4.23] for homogeneous medium and continuous densities.

Lemma 3.5. *Assume that the exterior of D is connected and that the wavenumber k_- is not a Maxwell eigenvalue for D. Then, $\frac{1}{2}I+M_D^m$ and $\frac{1}{2}I+M_D^{m\top}$ have trivial nullspace in $\boldsymbol{H}_{\mathrm{div}}^{-1/2}(\partial D)$ and $\boldsymbol{H}_{\mathrm{curl}}^{-1/2}(\partial D)$, respectively.*

Proof. Let $\boldsymbol{a}\in\mathcal{N}\big(\frac{1}{2}I+M_D^m\big)$ and define the electromagnetic field $(\boldsymbol{E},\boldsymbol{H})$ by

$$\boldsymbol{E}:=\frac{\varepsilon_-}{\varepsilon}\mathbf{curl}\mathcal{A}_D^k\boldsymbol{a},\quad \boldsymbol{H}:=\frac{1}{\mathrm{i}\,\omega\mu}\mathbf{curl}\boldsymbol{E}\qquad\text{in }\mathbb{R}^3\setminus\partial D.$$

Then, $\boldsymbol{E}$ and $\boldsymbol{H}$ form a radiating solution of Maxwell's equations, and by (3.30),

$$\boldsymbol{\nu}\times\boldsymbol{E}\big|_{\partial D}^{+}=\Big(\frac{1}{2}I+M_D^m\Big)\boldsymbol{a}=0.$$

From the uniqueness of solutions of the exterior Maxwell boundary value problem (cf. Appendix C) we find that $\boldsymbol{E}=0$ in $\mathbb{R}^3\setminus\overline{D}$. Because by (3.31) $\mathrm{i}\,\omega\mu\boldsymbol{H}=\mathbf{curl}\frac{\varepsilon_-}{\varepsilon}\mathbf{curl}\mathcal{A}_D^k\boldsymbol{a}$ has continuous tangential components across the boundary ∂D, we obtain that $\boldsymbol{\nu}\times\boldsymbol{H}\big|_{\partial D}^{-}=0$. Therefore, $(\boldsymbol{H},-\frac{\varepsilon_-}{\mu_-}\boldsymbol{E})$ forms a solution to the interior Maxwell problem with homogeneous boundary condition. Recalling the assumption on k_-, we find that $\boldsymbol{H}=\boldsymbol{E}=0$ in D. Finally, again from (3.30), we obtain that $\boldsymbol{a}=\boldsymbol{\nu}\times\boldsymbol{E}\big|_{\partial D}^{+}-\boldsymbol{\nu}\times\boldsymbol{E}\big|_{\partial D}^{-}=0$. Therefore, $\mathcal{N}\big(\frac{1}{2}I+M_D^m\big)=\{0\}$ in $\boldsymbol{H}_{\mathrm{div}}^{-1/2}(\partial D)$.

By Theorem 2.1, $\mathcal{N}\big(\frac{1}{2}I+M_D^{m\top}\big)=\{0\}$ in $\boldsymbol{H}_{\mathrm{curl}}^{-1/2}(\partial D)$ also. □

So, if the exterior of D is connected and k_- is not a Maxwell eigenvalue for D, we find from Lemma 3.5 and Theorem 2.1 that $\frac{1}{2}I+M_D^m$ and $\frac{1}{2}I+M_D^{m\top}$ are invertible on $\boldsymbol{H}_{\mathrm{div}}^{-1/2}(\partial D)$ and $\boldsymbol{H}_{\mathrm{curl}}^{-1/2}(\partial D)$, respectively.

3.4 Mathematical Setting

In this section, we set up the mathematical model we are going to use. We decompose the space $\mathbb{R}^3=\mathbb{R}^3_+\cup\Sigma_0\cup\mathbb{R}^3_-$ as in Section 3.2.2 in a hyperplane Σ_0 corresponding to the surface of the ground and the two halfspaces $\mathbb{R}^3_+$

and $\mathbb{R}^3_-$ above and below Σ_0 representing air and ground, respectively. As above, both halfspaces are filled with homogeneous materials with electric permittivity ε and magnetic permeability μ given by (3.8), and we require that ε_+ as well as $\mu_\pm$ are positive numbers, whereas ε_- may be complex with positive real and nonnegative imaginary part to allow for soil materials that are conducting. The associated (discontinuous) wavenumber is $k := \omega\sqrt{\varepsilon\mu}$, where we assume $\omega > 0$. If $\varepsilon_- \notin \mathbb{R}$, then k is taken to have positive imaginary part.

In the following, we investigate *radiating solutions* of time–harmonic *Maxwell's equations*

$$\mathbf{curl}\boldsymbol{H} + \mathrm{i}\,\omega\varepsilon\boldsymbol{E} = 0, \quad \mathbf{curl}\boldsymbol{E} - \mathrm{i}\,\omega\mu\boldsymbol{H} = 0 \tag{3.32}$$

in the exterior of some compact set $C \subset \mathbb{R}^3$. By this, we understand (cf., e.g., [43, 88]), solutions $\boldsymbol{E}, \boldsymbol{H} \in \boldsymbol{H}_{\mathrm{loc}}(\mathbf{curl}, \mathbb{R}^3 \setminus C)$ which obey the integral radiation condition

$$\int_{\partial B_R(0)} \left| \frac{\boldsymbol{x}}{R} \times \boldsymbol{H}(\boldsymbol{x}) + \Big(\frac{\varepsilon(\boldsymbol{x})}{\mu(\boldsymbol{x})}\Big)^{1/2} \boldsymbol{E}(\boldsymbol{x}) \right|^2 \mathrm{d}s(\boldsymbol{x}) = o(1) \qquad \text{as } R \to \infty. \tag{3.33}$$

As mentioned by Kirsch [75], the radiation condition (3.33) makes sense due to the following regularity result by Weber [100]: Let $R > 0$ be such that C is contained in the open ball $B_R(0)$ and set $G := \mathbb{R}^3 \setminus \overline{B_R(0)}$. Observing that the boundary condition on ∂G is not necessary to derive the regularity results in G in Theorem 2.2 and Theorem 2.9 in [100], we obtain from Theorem 2.9 in [100] that the solutions $\boldsymbol{E}$, $\boldsymbol{H}$ of (3.32) belonging to $\boldsymbol{H}_{\mathrm{loc}}(\mathbf{curl}, \mathbb{R}^3 \setminus C)$ satisfy $\boldsymbol{E}|_{M\cap G_\pm}$, $\boldsymbol{H}|_{M\cap G_\pm} \in H^s(M \cap G_\pm; \mathbb{C})^3$ for all $s \in \mathbb{N}$ and all open bounded sets M such that $\overline{M} \subset G$, where $G_\pm := \mathbb{R}^3_\pm \setminus \overline{B_R(0)}$. Sobolev's embedding theorem (cf. Agmon [1, Theorem 3.9]), yields that $\boldsymbol{E}|_{G_\pm}$, $\boldsymbol{H}|_{G_\pm} \in C^s(\overline{G_\pm}; \mathbb{C})^3$ for all $s \in \mathbb{N}$.

Recalling the electric and the magnetic dyadic Green's function $\mathbb{G}^e$ and $\mathbb{G}^m$ from Section 3.2.2, we mention that for any $\boldsymbol{d} \in \mathbb{C}^3$ and $\boldsymbol{y} \in \mathbb{R}^3_0$ it holds that $(\mathbb{G}^e(\cdot,\boldsymbol{y})\boldsymbol{d}, \frac{1}{\mathrm{i}\,\omega\mu}\mathbf{curl}_x\,\mathbb{G}^e(\cdot,\boldsymbol{y})\boldsymbol{d})$ and $(-\frac{1}{\mathrm{i}\,\omega\varepsilon}\mathbf{curl}_x\,\mathbb{G}^m(\cdot,\boldsymbol{y})\boldsymbol{d}, \mathbb{G}^m(\cdot,\boldsymbol{y})\boldsymbol{d})$ are radiating solutions of Maxwell's equations (3.32) in $\mathbb{R}^3 \setminus \{\boldsymbol{y}\}$.

We denote by

$$\Sigma_d := \{\boldsymbol{x} \in \mathbb{R}^3_+ \mid \boldsymbol{x} \cdot \boldsymbol{e}_3 = d\} \subset \mathbb{R}^3_+$$

the hyperplane parallel to the surface of the ground at height $d > 0$, and we assume that measurements and excitations are restricted to an open bounded sheet $\mathcal{M} \subset \Sigma_d$ supporting the measurement device. A time–harmonic excitation given by a *magnetic dipole density* $\boldsymbol{\varphi} \in \boldsymbol{L}^2(\mathcal{M}) := L^2(\mathcal{M}; \mathbb{C})^3$ on $\mathcal{M}$ leads to a primary electromagnetic field $(\boldsymbol{E}^i, \boldsymbol{H}^i)$ satisfying (3.32) in $\mathbb{R}^3 \setminus \mathcal{M}$, where the magnetic field has the form

$$\boldsymbol{H}^i = k_+^2 \int_{\mathcal{M}} \mathbb{G}^m(\cdot,\boldsymbol{y})\boldsymbol{\varphi}(\boldsymbol{y})\, \mathrm{d}s(\boldsymbol{y}); \tag{3.34}$$

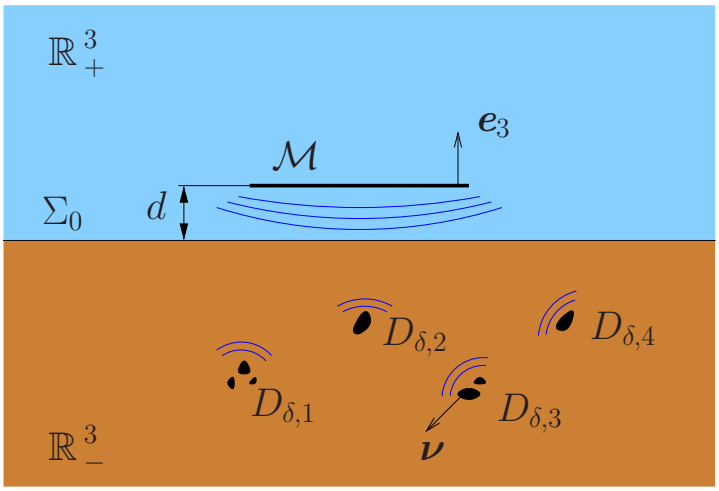

Figure 3.1: Sketch of the geometrical setup.

cf. [99].

We suppose that $\mathbb{R}^3_-$ contains a finite number of *well separated* small perfectly conducting scatterers, each of the form $D_{\delta,l} := \boldsymbol{z}_l + \delta B_l$, $1 \leq l \leq m$, where $B_l \subset \mathbb{R}^3$ is a bounded open set of class $C^{2,\alpha}$, $0 < \alpha < 1$, containing the origin, that consists of finitely many domains such that every component of B_l is simply connected and its boundary is connected. The points $\boldsymbol{z}_l \in \mathbb{R}^3_-$, $1 \leq l \leq m$, that determine the *position* of the scatterers are assumed to satisfy

$$|\boldsymbol{z}_j - \boldsymbol{z}_l| \geq d_0 \quad \text{for } j \neq l \quad \text{and} \quad \operatorname{dist}(\boldsymbol{z}_l, \Sigma_0) \geq d_0$$

for some constant $d_0 > 0$, $1 \leq j, l \leq m$. The value of $0 < \delta \leq 1$, the common order of magnitude of the *size of the scatterers*, is assumed to be small enough such that the scatterers are disjoint and compactly contained in $\mathbb{R}^3_-$. So, the total collection of scatterers takes the form $D_\delta := \bigcup_{l=1}^m (\boldsymbol{z}_l + \delta B_l)$. Throughout, we denote by $\boldsymbol{\nu}$ the unit outward normal to $\partial D_{\delta,l}$ and ∂B_l relative to $D_{\delta,l}$ and B_l, $1 \leq l \leq m$, respectively.

The *perfect conductor* sitting in D_δ induces a secondary field $(\boldsymbol{E}^s, \boldsymbol{H}^s)$ which is a radiating solution of (3.32) in $\mathbb{R}^3 \setminus \overline{D_\delta}$ subject to the boundary condition

$$\boldsymbol{\nu} \times \boldsymbol{E}^s = -\boldsymbol{\nu} \times \boldsymbol{E}^i \qquad \text{on } \partial D_\delta. \tag{3.35}$$

For a mathematical treatment of this direct problem we refer the reader to [43, 46, 88]. We define the *near field measurement operator* G_δ, which maps given excitations $\boldsymbol{\varphi}$ to the corresponding secondary magnetic fields $\boldsymbol{H}^s|_{\mathcal{M}}$ on $\mathcal{M}$, i.e.,

$$G_\delta : \boldsymbol{L}^2(\mathcal{M}) \to \boldsymbol{L}^2(\mathcal{M}), \quad G_\delta \boldsymbol{\varphi} := \boldsymbol{H}^s|_{\mathcal{M}}. \tag{3.36}$$

Note that, because $\boldsymbol{H}^s$ is analytic in a neighborhood of $\mathcal{M}$, its trace on $\mathcal{M}$ is a well–defined member of $\boldsymbol{L}^2(\mathcal{M})$. As in Gebauer et al. [52, Theorem 2.1], it can be seen that G_δ is a compact operator.

3.5 Factorization of G_δ

In this section, we derive a factorization of the measurement operator G_δ from (3.36) similar to the one developed in [52], but here we do not restrict ourselves to tangential excitations and measurements.

We consider an arbitrary tangential vector field $\boldsymbol{\psi} \in \boldsymbol{H}_{\mathrm{div}}^{-1/2}(\partial D_\delta)$ and denote by $(\boldsymbol{E}^\psi, \boldsymbol{H}^\psi)$ the associated radiating solution of the exterior Maxwell boundary value problem

$$\mathbf{curl}\boldsymbol{H}^\psi + \mathrm{i}\,\omega\varepsilon\boldsymbol{E}^\psi = 0, \quad \mathbf{curl}\boldsymbol{E}^\psi - \mathrm{i}\,\omega\mu\boldsymbol{H}^\psi = 0 \quad \text{in } \mathbb{R}^3 \setminus \overline{D_\delta}, \tag{3.37a}$$

$$\boldsymbol{\nu} \times \boldsymbol{E}^\psi = \boldsymbol{\psi} \quad \text{on } \partial D_\delta. \tag{3.37b}$$

Uniqueness of solutions of this problem is stated in Appendix C, and existence of solutions will be shown in the next sections by reducing the boundary value problem to an integral equation of the second kind and applying Riesz–Fredholm theory. We define

$$L_\delta : \boldsymbol{H}_{\mathrm{div}}^{-1/2}(\partial D_\delta) \to \boldsymbol{L}^2(\mathcal{M}), \quad L_\delta\boldsymbol{\psi} := \boldsymbol{H}^\psi|_{\mathcal{M}}. \tag{3.38}$$

Then, L_δ is a bounded linear operator. In particular, we mention that if $\boldsymbol{E}^i$ and $\boldsymbol{H}^s$ are the primary electric and secondary magnetic fields introduced in Section 3.4, respectively, then $\boldsymbol{\psi} := -\boldsymbol{\nu} \times \boldsymbol{E}^i|_{\partial D_\delta}$ belongs to $\boldsymbol{H}_{\mathrm{div}}^{-1/2}(\partial D_\delta)$, and this choice of $\boldsymbol{\psi}$ yields $\boldsymbol{H}^\psi = \boldsymbol{H}^s$. This means that $L_\delta : -\boldsymbol{\nu} \times \boldsymbol{E}^i|_{\partial D_\delta} \mapsto \boldsymbol{H}^s|_{\mathcal{M}}$.

Next, we introduce the bilinear form

$$\langle \boldsymbol{\varphi}_1, \boldsymbol{\varphi}_2 \rangle_{\mathcal{M}} := \int_{\mathcal{M}} \boldsymbol{\varphi}_1 \cdot \boldsymbol{\varphi}_2 \, \mathrm{d}s \qquad \text{for } \boldsymbol{\varphi}_1, \boldsymbol{\varphi}_2 \in \boldsymbol{L}^2(\mathcal{M}), \tag{3.39}$$

and denote by $L_\delta^\top : \boldsymbol{L}^2(\mathcal{M}) \to \boldsymbol{H}_{\mathrm{curl}}^{-1/2}(\partial D_\delta)$ the corresponding transpose of L_δ.

Proposition 3.6. *Let $\boldsymbol{\varphi} \in \boldsymbol{L}^2(\mathcal{M})$ and denote by $\boldsymbol{H}^i$ and $\boldsymbol{H}^s$ the associated primary and secondary magnetic fields introduced in Section 3.4. Then,*

$$L_\delta^\top \boldsymbol{\varphi} = \frac{1}{\mathrm{i}\,\omega\mu_+}(\boldsymbol{\nu} \times \boldsymbol{H}|_{\partial D_\delta}) \times \boldsymbol{\nu} \qquad \text{on } \partial D_\delta, \tag{3.40}$$

where $\boldsymbol{H} = \boldsymbol{H}^i + \boldsymbol{H}^s$ is the total magnetic field.

Proof. Given $\boldsymbol{\psi} \in \boldsymbol{H}_{\mathrm{div}}^{-1/2}(\partial D_\delta)$, let $(\boldsymbol{E}^{\boldsymbol{\psi}}, \boldsymbol{H}^{\boldsymbol{\psi}})$ be the radiating solution of (3.37). From Theorem B.1, we obtain that for any $\boldsymbol{y} \in \mathbb{R}^3 \setminus \overline{D_\delta}$,

$$\boldsymbol{H}^{\boldsymbol{\psi}}(\boldsymbol{y}) = \int_{\partial D_\delta} \frac{\varepsilon(\boldsymbol{y})}{\varepsilon(\boldsymbol{x})} \Big(\mathbb{G}^{m\top}(\boldsymbol{x},\boldsymbol{y})(\boldsymbol{\nu} \times \mathbf{curl} \boldsymbol{H}^{\boldsymbol{\psi}})(\boldsymbol{x}) + (\mathbf{curl}_x \mathbb{G}^m)^\top(\boldsymbol{x},\boldsymbol{y})(\boldsymbol{\nu} \times \boldsymbol{H}^{\boldsymbol{\psi}})(\boldsymbol{x}) \Big) \, \mathrm{d}s(\boldsymbol{x}).$$

Therefore, applying (3.37a) and (3.37b), we find that

$$\begin{aligned}
&\mathrm{i}\,\omega\mu_+ \langle \boldsymbol{\varphi}, L_\delta \boldsymbol{\psi} \rangle_{\mathcal{M}} = \mathrm{i}\,\omega\mu_+ \int_{\mathcal{M}} \boldsymbol{\varphi}(\boldsymbol{y}) \cdot \boldsymbol{H}^{\boldsymbol{\psi}}(\boldsymbol{y}) \, \mathrm{d}s(\boldsymbol{y}) \\
&= \mathrm{i}\,\omega\mu_+ \int_{\mathcal{M}} \boldsymbol{\varphi}(\boldsymbol{y}) \cdot \left(\int_{\partial D_\delta} \frac{\varepsilon_+}{\varepsilon_-} \Big(\mathbb{G}^{m\top}(\boldsymbol{x},\boldsymbol{y})(\boldsymbol{\nu} \times \mathbf{curl} \boldsymbol{H}^{\boldsymbol{\psi}})(\boldsymbol{x}) + (\mathbf{curl}_x \mathbb{G}^m)^\top(\boldsymbol{x},\boldsymbol{y})(\boldsymbol{\nu} \times \boldsymbol{H}^{\boldsymbol{\psi}})(\boldsymbol{x}) \Big) \, \mathrm{d}s(\boldsymbol{x}) \right) \mathrm{d}s(\boldsymbol{y}) \\
&= \int_{\partial D_\delta} \boldsymbol{\psi}(\boldsymbol{x}) \cdot k_+^2 \int_{\mathcal{M}} \mathbb{G}^m(\boldsymbol{x},\boldsymbol{y}) \boldsymbol{\varphi}(\boldsymbol{y}) \, \mathrm{d}s(\boldsymbol{y}) \, \mathrm{d}s(\boldsymbol{x}) \\
&\quad + \int_{\partial D_\delta} (\boldsymbol{\nu} \times \boldsymbol{H}^{\boldsymbol{\psi}})(\boldsymbol{x}) \cdot \frac{\mathrm{i}\,\omega\mu_+\varepsilon_+}{\varepsilon_-} \int_{\mathcal{M}} \mathbf{curl}_x \mathbb{G}^m(\boldsymbol{x},\boldsymbol{y}) \boldsymbol{\varphi}(\boldsymbol{y}) \, \mathrm{d}s(\boldsymbol{y}) \, \mathrm{d}s(\boldsymbol{x}).
\end{aligned}$$

Recalling formula (3.34) for the incident field and the boundary condition (3.35), we obtain

$$\begin{aligned}
&\mathrm{i}\,\omega\mu_+ \langle \boldsymbol{\varphi}, L_\delta \boldsymbol{\psi} \rangle_{\mathcal{M}} \\
&= \int_{\partial D_\delta} \boldsymbol{\psi}(\boldsymbol{x}) \cdot \boldsymbol{H}^i(\boldsymbol{x}) \, \mathrm{d}s(\boldsymbol{x}) - \frac{1}{\mathrm{i}\,\omega\varepsilon_-} \int_{\partial D_\delta} (\boldsymbol{\nu} \times \boldsymbol{H}^{\boldsymbol{\psi}})(\boldsymbol{x}) \cdot \mathbf{curl} \boldsymbol{H}^i(\boldsymbol{x}) \, \mathrm{d}s(\boldsymbol{x}) \\
&= \int_{\partial D_\delta} \boldsymbol{\psi}(\boldsymbol{x}) \cdot \boldsymbol{H}^i(\boldsymbol{x}) \, \mathrm{d}s(\boldsymbol{x}) + \int_{\partial D_\delta} \boldsymbol{H}^{\boldsymbol{\psi}}(\boldsymbol{x}) \cdot (\boldsymbol{\nu} \times \boldsymbol{E}^s)(\boldsymbol{x}) \, \mathrm{d}s(\boldsymbol{x}).
\end{aligned}$$

Then, integration by parts (cf. (3.1)) and applying Maxwell's equations gives for the second term

$$\begin{aligned}
&\int_{\partial D_\delta} \boldsymbol{H}^{\boldsymbol{\psi}}(\boldsymbol{x}) \cdot (\boldsymbol{\nu} \times \boldsymbol{E}^s)(\boldsymbol{x}) \, \mathrm{d}s(\boldsymbol{x}) \\
&\qquad = \int_{B_R(0) \setminus \overline{D_\delta}} \big(\mathbf{curl} \boldsymbol{H}^{\boldsymbol{\psi}}(\boldsymbol{x}) \cdot \boldsymbol{E}^s(\boldsymbol{x}) - \boldsymbol{H}^{\boldsymbol{\psi}}(\boldsymbol{x}) \cdot \mathbf{curl} \boldsymbol{E}^s(\boldsymbol{x}) \big) \, \mathrm{d}\boldsymbol{x} \\
&\qquad\quad + \int_{\partial B_R(0)} \frac{\boldsymbol{x}}{R} \times \boldsymbol{E}^s(\boldsymbol{x}) \cdot \boldsymbol{H}^{\boldsymbol{\psi}}(\boldsymbol{x}) \, \mathrm{d}s(\boldsymbol{x}) \\
&\qquad = \int_{B_R(0) \setminus \overline{D_\delta}} \big(\boldsymbol{E}^{\boldsymbol{\psi}}(\boldsymbol{x}) \cdot \mathbf{curl} \boldsymbol{H}^s(\boldsymbol{x}) - \mathbf{curl} \boldsymbol{E}^{\boldsymbol{\psi}}(\boldsymbol{x}) \cdot \boldsymbol{H}^s(\boldsymbol{x}) \big) \, \mathrm{d}\boldsymbol{x} \\
&\qquad\quad - \int_{\partial B_R(0)} \boldsymbol{E}^s(\boldsymbol{x}) \cdot \frac{\boldsymbol{x}}{R} \times \boldsymbol{H}^{\boldsymbol{\psi}}(\boldsymbol{x}) \, \mathrm{d}s(\boldsymbol{x}).
\end{aligned}$$

With another partial integration, we thus obtain

$$\begin{aligned}
&\int_{\partial D_\delta} \boldsymbol{H}^{\psi}(\boldsymbol{x}) \cdot (\boldsymbol{\nu} \times \boldsymbol{E}^{s})(\boldsymbol{x}) \, \mathrm{d}s(\boldsymbol{x}) = \int_{\partial B_R(0)} \frac{\boldsymbol{x}}{R} \times \boldsymbol{H}^{s}(\boldsymbol{x}) \cdot \boldsymbol{E}^{\psi}(\boldsymbol{x}) \, \mathrm{d}s(\boldsymbol{x}) \\
&- \int_{\partial D_\delta} (\boldsymbol{\nu} \times \boldsymbol{H}^{s})(\boldsymbol{x}) \cdot \boldsymbol{E}^{\psi}(\boldsymbol{x}) \, \mathrm{d}s(\boldsymbol{x}) - \int_{\partial B_R(0)} \boldsymbol{E}^{s}(\boldsymbol{x}) \cdot \frac{\boldsymbol{x}}{R} \times \boldsymbol{H}^{\psi}(\boldsymbol{x}) \, \mathrm{d}s(\boldsymbol{x}) \\
&= \int_{\partial D_\delta} \boldsymbol{H}^{s}(\boldsymbol{x}) \cdot (\boldsymbol{\nu} \times \boldsymbol{E}^{\psi})(\boldsymbol{x}) \, \mathrm{d}s(\boldsymbol{x}) \\
&+ \int_{\partial B_R(0)} \left(\frac{\boldsymbol{x}}{R} \times \boldsymbol{H}^{s}(\boldsymbol{x}) + \Big(\frac{\varepsilon(\boldsymbol{x})}{\mu(\boldsymbol{x})} \Big)^{1/2} \boldsymbol{E}^{s}(\boldsymbol{x}) \right) \cdot \boldsymbol{E}^{\psi}(\boldsymbol{x}) \, \mathrm{d}s(\boldsymbol{x}) \\
&- \int_{\partial B_R(0)} \boldsymbol{E}^{s}(\boldsymbol{x}) \cdot \left(\frac{\boldsymbol{x}}{R} \times \boldsymbol{H}^{\psi}(\boldsymbol{x}) + \Big(\frac{\varepsilon(\boldsymbol{x})}{\mu(\boldsymbol{x})} \Big)^{1/2} \boldsymbol{E}^{\psi}(\boldsymbol{x}) \right) \mathrm{d}s(\boldsymbol{x}).
\end{aligned}$$

From the radiation condition (3.33) and the finiteness condition (B.9), we obtain that the integrals over $\partial B_R(0)$ vanish as $R \to \infty$. Therefore, recalling (3.37b),

$$\mathrm{i}\,\omega\mu_+ \langle \boldsymbol{\varphi}, L_\delta \boldsymbol{\psi} \rangle_{\mathcal{M}} = \int_{\partial D_\delta} \boldsymbol{H}(\boldsymbol{x}) \cdot \boldsymbol{\psi}(\boldsymbol{x}) \, \mathrm{d}s(\boldsymbol{x}) = \big\langle (\boldsymbol{\nu} \times \boldsymbol{H}|_{\partial D_\delta}) \times \boldsymbol{\nu}, \boldsymbol{\psi} \big\rangle_{D_\delta}.$$

□

Finally, we consider the diffraction problem

$$\mathbf{curl} \boldsymbol{H}^{d} + \mathrm{i}\,\omega\varepsilon \boldsymbol{E}^{d} = 0, \quad \mathbf{curl} \boldsymbol{E}^{d} - \mathrm{i}\,\omega\mu \boldsymbol{H}^{d} = 0 \qquad \text{in } \mathbb{R}^3 \setminus \partial D_\delta, \quad (3.41a)$$

with the jump conditions

$$\big[(\boldsymbol{\nu} \times \boldsymbol{H}^{d}) \times \boldsymbol{\nu} \big]_{\partial D_\delta} = \boldsymbol{\chi}, \qquad \big[\boldsymbol{\nu} \times \boldsymbol{E}^{d} \big]_{\partial D_\delta} = 0 \qquad \text{on } \partial D_\delta. \qquad (3.41b)$$

Here, $\boldsymbol{\chi} \in \boldsymbol{H}^{-1/2}_{\mathrm{curl}}(\partial D_\delta)$ is a given tangential field on ∂D_δ, and the square brackets denote the differences between the respective traces from outside and inside. We are looking for a radiating solution $(\boldsymbol{E}^{d}, \boldsymbol{H}^{d})$ of this problem. Uniqueness of solutions is stated in Appendix C, and existence of solutions will be shown later by writing them in terms of layer potentials. Given the solution, we define

$$F_\delta : \boldsymbol{H}^{-1/2}_{\mathrm{curl}}(\partial D_\delta) \to \boldsymbol{H}^{-1/2}_{\mathrm{div}}(\partial D_\delta), \quad F_\delta \boldsymbol{\chi} := \boldsymbol{\nu} \times \boldsymbol{E}^{d}|_{\partial D_\delta}. \qquad (3.42)$$

Then, F_δ is a bounded linear operator. For $\boldsymbol{\chi} = (\boldsymbol{\nu} \times \boldsymbol{H}|_{\partial D_\delta}) \times \boldsymbol{\nu}$, i.e., the tangential component of the total magnetic field corresponding to some excitation $\boldsymbol{\varphi} \in \boldsymbol{L}^2(\mathcal{M})$ as described in Section 3.4, the solution of the diffraction problem (3.41) can be constructed from the corresponding primary and the secondary fields, namely

$$\boldsymbol{E}^{d} = \begin{cases} \boldsymbol{E}^{s}, & x \in \mathbb{R}^3 \setminus \overline{D_\delta}, \\ -\boldsymbol{E}^{i}, & x \in D_\delta, \end{cases} \qquad \boldsymbol{H}^{d} = \begin{cases} \boldsymbol{H}^{s}, & x \in \mathbb{R}^3 \setminus \overline{D_\delta}, \\ -\boldsymbol{H}^{i}, & x \in D_\delta. \end{cases}$$

Consequently,

$$F_\delta : (\boldsymbol{\nu} \times \boldsymbol{H}|_{\partial D_\delta}) \times \boldsymbol{\nu} \mapsto \boldsymbol{\nu} \times \boldsymbol{E}^s|_{\partial D_\delta} = -\boldsymbol{\nu} \times \boldsymbol{E}^i|_{\partial D_\delta}.$$

In sum, we have shown that the following diagram is commutative:

$$\begin{array}{ccc} \boldsymbol{L}^2(\mathcal{M}) & \xrightarrow{G_\delta} & \boldsymbol{L}^2(\mathcal{M}) \\ \downarrow{\scriptstyle \mathrm{i}\,\omega\mu_+ L_\delta^\top} & & \uparrow{\scriptstyle L_\delta} \\ \boldsymbol{H}_{\mathrm{curl}}^{-1/2}(\partial D_\delta) & \xrightarrow{F_\delta} & \boldsymbol{H}_{\mathrm{div}}^{-1/2}(\partial D_\delta) \end{array} \qquad \begin{array}{ccc} \boldsymbol{\varphi} & \longmapsto & \boldsymbol{H}^s|_{\mathcal{M}} \\ \downarrow & & \uparrow \\ (\boldsymbol{\nu} \times \boldsymbol{H}|_{\partial D_\delta}) \times \boldsymbol{\nu} & \longmapsto & -\boldsymbol{\nu} \times \boldsymbol{E}^i|_{\partial D_\delta} \end{array}$$

This yields the following theorem; cf. [52] for a corresponding result for tangential densities $\boldsymbol{\varphi}$ on $\mathcal{M}$.

Theorem 3.7. *Given L_δ from* (3.38) *and F_δ from* (3.42)*, the measurement operator G_δ from* (3.36) *admits the factorization*

$$G_\delta = \mathrm{i}\,\omega\mu_+ L_\delta F_\delta L_\delta^\top. \tag{3.43}$$

3.6 First Estimates

In the following two sections, we restrict ourselves to the case of a single scatterer, i.e., $D_\delta = \boldsymbol{z} + \delta B$. Multiple scatterers are studied in Section 3.8.

We often have to deal with changes of coordinates. For this purpose, we apply the notation introduced in (2.19) also to functions in $\boldsymbol{H}_{\mathrm{div}}^{-1/2}(\partial D_\delta)$ or $\boldsymbol{H}_{\mathrm{curl}}^{-1/2}(\partial D_\delta)$ and $\boldsymbol{H}_{\mathrm{div}}^{-1/2}(\partial B)$ or $\boldsymbol{H}_{\mathrm{curl}}^{-1/2}(\partial B)$, respectively.

For bounded open sets $D \subset \mathbb{R}^3$ of class $C^{2,\alpha}$, $0 < \alpha < 1$, we use the following norms on $\boldsymbol{H}_{\mathrm{div}}^{-1/2}(\partial D)$ and $\boldsymbol{H}_{\mathrm{curl}}^{-1/2}(\partial D)$:

$$\|\boldsymbol{a}\|_{\boldsymbol{H}_{\mathrm{div}}^{-1/2}(\partial D)} := \inf_{\substack{\boldsymbol{u} \in \boldsymbol{H}(\mathbf{curl}, D) \\ \gamma_t(\boldsymbol{u}) = \boldsymbol{a}}} \|\boldsymbol{u}\|_{\boldsymbol{H}(\mathbf{curl}, D)} \qquad \text{for } \boldsymbol{a} \in \boldsymbol{H}_{\mathrm{div}}^{-1/2}(\partial D),$$

$$\|\boldsymbol{b}\|_{\boldsymbol{H}_{\mathrm{curl}}^{-1/2}(\partial D)} := \inf_{\substack{\boldsymbol{u} \in \boldsymbol{H}(\mathbf{curl}, D) \\ \pi_t(\boldsymbol{u}) = \boldsymbol{b}}} \|\boldsymbol{u}\|_{\boldsymbol{H}(\mathbf{curl}, D)} \qquad \text{for } \boldsymbol{b} \in \boldsymbol{H}_{\mathrm{curl}}^{-1/2}(\partial D).$$

A simple calculation (cf. Lemma 2.5 for a similar result) yields the following scaling properties of these norms under changes of coordinates as in (2.19). Suppose $\boldsymbol{a} \in \boldsymbol{H}_{\mathrm{div}}^{-1/2}(\partial D_\delta)$, $\boldsymbol{b} \in \boldsymbol{H}_{\mathrm{curl}}^{-1/2}(\partial D_\delta)$ and assume $0 < \delta \leq 1$. Then

$$\delta^{\frac{3}{2}} \|\hat{\boldsymbol{a}}\|_{\boldsymbol{H}_{\mathrm{div}}^{-1/2}(\partial B)} \leq \|\boldsymbol{a}\|_{\boldsymbol{H}_{\mathrm{div}}^{-1/2}(\partial D_\delta)} \leq \delta^{\frac{1}{2}} \|\hat{\boldsymbol{a}}\|_{\boldsymbol{H}_{\mathrm{div}}^{-1/2}(\partial B)}, \tag{3.44a}$$

$$\delta^{\frac{3}{2}} \|\hat{\boldsymbol{b}}\|_{\boldsymbol{H}_{\mathrm{curl}}^{-1/2}(\partial B)} \leq \|\boldsymbol{b}\|_{\boldsymbol{H}_{\mathrm{curl}}^{-1/2}(\partial D_\delta)} \leq \delta^{\frac{1}{2}} \|\hat{\boldsymbol{b}}\|_{\boldsymbol{H}_{\mathrm{curl}}^{-1/2}(\partial B)}. \tag{3.44b}$$

In order to derive the asymptotic expansion in Section 3.7, we need to expand the fundamental solution

$$\Phi_{k_-}(\boldsymbol{x} - \boldsymbol{y}) = \Phi_{k_-}\big((\delta\boldsymbol{\xi} + \boldsymbol{z}) - (\delta\boldsymbol{\eta} + \boldsymbol{z})\big) = \Phi_{k_-}\big(\delta(\boldsymbol{\xi} - \boldsymbol{\eta})\big)$$

for $\boldsymbol{x} = \delta\boldsymbol{\xi} + \boldsymbol{z} \neq \delta\boldsymbol{\eta} + \boldsymbol{z} = \boldsymbol{y} \in \partial D_\delta$, i.e., $\boldsymbol{\xi} \neq \boldsymbol{\eta} \in \partial B$, as $\delta \to 0$. From

$$e^{\mathrm{i}\, k_-\delta|\boldsymbol{\xi}-\boldsymbol{\eta}|} = 1 + \mathrm{i}\, k_-\delta|\boldsymbol{\xi}-\boldsymbol{\eta}| - \frac{{k_-}^2\delta^2|\boldsymbol{\xi}-\boldsymbol{\eta}|^2}{2} - \frac{\mathrm{i}\, {k_-}^3\delta^3|\boldsymbol{\xi}-\boldsymbol{\eta}|^3}{6} + \mathcal{O}(\delta^4)$$

follows that

$$\begin{aligned}&\Phi_{k_-}(\boldsymbol{x}-\boldsymbol{y})\\ &\quad= \frac{1}{\delta}\left(\frac{1}{4\pi|\boldsymbol{\xi}-\boldsymbol{\eta}|} + \frac{\mathrm{i}\, k_-\delta}{4\pi} - \frac{{k_-}^2\delta^2|\boldsymbol{\xi}-\boldsymbol{\eta}|}{8\pi} - \frac{\mathrm{i}\, {k_-}^3\delta^3|\boldsymbol{\xi}-\boldsymbol{\eta}|^2}{24\pi} + \mathcal{O}(\delta^4)\right).\end{aligned} \tag{3.45}$$

Furthermore, we need an asymptotic expansion for

$$\nabla_x\Phi_{k_-}(\boldsymbol{x}-\boldsymbol{y}) = \left(\mathrm{i}\, k_- - \frac{1}{|\boldsymbol{x}-\boldsymbol{y}|}\right)\Phi_{k_-}(\boldsymbol{x}-\boldsymbol{y})\frac{\boldsymbol{x}-\boldsymbol{y}}{|\boldsymbol{x}-\boldsymbol{y}|}. \tag{3.46}$$

With (3.45), it follows that

$$\begin{aligned}&\nabla_x\Phi_{k_-}(\boldsymbol{x}-\boldsymbol{y})\\ &\qquad= \frac{1}{\delta^2}\left(-\frac{1}{4\pi|\boldsymbol{\xi}-\boldsymbol{\eta}|^2} - \frac{{k_-}^2\delta^2}{8\pi} - \frac{\mathrm{i}\, {k_-}^3\delta^3|\boldsymbol{\xi}-\boldsymbol{\eta}|}{12\pi} + \mathcal{O}(\delta^4)\right)\frac{\boldsymbol{\xi}-\boldsymbol{\eta}}{|\boldsymbol{\xi}-\boldsymbol{\eta}|}.\end{aligned}$$

In sum, we obtain the following formulas:

$$\Phi_{k_-}(\boldsymbol{x}-\boldsymbol{y}) = \frac{1}{\delta}\left(\Phi_0(\boldsymbol{\xi}-\boldsymbol{\eta}) + \frac{\mathrm{i}\, k_-\delta}{4\pi} + \mathcal{O}(\delta^2)\right) \qquad \text{as } \delta \to 0, \tag{3.47}$$

$$\nabla_x\Phi_{k_-}(\boldsymbol{x}-\boldsymbol{y}) = \frac{1}{\delta^2}\left(\nabla_\xi\Phi_0(\boldsymbol{\xi}-\boldsymbol{\eta}) - \frac{{k_-}^2\delta^2}{8\pi}\frac{\boldsymbol{\xi}-\boldsymbol{\eta}}{|\boldsymbol{\xi}-\boldsymbol{\eta}|} + \mathcal{O}(\delta^3)\right) \quad \text{as } \delta \to 0. \tag{3.48}$$

Remark 3.8 (Eigenvalues). In Section 3.3.3, we had to assume that the wavenumber k_- is not a *Maxwell eigenvalue* for the bounded open set D, to obtain the invertibility of the operators $\frac{1}{2}I + M_D^m$ and $\frac{1}{2}I + M_D^{m\top}$. Now, we explain, why this assumption yields no restrictions for our analysis.

Maxwell eigenvalues for D are wavenumbers κ so that Maxwell's equations (3.32) in D with homogeneous boundary condition $\boldsymbol{\nu} \times \boldsymbol{E}|_{\partial D} = 0$ have a nontrivial solution. That means, if κ is a Maxwell eigenvalue for D, the variational problem of finding

$$\boldsymbol{E} \in \boldsymbol{H}_0(\mathbf{curl}, D) := \left\{\boldsymbol{v} \in \boldsymbol{H}(\mathbf{curl}, D) \;\middle|\; \boldsymbol{\nu} \times \boldsymbol{v}|_{\partial D} = 0\right\}$$

such that

$$\int_D \mathbf{curl}\boldsymbol{E} \cdot \mathbf{curl}\boldsymbol{v}\, \mathrm{d}\boldsymbol{x} = \kappa^2 \int_D \boldsymbol{E} \cdot \boldsymbol{v}\, \mathrm{d}\boldsymbol{x} \qquad \text{for all } \boldsymbol{v} \in \boldsymbol{H}_0(\mathbf{curl}, D), \tag{3.49}$$

has a nontrivial solution; cf. [88, pp. 95–98]. If $\operatorname{Im}\kappa > 0$, it is well known that solutions of the interior Maxwell problem are unique (cf. [88, Theorem 4.17]) and thus κ is no eigenvalue. On the other hand there exists a discrete set of real eigenvalues $\kappa_j > 0$, $j \in \mathbb{N}$, for D that accumulates only at infinity; cf. [88, Theorem 4.18].

Let $\{k_j\}_{j\in\mathbb{N}}$ be the set of Maxwell eigenvalues corresponding to the reference set B. By a change of coordinates in the variational formulation (3.49), we find that $\{\delta^{-1}k_j\}_{j\in\mathbb{N}}$ is the set of eigenvalues corresponding to the set $D_\delta = \boldsymbol{z} + \delta B$, $0 < \delta \leq 1$. Therefore, we can assume henceforth in the derivation of the asymptotic expansion without loss of generality that δ is small enough so that $k_- \notin \{\delta^{-1}k_j\}_{j\in\mathbb{N}}$, i.e., that k_- is no Maxwell eigenvalue for the sets D_δ considered hereafter.

In the next lemma, we investigate the scaling properties of the integral operator $M^m_{D_\delta}$.

Lemma 3.9. *Let $\boldsymbol{a} \in \boldsymbol{H}^{-1/2}_{\mathrm{div}}(\partial D_\delta)$. Then,*

$$M^m_{D_\delta}\boldsymbol{a} = (M^0_B\hat{\boldsymbol{a}})^\vee + (E^m_M\hat{\boldsymbol{a}})^\vee,$$

where E^m_M is a bounded linear operator, independent of $\boldsymbol{a}$, which is $\mathcal{O}(\delta^2)$ in $\mathcal{L}(\boldsymbol{H}^{-1/2}_{\mathrm{div}}(\partial B))$ as $\delta \to 0$.

Proof. Let $\boldsymbol{a} \in \boldsymbol{H}^{-1/2}_{\mathrm{div}}(\partial D_\delta)$ and $\boldsymbol{a}_j \in \boldsymbol{T}_{\mathrm{div}}(\partial D_\delta)$, $j \in \mathbb{N}$, such that $\boldsymbol{a}_j$ converges to $\boldsymbol{a}$ in $\boldsymbol{H}^{-1/2}_{\mathrm{div}}(\partial D_\delta)$. For fixed j and $\boldsymbol{x} \in D_\delta$, we observe by a change of variables $\boldsymbol{\xi} := \frac{\boldsymbol{x}-\boldsymbol{z}}{\delta}$ and $\boldsymbol{\eta} := \frac{\boldsymbol{y}-\boldsymbol{z}}{\delta}$ that

$$\begin{aligned}
(M^0_{D_\delta}\boldsymbol{a}_j)(\boldsymbol{x}) &= \int_{\partial D_\delta} \boldsymbol{\nu}(\boldsymbol{x}) \times \mathbf{curl}_x \left(\boldsymbol{a}_j(\boldsymbol{y}) \frac{1}{4\pi|\boldsymbol{x}-\boldsymbol{y}|} \right) \mathrm{d}s(\boldsymbol{y}) \\
&= \int_{\partial B} \boldsymbol{\nu}(\boldsymbol{\xi}) \times \frac{1}{\delta}\mathbf{curl}_\xi \left(\hat{\boldsymbol{a}}_j(\boldsymbol{\eta}) \frac{1}{4\pi\delta|\boldsymbol{\xi}-\boldsymbol{\eta}|} \right) \delta^2 \, \mathrm{d}s(\boldsymbol{\eta}) \\
&= (M^0_B\hat{\boldsymbol{a}}_j)(\boldsymbol{\xi}),
\end{aligned}$$

i.e., $M^0_{D_\delta}\boldsymbol{a}_j = (M^0_B\hat{\boldsymbol{a}}_j)^\vee$. From (3.48), we find that

$$\nabla_x(\Phi_{k_-} - \Phi_0)(\boldsymbol{x}-\boldsymbol{y}) = \frac{1}{\delta^2}\left(-\frac{{k_-}^2\delta^2}{8\pi}\frac{\boldsymbol{\xi}-\boldsymbol{\eta}}{|\boldsymbol{\xi}-\boldsymbol{\eta}|} + \mathcal{O}(\delta^3) \right)$$

for $\boldsymbol{x} \neq \boldsymbol{y}$ as $\delta \to 0$. Again by a change of coordinates, we calculate for $\boldsymbol{x} \in \partial D_\delta$,

$$\begin{aligned}
\big((M^{k_-}_{D_\delta} - M^0_{D_\delta})\boldsymbol{a}_j\big)(\boldsymbol{x}) &= \int_{\partial D_\delta} \boldsymbol{\nu}(\boldsymbol{x}) \times \big(\nabla_x(\Phi_{k_-} - \Phi_0)(\boldsymbol{x}-\boldsymbol{y}) \times \boldsymbol{a}_j(\boldsymbol{y})\big) \, \mathrm{d}s(\boldsymbol{y}) \\
&= \int_{\partial B} \boldsymbol{\nu}(\boldsymbol{\xi}) \times \left(\frac{1}{\delta^2}\left(-\frac{{k_-}^2\delta^2}{8\pi}\frac{\boldsymbol{\xi}-\boldsymbol{\eta}}{|\boldsymbol{\xi}-\boldsymbol{\eta}|} + \mathcal{O}(\delta^3) \right) \times \hat{\boldsymbol{a}}_j(\boldsymbol{\eta}) \right) \delta^2 \, \mathrm{d}s(\boldsymbol{\eta}) \\
&= \delta^2 \int_{\partial B} \boldsymbol{\nu}(\boldsymbol{\xi}) \times \left(\left(-\frac{{k_-}^2}{8\pi}\frac{\boldsymbol{\xi}-\boldsymbol{\eta}}{|\boldsymbol{\xi}-\boldsymbol{\eta}|} + \mathcal{O}(\delta) \right) \times \hat{\boldsymbol{a}}_j(\boldsymbol{\eta}) \right) \mathrm{d}s(\boldsymbol{\eta}) \\
&=: (E^{k_-}_M\hat{\boldsymbol{a}}_j)(\boldsymbol{\xi}).
\end{aligned}$$

The kernel of E_M^{k-} is pseudo–homogeneous of class -2 (cf. [91, pp. 168–175]) and hence E_M^{k-} is continuous from $H^{-1/2}(\partial B;\mathbb{C})^3$ into $H^{3/2}(\partial B;\mathbb{C})^3$; cf. [91, Theorem 4.3.2]. So E_M^{k-} is also continuous from $\boldsymbol{H}_{\rm div}^{-1/2}(\partial B)$ into $\boldsymbol{H}_{\rm div}^{-1/2}(\partial B)$, in particular it is $\mathcal{O}(\delta^2)$ in $\mathcal{L}(\boldsymbol{H}_{\rm div}^{-1/2}(\partial B))$ as $\delta\to 0$. Thus, by the continuity properties of the operators $M_{D_\delta}^{k-}$, M_B^0, and E_M^{k-}, letting $j\to\infty$, we obtain that

$$M_{D_\delta}^{k-}\boldsymbol{a} = (M_B^0\hat{\boldsymbol{a}})^\vee + (E_M^{k-}\hat{\boldsymbol{a}})^\vee.$$

Recalling (3.29), it remains to estimate the norm of $R_{D_\delta}^m\boldsymbol{a}$. For this purpose, we denote by $\tilde{R}_{D_\delta}^m\boldsymbol{a}$ the extension of $R_{D_\delta}^m\boldsymbol{a}$ to $\boldsymbol{H}(\mathbf{curl},D_\delta)$ (with respect to the trace operator γ_t), which is obtained canonically from (3.28) via

$$\tilde{R}_{D_\delta}^m\boldsymbol{a} := \int_{\partial D_\delta}\mathbf{curl}_x F^m(\cdot,\boldsymbol{y})\boldsymbol{a}(\boldsymbol{y})\,\mathrm{d}s(\boldsymbol{y}) \qquad \text{in } D_\delta.$$

Then, because F^m is smooth near the scatterer,

$$\begin{aligned}
\|R_{D_\delta}^m\boldsymbol{a}\|^2_{\boldsymbol{H}_{\rm div}^{-1/2}(\partial D_\delta)} &= \inf_{\substack{\boldsymbol{u}\in\boldsymbol{H}(\mathbf{curl},D_\delta)\\ \gamma_t(\boldsymbol{u})=R_{D_\delta}^m\boldsymbol{a}}}\|\boldsymbol{u}\|^2_{\boldsymbol{H}(\mathbf{curl},D_\delta)} \le \|\tilde{R}_{D_\delta}^m\boldsymbol{a}\|^2_{\boldsymbol{H}(\mathbf{curl},D_\delta)}\\
&= \int_{D_\delta}\Big|\int_{\partial D_\delta}\mathbf{curl}_x F^m(\boldsymbol{x},\boldsymbol{y})\boldsymbol{a}(\boldsymbol{y})\,\mathrm{d}s(\boldsymbol{y})\Big|^2\,\mathrm{d}\boldsymbol{x}\\
&\quad+\int_{D_\delta}\Big|\mathbf{curl}_x\int_{\partial D_\delta}\mathbf{curl}_x F^m(\boldsymbol{x},\boldsymbol{y})\boldsymbol{a}(\boldsymbol{y})\,\mathrm{d}s(\boldsymbol{y})\Big|^2\,\mathrm{d}\boldsymbol{x}\\
&\le \int_{D_\delta}\Big(\|\mathbf{curl}_x F^m(\boldsymbol{x},\cdot)\|^2_{\boldsymbol{H}_{\rm curl}^{-1/2}(\partial D_\delta)}\\
&\qquad+\|\mathbf{curl}_x\,\mathbf{curl}_x F^m(\boldsymbol{x},\cdot)\|^2_{\boldsymbol{H}_{\rm curl}^{-1/2}(\partial D_\delta)}\Big)\|\boldsymbol{a}\|^2_{\boldsymbol{H}_{\rm div}^{-1/2}(\partial D_\delta)}\,\mathrm{d}\boldsymbol{x}\\
&\le C\delta^3\|\boldsymbol{a}\|^2_{\boldsymbol{H}_{\rm div}^{-1/2}(\partial D_\delta)}\int_{D_\delta}1\,\mathrm{d}\boldsymbol{x} \le C\delta^6\|\boldsymbol{a}\|^2_{\boldsymbol{H}_{\rm div}^{-1/2}(\partial D_\delta)}.
\end{aligned}$$

Using (3.44), we find that

$$\begin{aligned}
\|(R_{D_\delta}^m\boldsymbol{a})^\wedge\|_{\boldsymbol{H}_{\rm div}^{-1/2}(\partial B)} &\le \delta^{-\frac{3}{2}}\|R_{D_\delta}^m\boldsymbol{a}\|_{\boldsymbol{H}_{\rm div}^{-1/2}(\partial D_\delta)} \le \delta^{-\frac{3}{2}}C\delta^3\|\boldsymbol{a}\|_{\boldsymbol{H}_{\rm div}^{-1/2}(\partial D_\delta)}\\
&\le \delta^{\frac{1}{2}}C\delta^{\frac{3}{2}}\|\hat{\boldsymbol{a}}\|_{\boldsymbol{H}_{\rm div}^{-1/2}(\partial B)} = C\delta^2\|\hat{\boldsymbol{a}}\|_{\boldsymbol{H}_{\rm div}^{-1/2}(\partial B)}.
\end{aligned}$$

Thus, we define

$$E_M^m\boldsymbol{b} := E_M^{k-}\boldsymbol{b} + (R_{D_\delta}^m\check{\boldsymbol{b}})^\wedge, \qquad \boldsymbol{b}\in\boldsymbol{H}_{\rm div}^{-1/2}(\partial B),$$

and obtain the desired result. □

For $\boldsymbol{a} \in \boldsymbol{H}_{\mathrm{div}}^{-1/2}(\partial D_\delta)$, Lemma 3.9 yields

$$\Big(\frac{1}{2}I + M_{D_\delta}^m\Big)\boldsymbol{a} = \Big(\Big(\frac{1}{2}I + M_B^0 + E_M^m\Big)\hat{\boldsymbol{a}}\Big)^\vee$$

and thus,

$$\Big(\frac{1}{2}I + M_{D_\delta}^m\Big)^{-1}\boldsymbol{a} = \Big(\Big(\frac{1}{2}I + M_B^0 + E_M^m\Big)^{-1}\hat{\boldsymbol{a}}\Big)^\vee.$$

So, we obtain from Lemma 2.2 that

$$\Big(\frac{1}{2}I + M_{D_\delta}^m\Big)^{-1}\boldsymbol{a} = \Big(\Big(\frac{1}{2}I + M_B^0\Big)^{-1}\hat{\boldsymbol{a}}\Big)^\vee + (\tilde{E}_M^m\hat{\boldsymbol{a}})^\vee, \tag{3.50}$$

where $\tilde{E}_M^m$ is a bounded linear operator, independent of $\boldsymbol{a}$, which is $\mathcal{O}(\delta^2)$ in $\mathcal{L}(\boldsymbol{H}_{\mathrm{div}}^{-1/2}(\partial B))$ as $\delta \to 0$.

3.7 Asymptotic Expansion

In this section, we first expand the three operators L_δ, $L_\delta^\top$, and F_δ occurring in the factorization (3.43) of the measurement operator G_δ separately as the inhomogeneity size δ tends to zero. Then, we use these expansions to calculate the leading order term in the asymptotic expansion of G_δ.

First, we consider the exterior Maxwell problem (3.37) and study the asymptotic behavior of the operator L_δ from (3.38). A radiating solution of this problem is given by

$$\begin{aligned}
\boldsymbol{E}^\psi &:= \frac{\varepsilon_-}{\varepsilon}\mathbf{curl}\mathcal{A}_{D_\delta}^m\Big(\frac{1}{2}I + M_{D_\delta}^m\Big)^{-1}\boldsymbol{\psi} && \text{in } \mathbb{R}^3_0 \setminus \overline{D_\delta},\\
\boldsymbol{H}^\psi &:= \frac{1}{\mathrm{i}\,\omega\mu}\mathbf{curl}\boldsymbol{E}^\psi\\
&= -\mathrm{i}\,\omega\varepsilon_- \int_{\partial D_\delta} \mathbb{G}^m(\cdot,\boldsymbol{y})\Big(\Big(\frac{1}{2}I + M_{D_\delta}^m\Big)^{-1}\boldsymbol{\psi}\Big)(\boldsymbol{y})\,\mathrm{d}s(\boldsymbol{y}) && \text{in } \mathbb{R}^3_0 \setminus \overline{D_\delta}.
\end{aligned}$$

By Taylor expansion, we obtain for $\boldsymbol{x} \in \mathcal{M}$ and $\boldsymbol{\eta} \in \partial B$ as $\delta \to 0$ that

$$\mathbb{G}^m(\boldsymbol{x}, \delta\boldsymbol{\eta} + \boldsymbol{z}) = \mathbb{G}^m(\boldsymbol{x},\boldsymbol{z}) + \delta\sum_{j=1}^3 \frac{\partial\,\mathbb{G}^m}{\partial y_j}(\boldsymbol{x},\boldsymbol{z})\eta_j + \mathcal{O}(\delta^2).$$

Thus, by a change of coordinates, $\boldsymbol{\eta} := \frac{\boldsymbol{y}-\boldsymbol{z}}{\delta}$, and applying (3.50), we have

$$\begin{aligned}
\boldsymbol{H}^\psi(\boldsymbol{x}) &= -\mathrm{i}\,\omega\varepsilon_- \int_{\partial B} \mathbb{G}^m(\boldsymbol{x},\delta\boldsymbol{\eta}+\boldsymbol{z})\Big(\Big(\frac{1}{2}I + M_{D_\delta}^m\Big)^{-1}\boldsymbol{\psi}\Big)(\delta\boldsymbol{\eta}+\boldsymbol{z})\delta^2\,\mathrm{d}s(\boldsymbol{\eta})\\
&= -\mathrm{i}\,\omega\varepsilon_-\delta^2 \int_{\partial B} \mathbb{G}^m(\boldsymbol{x},\delta\boldsymbol{\eta}+\boldsymbol{z})\Big(\Big(\frac{1}{2}I + M_B^0\Big)^{-1}\hat{\boldsymbol{\psi}}\Big)(\boldsymbol{\eta})\,\mathrm{d}s(\boldsymbol{\eta}) + \mathcal{O}(\delta^4)\\
&= -\mathrm{i}\,\omega\varepsilon_-\delta^2\,\mathbb{G}^m(\boldsymbol{x},\boldsymbol{z}) \int_{\partial B} \Big(\Big(\frac{1}{2}I + M_B^0\Big)^{-1}\hat{\boldsymbol{\psi}}\Big)(\boldsymbol{\eta})\,\mathrm{d}s(\boldsymbol{\eta})\\
&\quad -\mathrm{i}\,\omega\varepsilon_-\delta^3 \int_{\partial B}\sum_{j=1}^3 \eta_j \frac{\partial\,\mathbb{G}^m}{\partial y_j}(\boldsymbol{x},\boldsymbol{z})\Big(\Big(\frac{1}{2}I + M_B^0\Big)^{-1}\hat{\boldsymbol{\psi}}\Big)(\boldsymbol{\eta})\,\mathrm{d}s(\boldsymbol{\eta}) + \mathcal{O}(\delta^4)
\end{aligned}$$

for $\boldsymbol{x} \in \mathcal{M}$ as $\delta \to 0$. The last term on the right–hand side is bounded by $C\delta^4 \|\hat{\boldsymbol{\psi}}\|_{\boldsymbol{H}_{\mathrm{div}}^{-1/2}(\partial B)}$ uniformly for $\boldsymbol{x} \in \mathcal{M}$, where the constant $C > 0$ is independent of δ and $\boldsymbol{\psi}$. We define $L_0 : \boldsymbol{H}_{\mathrm{div}}^{-1/2}(\partial B) \to \boldsymbol{L}^2(\mathcal{M})$,

$$L_0 \boldsymbol{a} := -\,\mathrm{i}\,\omega\varepsilon_-\, \mathbb{G}^m(\cdot, \boldsymbol{z}) \int_{\partial B} \Big(\Big(\frac{1}{2} I + M_B^0 \Big)^{-1} \boldsymbol{a} \Big)(\boldsymbol{\eta})\, \mathrm{d}s(\boldsymbol{\eta}), \tag{3.51}$$

and $L_1 : \boldsymbol{H}_{\mathrm{div}}^{-1/2}(\partial B) \to \boldsymbol{L}^2(\mathcal{M})$,

$$L_1 \boldsymbol{a} := -\,\mathrm{i}\,\omega\varepsilon_- \int_{\partial B} \sum_{j=1}^{3} \eta_j \frac{\partial\, \mathbb{G}^m}{\partial y_j}(\cdot, \boldsymbol{z}) \Big(\Big(\frac{1}{2} I + M_B^0 \Big)^{-1} \boldsymbol{a} \Big)(\boldsymbol{\eta})\, \mathrm{d}s(\boldsymbol{\eta}). \tag{3.52}$$

Then, L_0 and L_1 are bounded linear operators, and we have shown the following asymptotic behavior.

Proposition 3.10. *For all $\boldsymbol{\psi} \in \boldsymbol{H}_{\mathrm{div}}^{-1/2}(\partial D_\delta)$,*

$$L_\delta \boldsymbol{\psi} = \delta^2 L_0 \hat{\boldsymbol{\psi}} + \delta^3 L_1 \hat{\boldsymbol{\psi}} + E_L \hat{\boldsymbol{\psi}},$$

where E_L is a bounded linear operator, independent of $\boldsymbol{\psi}$, which is $\mathcal{O}(\delta^4)$ in $\mathcal{L}(\boldsymbol{H}_{\mathrm{div}}^{-1/2}(\partial B), \boldsymbol{L}^2(\mathcal{M}))$ as $\delta \to 0$.

Remark 3.11. Note that by duality the transpose $E_L^\top$ of E_L is $\mathcal{O}(\delta^4)$ in $\mathcal{L}(\boldsymbol{L}^2(\mathcal{M}), \boldsymbol{H}_{\mathrm{curl}}^{-1/2}(\partial B))$.

Next, we consider the asymptotic behavior of the operator $L_\delta^\top$ from (3.40). Let $\boldsymbol{\varphi} \in \boldsymbol{L}^2(\mathcal{M})$ and $\boldsymbol{\psi} \in \boldsymbol{H}_{\mathrm{div}}^{-1/2}(\partial D_\delta)$. For $X \in \{B, D_\delta\}$, we denote by $\langle \cdot, \cdot \rangle_{\partial X}$ the dual pairing between $\boldsymbol{H}_{\mathrm{div}}^{-1/2}(\partial X)$ and $\boldsymbol{H}_{\mathrm{curl}}^{-1/2}(\partial X)$, and $\langle \cdot, \cdot \rangle_{\mathcal{M}}$ is the bilinear form from (3.39). Using Proposition 3.10, we can calculate

$$\begin{aligned}
\langle L_\delta^\top \boldsymbol{\varphi}, \boldsymbol{\psi} \rangle_{\partial D_\delta} &= \big\langle \boldsymbol{\varphi}, L_\delta \boldsymbol{\psi} \big\rangle_{\mathcal{M}} = \big\langle \boldsymbol{\varphi}, \delta^2 L_0 \hat{\boldsymbol{\psi}} + \delta^3 L_1 \hat{\boldsymbol{\psi}} + E_L \hat{\boldsymbol{\psi}} \big\rangle_{\mathcal{M}} \\
&= \big\langle \delta^2 L_0^\top \boldsymbol{\varphi} + \delta^3 L_1^\top \boldsymbol{\varphi} + E_L^\top \boldsymbol{\varphi}, \hat{\boldsymbol{\psi}} \big\rangle_{\partial B} \\
&= \big\langle (L_0^\top \boldsymbol{\varphi})^\vee + \delta (L_1^\top \boldsymbol{\varphi})^\vee + \delta^{-2} (E_L^\top \boldsymbol{\varphi})^\vee, \boldsymbol{\psi} \big\rangle_{\partial D_\delta},
\end{aligned}$$

where $L_0^\top, L_1^\top : \boldsymbol{L}^2(\mathcal{M}) \to \boldsymbol{H}_{\mathrm{curl}}^{-1/2}(\partial B)$ are the dual operators of L_0 and L_1, respectively. Recalling Remark 3.11, we obtain the following asymptotic behavior.

Proposition 3.12. *For all $\boldsymbol{\varphi} \in \boldsymbol{L}^2(\mathcal{M})$,*

$$L_\delta^\top \boldsymbol{\varphi} = (L_0^\top \boldsymbol{\varphi})^\vee + \delta (L_1^\top \boldsymbol{\varphi})^\vee + \delta^{-2} (E_L^\top \boldsymbol{\varphi})^\vee,$$

where $E_L^\top$ is a bounded linear operator, independent of $\boldsymbol{\varphi}$, which is $\mathcal{O}(\delta^4)$ in $\mathcal{L}(\boldsymbol{L}^2(\mathcal{M}), \boldsymbol{H}_{\mathrm{curl}}^{-1/2}(\partial B))$ as $\delta \to 0$.

Now, we calculate the operators $L_0^\top$ and $L_1^\top$ explicitly. Let $\boldsymbol{\varphi} \in \boldsymbol{L}^2(\mathcal{M})$ and $\boldsymbol{a} \in \boldsymbol{H}_{\mathrm{div}}^{-1/2}(\partial B)$. Recalling the definition of the operator L_0 from (3.51), we find that

$$\begin{aligned}
&\langle \boldsymbol{\varphi}, L_0 \boldsymbol{a} \rangle_{\mathcal{M}} \\
&= \int_{\mathcal{M}} \Big(-\mathrm{i}\,\omega\varepsilon_- \, \mathbb{G}^m(\boldsymbol{x}, \boldsymbol{z}) \int_{\partial B} \Big(\Big(\frac{1}{2} I + M_B^0 \Big)^{-1} \boldsymbol{a} \Big)(\boldsymbol{\eta}) \, \mathrm{d}s(\boldsymbol{\eta}) \Big) \cdot \boldsymbol{\varphi}(\boldsymbol{x}) \, \mathrm{d}s(\boldsymbol{x}) \\
&= \Big(-\mathrm{i}\,\omega\varepsilon_- \int_{\mathcal{M}} \mathbb{G}^{m\top}(\boldsymbol{x}, \boldsymbol{z}) \boldsymbol{\varphi}(\boldsymbol{x}) \, \mathrm{d}s(\boldsymbol{x}) \Big) \cdot \int_{\partial B} \Big(\Big(\frac{1}{2} I + M_B^0 \Big)^{-1} \boldsymbol{a} \Big)(\boldsymbol{\eta}) \, \mathrm{d}s(\boldsymbol{\eta}).
\end{aligned}$$

Recalling (B.7b) and (3.34), we obtain

$$\begin{aligned}
\langle \boldsymbol{\varphi}, L_0 \boldsymbol{a} \rangle_{\mathcal{M}} &= \frac{1}{\mathrm{i}\,\omega\mu_+} \boldsymbol{H}^i(\boldsymbol{z}) \cdot \int_{\partial B} \Big(\Big(\frac{1}{2} I + M_B^0 \Big)^{-1} \boldsymbol{a} \Big)(\boldsymbol{\eta}) \, \mathrm{d}s(\boldsymbol{\eta}) \\
&= \int_{\partial B} \frac{1}{\mathrm{i}\,\omega\mu_+} \Big(\Big(\frac{1}{2} I + M_B^{0\top} \Big)^{-1} \pi_t\big(\boldsymbol{H}^i(\boldsymbol{z}) \big) \Big)(\boldsymbol{\xi}) \cdot \boldsymbol{a}(\boldsymbol{\xi}) \, \mathrm{d}s(\boldsymbol{\xi}),
\end{aligned}$$

where π_t denotes the projection on the tangent plane to ∂B. Therefore, we have

$$L_0^\top \boldsymbol{\varphi} = \frac{1}{\mathrm{i}\,\omega\mu_+} \Big(\frac{1}{2} I + M_B^{0\top} \Big)^{-1} \pi_t(\boldsymbol{H}^i(\boldsymbol{z})). \tag{3.53}$$

In the same way, we obtain from (3.52) that

$$\begin{aligned}
&\langle \boldsymbol{\varphi}, L_1 \boldsymbol{a} \rangle_{\mathcal{M}} \\
&= \int_{\mathcal{M}} \Big(-\mathrm{i}\,\omega\varepsilon_- \int_{\partial B} \sum_{j=1}^3 \eta_j \frac{\partial \, \mathbb{G}^m}{\partial y_j}(\boldsymbol{x}, \boldsymbol{z}) \Big(\Big(\frac{1}{2} I + M_B^0 \Big)^{-1} \boldsymbol{a} \Big)(\boldsymbol{\eta}) \, \mathrm{d}s(\boldsymbol{\eta}) \Big) \\
&\qquad \cdot \boldsymbol{\varphi}(\boldsymbol{x}) \, \mathrm{d}s(\boldsymbol{x}) \\
&= \sum_{j=1}^3 \Big(-\mathrm{i}\,\omega\varepsilon_- \int_{\mathcal{M}} \Big(\frac{\partial \, \mathbb{G}^m}{\partial y_j}(\boldsymbol{x}, \boldsymbol{z}) \Big)^\top \boldsymbol{\varphi}(\boldsymbol{x}) \, \mathrm{d}s(\boldsymbol{x}) \Big) \\
&\qquad \cdot \int_{\partial B} \eta_j \Big(\Big(\frac{1}{2} I + M_B^0 \Big)^{-1} \boldsymbol{a} \Big)(\boldsymbol{\eta}) \, \mathrm{d}s(\boldsymbol{\eta}) \\
&= \sum_{j=1}^3 \Big(\frac{1}{\mathrm{i}\,\omega\mu_+} \frac{\partial \boldsymbol{H}^i}{\partial y_j}(\boldsymbol{z}) \Big) \cdot \int_{\partial B} \eta_j \Big(\Big(\frac{1}{2} I + M_B^0 \Big)^{-1} \boldsymbol{a} \Big)(\boldsymbol{\eta}) \, \mathrm{d}s(\boldsymbol{\eta}) \\
&= \int_{\partial B} \frac{1}{\mathrm{i}\,\omega\mu_+} \Big(\Big(\frac{1}{2} I + M_B^{0\top} \Big)^{-1} \pi_t \Big(\sum_{j=1}^3 \eta_j \frac{\partial \boldsymbol{H}^i}{\partial y_j}(\boldsymbol{z}) \Big) \Big)(\boldsymbol{\xi}) \cdot \boldsymbol{a}(\boldsymbol{\xi}) \, \mathrm{d}s(\boldsymbol{\xi}).
\end{aligned}$$

Note that in the last line of this computation η_j is the jth component of the surface variable on ∂B. Therefore, we have

$$L_1^\top \boldsymbol{\varphi} = \frac{1}{\mathrm{i}\,\omega\mu_+} \Big(\frac{1}{2} I + M_B^{0\top} \Big)^{-1} \pi_t \Big(\sum_{j=1}^3 \eta_j \frac{\partial \boldsymbol{H}^i}{\partial y_j}(\boldsymbol{z}) \Big). \tag{3.54}$$

We return to the diffraction problem (3.41) and the operator F_δ from (3.42). Given $\boldsymbol{\chi} \in \boldsymbol{H}_{\mathrm{curl}}^{-1/2}(\partial D_\delta)$, we define

$$\begin{aligned}
\boldsymbol{E}^d &:= -\frac{1}{\mathrm{i}\,\omega\varepsilon}\mathbf{curl}\frac{\mu_-}{\mu}\mathbf{curl}\mathcal{A}^e_{D_\delta}(\boldsymbol{\nu}\times\boldsymbol{\chi}) && \text{in } \mathbb{R}^3_0 \setminus \partial D_\delta,\\
\boldsymbol{H}^d &:= \frac{\mu_-}{\mu}\mathbf{curl}\mathcal{A}^e_{D_\delta}(\boldsymbol{\nu}\times\boldsymbol{\chi}) && \text{in } \mathbb{R}^3_0 \setminus \partial D_\delta.
\end{aligned}$$

Then, $(\boldsymbol{E}^d, \boldsymbol{H}^d)$ is a radiating solution to (3.41), and recalling (3.14), (3.22), and (3.2), we find that

$$\begin{aligned}
&\boldsymbol{\nu}\times\boldsymbol{E}^d\big|_{\partial D_\delta}(\boldsymbol{x})\\
&\qquad= -\frac{1}{\mathrm{i}\,\omega\varepsilon_-}\boldsymbol{\nu}(\boldsymbol{x})\times\mathbf{curl}_x\,\mathbf{curl}_x\int_{\partial D_\delta}\Pi^e(\boldsymbol{x},\boldsymbol{y})(\boldsymbol{\nu}\times\boldsymbol{\chi})(\boldsymbol{y})\,\mathrm{d}s(\boldsymbol{y})\\
&\qquad= \mathrm{i}\,\omega\mu_-\boldsymbol{\nu}(\boldsymbol{x})\times\int_{\partial D_\delta}\Phi_{k_-}(\boldsymbol{x}-\boldsymbol{y})(\boldsymbol{\nu}\times\boldsymbol{\chi})(\boldsymbol{y})\,\mathrm{d}s(\boldsymbol{y})\\
&\qquad\quad+\frac{1}{\mathrm{i}\,\omega\varepsilon_-}\boldsymbol{\nu}(\boldsymbol{x})\times\int_{\partial D_\delta}\nabla_x\Phi_{k_-}(\boldsymbol{x}-\boldsymbol{y})(\mathrm{curl}_{\partial D_\delta}\boldsymbol{\chi})(\boldsymbol{y})\,\mathrm{d}s(\boldsymbol{y})\\
&\qquad\quad-\frac{1}{\mathrm{i}\,\omega\varepsilon_-}\boldsymbol{\nu}(\boldsymbol{x})\times\mathbf{curl}_x\,\mathbf{curl}_x\int_{\partial D_\delta}F^e(\boldsymbol{x},\boldsymbol{y})(\boldsymbol{\nu}\times\boldsymbol{\chi})(\boldsymbol{y})\,\mathrm{d}s(\boldsymbol{y})\,.
\end{aligned}$$

Remark 3.13. The previous formula employs a slight abuse of notation, because pointwise evaluation is not defined for elements of $\boldsymbol{H}_{\mathrm{div}}^{-1/2}(\partial D_\delta)$. Nontheless, we prefer this notation for the sake of readability.

Define $P_{D_\delta} : \boldsymbol{H}_{\mathrm{curl}}^{-1/2}(\partial D_\delta) \to \boldsymbol{H}_{\mathrm{div}}^{-1/2}(\partial D_\delta)$ by

$$P_{D_\delta}\boldsymbol{a} := -\frac{1}{\mathrm{i}\,\omega\varepsilon_-}\boldsymbol{\nu}\times\mathbf{curl}\,\mathbf{curl}\int_{\partial D_\delta}F^e(\cdot,\boldsymbol{y})(\boldsymbol{\nu}\times\boldsymbol{a})(\boldsymbol{y})\,\mathrm{d}s(\boldsymbol{y})$$

for $\boldsymbol{a} \in \boldsymbol{H}_{\mathrm{curl}}^{-1/2}(\partial D_\delta)$. Then, we can see as in the proof of Lemma 3.9 that

$$\|(P_{D_\delta}\boldsymbol{a})^\wedge\|_{\boldsymbol{H}_{\mathrm{div}}^{-1/2}(\partial B)} \le C\delta^2\|\hat{\boldsymbol{a}}\|_{\boldsymbol{H}_{\mathrm{curl}}^{-1/2}(\partial B)}.$$

Therefore, by a change of coordinates, applying (3.47) and (3.48), we obtain

$$\begin{aligned}
&\big(\boldsymbol{\nu}\times\boldsymbol{E}^d\big|_{\partial D_\delta}\big)^\wedge(\boldsymbol{\xi})\\
&\quad= \mathrm{i}\,\omega\mu_-\boldsymbol{\nu}(\delta\boldsymbol{\xi}+\boldsymbol{z})\times\int_{\partial B}\Phi_{k_-}(\delta(\boldsymbol{\xi}-\boldsymbol{\eta}))(\boldsymbol{\nu}\times\boldsymbol{\chi})(\delta\boldsymbol{\eta}+\boldsymbol{z})\delta^2\,\mathrm{d}s(\boldsymbol{\eta})\\
&\qquad+\frac{1}{\mathrm{i}\,\omega\varepsilon_-}\boldsymbol{\nu}(\delta\boldsymbol{\xi}+\boldsymbol{z})\times\int_{\partial B}\nabla_x\Phi_{k_-}(\delta(\boldsymbol{\xi}-\boldsymbol{\eta}))(\mathrm{curl}_{\partial D_\delta}\boldsymbol{\chi})(\delta\boldsymbol{\eta}+\boldsymbol{z})\delta^2\,\mathrm{d}s(\boldsymbol{\eta})\\
&\qquad+\mathcal{O}(\delta^2)\\
&\quad= \delta^{-1}\frac{1}{\mathrm{i}\,\omega\varepsilon_-}\boldsymbol{\nu}(\boldsymbol{\xi})\times\int_{\partial B}\nabla_{\boldsymbol{\xi}}\Phi_0(\boldsymbol{\xi}-\boldsymbol{\eta})(\mathrm{curl}_{\partial B}\hat{\boldsymbol{\chi}})(\boldsymbol{\eta})\,\mathrm{d}s(\boldsymbol{\eta})\\
&\qquad+\delta\,\mathrm{i}\,\omega\mu_-\boldsymbol{\nu}(\boldsymbol{\xi})\times\int_{\partial B}\Phi_0(\boldsymbol{\xi}-\boldsymbol{\eta})(\boldsymbol{\nu}\times\hat{\boldsymbol{\chi}})(\boldsymbol{\eta})\,\mathrm{d}s(\boldsymbol{\eta})\\
&\qquad+\delta\,\mathrm{i}\,\omega\mu_-\boldsymbol{\nu}(\boldsymbol{\xi})\times\int_{\partial B}\frac{1}{8\pi}\frac{\boldsymbol{\xi}-\boldsymbol{\eta}}{|\boldsymbol{\xi}-\boldsymbol{\eta}|}(\mathrm{curl}_{\partial B}\hat{\boldsymbol{\chi}})(\boldsymbol{\eta})\,\mathrm{d}s(\boldsymbol{\eta})+\mathcal{O}(\delta^2)
\end{aligned}$$

as $\delta \to 0$. The $\mathcal{O}(\delta^2)$–term in (3.47) and the $\mathcal{O}(\delta^3)$–term in (3.48) define pseudo–homogeneous kernels of class -3 (cf. [91, pp. 168–174]), i.e., the corresponding integral operators are continuous from $H^{-1/2}(\partial B;\mathbb{C})^3$ to $H^{3/2}(\partial B;\mathbb{C})^3$ ($H^{5/2}(\partial B;\mathbb{C})^3$ if ∂B is smooth enough); cf. [91, Theorem 4.4.1]. Thus, these operators are also continuous from $\boldsymbol{H}_{\mathrm{curl}}^{-1/2}(\partial B)$ to $\boldsymbol{H}_{\mathrm{div}}^{-1/2}(\partial B)$, and together with the (constant) $\mathcal{O}(\delta)$–term in (3.47) they lead to terms of order $\mathcal{O}(\delta^2)$ in $\boldsymbol{H}_{\mathrm{div}}^{-1/2}(\partial B)$ in the asymptotic expansion of $\boldsymbol{\nu}\times\boldsymbol{E}^d|_{\partial D_\delta}$ as $\delta\to 0$.

We define $F_0 : \boldsymbol{H}_{\mathrm{curl}}^{-1/2}(\partial B) \to \boldsymbol{H}_{\mathrm{div}}^{-1/2}(\partial B)$,

$$\begin{aligned}(F_0\boldsymbol{a})(\boldsymbol{\xi}) :=& \frac{1}{\mathrm{i}\,\omega\varepsilon_-}\boldsymbol{\nu}(\boldsymbol{\xi})\times\int_{\partial B}\nabla_{\boldsymbol{\xi}}\Phi_0(\boldsymbol{\xi}-\boldsymbol{\eta})(\mathrm{curl}_{\partial B}\,\boldsymbol{a})(\boldsymbol{\eta})\,\mathrm{d}s(\boldsymbol{\eta})\\ =& -\frac{1}{\mathrm{i}\,\omega\varepsilon_-}N_B^0\boldsymbol{a},\end{aligned} \tag{3.55}$$

and $F_1 :\ \boldsymbol{H}_{\mathrm{curl}}^{-1/2}(\partial B) \to \boldsymbol{H}_{\mathrm{div}}^{-1/2}(\partial B)$,

$$\begin{aligned}(F_1\boldsymbol{a})(\boldsymbol{\xi}) :=& \,\mathrm{i}\,\omega\mu_-\big(\boldsymbol{\nu}\times\mathcal{A}_B^0(\boldsymbol{\nu}\times\boldsymbol{a})\big|_{\partial B}\big)(\boldsymbol{\xi})\\ &+\mathrm{i}\,\omega\mu_-\boldsymbol{\nu}(\boldsymbol{\xi})\times\int_{\partial B}\frac{1}{8\pi}\frac{\boldsymbol{\xi}-\boldsymbol{\eta}}{|\boldsymbol{\xi}-\boldsymbol{\eta}|}(\mathrm{curl}_{\partial B}\,\boldsymbol{a})(\boldsymbol{\eta})\,\mathrm{d}s(\boldsymbol{\eta}).\end{aligned} \tag{3.56}$$

From Lemma 3.2 (in the potential theoretic limit), we find that F_0 and the first part of F_1 are bounded. Moreover, because the kernel of the second part of F_1 is homogeneous of class -2 (cf. [91, Sec. 4.3.2]) also the second part of F_1 is continuous. We obtain the following asymptotic behavior.

Proposition 3.14. *For all $\boldsymbol{\chi}\in\boldsymbol{H}_{\mathrm{curl}}^{-1/2}(\partial D_\delta)$,*

$$F_\delta\boldsymbol{\chi} = \delta^{-1}(F_0\hat{\boldsymbol{\chi}})^\vee + \delta(F_1\hat{\boldsymbol{\chi}})^\vee + (E_F\hat{\boldsymbol{\chi}})^\vee, \tag{3.57}$$

where E_F is a bounded linear operator, independent of $\boldsymbol{\chi}$, which is $\mathcal{O}(\delta^2)$ in $\mathcal{L}(\boldsymbol{H}_{\mathrm{curl}}^{-1/2}(\partial B),\boldsymbol{H}_{\mathrm{div}}^{-1/2}(\partial B))$ as $\delta\to 0$.

Next, we consider the boundary value problem of finding $\boldsymbol{u}\in\boldsymbol{H}(\mathbf{curl},B)$ such that

$$\mathbf{curl}\,\mathbf{curl}\,\boldsymbol{u} = 0 \qquad \text{in } B, \tag{3.58a}$$

$$\mathrm{div}\,\boldsymbol{u} = 0 \qquad \text{in } B, \tag{3.58b}$$

$$\boldsymbol{\nu}\times\boldsymbol{u} = \boldsymbol{c} \qquad \text{on } \partial B, \tag{3.58c}$$

where $\boldsymbol{c}\in\boldsymbol{H}_{\mathrm{div}}^{-1/2}(\partial B)$ is a given tangential function. We show that (3.58) has at most one solution and use this fact to prove that $L_0F_0 = 0$ on $\boldsymbol{H}_{\mathrm{curl}}^{-1/2}(\partial B)$ and $F_0L_0^\top = 0$ on $\boldsymbol{L}^2(\mathcal{M})$.

Lemma 3.15. *Let* $\boldsymbol{c} \in \boldsymbol{H}_{\mathrm{div}}^{-1/2}(\partial B)$. *Then, the boundary value problem* (3.58) *has at most one solution in* $\boldsymbol{H}(\mathbf{curl}, B)$.

Proof. Applying an integration by parts (3.1), we obtain for any solution $\boldsymbol{u} \in \boldsymbol{H}_0(\mathbf{curl}, B)$ of (3.58) with homogeneous boundary condition $\boldsymbol{c} = 0$ that

$$\begin{aligned} 0 &= \int_B \mathbf{curl}\,\mathbf{curl}\boldsymbol{u}(\boldsymbol{x}) \cdot \overline{\boldsymbol{u}(\boldsymbol{x})}\,\mathrm{d}\boldsymbol{x} \\ &= \int_B |\mathbf{curl}\boldsymbol{u}(\boldsymbol{x})|^2\,\mathrm{d}\boldsymbol{x} + \big\langle \gamma_t(\mathbf{curl}\boldsymbol{u}), \overline{\pi_t(\boldsymbol{u})}\big\rangle_{\partial B} = \int_B |\mathbf{curl}\boldsymbol{u}(\boldsymbol{x})|^2\,\mathrm{d}\boldsymbol{x}. \end{aligned}$$

Hence, $\mathbf{curl}\boldsymbol{u} = 0$ in B, and because the boundaries of all components of B are assumed to be connected, we obtain from [88, Theorems 3.41 and 3.42] a scalar potential $p \in H^1(B;\mathbb{C})$ with $\gamma_0(p) = 0$ on ∂B such that $\boldsymbol{u} = \nabla p$. Because $\Delta p = \operatorname{div}\boldsymbol{u} = 0$ in B by (3.58b), we have $p = 0$ in B. Hence, $\boldsymbol{u} = \nabla p = 0$ in B. □

Proposition 3.16. *Let* $\boldsymbol{\varphi} \in \boldsymbol{L}^2(\mathcal{M})$ *and* $\boldsymbol{a} \in \boldsymbol{H}_{\mathrm{curl}}^{-1/2}(\partial B)$. *Then,* $L_0 F_0 \boldsymbol{a} = 0$ *and* $F_0 L_0^\top \boldsymbol{\varphi} = 0$.

Proof. Given $\boldsymbol{\varphi} \in \boldsymbol{L}^2(\mathcal{M})$, we find by (3.53) and (3.55) that on ∂B

$$\begin{aligned} F_0 L_0^\top \boldsymbol{\varphi} =& \frac{1}{\omega^2\varepsilon_-\mu_+} N_B^0 \Big(\frac{1}{2}I + {M_B^0}^\top\Big)^{-1} \pi_t\big(\boldsymbol{H}^i(\boldsymbol{z})\big) \\ =& \frac{1}{\omega^2\varepsilon_-\mu_+} \boldsymbol{\nu} \times \mathbf{curl}\,\mathbf{curl}\mathcal{A}_B^0\Big(\boldsymbol{\nu} \times \Big(\frac{1}{2}I + {M_B^0}^\top\Big)^{-1} \pi_t\big(\boldsymbol{H}^i(\boldsymbol{z})\big)\Big), \end{aligned}$$

where $\boldsymbol{H}^i(\boldsymbol{z})$ is given by (3.34). An easy computation applying (3.25) (for $k = 0$) shows that

$$\boldsymbol{\nu} \times \Big(\pm\frac{1}{2}I + {M_B^0}^\top\Big)^{-1} \pi_t(\cdot) = -\Big(\mp\frac{1}{2}I + M_B^0\Big)^{-1} \gamma_t(\cdot). \tag{3.59}$$

Therefore,

$$F_0 L_0^\top \boldsymbol{\varphi} = -\frac{1}{\omega^2\varepsilon_-\mu_+} \boldsymbol{\nu} \times \mathbf{curl}\,\mathbf{curl}\mathcal{A}_B^0\Big(-\frac{1}{2}I + M_B^0\Big)^{-1} \gamma_t\big(\boldsymbol{H}^i(\boldsymbol{z})\big).$$

Now, let

$$\boldsymbol{u} := \mathbf{curl}\mathcal{A}_B^0\Big(-\frac{1}{2}I + M_B^0\Big)^{-1} \gamma_t\big(\boldsymbol{H}^i(\boldsymbol{z})\big) \qquad \text{in } B.$$

Then, $\boldsymbol{u}$ is a solution to (3.58) with $\boldsymbol{c} = \gamma_t\big(\boldsymbol{H}^i(\boldsymbol{z})\big)$. Because solutions to (3.58) are unique by Lemma 3.15 and obviously the constant function $\boldsymbol{v} := \boldsymbol{H}^i(\boldsymbol{z})$, in B, is a solution for (3.58) with $\boldsymbol{\nu} \times \boldsymbol{v}|_{\partial B} = \gamma_t\big(\boldsymbol{H}^i(\boldsymbol{z})\big)$ too, we obtain that $\boldsymbol{u} = \boldsymbol{H}^i(\boldsymbol{z})$ is constant in B. Hence,

$$F_0 L_0^\top \boldsymbol{\varphi} = -\frac{1}{\omega^2\varepsilon_-\mu_+} \gamma_t(\mathbf{curl}\boldsymbol{u}) = 0 \qquad \text{on } \partial B.$$

Because N_0 and therefore also F_0 is symmetric with respect to the dual pairing $\langle\cdot,\cdot\rangle_{\partial B}$ between $\boldsymbol{H}^{-1/2}_{\mathrm{curl}}(\partial B)$ and $\boldsymbol{H}^{-1/2}_{\mathrm{div}}(\partial B)$, also $L_0F_0\boldsymbol{a}=0$ for each $\boldsymbol{a}\in\boldsymbol{H}^{-1/2}_{\mathrm{curl}}(\partial B)$. □

Recalling Theorem 3.7, we can put our results together and obtain the following asymptotic expansion of the measurement operator G_δ.

Theorem 3.17. *Let $\boldsymbol{\varphi}\in\boldsymbol{L}^2(\mathcal{M})$. Then,*

$$G_\delta\boldsymbol{\varphi}=\mathrm{i}\,\omega\mu_+\delta^3\big(L_0F_1L_0^\top\boldsymbol{\varphi}+L_1F_0L_1^\top\boldsymbol{\varphi}\big)+\mathcal{O}(\delta^4)$$

in $\boldsymbol{L}^2(\mathcal{M})$ as $\delta\to0$. More precisely, the last term on the right–hand side is bounded by $C\delta^4\|\boldsymbol{\varphi}\|_{\boldsymbol{L}^2(\mathcal{M})}$, where the constant $C>0$ is independent of δ and $\boldsymbol{\varphi}$.

The proof of this theorem follows straightforwardly from the previous propositions and Theorem 3.7.

Finally, we calculate $L_0F_1L_0^\top\boldsymbol{\varphi}$ and $L_1F_0L_1^\top\boldsymbol{\varphi}$ for $\boldsymbol{\varphi}\in\boldsymbol{L}^2(\mathcal{M})$ explicitly.

Lemma 3.18. *For each $\boldsymbol{\varphi}\in\boldsymbol{L}^2(\mathcal{M})$, we have*

$$F_0L_1^\top\boldsymbol{\varphi}=-\frac{1}{\omega^2\varepsilon_-\mu_+}\gamma_t\big(\mathbf{curl}\boldsymbol{H}^i(\boldsymbol{z})\big)\qquad\text{on }\partial B.\tag{3.60}$$

Proof. Given $\boldsymbol{\varphi}\in\boldsymbol{L}^2(\mathcal{M})$, we find from (3.54) and (3.55) by applying (3.59) that

$$\begin{aligned}
F_0L_1^\top\boldsymbol{\varphi}&=\frac{1}{\omega^2\varepsilon_-\mu_+}N_B^0\Big(\frac{1}{2}I+{M_B^0}^\top\Big)^{-1}\pi_t\bigg(\sum_{j=1}^3\eta_j\frac{\partial\boldsymbol{H}^i}{\partial y_j}(\boldsymbol{z})\bigg)\\
&=\frac{1}{\omega^2\varepsilon_-\mu_+}\boldsymbol{\nu}\times\mathbf{curl}\,\mathbf{curl}\mathcal{A}_B^0\bigg(\boldsymbol{\nu}\times\Big(\frac{1}{2}I+{M_B^0}^\top\Big)^{-1}\pi_t\bigg(\sum_{j=1}^3\eta_j\frac{\partial\boldsymbol{H}^i}{\partial y_j}(\boldsymbol{z})\bigg)\bigg)\\
&=-\frac{1}{\omega^2\varepsilon_-\mu_+}\boldsymbol{\nu}\times\mathbf{curl}\,\mathbf{curl}\mathcal{A}_B^0\Big(-\frac{1}{2}I+M_B^0\Big)^{-1}\gamma_t\bigg(\sum_{j=1}^3\eta_j\frac{\partial\boldsymbol{H}^i}{\partial y_j}(\boldsymbol{z})\bigg).
\end{aligned}$$

Let

$$\boldsymbol{u}:=\mathbf{curl}\mathcal{A}_B^0\Big(-\frac{1}{2}I+M_B^0\Big)^{-1}\gamma_t\bigg(\sum_{j=1}^3\eta_j\frac{\partial\boldsymbol{H}^i}{\partial y_j}(\boldsymbol{z})\bigg)\qquad\text{in }B.$$

Then, $\boldsymbol{u}$ is a solution to (3.58) with $\boldsymbol{c}=\gamma_t\big(\sum_{j=1}^3\eta_j\frac{\partial\boldsymbol{H}^i}{\partial y_j}(\boldsymbol{z})\big)$. Because solutions to (3.58) are unique by Lemma 3.15 and $\boldsymbol{v}(\boldsymbol{\xi}):=\sum_{j=1}^3\xi_j\frac{\partial\boldsymbol{H}^i}{\partial y_j}(\boldsymbol{z})$, $\boldsymbol{\xi}\in B$, is a solution to (3.58) with $\boldsymbol{\nu}\times\boldsymbol{v}|_{\partial B}=\gamma_t\left(\sum_{j=1}^3\eta_j\frac{\partial\boldsymbol{H}^i}{\partial y_j}(\boldsymbol{z})\right)$ too, we obtain that $\boldsymbol{u}(\boldsymbol{\xi})=\sum_{j=1}^3\xi_j\frac{\partial\boldsymbol{H}^i}{\partial y_j}(\boldsymbol{z})$ for a.e. $\boldsymbol{\xi}\in B$. An easy calculation shows that $\mathbf{curl}\boldsymbol{u}=\mathbf{curl}\boldsymbol{H}^i(\boldsymbol{z})$ in B, which ends the proof. □

Lemma 3.19. *For each $\boldsymbol{\varphi} \in \boldsymbol{L}^2(\mathcal{M})$ we have*

$$F_1 L_0^\top \boldsymbol{\varphi} = -\frac{\mu_-}{\mu_+}\gamma_t\Big(\mathcal{A}_B^0\Big(-\frac{1}{2}I + M_B^0\Big)^{-1}\gamma_t\big(\boldsymbol{H}^i(\boldsymbol{z})\big)\Big) \qquad \text{on } \partial B. \tag{3.61}$$

Proof. Given $\boldsymbol{\varphi} \in \boldsymbol{L}^2(\mathcal{M})$, we find from (3.53) and (3.56) by applying (3.2) and (3.59) that on ∂B

$$\begin{aligned}
(F_1 L_0^\top \boldsymbol{\varphi})(\boldsymbol{\xi}) =& \frac{\mu_-}{\mu_+}\Big(\gamma_t\Big(\mathcal{A}_B^0\Big(\boldsymbol{\nu}\times\Big(\frac{1}{2}I + {M_B^0}^\top\Big)^{-1}\pi_t\big(\boldsymbol{H}^i(\boldsymbol{z})\big)\Big)\Big)\Big)(\boldsymbol{\xi}) \\
+\frac{\mu_-}{\mu_+}\boldsymbol{\nu}(\boldsymbol{\xi})\times\int_{\partial B}\frac{1}{8\pi}\frac{\boldsymbol{\xi}-\boldsymbol{\eta}}{|\boldsymbol{\xi}-\boldsymbol{\eta}|}&\Big(\mathrm{curl}_{\partial B}\Big(\frac{1}{2}I + {M_B^0}^\top\Big)^{-1}\pi_t\big(\boldsymbol{H}^i(\boldsymbol{z})\big)\Big)(\boldsymbol{\eta})\,\mathrm{d}s(\boldsymbol{\eta}) \\
=& -\frac{\mu_-}{\mu_+}\Big(\gamma_t\Big(\mathcal{A}_B^0\Big(-\frac{1}{2}I + M_B^0\Big)^{-1}\gamma_t\big(\boldsymbol{H}^i(\boldsymbol{z})\big)\Big)\Big)(\boldsymbol{\xi}) \\
+\frac{\mu_-}{\mu_+}\boldsymbol{\nu}(\boldsymbol{\xi})\times\int_{\partial B}\frac{1}{8\pi}\frac{\boldsymbol{\xi}-\boldsymbol{\eta}}{|\boldsymbol{\xi}-\boldsymbol{\eta}|}&\Big(\mathrm{div}_{\partial B}\Big(\Big(-\frac{1}{2}I + M_B^0\Big)^{-1}\gamma_t\big(\boldsymbol{H}^i(\boldsymbol{z})\big)\Big)\Big)(\boldsymbol{\eta})\,\mathrm{d}s(\boldsymbol{\eta}).
\end{aligned} \tag{3.62}$$

By Lemma 3.4 (i), $-\frac{1}{2}I + M_B^0$ is an isomorphism on $\boldsymbol{H}^{-1/2}_{\mathrm{div},0}(\partial B)$. Therefore, because

$$\mathrm{div}_{\partial B}\,\gamma_t\big(\boldsymbol{H}^i(\boldsymbol{z})\big) = -\gamma_n\big(\mathbf{curl}\big(\boldsymbol{H}^i(\boldsymbol{z})\big)\big) = 0$$

by virtue of (3.5), we find that

$$\mathrm{div}_{\partial B}\Big(\Big(-\frac{1}{2}I + M_B^0\Big)^{-1}\gamma_t\big(\boldsymbol{H}^i(\boldsymbol{z})\big)\Big) = 0.$$

Hence, the second term on the right–hand side of (3.62) vanishes and we obtain the desired result. □

Proposition 3.20. *For each $\boldsymbol{\varphi} \in \boldsymbol{L}^2(\mathcal{M})$, we have*

$$L_1 F_0 L_1^\top \boldsymbol{\varphi} = \frac{1}{\mathrm{i}\,\omega\mu_+}\frac{\mu_-}{\mu_+}\mathbf{curl}_x\,\mathbb{G}^e(\cdot,\boldsymbol{z})\,\mathbb{M}_B^\infty\mathbf{curl}\boldsymbol{H}^i(\boldsymbol{z}) \qquad \text{on } \mathcal{M},$$

where the matrix $\mathbb{M}_B^\infty \in \mathbb{R}^{3\times 3}$ is the electric polarizability tensor corresponding to B; cf. Definition A.1.

Proof. Let $\boldsymbol{\varphi} \in \boldsymbol{L}^2(\mathcal{M})$. By (3.60) and (3.52),

$$\begin{aligned}
&L_1 F_0 L_1^\top \boldsymbol{\varphi} \\
&= -\frac{1}{\mathrm{i}\,\omega\mu_+}\int_{\partial B}\sum_{j=1}^{3}\eta_j\frac{\partial\,\mathbb{G}^m}{\partial y_j}(\cdot,\boldsymbol{z})\Big(\Big(\frac{1}{2}I + M_B^0\Big)^{-1}\gamma_t\big(\mathbf{curl}\boldsymbol{H}^i(\boldsymbol{z})\big)\Big)(\boldsymbol{\eta})\,\mathrm{d}s(\boldsymbol{\eta})
\end{aligned}$$

on $\mathcal{M}$. Applying (3.59), we find that

$$
\begin{aligned}
&-\int_{\partial B}\sum_{j=1}^{3}\eta_j\frac{\partial\,\mathbb{G}^m}{\partial y_j}(\cdot,\boldsymbol{z})\Big(\Big(\frac{1}{2}I+M_B^0\Big)^{-1}\gamma_t\big(\mathbf{curl}\boldsymbol{H}^i(\boldsymbol{z})\big)\Big)(\boldsymbol{\eta})\;\mathrm{d}s(\boldsymbol{\eta})\\
&=\sum_{j=1}^{3}\frac{\partial\,\mathbb{G}^m}{\partial y_j}(\cdot,\boldsymbol{z})\int_{\partial B}\eta_j\,\mathbb{I}_3\Big(\boldsymbol{\nu}\times\Big(-\frac{1}{2}I+{M_B^0}^{\top}\Big)^{-1}\pi_t\big(\mathbf{curl}\boldsymbol{H}^i(\boldsymbol{z})\big)\Big)(\boldsymbol{\eta})\;\mathrm{d}s(\boldsymbol{\eta})
\end{aligned}
$$

on $\mathcal{M}$. Because by (3.3),

$$
\pi_t\big(\mathbf{curl}\boldsymbol{H}^i(\boldsymbol{z})\big)=\pi_t\big(\nabla_\eta\big(\mathbf{curl}\boldsymbol{H}^i(\boldsymbol{z})\cdot\boldsymbol{\eta}\big)\big)=\nabla_{\partial B}\big(\mathbf{curl}\boldsymbol{H}^i(\boldsymbol{z})\cdot\boldsymbol{\eta}\big),
$$

on ∂B, where $\boldsymbol{\eta}$ denotes the coordinate function in a neighborhood of ∂B, we can apply (3.26) and (3.4) to obtain for $1\le j\le 3$ that

$$
\begin{aligned}
&\int_{\partial B}\eta_j\,\mathbb{I}_3\Big(\boldsymbol{\nu}\times\Big(-\frac{1}{2}I+{M_B^0}^{\top}\Big)^{-1}\pi_t\big(\mathbf{curl}\boldsymbol{H}^i(\boldsymbol{z})\big)\Big)(\boldsymbol{\eta})\;\mathrm{d}s(\boldsymbol{\eta})\\
&\qquad=\int_{\partial B}\pi_t(\eta_j\,\mathbb{I}_3)^{\top}\Big(\mathbf{curl}_{\partial B}\Big(\frac{1}{2}I+K_B^0\Big)^{-1}\big(\mathbf{curl}\boldsymbol{H}^i(\boldsymbol{z})\cdot\boldsymbol{\eta}\big)\Big)(\boldsymbol{\eta})\;\mathrm{d}s(\boldsymbol{\eta}).
\end{aligned}
$$

From the duality of $\mathbf{curl}_{\partial B}$ and $\mathrm{curl}_{\partial B}$ and from (3.5), we find

$$
\begin{aligned}
&\int_{\partial B}\pi_t(\eta_j\,\mathbb{I}_3)^{\top}\Big(\mathbf{curl}_{\partial B}\Big(\frac{1}{2}I+K_B^0\Big)^{-1}\big(\mathbf{curl}\boldsymbol{H}^i(\boldsymbol{z})\cdot\boldsymbol{\eta}\big)\Big)(\boldsymbol{\eta})\;\mathrm{d}s(\boldsymbol{\eta})\\
&\quad=\int_{\partial B}\big(\boldsymbol{\nu}\cdot\mathbf{curl}(\eta_j\,\mathbb{I}_3)\big)^{\top}(\boldsymbol{\xi})\left(\Big(\Big(\frac{1}{2}I+K_B^0\Big)^{-1}\boldsymbol{\eta}\Big)(\boldsymbol{\xi})\cdot\mathbf{curl}\boldsymbol{H}^i(\boldsymbol{z})\right)\mathrm{d}s(\boldsymbol{\xi}).
\end{aligned}
$$

An easy calculation reveals that

$$
\sum_{j=1}^{3}\frac{\partial\,\mathbb{G}^m}{\partial y_j}(\cdot,\boldsymbol{z})\mathbf{curl}_\eta(\eta_j\,\mathbb{I}_3)^{\top}=\big(\mathbf{curl}_y\,\mathbb{G}^{m\top}\big)^{\top}(\cdot,\boldsymbol{z}).
$$

Applying (B.7b) and (B.8), we observe that

$$
\big(\mathbf{curl}_y\,\mathbb{G}^{m\top}\big)^{\top}(\cdot,\boldsymbol{z})=\frac{\mu_-}{\mu_+}\mathbf{curl}_x\,\mathbb{G}^e(\cdot,\boldsymbol{z}).
$$

So, we find that

$$
\begin{aligned}
&\mathrm{i}\,\omega\mu_+L_1F_0L_1^{\top}\boldsymbol{\varphi}\\
&\quad=\frac{\mu_-}{\mu_+}\mathbf{curl}_x\,\mathbb{G}^e(\cdot,\boldsymbol{z})\int_{\partial B}\boldsymbol{\nu}(\boldsymbol{\xi})\left(\Big(\Big(\frac{1}{2}I+K_B^0\Big)^{-1}\boldsymbol{\eta}\Big)(\boldsymbol{\xi})\cdot\mathbf{curl}\boldsymbol{H}^i(\boldsymbol{z})\right)\mathrm{d}s(\boldsymbol{\xi})\\
&\quad=\frac{\mu_-}{\mu_+}\mathbf{curl}_x\,\mathbb{G}^e(\cdot,\boldsymbol{z})\left(\int_{\partial B}\Big(\Big(\frac{1}{2}I+{K_B^0}^{\top}\Big)^{-1}\boldsymbol{\nu}\Big)(\boldsymbol{\eta})\boldsymbol{\eta}^{\top}\;\mathrm{d}s(\boldsymbol{\eta})\right)\mathbf{curl}\boldsymbol{H}^i(\boldsymbol{z})\\
&\quad=\frac{\mu_-}{\mu_+}\mathbf{curl}_x\,\mathbb{G}^e(\cdot,\boldsymbol{z})\,\mathbb{M}_B^{\infty}\mathbf{curl}\boldsymbol{H}^i(\boldsymbol{z}),
\end{aligned}
$$

where the matrix $\mathbb{M}_B^{\infty}\in\mathbb{R}^{3\times3}$ is the electric polarizability tensor corresponding to B; cf. Definition A.1. □

Proposition 3.21. *For each $\boldsymbol{\varphi} \in \boldsymbol{L}^2(\mathcal{M})$, we have*

$$L_0 F_1 L_0^\top \boldsymbol{\varphi} = \mathrm{i}\,\omega\varepsilon_- \frac{\mu_-}{\mu_+}\, \mathbb{G}^m(\cdot, \boldsymbol{z})\, \mathbb{M}_B^0 \boldsymbol{H}^i(\boldsymbol{z}),$$

where $\mathbb{M}_B^0 \in \mathbb{R}^{3\times 3}$ is the magnetic polarizability tensor corresponding to B; cf. Definition A.1.

Proof. Let $\boldsymbol{\varphi} \in \boldsymbol{L}^2(\mathcal{M})$ and set

$$\boldsymbol{w} := \mathcal{A}_B^0 \Big(-\frac{1}{2} I + M_B^0\Big)^{-1} \gamma_t\big(\boldsymbol{H}^i(z)\big) \qquad \text{in } B.$$

As in the proof of Proposition 3.16, we find that $\mathbf{curl}\boldsymbol{w} = \boldsymbol{H}^i(\boldsymbol{z})$ in B. So, recalling (3.20), we obtain that

$$\gamma_n\Big(\mathbf{curl}\mathcal{A}_B^0\Big(-\frac{1}{2} I + M_B^0\Big)^{-1} \gamma_t\big(\boldsymbol{H}^i(z)\big)\Big) = \boldsymbol{\nu} \cdot \boldsymbol{H}^i(\boldsymbol{z}) \qquad \text{on } \partial B. \tag{3.63}$$

By (3.61) and (3.51),

$$L_0 F_1 L_0^\top \boldsymbol{\varphi} = \mathrm{i}\,\omega\varepsilon_- \frac{\mu_-}{\mu_+}\, \mathbb{G}^m(\cdot, \boldsymbol{z}) \int_{\partial B} \Big(\Big(\frac{1}{2} I + M_B^0\Big)^{-1} \gamma_t(\boldsymbol{w})\Big)(\boldsymbol{\eta})\, \mathrm{d}s(\boldsymbol{\eta})$$

on $\mathcal{M}$. Observing that $\mathbb{I}_3 = \nabla_\eta \boldsymbol{\eta}$ on ∂B, where $\boldsymbol{\eta}$ again denotes the surface variable on ∂B, and applying (3.3), we can calculate

$$\begin{aligned}
&\int_{\partial B} \Big(\Big(\frac{1}{2} I + M_B^0\Big)^{-1} \gamma_t(\boldsymbol{w})\Big)(\boldsymbol{\eta})\, \mathrm{d}s(\boldsymbol{\eta}) \\
&\qquad = \int_{\partial B} \pi_t(\mathbb{I}_3)^\top \Big(\Big(\frac{1}{2} I + M_B^0\Big)^{-1} \gamma_t(\boldsymbol{w})\Big)(\boldsymbol{\eta})\, \mathrm{d}s(\boldsymbol{\eta}) \\
&\qquad = \int_{\partial B} \Big(\Big(\frac{1}{2} I + {M_B^0}^\top\Big)^{-1} \nabla_{\partial B}\boldsymbol{\eta}\Big)^\top (\boldsymbol{\xi}) \gamma_t(\boldsymbol{w})(\boldsymbol{\xi})\, \mathrm{d}s(\boldsymbol{\xi}).
\end{aligned}$$

Applying (3.26), the duality of $-\nabla_{\partial B}$ and $\mathrm{div}_{\partial B}$, and (3.5), we have

$$\begin{aligned}
&\int_{\partial B} \Big(\Big(\frac{1}{2} I + {M_B^0}^\top\Big)^{-1} \nabla_{\partial B}\boldsymbol{\eta}\Big)^\top (\boldsymbol{\xi}) \gamma_t(\boldsymbol{w})(\boldsymbol{\xi})\, \mathrm{d}s(\boldsymbol{\xi}) \\
&\qquad = \int_{\partial B} \Big(-\nabla_{\partial B}\Big(-\frac{1}{2} I + K_B^0\Big)^{-1} \boldsymbol{\eta}\Big)^\top (\boldsymbol{\xi}) \gamma_t(\boldsymbol{w})(\boldsymbol{\xi})\, \mathrm{d}s(\boldsymbol{\xi}) \\
&\qquad = \int_{\partial B} \Big(\Big(-\frac{1}{2} I + K_B^0\Big)^{-1} \boldsymbol{\eta}\Big)(\boldsymbol{\eta}) (-\gamma_n(\mathbf{curl}\boldsymbol{w}))(\boldsymbol{\eta})\, \mathrm{d}s(\boldsymbol{\eta}).
\end{aligned}$$

Finally, recalling (3.63), we obtain

$$\begin{aligned}
&\int_{\partial B} \Big(\Big(-\frac{1}{2} I + K_B^0\Big)^{-1} \boldsymbol{\eta}\Big)(\boldsymbol{\eta}) (-\gamma_n(\mathbf{curl}\boldsymbol{w}))(\boldsymbol{\eta})\, \mathrm{d}s(\boldsymbol{\eta}) \\
&\qquad = -\int_{\partial B} \Big(\Big(-\frac{1}{2} I + K_B^0\Big)^{-1} \boldsymbol{\eta}\Big)(\boldsymbol{\eta}) \big(\boldsymbol{\nu}(\boldsymbol{\eta}) \cdot \boldsymbol{H}^i(\boldsymbol{z})\big)\, \mathrm{d}s(\boldsymbol{\eta}) \\
&\qquad = -\int_{\partial B} \boldsymbol{\xi}\Big(\Big(-\frac{1}{2} I + {K_B^0}^\top\Big)^{-1} \big(\boldsymbol{\nu} \cdot \boldsymbol{H}^i(\boldsymbol{z})\big)\Big)(\boldsymbol{\xi})\, \mathrm{d}s(\boldsymbol{\xi}) \\
&\qquad = \mathbb{M}_B^0 \boldsymbol{H}^i(\boldsymbol{z}),
\end{aligned}$$

where the matrix $\mathbb{M}_B^0 \in \mathbb{R}^{3\times 3}$ is the magnetic polarizability tensor corresponding to B; cf. Definition A.1. □

From Theorem 3.17, Proposition 3.20, and Proposition 3.21, we obtain the following corollary.

Corollary 3.22. *Let $\boldsymbol{\varphi} \in \boldsymbol{L}^2(\mathcal{M})$ and let $\boldsymbol{H}^i$ be the corresponding incident field from* (3.34)*. Then,*

$$G_\delta \boldsymbol{\varphi} = \delta^3 \Big(-k_-^2\, \mathbb{G}^m(\cdot, \boldsymbol{z})\, \mathbb{M}_B^0 \boldsymbol{H}^i(\boldsymbol{z}) + \frac{\mu_-}{\mu_+} \mathbf{curl}_x\, \mathbb{G}^e(\cdot, \boldsymbol{z})\, \mathbb{M}_B^\infty \mathbf{curl} \boldsymbol{H}^i(\boldsymbol{z}) \Big) + \mathcal{O}(\delta^4)$$

in $\boldsymbol{L}^2(\mathcal{M})$ as $\delta \to 0$. More precisely, the last term on the right–hand side is bounded by $C\delta^4 \|\boldsymbol{\varphi}\|_{\boldsymbol{L}^2(\mathcal{M})}$, where the constant $C > 0$ is independent of δ and $\boldsymbol{\varphi}$.

3.8 Multiple Scatterers

The results of the previous sections can be extended to the practically important case of finitely many well separated small scatterers as introduced in Section 3.4. This generalization works essentially in the same way as in Section 2.7 for the electrostatic case. However, we include the main steps for the sake of completeness.

Again we set $\partial D_\delta := \partial D_{\delta,1} \times \cdots \times \partial D_{\delta,m}$ and $\partial B := \partial B_1 \times \cdots \times \partial B_m$ and interpret the relevant Sobolev spaces accordingly as product spaces. Boundary conditions on ∂D_δ should be understood component–wise.

We start by reconsidering the operator L_δ introduced in (3.38). For any $\boldsymbol{\psi} = (\boldsymbol{\psi}_1, \ldots, \boldsymbol{\psi}_m) \in \boldsymbol{H}_{\mathrm{div}}^{-1/2}(\partial D_\delta)$, we define $\boldsymbol{H}^\psi \in \boldsymbol{H}_{\mathrm{loc}}(\mathbf{curl}, \mathbb{R}^3 \setminus \overline{D_\delta})$ by

$$\boldsymbol{H}^\psi = -\mathrm{i}\,\omega\varepsilon_- \sum_{l=1}^m \int_{\partial D_{\delta,l}} \mathbb{G}^m(\cdot, \boldsymbol{y}) \boldsymbol{a}_l(\boldsymbol{y})\, \mathrm{d}s(\boldsymbol{y}),$$

where $\boldsymbol{a} := (\boldsymbol{a}_1, \ldots, \boldsymbol{a}_m)^\top \in \boldsymbol{H}_{\mathrm{div}}^{-1/2}(\partial D_\delta)$ solves the system of integral equations

$$\mathbb{A}\boldsymbol{a} = \boldsymbol{\psi},$$

with $\mathbb{A}$ given by

$$\begin{pmatrix} \frac{1}{2}I + M_{D_{\delta,1}}^m & \boldsymbol{\nu} \times \mathbf{curl} \mathcal{A}_{D_{\delta,2}}^m\big|_{\partial D_{\delta,1}} & \ldots & \boldsymbol{\nu} \times \mathbf{curl} \mathcal{A}_{D_{\delta,m}}^m\big|_{\partial D_{\delta,1}} \\ \boldsymbol{\nu} \times \mathbf{curl} \mathcal{A}_{D_{\delta,1}}^m\big|_{\partial D_{\delta,2}} & \frac{1}{2}I + M_{D_{\delta,2}}^m & \ldots & \boldsymbol{\nu} \times \mathbf{curl} \mathcal{A}_{D_{\delta,m}}^m\big|_{\partial D_{\delta,2}} \\ \ldots & \ldots & \ldots & \ldots \\ \boldsymbol{\nu} \times \mathbf{curl} \mathcal{A}_{D_{\delta,1}}^m\big|_{\partial D_{\delta,m}} & \boldsymbol{\nu} \times \mathbf{curl} \mathcal{A}_{D_{\delta,2}}^m\big|_{\partial D_{\delta,m}} & \ldots & \frac{1}{2}I + M_{D_{\delta,m}}^m \end{pmatrix}.$$

Because the small scatterers are assumed to be well separated from each other and from the interface Σ_0, we can estimate the nondiagonal entries of the matrix $\mathbb{A}$ using the regularity of $\mathcal{A}^m_{D_{\delta,l}}\boldsymbol{b}_l$, $\boldsymbol{b}_l \in \boldsymbol{H}^{-1/2}_{\rm div}(\partial D_{\delta,l})$, away from $\partial D_{\delta,l}$, $1 \le l \le m$. Set

$$\mathbb{B} := \begin{pmatrix} \frac{1}{2}I + M^m_{B_1} & 0 & \dots & 0 \\ 0 & \frac{1}{2}I + M^m_{B_2} & \dots & 0 \\ \dots & \dots & \dots & \dots \\ 0 & 0 & \dots & \frac{1}{2}I + M^m_{B_m} \end{pmatrix},$$

and note that $\mathbb{B}$ is invertible by Lemma 3.5 and Theorem 2.1. In the same way as in the proof of Lemma 3.5 we obtain that the nullspace of $\mathbb{A}$ is trivial, too. Because $\mathbb{A}$ is just a compact perturbation of $\frac{1}{2}\,\mathbb{I}$, where $\mathbb{I}$ denotes the identity operator on $\boldsymbol{H}^{-1/2}_{\rm div}(\partial D_\delta)$, Theorem 2.1 yields that $\mathbb{A}$ is invertible. Similar to Lemma 3.9 we get the following result, where we use the maximum row sum of $\mathcal{L}(\boldsymbol{H}^{-1/2}_{\rm div}(\partial B_j), \boldsymbol{H}^{-1/2}_{\rm div}(\partial B_l))$ norms, $1 \le j, l \le m$, as norm on $\mathcal{L}(\boldsymbol{H}^{-1/2}_{\rm div}(\partial B))$ in this context.

Lemma 3.23. *Let $\boldsymbol{b} \in \boldsymbol{H}^{-1/2}_{\rm div}(\partial D_\delta)$. Then*

$$\mathbb{A}\boldsymbol{b} = (\,\mathbb{B}\hat{\boldsymbol{b}})^\vee + (\,\mathbb{E}_A\hat{\boldsymbol{b}})^\vee,$$

where $\mathbb{E}_A$ is a bounded linear operator, independent of $\boldsymbol{b}$, which is $\mathcal{O}(\delta^2)$ in $\mathcal{L}(\boldsymbol{H}^{-1/2}_{\rm div}(\partial B))$ as $\delta \to 0$.

Proof. Let $\boldsymbol{b} = (\boldsymbol{b}_1, \dots, \boldsymbol{b}_m) \in \boldsymbol{H}^{-1/2}_{\rm div}(\partial D_\delta)$ and $1 \le j \ne l \le m$. Using the regularity of $\Pi^m(\boldsymbol{x}, \boldsymbol{y})$ in a neighborhood of $(\boldsymbol{x}, \boldsymbol{y}) \in \mathbb{R}^3_- \times \mathbb{R}^3_-$ with $\boldsymbol{x} \ne \boldsymbol{y}$, we obtain as in the proof of Lemma 3.9 that

$$\big\|\big(\boldsymbol{\nu} \times \mathbf{curl}\mathcal{A}^m_{D_{\delta,j}}\boldsymbol{b}_j\big|_{\partial D_{\delta,l}}\big)^{\wedge_l}\big\|_{\boldsymbol{H}^{-1/2}_{\rm div}(\partial B_l)} \le C\delta^2\|\boldsymbol{b}_j^{\wedge_j}\|_{\boldsymbol{H}^{-1/2}_{\rm div}(\partial B_j)}.$$

Here, $(\cdot)^{\wedge_l}$ denotes the transformation from (2.19), applied to the lth scatterer $D_{\delta,l}$, $1 \le l \le m$. □

So, we find from Lemma 2.2 that for any $\boldsymbol{b} \in \boldsymbol{H}^{-1/2}_{\rm div}(\partial D_\delta)$

$$\mathbb{A}^{-1}\boldsymbol{b} = (\,\mathbb{B}^{-1}\hat{\boldsymbol{b}})^\vee + (\,\tilde{\mathbb{E}}_A\hat{\boldsymbol{b}})^\vee,$$

where $\tilde{\mathbb{E}}_A$ is a bounded linear operator, independent of $\boldsymbol{b}$, which is $\mathcal{O}(\delta^2)$ in $\mathcal{L}(\boldsymbol{H}^{-1/2}_{\rm div}(\partial B))$ as $\delta \to 0$. Calculating along the lines of Section 3.7 we obtain the following asymptotic formula:

$$\begin{aligned}\boldsymbol{H}^\psi|_{\mathcal{M}} = &-\mathrm{i}\,\omega\varepsilon_-\delta^3\sum_{l=1}^m \mathbb{G}^m(\cdot, \boldsymbol{z}_l)\int_{\partial B_l}\Big(\Big(\frac{1}{2}I + M^0_{B_l}\Big)^{-1}\boldsymbol{\psi}_l{}^{\wedge_l}\Big)(\boldsymbol{\eta})\,\mathrm{d}s(\boldsymbol{\eta}) \\ &-\mathrm{i}\,\omega\varepsilon_-\delta^3\sum_{l=1}^m\int_{\partial B_l}\sum_{j=1}^3\eta_j\frac{\partial\,\mathbb{G}^m}{\partial y_j}(\cdot, \boldsymbol{z}_l)\Big(\Big(\frac{1}{2}I + M^0_{B_l}\Big)^{-1}\boldsymbol{\psi}_l{}^{\wedge_l}\Big)(\boldsymbol{\eta})\,\mathrm{d}s(\boldsymbol{\eta}) \\ &+\mathcal{O}(\delta^4)\end{aligned}$$

in $\boldsymbol{L}^2(\mathcal{M})$ as $\delta \to 0$. The last term on the right–hand side is bounded by $C\delta^4 \max_{1\le l\le m} \|\boldsymbol{\psi}_l{}^{\wedge_l}\|_{\boldsymbol{H}_{\rm div}^{-1/2}(\partial B_l)}$, where the constant $C > 0$ is independent of δ and $\boldsymbol{\psi}$. Therefore, if we define $L_0 : \boldsymbol{H}_{\rm div}^{-1/2}(\partial B) \to \boldsymbol{L}^2(\mathcal{M})$,

$$L_0\boldsymbol{a} := -\,\mathrm{i}\,\omega\varepsilon_- \sum_{l=1}^{m} \mathbb{G}^m(\cdot,\boldsymbol{z}_l) \int_{\partial B_l} \Big(\Big(\frac{1}{2}I + M_{B_l}^0\Big)^{-1}\boldsymbol{a}_l\Big)(\boldsymbol{\eta})\,\mathrm{d}s(\boldsymbol{\eta}), \quad (3.64)$$

and $L_1 : \boldsymbol{H}_{\rm div}^{-1/2}(\partial B) \to \boldsymbol{L}^2(\mathcal{M})$,

$$L_1\boldsymbol{a} := -\,\mathrm{i}\,\omega\varepsilon_- \sum_{l=1}^{m} \int_{\partial B_l} \sum_{j=1}^{3} \eta_j \frac{\partial\,\mathbb{G}^m}{\partial y_j}(\cdot,\boldsymbol{z}_l)\Big(\Big(\frac{1}{2}I + M_{B_l}^0\Big)^{-1}\boldsymbol{a}_l\Big)(\boldsymbol{\eta})\,\mathrm{d}s(\boldsymbol{\eta}), \quad (3.65)$$

Proposition 3.10 remains valid in the case of finitely many well separated small scatterers.

As in Section 3.7, we find by duality that Proposition 3.12 remains valid in the case of finitely many well separated small scatterers too and that the dual operators of L_0 and L_1 are given by $L_0^\top : \boldsymbol{L}^2(\mathcal{M}) \to \boldsymbol{H}_{\rm curl}^{-1/2}(\partial B)$,

$$L_0^\top\boldsymbol{\varphi} = \Big(\frac{1}{\mathrm{i}\,\omega\mu_+}\Big(\frac{1}{2}I + M_{B_1}^0{}^\top\Big)^{-1}\pi_t\big(\boldsymbol{H}^i(\boldsymbol{z}_1)\big),\ldots, \frac{1}{\mathrm{i}\,\omega\mu_+}\Big(\frac{1}{2}I + M_{B_m}^0{}^\top\Big)^{-1}\pi_t\big(\boldsymbol{H}^i(\boldsymbol{z}_m)\big)\Big), \quad (3.66)$$

and $L_1^\top : \boldsymbol{L}^2(\mathcal{M}) \to \boldsymbol{H}_{\rm curl}^{-1/2}(\partial B)$,

$$L_1^\top\boldsymbol{\varphi} = \Big(\frac{1}{\mathrm{i}\,\omega\mu_+}\Big(\frac{1}{2}I + M_{B_1}^0{}^\top\Big)^{-1}\pi_t\Big(\sum_{j=1}^{3}\eta_j\frac{\partial\boldsymbol{H}^i}{\partial y_j}(\boldsymbol{z}_1)\Big),\ldots, \frac{1}{\mathrm{i}\,\omega\mu_+}\Big(\frac{1}{2}I + M_{B_m}^0{}^\top\Big)^{-1}\pi_t\Big(\sum_{j=1}^{3}\eta_j\frac{\partial\boldsymbol{H}^i}{\partial y_j}(\boldsymbol{z}_m)\Big)\Big), \quad (3.67)$$

where $\boldsymbol{H}^i$ is the corresponding incident field from (3.34).

We return to the diffraction problem (3.41) and the operator F_δ from (3.42). For $\boldsymbol{\chi} = (\boldsymbol{\chi}_1,\ldots,\boldsymbol{\chi}_m) \in \boldsymbol{H}_{\rm curl}^{-1/2}(\partial D_\delta)$, we define

$$\boldsymbol{E}^d := -\frac{1}{\mathrm{i}\,\omega\varepsilon}\sum_{l=1}^{m}\mathbf{curl}\frac{\mu_-}{\mu}\mathbf{curl}\mathcal{A}^e_{D_{\delta,l}}(\boldsymbol{\nu}\times\boldsymbol{\chi}_l) \qquad \text{in } \mathbb{R}^3_0\setminus\partial D_\delta,$$

$$\boldsymbol{H}^d := \frac{\mu_-}{\mu}\sum_{l=1}^{m}\mathbf{curl}\mathcal{A}^e_{D_{\delta,l}}(\boldsymbol{\nu}\times\boldsymbol{\chi}_l) \qquad \text{in } \mathbb{R}^3_0\setminus\partial D_\delta.$$

Then, $(\boldsymbol{E}^d, \boldsymbol{H}^d)$ is a radiating solution to (3.41) and for $1 \le j \le m$,

$$\begin{aligned}\boldsymbol{\nu} \times \boldsymbol{E}^d\big|_{\partial D_{\delta,j}} = &-\frac{1}{\mathrm{i}\,\omega\varepsilon_-}\boldsymbol{\nu} \times \mathbf{curl}\,\mathbf{curl}\mathcal{A}^e_{D_{\delta,j}}(\boldsymbol{\nu} \times \boldsymbol{\chi}_j)\big|_{\partial D_{\delta,j}} \\ &- \frac{1}{\mathrm{i}\,\omega\varepsilon_-}\sum_{\substack{l=1\\ l\neq j}}^{m} \boldsymbol{\nu} \times \mathbf{curl}\,\mathbf{curl}\mathcal{A}^e_{D_{\delta,l}}(\boldsymbol{\nu} \times \boldsymbol{\chi}_l)\big|_{\partial D_{\delta,j}}.\end{aligned}$$

As in the proof of Lemma 3.23, we can estimate for $1 \le l \le m$ that

$$\Big\|\Big(\boldsymbol{\nu} \times \mathbf{curl}\,\mathbf{curl}\mathcal{A}^e_{D_{\delta,l}}(\boldsymbol{\nu} \times \boldsymbol{\chi}_l)\big|_{\partial D_{\delta,j}}\Big)^{\wedge_j}\Big\|_{\boldsymbol{H}^{-1/2}_{\mathrm{div}}(\partial B_j)} \le C\delta^2\|\boldsymbol{\chi}_l^{\wedge_l}\|_{\boldsymbol{H}^{-1/2}_{\mathrm{curl}}(\partial B_l)}.$$

Thus,

$$\begin{aligned}\Big\|\Big(\frac{1}{\mathrm{i}\,\omega\varepsilon_-}\sum_{\substack{l=1\\ l\neq j}}^{m} \boldsymbol{\nu} \times \mathbf{curl}\,\mathbf{curl}\mathcal{A}^e_{D_{\delta,l}}(\boldsymbol{\nu} \times \boldsymbol{\chi}_l)\big|_{\partial D_{\delta,j}}\Big)^{\wedge_j}\Big\|_{\boldsymbol{H}^{-1/2}_{\mathrm{div}}(\partial B_j)} \\ \le C\delta^2 \max_{1\le l\le m}\|\boldsymbol{\chi}_l^{\wedge_l}\|_{\boldsymbol{H}^{-1/2}_{\mathrm{curl}}(\partial B_l)},\end{aligned} \tag{3.68}$$

where the constant $C > 0$ is independent of δ and $\boldsymbol{\chi}$. Recalling (3.55) and (3.56), we define $F_0 : \boldsymbol{H}^{-1/2}_{\mathrm{curl}}(\partial B) \to \boldsymbol{H}^{-1/2}_{\mathrm{div}}(\partial B)$,

$$F_0\boldsymbol{a} = \Big(-\frac{1}{\mathrm{i}\,\omega\varepsilon_-}N^0_{B_1}\boldsymbol{a}_1, \dots, -\frac{1}{\mathrm{i}\,\omega\varepsilon_-}N^0_{B_m}\boldsymbol{a}_m\Big), \tag{3.69}$$

and $F_1 : \boldsymbol{H}^{-1/2}_{\mathrm{curl}}(\partial B) \to \boldsymbol{H}^{-1/2}_{\mathrm{div}}(\partial B)$,

$$\begin{aligned}(F_1\boldsymbol{a})(\boldsymbol{\xi}) := \Big(&\mathrm{i}\,\omega\mu_-\big(\boldsymbol{\nu} \times \mathcal{A}^0_{B_1}(\boldsymbol{\nu} \times \boldsymbol{a}_1)\big|_{\partial B_1}\big)(\boldsymbol{\xi}) \\ &+ \mathrm{i}\,\omega\mu_-\boldsymbol{\nu}(\boldsymbol{\xi}) \times \int_{\partial B_1}\frac{1}{8\pi}\frac{\boldsymbol{\xi}-\boldsymbol{\eta}}{|\boldsymbol{\xi}-\boldsymbol{\eta}|}(\mathrm{curl}_{\partial B_1}\,\boldsymbol{a}_1)(\boldsymbol{\eta})\,\mathrm{d}s(\boldsymbol{\eta}), \dots, \\ &\mathrm{i}\,\omega\mu_-\big(\boldsymbol{\nu} \times \mathcal{A}^0_{B_m}(\boldsymbol{\nu} \times \boldsymbol{a}_m)\big|_{\partial B_m}\big)(\boldsymbol{\xi}) \\ &+ \mathrm{i}\,\omega\mu_-\boldsymbol{\nu}(\boldsymbol{\xi}) \times \int_{\partial B_m}\frac{1}{8\pi}\frac{\boldsymbol{\xi}-\boldsymbol{\eta}}{|\boldsymbol{\xi}-\boldsymbol{\eta}|}(\mathrm{curl}_{\partial B_m}\,\boldsymbol{a}_m)(\boldsymbol{\eta})\,\mathrm{d}s(\boldsymbol{\eta})\Big).\end{aligned} \tag{3.70}$$

Combining (3.68) with the derivation of (3.57) in Section 3.7, we find that Proposition 3.14 remains true in the case of finitely many well separated small scatterers.

Proposition 3.24. *Theorem 3.17 holds true in the case of finitely many well separated small scatterers, if L_0, L_1, F_0, F_1, $L_0^\top$, and $L_1^\top$ are given as in* (3.64), (3.65), (3.69), (3.70), (3.66), *and* (3.67), *respectively.*

Finally, let $\mathbb{M}^0_{B_1}, \dots, \mathbb{M}^0_{B_m}$ and $\mathbb{M}^\infty_{B_1}, \dots, \mathbb{M}^\infty_{B_m}$ denote the magnetic and electric polarizability tensors corresponding to $B_1, \dots, B_m$, respectively. In the case of multiple scatterers, Corollary 3.22 reads as follows.

Corollary 3.25. *Let $\boldsymbol{\varphi} \in \boldsymbol{L}^2(\mathcal{M})$ and let $\boldsymbol{H}^i$ be the corresponding incident field from* (3.34)*. Then,*

$$G_\delta \boldsymbol{\varphi} = \delta^3 \sum_{l=1}^{m} \Big(-k_-^2 \, \mathbb{G}^m(\cdot, z_l) \, \mathbb{M}_{B_l}^0 \boldsymbol{H}^i(z_l) + \frac{\mu_-}{\mu_+} \mathbf{curl}_x \, \mathbb{G}^e(\cdot, z_l) \, \mathbb{M}_{B_l}^\infty \mathbf{curl} \boldsymbol{H}^i(z_l) \Big) + \mathcal{O}(\delta^4) \quad (3.71)$$

in $\boldsymbol{L}^2(\mathcal{M})$ as $\delta \to 0$. More precisely, the last term on the right–hand side is bounded by $C\delta^4 \|\boldsymbol{\varphi}\|_{\boldsymbol{L}^2(\mathcal{M})}$, where the constant $C > 0$ is independent of δ and $\boldsymbol{\varphi}$.

Chapter 4

Reconstruction of Small Scatterers from Near Field Measurements

In this chapter, we study the inverse obstacle scattering problem outlined in the introduction and reconstruct the number and the positions of a collection of finitely many small perfectly conducting scatterers buried within the lower halfspace of an unbounded two–layered background medium using near field measurements of scattered electromagnetic waves.

We consider the same measurement setup as studied in the previous chapter (cf. Section 3.4), and we apply the asymptotic expansion of the near field measurement operator as the size of the scatterers tends to zero from Corollary 3.25 to justify a noniterative MUSIC–type reconstruction method for the numerical solution of the inverse problem. This reconstruction method is an extension of a reconstruction method, which was originally developed for electrical impedance tomography by Brühl, Hanke, and Vogelius [22]. Similar methods have recently been suggested by Ammari et al. [4] for homogeneous background media and by Iakovleva et al. [62] for two–layered background media.

Considering only the leading order term in the asymptotic expansion of the measurement operator, we construct a criterion on the range of this leading order term that tells us, whether a given point in the lower halfspace belongs to the set of asymptotically small scatterers or not. We derive this characterization for three different measurement setups: First, we study excitations of the incident field due to magnetic dipole distributions on the measurement device with arbitrary three–dimensional polarizations and measure the complete scattered field on the same device; secondly, we study incident fields excited by magnetic dipole distributions on the measurement device with polarizations tangential to the measurement device and measure only the tangential components of the scattered fields on the same device; and thirdly, we consider excitations of the incident field corresponding to

magnetic dipoles on the measurement device with polarizations normal to the measurement device and measure only the normal components of the scattered fields. The last case is particularly relevant for applications of our reconstruction method to more realistic models for the measurement device including special coil geometries; cf., e.g., Delbary et al. [46].

So far, the characterization of the positions of the scatterers holds only in case of asymptotically small scatterers. But recalling the asymptotic expansion of the measurement operator and applying perturbation theory for linear operators, we derive a similar criterion on the range of the full measurement operator, which tells us whether a point in the lower halfspace can be assumed to be close to an extended small buried scatterer or not.

Sampling a search domain in the lower halfspace, using a finite collection of points, we implement this characterization numerically using orthogonal projections on appropriate subspaces of the range of the measurement operator. This procedure leads to a noniterative visualization method for the approximate positions of the unknown small scatterers.

This chapter is organized as follows. In Section 4.1, we derive characterizations of the positions of the scatterers for the three different measurement setups, and the numerical implementation of these criteria in a sampling method is outlined in Section 4.2 and Section 4.3. Finally, in Section 4.4, we present numerical results obtained with this reconstruction method for numerically simulated forward data.

4.1 A Characterization of the Scatterers

In this section, we derive a characterization of the positions of the scatterers in terms of the range of the leading order term of the asymptotic expansion of the measurement operator G_δ as the size of the scatterers tends to zero. We study three different measurement setups:

- three–dimensional excitations and three-dimensional measurements,
- tangential excitations and tangential measurements,
- normal excitations and normal measurements.

4.1.1 Three–Dimensional Excitations and Measurements

First, we study the measurement setup as introduced in Section 3.4, i.e., the incident fields $(\boldsymbol{E}^i, \boldsymbol{H}^i)$ are given as superpositions of electromagnetic fields due to magnetic dipole distributions on $\mathcal{M}$ with arbitrary three–dimensional dipole densities $\boldsymbol{\varphi} \in \boldsymbol{L}^2(\mathcal{M})$ (cf. (3.34)), and we measure all three components of the corresponding scattered magnetic fields $\boldsymbol{H}^s$ on $\mathcal{M}$.

We introduce the operator $T:\ \boldsymbol{L}^2(\mathcal{M}) \to \boldsymbol{L}^2(\mathcal{M})$, describing the leading order term in the asymptotic expansion (3.71), given by

$$T\boldsymbol{\varphi} := \sum_{l=1}^{m} \Big(-k_-^2\, \mathbb{G}^m(\cdot, \boldsymbol{z}_l)\, \mathbb{M}_{B_l}^0 \boldsymbol{H}^i(\boldsymbol{z}_l) + \frac{\mu_-}{\mu_+} \mathbf{curl}_x\, \mathbb{G}^e(\cdot, \boldsymbol{z}_l)\, \mathbb{M}_{B_l}^\infty \mathbf{curl} \boldsymbol{H}^i(\boldsymbol{z}_l) \Big). \tag{4.1}$$

Because (3.34) implies that $\boldsymbol{H}^i$ depends linearly on $\boldsymbol{\varphi}$, it follows that T is linear. From Corollary 3.25, we obtain that

$$G_\delta = \delta^3 T + \mathcal{O}(\delta^4) \tag{4.2}$$

as $\delta \to 0$ in $\mathcal{L}(\boldsymbol{L}^2(\mathcal{M}))$. Next, we define the operator $R:\ \mathbb{C}^{3\times 2m} \to \boldsymbol{L}^2(\mathcal{M})$ by

$$R\boldsymbol{a} := k_-^2 \sum_{l=1}^{m} \Big(\mathbb{G}^m(\cdot, \boldsymbol{z}_l) \boldsymbol{a}_l + \frac{\mu_-}{\mu_+} \mathbf{curl}_x\, \mathbb{G}^e(\cdot, \boldsymbol{z}_l) \boldsymbol{a}_{m+l} \Big) \tag{4.3}$$

for $\boldsymbol{a} = (\boldsymbol{a}_1, \dots, \boldsymbol{a}_{2m}) \in \mathbb{C}^{3\times 2m}$, $\boldsymbol{a}_l \in \mathbb{C}^3$. Endowing $\mathbb{C}^{3\times 2m}$ with the bilinear form

$$\langle \boldsymbol{a}, \boldsymbol{b} \rangle_{\mathbb{C}^{3\times 2m}} := \sum_{l=1}^{2m} \boldsymbol{a}_l \cdot \boldsymbol{b}_l$$

for $\boldsymbol{a} = (\boldsymbol{a}_1, \dots, \boldsymbol{a}_{2m})$, $\boldsymbol{b} = (\boldsymbol{b}_1, \dots, \boldsymbol{b}_{2m}) \in \mathbb{C}^{3\times 2m}$ with $\boldsymbol{a}_l,\ \boldsymbol{b}_l \in \mathbb{C}^3$, using (3.34), (B.7b), and (B.8), we obtain that

$$\begin{aligned}
\langle R\boldsymbol{a}, \boldsymbol{\varphi} \rangle_{\mathcal{M}} &= \Big\langle k_-^2 \sum_{l=1}^{m} \Big(\mathbb{G}^m(\cdot, \boldsymbol{z}_l) \boldsymbol{a}_l + \frac{\mu_-}{\mu_+} \mathbf{curl}_x\, \mathbb{G}^e(\cdot, \boldsymbol{z}_l) \boldsymbol{a}_{m+l} \Big), \boldsymbol{\varphi} \Big\rangle_{\mathcal{M}} \\
&= \sum_{l=1}^{m} \boldsymbol{a}_l \cdot k_-^2 \int_{\mathcal{M}} \mathbb{G}^{m\top}(\boldsymbol{x}, \boldsymbol{z}_l) \boldsymbol{\varphi}(\boldsymbol{x})\, \mathrm{d}s(\boldsymbol{x}) \\
&\quad + \sum_{l=1}^{m} \boldsymbol{a}_{l+m} \cdot k_-^2 \frac{\mu_-}{\mu_+} \int_{\mathcal{M}} (\mathbf{curl}_x\, \mathbb{G}^e)^\top(\boldsymbol{x}, \boldsymbol{z}_l) \boldsymbol{\varphi}(\boldsymbol{x})\, \mathrm{d}s(\boldsymbol{x}) \\
&= \sum_{l=1}^{m} \Big(\boldsymbol{a}_l \cdot \frac{\mu_-}{\mu_+} \boldsymbol{H}^i(\boldsymbol{z}_l) + \boldsymbol{a}_{l+m} \cdot \frac{\mu_-}{\mu_+} \mathbf{curl} \boldsymbol{H}^i(\boldsymbol{z}_l) \Big)
\end{aligned}$$

for $\boldsymbol{a} \in \mathbb{C}^{3\times 2m}$ and $\boldsymbol{\varphi} \in \boldsymbol{L}^2(\mathcal{M})$. So, the transpose $R^\top:\ \boldsymbol{L}^2(\mathcal{M}) \to \mathbb{C}^{3\times 2m}$ of R is given by

$$R^\top \boldsymbol{\varphi} = \frac{\mu_-}{\mu_+} \big(\boldsymbol{H}^i(\boldsymbol{z}_1), \dots, \boldsymbol{H}^i(\boldsymbol{z}_m), \mathbf{curl} \boldsymbol{H}^i(\boldsymbol{z}_1), \dots, \mathbf{curl} \boldsymbol{H}^i(\boldsymbol{z}_m) \big). \tag{4.4}$$

Lemma 4.1. *The operator R is injective.*

Proof. Suppose $\boldsymbol{a} \in \mathbb{C}^{3\times 2m}$ such that $R\boldsymbol{a} = 0$, i.e.,

$$k_-^2 \sum_{l=1}^{m} \Big(\mathbb{G}^m(\cdot, \boldsymbol{z}_l) \boldsymbol{a}_l + \frac{\mu_-}{\mu_+} \mathbf{curl}_x\, \mathbb{G}^e(\cdot, \boldsymbol{z}_l) \boldsymbol{a}_{m+l} \Big) = 0 \qquad \text{on } \mathcal{M}.$$

Then,

$$\tilde{\boldsymbol{H}} := k_-^2 \sum_{l=1}^{m} \Big(\mathbb{G}^m(\cdot, \boldsymbol{z}_l)\boldsymbol{a}_l + \frac{\mu_-}{\mu} \mathbf{curl}_x \, \mathbb{G}^e(\cdot, \boldsymbol{z}_l)\boldsymbol{a}_{m+l} \Big)$$

together with the associated electric field $\tilde{\boldsymbol{E}} := -1/(\mathrm{i}\,\omega\varepsilon)\mathbf{curl}\tilde{\boldsymbol{H}}$ is a radiating solution of Maxwell's equations (3.32) in $\mathbb{R}^3 \setminus \bigcup_{l=1}^m \{\boldsymbol{z}_l\}$ that satisfies $\tilde{\boldsymbol{H}}|_{\mathcal{M}} = 0$. Now, we follow the proof of Gebauer et al. [52, Theorem 3.2]: Because $\tilde{\boldsymbol{H}}$ has analytic Cartesian components in $\mathbb{R}^3_0 \setminus \bigcup_{l=1}^m \{\boldsymbol{z}_l\}$, the tangential projection $(\boldsymbol{e}_3 \times \tilde{\boldsymbol{H}}|_{\Sigma_d}) \times \boldsymbol{e}_3$ has analytic components, too. Because they vanish on $\mathcal{M}$, they must vanish everywhere in Σ_d, i.e., $(\tilde{\boldsymbol{E}}, \tilde{\boldsymbol{H}})$ is a radiating solution of Maxwell's equations (3.32) in the halfspace $\{\boldsymbol{x} \in \mathbb{R}^3 \mid \boldsymbol{x} \cdot \boldsymbol{e}_3 > d\}$ with $(\boldsymbol{e}_3 \times \tilde{\boldsymbol{H}}|_{\Sigma_d}) \times \boldsymbol{e}_3 = 0$. We can apply the reflection principle and extend $\tilde{\boldsymbol{H}}$ to all of $\mathbb{R}^3$ by

$$\tilde{\boldsymbol{H}}^e(\boldsymbol{x}) := \begin{cases} \tilde{\boldsymbol{H}}(\boldsymbol{x}), & \boldsymbol{x} \cdot \boldsymbol{e}_3 \geq d, \\ -\alpha(\tilde{\boldsymbol{H}}(\alpha(\boldsymbol{x}))), & \boldsymbol{x} \cdot \boldsymbol{e}_3 < d, \end{cases}$$

where α denotes the reflection operator

$$\alpha : \mathbb{R}^3 \to \mathbb{R}^3, \quad \alpha(\boldsymbol{x}) := \boldsymbol{x} - 2(\boldsymbol{x} \cdot \boldsymbol{e}_3 - d)\boldsymbol{e}_3. \tag{4.5}$$

Because by construction the tangential components of $\tilde{\boldsymbol{H}}^e$ and $\mathbf{curl}\tilde{\boldsymbol{H}}^e$ are continuous across Σ_d and $(\tilde{\boldsymbol{E}}^e, \tilde{\boldsymbol{H}}^e)$ with $\tilde{\boldsymbol{E}}^e := -1/(\mathrm{i}\,\omega\varepsilon_+)\mathbf{curl}\tilde{\boldsymbol{H}}^e$ satisfies the Silver–Müller radiation condition, we find that $(\tilde{\boldsymbol{E}}^e, \tilde{\boldsymbol{H}}^e)$ is a radiating solution of Maxwell's equations with constant coefficients

$$\mathbf{curl}\tilde{\boldsymbol{H}}^e + \mathrm{i}\,\omega\varepsilon_+\tilde{\boldsymbol{E}}^e = 0, \quad \mathbf{curl}\tilde{\boldsymbol{E}}^e - \mathrm{i}\,\omega\mu_+\tilde{\boldsymbol{H}}^e = 0 \qquad \text{in } \mathbb{R}^3.$$

As a consequence (cf. Colton and Kress [39, p. 163]), $\tilde{\boldsymbol{H}}^e$ vanishes everywhere in $\mathbb{R}^3$, and therefore $\tilde{\boldsymbol{H}}$ vanishes in $\{\boldsymbol{x} \in \mathbb{R}^3 \mid \boldsymbol{x} \cdot \boldsymbol{e}_3 > d\}$. Accordingly, $\tilde{\boldsymbol{H}} = 0$ in $\mathbb{R}^3_+$ because of its analyticity. In particular, $\tilde{\boldsymbol{E}}$ and $\tilde{\boldsymbol{H}}$ have vanishing tangential components on Σ_0. Because these tangential components are continuous across Σ_0, it now follows from Holmgren's theorem (cf. Kress [80, Theorem 2.4, p. 179]) that the field $(\tilde{\boldsymbol{E}}, \tilde{\boldsymbol{H}})$ is also zero in a neighborhood of Σ_0 in $\mathbb{R}^3_-$, because it is a solution of the homogeneous Maxwell equations with constant coefficients ε_- and μ_-. Accordingly, $\tilde{\boldsymbol{H}} = 0$ in $\mathbb{R}^3 \setminus \bigcup_{l=1}^m \{\boldsymbol{z}_l\}$ because of its analyticity.

Now, let $l \in \{1, \ldots, m\}$ and consider the asymptotic behavior of $\tilde{\boldsymbol{H}}(\boldsymbol{x})$ as $\boldsymbol{x} \to \boldsymbol{z}_l$. For any $\boldsymbol{b} \in \mathbb{R}^3$ we have $\lim_{t\to 0} \tilde{\boldsymbol{H}}(\boldsymbol{z}_l + t\boldsymbol{b}) = 0$. A short calculation shows that the singularity of $\mathbb{G}^m(\cdot, \boldsymbol{z}_l)$ in $\boldsymbol{z}_l$ is of order 3, while the singularity of $\mathbf{curl}_x \, \mathbb{G}^e(\cdot, \boldsymbol{z}_l)$ in $\boldsymbol{z}_l$ is of order 2; see Section B.3 for details. So, taking into account the structure of the singularity of $\mathbb{G}^m(\cdot, \boldsymbol{z}_l)$ (cf. (B.11)), we obtain from

$$\lim_{t\to 0} \mathbb{G}^m(\boldsymbol{z}_l + t\boldsymbol{e}_3, \boldsymbol{z}_l)\boldsymbol{a}_l = 0$$

that $\boldsymbol{a}_l = 0$. Indeed, otherwise the singularity of $\mathbb{G}^m(\cdot, \boldsymbol{z}_l)\boldsymbol{a}_l$ at $\boldsymbol{z}_l$ would imply that $\lim_{t\to 0} |\tilde{\boldsymbol{H}}(\boldsymbol{z}_l + t\boldsymbol{e}_3)| = \infty$. Then, considering the structure of the singularity of $\mathbf{curl}_x\, \mathbb{G}^e(\cdot, \boldsymbol{z}_l)$ (cf. (B.10)), we find from

$$\lim_{t\to 0} \mathbf{curl}_x\, \mathbb{G}^e(\boldsymbol{z}_l + t\boldsymbol{e}_1, \boldsymbol{z}_l)\boldsymbol{a}_{m+l} = 0,$$
$$\lim_{t\to 0} \mathbf{curl}_x\, \mathbb{G}^e(\boldsymbol{z}_l + t\boldsymbol{e}_2, \boldsymbol{z}_l)\boldsymbol{a}_{m+l} = 0$$

that $\boldsymbol{a}_{m+l} = 0$. As $l \in \{1, \ldots, m\}$ was arbitrary, we are done. □

Corollary 4.2. *The operator $R^\top$ is surjective.*

Proof. This result follows from Lemma 4.1 and the well–known relation $\mathcal{R}(R^\top) = \mathcal{N}(R)^a$ between ranges and null spaces of dual operators with finite rank. Here, $\mathcal{N}(R)^a$ denotes the annihilator of $\mathcal{N}(R)$ in $\mathbb{C}^{3\times 2m}$. □

Comparing the formulas (4.3) and (4.4) for R and $R^\top$ and the definition (4.1) of T, we find that these operators are related by

$$T = RMR^\top, \tag{4.6}$$

where the operator $M : \mathbb{C}^{3\times 2m} \to \mathbb{C}^{3\times 2m}$ is given by

$$M\boldsymbol{a} := \frac{\mu_+}{\mu_-}\Big(-\mathbb{M}^0_{B_1}\boldsymbol{a}_1, \ldots, -\mathbb{M}^0_{B_m}\boldsymbol{a}_m, \frac{1}{k_-^2}\mathbb{M}^\infty_{B_1}\boldsymbol{a}_{m+1}, \ldots, \frac{1}{k_-^2}\mathbb{M}^\infty_{B_m}\boldsymbol{a}_{2m}\Big).$$

From the symmetry and positive definiteness of the magnetic and electric polarizability tensors $\mathbb{M}^0_{B_1}, \ldots, \mathbb{M}^0_{B_m}$ and $\mathbb{M}^\infty_{B_1}, \ldots, \mathbb{M}^\infty_{B_m}$ (cf. Proposition A.6), we conclude that M is symmetric and invertible. Taking a closer look at the range of T, we first we observe that $\mathcal{R}(T) \subset \mathcal{R}(R)$. Next, we show that this inclusion is actually an equality.

Proposition 4.3. *The range of T has dimension $6m$ and is given by*

$$\mathcal{R}(T) = \operatorname{span}_{\mathbb{C}}\big\{\, \mathbb{G}^m(\cdot, \boldsymbol{z}_l)\boldsymbol{e}_j\,,\ \mathbf{curl}_x\, \mathbb{G}^e(\cdot, \boldsymbol{z}_l)\boldsymbol{e}_j \;\big|\; j = 1, 2, 3;\ l = 1, \ldots, m\big\}.$$

Proof. The surjectivity of $R^\top$ and M implies $\mathcal{R}(T) = \mathcal{R}(RMR^\top) = \mathcal{R}(R)$. The proposition is then an immediate consequence of (4.3) and Lemma 4.1. □

Now, we present the main tool for the reconstruction of the small scatterers, the characterization of their positions $\boldsymbol{z}_1, \ldots, \boldsymbol{z}_m$ in terms of the leading order term T of the asymptotic expansion of the measurement operator G_δ.

Proposition 4.4. *Let $\boldsymbol{d} = (\boldsymbol{d}_1, \boldsymbol{d}_2) \in (\mathbb{C}^3 \times \mathbb{C}^3) \setminus \{(0,0)\}$, $\boldsymbol{y} \in \mathbb{R}^3_-$ and*

$$\boldsymbol{g}_{y,d} := (\mathbb{G}^m(\cdot, \boldsymbol{y})\boldsymbol{d}_1 + \mathbf{curl}_x\, \mathbb{G}^e(\cdot, \boldsymbol{y})\boldsymbol{d}_2)|_{\mathcal{M}}.$$

Then, $\boldsymbol{g}_{y,d} \in \mathcal{R}(T)$ if and only if $\boldsymbol{y} \in \{\boldsymbol{z}_1, \ldots, \boldsymbol{z}_m\}$.

Proof. Assume that $\boldsymbol{g}_{y,d} \in \mathcal{R}(T)$. As a consequence of Proposition 4.3, $\boldsymbol{g}_{y,d}$ may be represented as

$$\boldsymbol{g}_{y,d} = \sum_{l=1}^{m} \big(\mathbb{G}^m(\cdot, \boldsymbol{z}_l)\boldsymbol{a}_l + \mathbf{curl}_x \mathbb{G}^e(\cdot, \boldsymbol{z}_{l+m})\boldsymbol{a}_{l+m} \big) \qquad \text{on } \mathcal{M},$$

with $\boldsymbol{a}_1, \ldots, \boldsymbol{a}_{2m} \in \mathbb{C}^3$. But then both,

$$\boldsymbol{H}^a := \sum_{l=1}^{m} \Big(\mathbb{G}^m(\cdot, \boldsymbol{z}_l)\boldsymbol{a}_l + \frac{\mu_+}{\mu} \mathbf{curl}_x \mathbb{G}^e(\cdot, \boldsymbol{z}_{l+m})\boldsymbol{a}_{l+m} \Big)$$

and

$$\boldsymbol{H}^b := \mathbb{G}^m(\cdot, \boldsymbol{y})\boldsymbol{d}_1 + \frac{\mu_+}{\mu} \mathbf{curl}_x \mathbb{G}^e(\cdot, \boldsymbol{y})\boldsymbol{d}_2$$

together with the corresponding electric fields are radiating solutions of Maxwell's equations (3.32) in $\mathbb{R}^3 \setminus (\bigcup_{l=1}^m \{\boldsymbol{z}_l\} \cup \{\boldsymbol{y}\})$ that coincide on $\mathcal{M}$. Hence, $\tilde{\boldsymbol{H}} := \boldsymbol{H}^a - \boldsymbol{H}^b$ together with the associated electric field $\tilde{\boldsymbol{E}}$ is a radiating solution of (3.32) in $\mathbb{R}^3 \setminus (\bigcup_{l=1}^m \{\boldsymbol{z}_l\} \cup \{\boldsymbol{y}\})$ that satisfies $\tilde{\boldsymbol{H}}|_{\mathcal{M}} = 0$. Following the proof of Lemma 4.1, we conclude that $(\tilde{\boldsymbol{E}}, \tilde{\boldsymbol{H}})$ vanishes everywhere in $\mathbb{R}^3 \setminus (\bigcup_{l=1}^m \{\boldsymbol{z}_l\} \cup \{\boldsymbol{y}\})$. Thus, $\boldsymbol{H}^a = \boldsymbol{H}^b$ in $\mathbb{R}^3 \setminus (\bigcup_{l=1}^m \{\boldsymbol{z}_l\} \cup \{\boldsymbol{y}\})$. This is only possible if $\boldsymbol{y} \in \{\boldsymbol{z}_1, \ldots, \boldsymbol{z}_m\}$, and we have established the necessity of this condition. The sufficiency follows from Proposition 4.3. □

4.1.2 Tangential Excitations and Measurements

In this section, we assume that the incident fields $(\boldsymbol{E}^i, \boldsymbol{H}^i)$ are given as superpositions of electromagnetic fields due to magnetic dipole distributions on $\mathcal{M}$ with *tangential dipole densities*

$$\boldsymbol{\varphi} \in \boldsymbol{L}_t^2(\mathcal{M}) := \big\{ \boldsymbol{a} \in \boldsymbol{L}^2(\mathcal{M}) \;\big|\; \boldsymbol{e}_3 \cdot \boldsymbol{a} = 0 \big\},$$

and we measure only the *tangential components* $(\boldsymbol{e}_3 \times \boldsymbol{H}^s|_{\mathcal{M}}) \times \boldsymbol{e}_3$ of the corresponding scattered magnetic fields on $\mathcal{M}$.

We introduce the projection operator $P_t : \boldsymbol{L}^2(\mathcal{M}) \to \boldsymbol{L}_t^2(\mathcal{M})$,

$$P_t\boldsymbol{\phi} := (\boldsymbol{e}_3 \times \boldsymbol{\phi}) \times \boldsymbol{e}_3,$$

and denote by $P_t^\top : \boldsymbol{L}_t^2(\mathcal{M}) \to \boldsymbol{L}^2(\mathcal{M})$ the corresponding transpose. Then, we can define the *tangential measurement operator* $G_{\delta,t} : \boldsymbol{L}_t^2(\mathcal{M}) \to \boldsymbol{L}_t^2(\mathcal{M})$,

$$G_{\delta,t}\boldsymbol{\varphi} := P_t G_\delta P_t^\top \boldsymbol{\varphi}.$$

Because P_t and $P_t^\top$ are bounded and linear, we find from Corollary 3.25 that

$$G_{\delta,t} = \delta^3 P_t T P_t^\top + \mathcal{O}(\delta^4) \tag{4.7}$$

in $\mathcal{L}(\boldsymbol{L}_t^2(\mathcal{M}))$ as $\delta \to 0$. The factorization (4.6) of the leading order term of the asymptotic expansion becomes

$$P_t T P_t^\top = (P_t R) M (P_t R)^\top.$$

Exactly as in Lemma 4.1, we can prove that $P_t R$ is injective, and thus $(P_t R)^\top$ is surjective. So, we find that $\mathcal{R}(P_t T P_t^\top) = \mathcal{R}(P_t R)$, and recalling (4.3), we obtain the following proposition.

Proposition 4.5. *The range of $P_t T P_t^\top$ has dimension $6m$ and is given by*

$$\mathcal{R}(P_t T P_t^\top) = \operatorname{span}_{\mathbb{C}} \big\{ P_t(\, \mathbb{G}^m(\cdot, \boldsymbol{z}_l)\boldsymbol{e}_j)\,, \\ P_t(\mathbf{curl}_x\, \mathbb{G}^e(\cdot, \boldsymbol{z}_l)\boldsymbol{e}_j) \;\big|\; j = 1,2,3;\ l = 1,\dots,m \big\}.$$

Using this result, the following range characterization of the positions of the scatterers $\boldsymbol{z}_1, \dots, \boldsymbol{z}_m$ can be verified in the same manner as Proposition 4.4.

Proposition 4.6. *Let $\boldsymbol{d} = (\boldsymbol{d}_1, \boldsymbol{d}_2) \in (\mathbb{C}^3 \times \mathbb{C}^3) \setminus \{(0,0)\}$, $\boldsymbol{y} \in \mathbb{R}^3_-$ and*

$$\boldsymbol{g}_{y,d}^t := P_t\big(\big(\mathbb{G}^m(\cdot, \boldsymbol{y})\boldsymbol{d}_1 + \mathbf{curl}_x\, \mathbb{G}^e(\cdot, \boldsymbol{y})\boldsymbol{d}_2 \big)\big|_{\mathcal{M}} \big).$$

Then, $\boldsymbol{g}_{y,d}^t \in \mathcal{R}(P_t T P_t^\top)$ if and only if $\boldsymbol{y} \in \{\boldsymbol{z}_1, \dots, \boldsymbol{z}_m\}$.

4.1.3 Normal Excitations and Measurements

In this section, we assume that the incident fields $(\boldsymbol{E}^i, \boldsymbol{H}^i)$ are given as superpositions of electromagnetic fields due to magnetic dipole distributions on $\mathcal{M}$ with *normal dipole densities*

$$\boldsymbol{\varphi} \in \boldsymbol{L}_n^2(\mathcal{M}) := \big\{ \boldsymbol{a} \in \boldsymbol{L}^2(\mathcal{M}) \;\big|\; \boldsymbol{e}_1 \cdot \boldsymbol{a} = \boldsymbol{e}_2 \cdot \boldsymbol{a} = 0 \big\},$$

and we measure only the *normal components* $\boldsymbol{e}_3 \cdot \boldsymbol{H}^s|_{\mathcal{M}}$ of the corresponding scattered magnetic field on $\mathcal{M}$.

We introduce the projection operator $P_n : \boldsymbol{L}^2(\mathcal{M}) \to \boldsymbol{L}_n^2(\mathcal{M})$,

$$P_n \boldsymbol{\phi} := (\boldsymbol{e}_3 \cdot \boldsymbol{\phi})\boldsymbol{e}_3,$$

and denote by $P_n^\top : \boldsymbol{L}_n^2(\mathcal{M}) \to \boldsymbol{L}^2(\mathcal{M})$ the corresponding transpose. Then, we can define the *normal measurement operator* $G_{\delta,n} : \boldsymbol{L}_n^2(\mathcal{M}) \to \boldsymbol{L}_n^2(\mathcal{M})$,

$$G_{\delta,n}\boldsymbol{\varphi} := P_n G_\delta P_n^\top \boldsymbol{\varphi}.$$

Because P_n and $P_n^\top$ are bounded and linear, we find from Corollary 3.25 that

$$G_{\delta,n} = \delta^3 P_n T P_n^\top + \mathcal{O}(\delta^4) \tag{4.8}$$

in $\mathcal{L}(\boldsymbol{L}_n^2(\mathcal{M}))$ as $\delta \to 0$. The factorization (4.6) of the leading order term of the asymptotic expansion becomes

$$P_n T P_n^\top = (P_n R) M (P_n R)^\top.$$

Lemma 4.7. *The operator $P_n R$ is not injective and*

$$\mathcal{N}(P_n R) = \{0\}^m \times (\mathbb{C}\, \boldsymbol{e}_3)^m.$$

Proof. Suppose $\boldsymbol{a} \in \mathbb{C}^{3\times 2m}$ such that $P_n R \boldsymbol{a} = 0$, i.e.,

$$k_-^2 \sum_{l=1}^{m} \Big(\boldsymbol{e}_3 \cdot \big(\mathbb{G}^m(\cdot, \boldsymbol{z}_l)\boldsymbol{a}_l \big) + \frac{\mu_-}{\mu_+} \boldsymbol{e}_3 \cdot \big(\mathbf{curl}_x\, \mathbb{G}^e(\cdot, \boldsymbol{z}_l)\boldsymbol{a}_{m+l} \big) \Big) = 0 \qquad \text{on } \mathcal{M}.$$

Then,

$$\tilde{\boldsymbol{H}} := k_-^2 \sum_{l=1}^{m} \Big(\mathbb{G}^m(\cdot, \boldsymbol{z}_l)\boldsymbol{a}_l + \frac{\mu_-}{\mu} \mathbf{curl}_x\, \mathbb{G}^e(\cdot, \boldsymbol{z}_l)\boldsymbol{a}_{m+l} \Big)$$

together with the associated electric field $\tilde{\boldsymbol{E}} := -1/(\mathrm{i}\,\omega\varepsilon)\mathbf{curl}\tilde{\boldsymbol{H}}$ is a radiating solution of Maxwell's equations (3.32) in $\mathbb{R}^3 \setminus \bigcup_{l=1}^m \{\boldsymbol{z}_l\}$ that satisfies $\boldsymbol{e}_3 \cdot \tilde{\boldsymbol{H}}|_{\mathcal{M}} = 0$. Because $\tilde{\boldsymbol{H}}$ has analytic Cartesian components in $\mathbb{R}^3_0 \setminus \bigcup_{l=1}^m \{\boldsymbol{z}_l\}$, the normal component $\boldsymbol{e}_3 \cdot \tilde{\boldsymbol{H}}|_{\Sigma_d}$ on Σ_d is analytic, too. Because it vanishes on $\mathcal{M}$, it must vanish everywhere on Σ_d, i.e., $\tilde{H}_3 := \boldsymbol{e}_3 \cdot \tilde{\boldsymbol{H}}$ is a radiating solution of Helmholtz's equation

$$\Delta \tilde{H}_3 + k_+^2 \tilde{H}_3 = 0 \tag{4.9}$$

in the halfspace $\{\boldsymbol{x} \in \mathbb{R}^3 \mid \boldsymbol{x} \cdot \boldsymbol{e}_3 > d\}$ with $\tilde{H}_3|_{\Sigma_d} = 0$. We can apply the reflection principle and extend $\tilde{H}_3$ to all of $\mathbb{R}^3$ by

$$\tilde{H}_3^e(\boldsymbol{x}) := \begin{cases} \tilde{H}_3(\boldsymbol{x}), & \boldsymbol{x} \cdot \boldsymbol{e}_3 \geq d, \\ -\tilde{H}_3(\alpha(\boldsymbol{x})), & \boldsymbol{x} \cdot \boldsymbol{e}_3 < d, \end{cases}$$

where α denotes the reflection operator from (4.5). Because by construction $\tilde{H}_3^e$ and $\frac{\partial \tilde{H}_3}{\partial \boldsymbol{e}_3}$ are continuous across Σ_d and $\tilde{H}_3^e$ satisfies the Sommerfeld radiation condition, we find that $\tilde{H}_3^e$ is a radiating solution of Helmholtz's equation (4.9) with constant coefficient in $\mathbb{R}^3$. As a consequence (cf. [39, p. 20]), $\tilde{H}_3^e$ vanishes everywhere in $\mathbb{R}^3$, and so $\tilde{H}_3$ vanishes in $\{\boldsymbol{x} \in \mathbb{R}^3 \mid \boldsymbol{x} \cdot \boldsymbol{e}_3 > d\}$. Accordingly, $\tilde{H}_3 = 0$ in $\mathbb{R}^3_+$ because of its analyticity. Because $[\mu \tilde{H}_3]_{\Sigma_0} = 0$ and $\left[\frac{\partial \tilde{H}_3}{\partial \boldsymbol{e}_3}\right]_{\Sigma_0} = 0$ (cf. Cutzach and Hazard [43, p. 439] or Cessenat [30, pp. 32–33]), it now follows from Holmgren's theorem (cf. Kress [81, Theorem 2.2, p. 41]), that $\tilde{H}_3$ is also zero in a neighborhood of Σ_0 in $\mathbb{R}^3_-$, because it is a solution of the homogeneous Helmholtz equation with constant coefficient k_-. Accordingly, $\tilde{H}_3 = 0$ in $\mathbb{R}^3 \setminus \bigcup_{l=1}^m \{\boldsymbol{z}_l\}$ because of its analyticity.

Now, let $l \in \{1, \ldots, m\}$ and consider the asymptotic behavior of $\tilde{H}_3(\boldsymbol{x})$ as $\boldsymbol{x} \to \boldsymbol{z}_l$. For any $\boldsymbol{b} \in \mathbb{R}^3$, we have $\lim_{t\to 0} \tilde{H}_3(\boldsymbol{z}_l + t\boldsymbol{b}) = 0$. As already mentioned, the singularity of $\mathbb{G}^m(\cdot, \boldsymbol{z}_l)$ in $\boldsymbol{z}_l$ is of order 3, while the singularity of $\mathbf{curl}_x\, \mathbb{G}^e(\cdot, \boldsymbol{z}_l)$ in $\boldsymbol{z}_l$ is of order 2; see Section B.3 for details. So,

taking into account the structure of the singularity of $\mathbb{G}^m(\cdot, \boldsymbol{z}_l)$ (cf. (B.11)), we obtain from

$$\begin{aligned}\lim_{t\to 0}\big(\boldsymbol{e}_3 \cdot \mathbb{G}^m(\boldsymbol{z}_l + t\boldsymbol{e}_3, \boldsymbol{z}_l)\boldsymbol{a}_l\big) &= 0,\\ \lim_{t\to 0}\big(\boldsymbol{e}_3 \cdot \mathbb{G}^m(\boldsymbol{z}_l + t(\boldsymbol{e}_1+\boldsymbol{e}_3), \boldsymbol{z}_l)\boldsymbol{a}_l\big) &= 0,\\ \lim_{t\to 0}\big(\boldsymbol{e}_3 \cdot \mathbb{G}^m(\boldsymbol{z}_l + t(\boldsymbol{e}_2+\boldsymbol{e}_3), \boldsymbol{z}_l)\boldsymbol{a}_l\big) &= 0\end{aligned}$$

that $\boldsymbol{a}_l = 0$. Then, considering the singularity of $\mathbf{curl}_x\, \mathbb{G}^e(\cdot, \boldsymbol{z}_l)$ in $\boldsymbol{z}_l$ (cf. (B.10)), we find from

$$\begin{aligned}\lim_{t\to 0}\big(\boldsymbol{e}_3 \cdot \mathbf{curl}_x\, \mathbb{G}^e(\boldsymbol{z}_l + t\boldsymbol{e}_1, \boldsymbol{z}_l)\boldsymbol{a}_{m+l}\big) &= 0,\\ \lim_{t\to 0}\big(\boldsymbol{e}_3 \cdot \mathbf{curl}_x\, \mathbb{G}^e(\boldsymbol{z}_l + t\boldsymbol{e}_2, \boldsymbol{z}_l)\boldsymbol{a}_{m+l}\big) &= 0\end{aligned}$$

that $\boldsymbol{e}_1 \cdot \boldsymbol{a}_{m+l} = \boldsymbol{e}_2 \cdot \boldsymbol{a}_{m+l} = 0$. Because $l \in \{1, \dots, m\}$ was arbitrary, we have shown that $\mathcal{N}(P_n R) \subset \{0\}^m \times (\,\mathbb{C}\,\boldsymbol{e}_3)^m$.

On the other hand, it follows from (B.10) that $\boldsymbol{e}_3 \cdot (\frac{1}{\mu}\mathbf{curl}_x\, \mathbb{G}^e(\cdot, \boldsymbol{z}_l)\boldsymbol{e}_3)$ is bounded in a neighborhood of $\boldsymbol{z}_l$, and therefore an entire solution of a transmission problem for Helmholtz's equation satisfying the Sommerfeld radiation condition. Thus, $\boldsymbol{e}_3 \cdot (\frac{1}{\mu}\mathbf{curl}_x\, \mathbb{G}^e(\cdot, \boldsymbol{z}_l)\boldsymbol{e}_3) = 0$; cf. Kristensson [83] if $k \in \mathbb{R}$ and Petry [92, Satz 2.3] if $k \notin \mathbb{R}$. So we obtain that $\{0\}^m \times (\,\mathbb{C}\,\boldsymbol{e}_3)^m \subset \mathcal{N}(P_n R)$. □

Again it is clear that $\mathcal{R}(P_n T P_n^\top) \subset \mathcal{R}(P_n R)$. Next, we show that this inclusion is actually an equality.

Proposition 4.8. *The range of $P_n T P_n^\top$ has dimension $5m$ and is given by*

$$\begin{aligned}\mathcal{R}\big(P_n T P_n^\top\big) = \operatorname{span}_{\mathbb{C}} \big\{ & P_n\big(\mathbb{G}^m(\cdot, \boldsymbol{z}_l)\boldsymbol{e}_{j_1}\big),\\ & P_n\big(\mathbf{curl}_x\, \mathbb{G}^e(\cdot, \boldsymbol{z}_l)\boldsymbol{e}_{j_2}\big) \;\big|\; j_1 = 1,2,3;\ j_2 = 1,2;\ l = 1,\dots,m\big\}.\end{aligned}$$

Proof. Because the range of $P_n R$ is finite dimensional and M is symmetric, we find that

$$\mathcal{R}(P_n R) = \mathcal{N}\big((P_n R)^\top\big)^a, \tag{4.10a}$$

$$\mathcal{R}\big((P_n R) M (P_n R)^\top\big) = \mathcal{N}\big((P_n R) M (P_n R)^\top\big)^a. \tag{4.10b}$$

Let $\boldsymbol{\phi} \in \mathcal{N}((P_n R) M (P_n R)^\top)$. Then,

$$0 = \big\langle \boldsymbol{\phi}, (P_n R) M (P_n R)^\top \boldsymbol{\phi} \big\rangle_{\mathcal{M}} = \big\langle (P_n R)^\top \boldsymbol{\phi}, M (P_n R)^\top \boldsymbol{\phi} \big\rangle_{\mathbb{C}^{3\times 2m}}$$

and because the electric and magnetic polarizability tensors are positive definite, we conclude that $\boldsymbol{\phi} \in \mathcal{N}((P_n R)^\top)$. Therefore,

$$\mathcal{N}((P_n R) M (P_n R)^\top) \subset \mathcal{N}((P_n R)^\top),$$

and from (4.10), we obtain that $\mathcal{R}(P_n R) \subset \mathcal{R}((P_n R) M (P_n R)^\top)$. This means that $\mathcal{R}(P_n R) = \mathcal{R}(P_n T P_n^\top)$. The proposition follows now from (4.3) and Lemma 4.7. □

Proposition 4.9. *Let* $\boldsymbol{d} = (\boldsymbol{d}_1, \boldsymbol{d}_2) \in (\mathbb{C}^3 \times \mathbb{C}^3) \setminus (\mathbb{C}(0, \boldsymbol{e}_3))$, $\boldsymbol{y} \in \mathbb{R}^3_-$ *and*

$$\boldsymbol{g}^n_{y,d} := P_n\big(\big(\mathbb{G}^m(\cdot, \boldsymbol{y})\boldsymbol{d}_1 + \mathbf{curl}_x\, \mathbb{G}^e(\cdot, \boldsymbol{y})\boldsymbol{d}_2\big)\big|_{\mathcal{M}}\big).$$

Then, $\boldsymbol{g}^n_{y,d} \in \mathcal{R}(P_n T P_n^\top)$ *if and only if* $\boldsymbol{y} \in \{\boldsymbol{z}_1, \ldots, \boldsymbol{z}_m\}$.

Proof. Assume that $\boldsymbol{g}^n_{y,d} \in \mathcal{R}(P_n T P_n^\top)$. As a consequence of Proposition 4.8, $\boldsymbol{g}^n_{y,d}$ may be represented as

$$\boldsymbol{g}^n_{y,d} = \sum_{l=1}^{m} \big(P_n(\mathbb{G}^m(\cdot, \boldsymbol{z}_l)\boldsymbol{a}_l) + P_n(\mathbf{curl}_x\, \mathbb{G}^e(\cdot, \boldsymbol{z}_{l+m})\boldsymbol{a}_{l+m})\big) \qquad \text{on } \mathcal{M},$$

with $\boldsymbol{a}_1, \ldots, \boldsymbol{a}_m \in \mathbb{C}^3$ and $\boldsymbol{a}_{m+1}, \ldots, \boldsymbol{a}_{2m} \in \mathbb{C}^3 \setminus (\mathbb{C}\,\boldsymbol{e}_3)$. But then both,

$$\boldsymbol{H}^a := \sum_{l=1}^{m} \Big(\mathbb{G}^m(\cdot, \boldsymbol{z}_l)\boldsymbol{a}_l + \frac{\mu_+}{\mu}\mathbf{curl}_x\, \mathbb{G}^e(\cdot, \boldsymbol{z}_{l+m})\boldsymbol{a}_{l+m}\Big)$$

and

$$\boldsymbol{H}^b := \mathbb{G}^m(\cdot, \boldsymbol{y})\boldsymbol{d}_1 + \frac{\mu_+}{\mu}\mathbf{curl}_x\, \mathbb{G}^e(\cdot, \boldsymbol{y})\boldsymbol{d}_2$$

together with the corresponding electric fields are radiating solutions of Maxwell's equations (3.32) in $\mathbb{R}^3 \setminus (\bigcup_{l=1}^m \{\boldsymbol{z}_l\} \cup \{\boldsymbol{y}\})$ and their normal components coincide on $\mathcal{M}$. Hence, $\tilde{\boldsymbol{H}} := \boldsymbol{H}^a - \boldsymbol{H}^b$ together with the associated electric field $\tilde{\boldsymbol{E}}$ is a radiating solution of (3.32) in $\mathbb{R}^3 \setminus (\bigcup_{l=1}^m \{\boldsymbol{z}_l\} \cup \{\boldsymbol{y}\})$ that satisfies $\boldsymbol{e}_3 \cdot \tilde{\boldsymbol{H}}|_{\mathcal{M}} = 0$. We follow the proof of Lemma 4.7 and conclude that $\tilde{H}_3$ vanishes everywhere in $\mathbb{R}^3 \setminus (\bigcup_{l=1}^m \{\boldsymbol{z}_l\} \cup \{\boldsymbol{y}\})$, which means that $H_3^a = H_3^b$ in $\mathbb{R}^3 \setminus (\bigcup_{l=1}^m \{\boldsymbol{z}_l\} \cup \{\boldsymbol{y}\})$. This is only possible if $\boldsymbol{y} \in \{\boldsymbol{z}_1, \ldots, \boldsymbol{z}_m\}$, and we have established the necessity of this condition. The sufficiency follows directly from Proposition 4.3. □

4.2 Determining the Positions of the Scatterers

In this section, we discuss an implementation of the range criteria developed in the previous section in a reconstruction algorithm. We focus only on the case of three–dimensional excitations and measurements. Tangential and normal excitations and measurements can be addressed in essentially the same manner.

To implement the range criterion from Proposition 4.4, we need orthogonal projections of the *test functions* $\boldsymbol{g}_{y,d}$ on the finite dimensional range space $\mathcal{R}(T)$ and its orthogonal complement. However, in practise we do not measure the leading order term T of the asymptotic expansion (4.2) but only the full measurement operator G_δ. By (4.2), G_δ is a good approximation of $\delta^3 T$ for small values of δ. Hence, we can use perturbation theory for linear operators to approximate the singular values and singular vectors of T by the singular values and singular vectors of G_δ.

Let $(\cdot,\cdot)_{\boldsymbol{L}^2(\mathcal{M})}$ denote the (complex) scalar product on $\boldsymbol{L}^2(\mathcal{M})$, and for any bounded linear operator $A \in \mathcal{L}(\boldsymbol{L}^2(\mathcal{M}))$ let $A^* \in \mathcal{L}(\boldsymbol{L}^2(\mathcal{M}))$ be the adjoint operator of A with respect to this scalar product. Because G_δ is a compact operator on $\boldsymbol{L}^2(\mathcal{M})$, it admits a singular value decomposition

$$G_\delta \boldsymbol{\varphi} = \sum_{l=1}^{\infty} \sigma_l^\delta (\boldsymbol{\varphi}, \boldsymbol{v}_l^\delta)_{\boldsymbol{L}^2(\mathcal{M})} \boldsymbol{u}_l^\delta, \qquad \boldsymbol{\varphi} \in \boldsymbol{L}^2(\mathcal{M}),$$

where $((\sigma_l^\delta)^2)_{l\in\mathbb{N}}$ are the eigenvalues of $G_\delta^* G_\delta$, written in decreasing order with multiplicity, $\sigma_l^\delta \geq 0$, $(\boldsymbol{v}_l^\delta)_{l\in\mathbb{N}}$ is a corresponding complete orthonormal system of eigenvectors of $G_\delta^* G_\delta$, and $(\boldsymbol{u}_l)_{l\in\mathbb{N}}$ is a complete orthonormal system of eigenvectors of $G_\delta G_\delta^*$; cf. Kress [79, Theorem 5.16]. Similarly, the finite rank operator T can be decomposed as

$$T\boldsymbol{\varphi} = \sum_{l=1}^{6m} \sigma_l (\boldsymbol{\varphi}, \boldsymbol{v}_l)_{\boldsymbol{L}^2(\mathcal{M})} \boldsymbol{u}_l, \qquad \boldsymbol{\varphi} \in \boldsymbol{L}^2(\mathcal{M}),$$

with $\sigma_1 \geq \sigma_2 \geq \cdots \geq \sigma_{6m} > 0$.

From (4.2), we obtain that

$$G_\delta^* G_\delta = \delta^6 T^* T + \mathcal{O}(\delta^7), \tag{4.11}$$

in $\mathcal{L}(\boldsymbol{L}^2(\mathcal{M}))$ as $\delta \to 0$. So, applying Theorem V.4.10 from Kato [68], we get the following asymptotic formula for the singular values as $\delta \to 0$:

$$(\sigma_l^\delta)^2 = \delta^6 \sigma_l^2 + \mathcal{O}(\delta^7), \qquad l \in \mathbb{N}, \tag{4.12}$$

where we have set $\sigma_l = 0$ for $l \geq 6m$. Next, let

$$\begin{aligned} P_l^\delta &: \boldsymbol{L}^2(\mathcal{M}) \to \operatorname{span}_{\mathbb{C}} \{\boldsymbol{u}_1^\delta, \ldots, \boldsymbol{u}_l^\delta\}, && l \in \mathbb{N}, \\ P_l &: \boldsymbol{L}^2(\mathcal{M}) \to \operatorname{span}_{\mathbb{C}} \{\boldsymbol{u}_1, \ldots, \boldsymbol{u}_l\}, && l = 1, \ldots, 6m, \end{aligned}$$

denote the orthogonal projections onto these subspaces, respectively. To simplify the presentation we suppose in the following that all eigenvalues of $G_\delta^* G_\delta$ and T^*T are simple. But this assumption is not essential and could be omitted by choosing the eigenvectors corresponding to multiple eigenvalues appropriately . For $1 \leq l \leq 6m$, let $\Gamma_{\delta,l}$ be a rectifiable, simple closed curve that encloses an open set containing the eigenvalues $(\sigma_1^\delta)^2, \ldots, (\sigma_l^\delta)^2$ in its interior and $(\sigma_{l+1}^\delta)^2, (\sigma_{l+2}^\delta)^2, \ldots$ in its exterior. Then, by [68, III-(6.19), p. 178] we can write

$$P_l^\delta = -\frac{1}{2\pi\,\mathrm{i}} \int_{\Gamma_{\delta,l}} \mathfrak{R}(\zeta, G_\delta G_\delta^*)\, \mathrm{d}\zeta,$$

where the operator valued function $\mathfrak{R}(\cdot, G_\delta G_\delta^*)$ is the resolvent of $G_\delta G_\delta^*$ (cf. [68, p. 173]). If δ is small enough, we find from (4.12) that $\Gamma_{\delta,l}$ also belongs to the resolvent set of $\delta^6 TT^*$, and thus we can write

$$P_l = -\frac{1}{2\pi\,\mathrm{i}} \int_{\Gamma_{\delta,l}} \mathfrak{R}(\zeta, \delta^6 TT^*)\, \mathrm{d}\zeta,$$

where $\mathfrak{R}(\cdot, \delta^6 TT^*)$ denotes the resolvent of $\delta^6 TT^*$. Therefore,

$$\begin{aligned} P_l^\delta - P_l &= -\frac{1}{2\pi\,\mathrm{i}} \int_{\Gamma_{\delta,l}} \big(\mathfrak{R}(\zeta, G_\delta G_\delta^*) - \mathfrak{R}(\zeta, \delta^6 TT^*)\big)\,\mathrm{d}\zeta \\ &= \frac{1}{2\pi\,\mathrm{i}} \int_{\Gamma_{\delta,l}} \mathfrak{R}(\zeta, G_\delta G_\delta^*)\big(G_\delta G_\delta^* - \delta^6 TT^*\big)\mathfrak{R}(\zeta, \delta^6 TT^*)\,\mathrm{d}\zeta, \end{aligned}$$

and so

$$\big\|P_l^\delta - P_l\big\| \le \frac{|\Gamma_{\delta,l}|}{2\pi\,\mathrm{i}} \max_{\zeta\in\Gamma_{\delta,l}} \big\|\mathfrak{R}(\zeta, G_\delta G_\delta^*)\big\| \big\|G_\delta G_\delta^* - \delta^6 TT^*\big\| \max_{\zeta\in\Gamma_{\delta,l}} \big\|\mathfrak{R}(\zeta, \delta^6 TT^*)\big\|.$$

Here, $\|\cdot\|$ denotes the operator norm in $\mathcal{L}(\boldsymbol{L}^2(\mathcal{M}))$, and $|\Gamma_{\delta,l}|$ is the length of $\Gamma_{\delta,l}$. Again from (4.12), we find that $\Gamma_{\delta,l}$ can be chosen such that $|\Gamma_{\delta,l}| = \mathcal{O}(\delta^6)$ as $\delta \to 0$. Moreover, by [68, V-(3.16), p. 272],

$$\begin{aligned} \big\|\mathfrak{R}(\zeta, G_\delta G_\delta^*)\big\| &= 1/\operatorname{dist}(\zeta, \Sigma(G_\delta G_\delta^*)), \\ \big\|\mathfrak{R}(\zeta, \delta^6 TT^*)\big\| &= 1/\operatorname{dist}(\zeta, \Sigma(\delta^6 TT^*)), \end{aligned}$$

where $\Sigma(G_\delta G_\delta^*)$ and $\Sigma(\delta^6 TT^*)$ denotes the spectrum of $G_\delta G_\delta^*$ and $\delta^6 TT^*$, respectively. So, we find that

$$\|\mathfrak{R}(\zeta, G_\delta G_\delta^*)\| = \|\mathfrak{R}(\zeta, \delta^6 TT^*)\| = \mathcal{O}(\delta^{-6})$$

uniformly for $\zeta \in \Gamma_{\delta,l}$ as $\delta \to 0$. Using this and recalling (4.11), we obtain that

$$P_l^\delta = P_l + \mathcal{O}(\delta), \qquad l = 1, \dots, 6m, \tag{4.13}$$

as $\delta \to 0$ in $\mathcal{L}(\boldsymbol{L}^2(\mathcal{M}))$.

In Proposition 4.4, we have seen that a test point $\boldsymbol{y} \in \mathbb{R}^3_-$ coincides with one of the positions $\boldsymbol{z}_l$, $l = 1, \dots, m$, if and only if $\boldsymbol{g}_{y,d} \in \mathcal{R}(T)$, or equivalently $(I - P_{6m})\boldsymbol{g}_{y,d} = 0$. That means, if we decompose the test function orthogonally as $\boldsymbol{g}_{y,d} = P_{6m}\boldsymbol{g}_{y,d} + (I - P_{6m})\boldsymbol{g}_{y,d}$ and define the angle $\beta(\boldsymbol{y}) \in [0, \pi/2]$ by

$$\cot\beta_{6m}(\boldsymbol{y}) := \frac{\|P_{6m}\boldsymbol{g}_{y,d}\|_{\boldsymbol{L}^2(\mathcal{M})}}{\|(I - P_{6m})\boldsymbol{g}_{y,d}\|_{\boldsymbol{L}^2(\mathcal{M})}},$$

then we have

$$\boldsymbol{y} \in \{\boldsymbol{z}_l \mid l = 1, \dots, m\} \Longleftrightarrow \beta_{6m}(\boldsymbol{y}) = 0 \Longleftrightarrow \cot\beta_{6m}(\boldsymbol{y}) = \infty.$$

As already mentioned, we cannot compute $\beta_{6m}(\boldsymbol{y})$, because P_{6m} corresponds to the leading order term T of the asymptotic expansion (4.2), but what we measure is the full measurement operator G_δ. However, in view of (4.13), for small values of δ the projected test function $P_{6m}\boldsymbol{g}_{y,d}$ is well approximated

by $P^\delta_{6m}\boldsymbol{g}_{y,d}$, and the projections P^δ_p can be computed for each $p \in \mathbb{N}$ by means of the singular value decomposition of the measurement operator G_δ. Hence, for $p \in \mathbb{N}$, we define the angle $\beta^\delta_p(\boldsymbol{y}) \in [0, \pi/2]$ by

$$\cot \beta^\delta_p(\boldsymbol{y}) := \frac{\|P^\delta_p \boldsymbol{g}_{y,d}\|_{\boldsymbol{L}^2(\mathcal{M})}}{\|(I - P^\delta_p)\boldsymbol{g}_{y,d}\|_{\boldsymbol{L}^2(\mathcal{M})}} = \left(\frac{\sum_{j \le p} |(\boldsymbol{u}^\delta_j, \boldsymbol{g}_{y,d})_{\boldsymbol{L}^2(\mathcal{M})}|^2}{\sum_{j > p} |(\boldsymbol{u}^\delta_j, \boldsymbol{g}_{y,d})_{\boldsymbol{L}^2(\mathcal{M})}|^2} \right)^{1/2}. \tag{4.14}$$

If we plot $\cot \beta^\delta_{6m}(\boldsymbol{y})$ (resp. $\beta^\delta_{6m}(\boldsymbol{y})$), we expect to see large values (resp. values close to zero) for points $\boldsymbol{y}$ which are close to the positions $\boldsymbol{z}_l$, $l = 1, \ldots, m$.

Estimating the number of scatterers

As the number m of unknown scatterers is usually not known a priori, it has to be estimated somehow. Two different strategies are available: On the one hand, recalling (4.12), m may be estimated by looking for a gap in the set of singular values σ^δ_l, $l \in \mathbb{N}$, of G_δ. This works if δ is small enough and the noise level is not too high. Otherwise it may give misleading results.

On the other hand, we can plot $\cot \beta^\delta_p(\boldsymbol{y})$ (resp. $\beta^\delta_p(\boldsymbol{y})$) for increasing values of p, until the number of reconstructed scatterers does not increase any more. This is reasonable, because for subspaces $U \subset \mathcal{R}(T)$ the assertion of Proposition 4.4 reduces to

$$\boldsymbol{g}_{y,d} \in U \quad \Longrightarrow \quad \boldsymbol{y} \in \{\boldsymbol{z}_1, \ldots, \boldsymbol{z}_m\}.$$

So, testing whether $\boldsymbol{g}_{y,d}$ is contained in a subspace $U \subset \mathcal{R}(T)$, we can only expect to reconstruct a (possibly empty) subset of $\{\boldsymbol{z}_1, \ldots, \boldsymbol{z}_m\}$. The number of reconstructed scatterers is monotonically increasing (not strictly) as $\dim(U)$ increases, until all m scatterers are reconstructed for $\dim(U) = 6m$. Numerical experiments indicate that the number of scatterers is constant for moderately sized $p > 6m$.

Both strategies have been successfully tested in [22] (for an inverse conductivity problem).

Approximation of the singular value decomposition of G_δ

In practise, we can of course not measure the full measurement operator G_δ, but only finitely many data corresponding to scattered fields excited by finitely many incident fields. In order to calculate approximations of the singular values and the singular vectors of the infinite dimensional operator G_δ from these discrete measurements, we follow Gebauer [51, pp. 90–91] (see also [52]) and proceed in the spirit of Galerkin methods. Here, we formulate this in a rather general way, but in the next section we present a concrete numerical implementation.

Let $J : \mathbb{C}^N \to \boldsymbol{L}^2(\mathcal{M})$ be an injective operator, and assume that the measurement data are collected in a matrix $M \in \mathbb{C}^{N \times N}$ such that

$$M \approx J^* G_\delta J. \tag{4.15}$$

Because $J^*J : \mathbb{C}^N \to \mathbb{C}^N$ is self–adjoint and positive definite, we can define the inverse of its square root $Q := (J^*J)^{-1/2}$. Then, $JQQJ^* : \boldsymbol{L}^2(\mathcal{M}) \to \boldsymbol{L}^2(\mathcal{M})$ is the orthogonal projection on the finite dimensional subspace $\mathcal{R}(J)$, and

$$JQQJ^*G_\delta JQQJ^* : \boldsymbol{L}^2(\mathcal{M}) \to \boldsymbol{L}^2(\mathcal{M}) \tag{4.16}$$

is called the *Galerkin projection* of G_δ on $\mathcal{R}(J)$. Let now $(\tilde{\sigma}_l)_{l=1}^N$, $(\tilde{\boldsymbol{v}}_l)_{l=1}^N$, and $(\tilde{\boldsymbol{u}}_l)_{l=1}^N$ be the singular values and singular vectors of QMQ. Then, $(\tilde{\sigma}_l)_{l=1}^N$, $(JQ\tilde{\boldsymbol{v}}_l)_{l=1}^N$, and $(JQ\tilde{\boldsymbol{u}}_l)_{l=1}^N$ are approximations of the singular values and singular vectors of the Galerkin projection of G_δ on $\mathcal{R}(J)$ from (4.16). Recalling (4.15), this can be seen as follows:

$$\begin{aligned} JQQJ^*G_\delta JQQJ^*(JQ\tilde{\boldsymbol{v}}_l) &= JQ(QJ^*G_\delta JQ)\tilde{\boldsymbol{v}}_l \\ &\approx JQ(QMQ)\tilde{\boldsymbol{v}}_l = \tilde{\sigma}_l(JQ\tilde{\boldsymbol{u}}_l). \end{aligned}$$

Using $(JQ\tilde{\boldsymbol{u}}_l)_{l=1}^N$ as approximations of the singular vectors $(\boldsymbol{u}_l^\delta)_{l=1}^N$ of G_δ, we get an approximation $\cot \tilde{\beta}_p^\delta(\boldsymbol{y})$ of $\cot \beta_p^\delta(\boldsymbol{y})$ from (4.14) for any $\boldsymbol{y} \in \mathbb{R}^3_-$ and $0 < p < N$. Depending on the data error

$$e := \|QJ^*G_\delta JQ - QMQ\|_2,$$

we have to decide how many of these singular values and singular vectors we actually use in the reconstruction algorithm.

Now, we are prepared to formulate Algorithm 4.2 for reconstructing the number and the positions of a collection of finitely many small perfectly conducting scatterers buried within the lower halfspace of an unbounded two–layered background medium.

Remark 4.10. In case of tangential or normal excitations and measurements as considered in Sections 4.1.2 and 4.1.3 the reconstruction method works essentially in the same way. We just have to use the modified test functions $\boldsymbol{g}_{y,d}^t$ and $\boldsymbol{g}_{y,d}^n$ according to Propositions 4.6 and 4.9 instead of $\boldsymbol{g}_{y,d}$. Moreover, in case of normal excitations and measurements the range of the leading order term $P_nTP_n^\top$ of the asymptotic expansion (4.8) of the normal measurement operator $G_{\delta,n}$ has dimension $5m$, where m is the number of scatterers, and not dimension $6m$ as in the other two cases. This has to be taken into account.

4.3 Numerical Implementation

In this section, we describe our numerical implementation of Algorithm 4.2.

First, we explain the approximation of the measurement operator G_δ by a finite dimensional matrix. For this purpose, we consider for any $\boldsymbol{y} \in \mathcal{M}$ the

Algorithm 4.1 Reconstruction of number and positions of the scatterers

Require: measurement data $M \in \mathbb{C}^{N\times N}$, $M \approx J^* G_\delta J$

compute the singular values $(\tilde\sigma_l)_{l=1}^N$ and singular vectors $(\tilde{\boldsymbol{u}}_l)_{l=1}^N$ of QMQ

according to the data error e consider in the following only the first N_0 singular values and singular vectors

choose the dipole polarization $\boldsymbol{d} = (\boldsymbol{d}_1, \boldsymbol{d}_2) \in (\mathbb{C}^3 \times \mathbb{C}^3) \setminus \{(0,0)\}$ for the test function $\boldsymbol{g}_{y,d}$

if the data error e and the scatterers are small enough **then**

  estimate the number of scatterers m by looking for a gap in the set of singular values $(\tilde\sigma_l)_{l=1}^{N_0}$

  on a sampling grid of points $\boldsymbol{y}_j \in \mathbb{R}^3_-$, $j = 1, 2, \ldots$, calculate

$$\cot \tilde\beta^\delta_{6m}(\boldsymbol{y}_j) := \left(\frac{\sum_{l\le 6m} |(JQ\tilde{\boldsymbol{u}}_l^\delta, \boldsymbol{g}_{y_j,d})_{\boldsymbol{L}^2(\mathcal{M})}|^2}{\sum_{6m<l\le N_0} |(JQ\tilde{\boldsymbol{u}}_l^\delta, \boldsymbol{g}_{y_j,d})_{\boldsymbol{L}^2(\mathcal{M})}|^2} \right)^{1/2}$$

  visualize $\cot \tilde\beta^\delta_{6m}(\boldsymbol{y}_j)$, $j = 1, 2, \ldots$

else

  $p = 6$

  repeat

    on a sampling grid of points $\boldsymbol{z}_j \in \mathbb{R}^3_-$, $j = 1, 2, \ldots$, calculate

$$\cot \tilde\beta^\delta_{p}(\boldsymbol{y}_j) := \left(\frac{\sum_{l\le p} |(JQ\tilde{\boldsymbol{u}}_l^\delta, \boldsymbol{g}_{y_j,d})_{\boldsymbol{L}^2(\mathcal{M})}|^2}{\sum_{p<l\le N_0} |(JQ\tilde{\boldsymbol{u}}_l^\delta, \boldsymbol{g}_{y_j,d})_{\boldsymbol{L}^2(\mathcal{M})}|^2} \right)^{1/2}$$

    visualize $\cot \tilde\beta^\delta_{p}(\boldsymbol{y}_j)$, $j = 1, 2, \ldots$

    $p = p + 6$

  until no further scatterers have been reconstructed in the last few steps or $p = N_0$

end if

matrix valued function $\boldsymbol{H}^s(\cdot, \boldsymbol{y})$ such that the jth component of $\boldsymbol{H}^s(\cdot, \boldsymbol{y})$ is the scattered field corresponding to the incident field excited by a magnetic dipole with polarization $\boldsymbol{e}_j$ in $\boldsymbol{y}$. Then, we discretize the measurement device $\mathcal{M}$ and replace it by an equidistant rectangular $n \times n$ grid $\mathcal{M}_h$ with step size h. For any $\boldsymbol{y} \in \mathcal{M}_h$ we evaluate $\boldsymbol{H}^s(\cdot, \boldsymbol{y})$ on $\mathcal{M}_h$ and collect these data column by column in a matrix $G_{\delta,h} \in \mathbb{C}^{3n^2\times 3n^2}$, henceforth called *discrete measurement operator*. With an appropriate ordering of rows and columns this is a complex symmetric matrix due to the reciprocity principle. We mention that $G_{\delta,h}$ is often also called the *multi–static response matrix*.

Next, in accordance with the discrete measurement operator $G_{\delta,h}$, let $J : \mathbb{C}^{3n^2} \to \boldsymbol{L}^2(\mathcal{M})$ be an injective operator that maps finite dimensional vectors $\boldsymbol{v} \in \mathbb{C}^{3n^2}$ on (sufficiently smooth) functions $\boldsymbol{V} \in \boldsymbol{L}^2(\mathcal{M})$ such

that the values of $\boldsymbol{V}$ on $\mathcal{M}_h$ (written as one column) are equal to $\boldsymbol{v}$. By superposition, we can represent G_δ as an integral operator (cf. [52, p. 2038]) such that for any $\boldsymbol{u} \in \mathbb{C}^{3n^2}$,

$$G_\delta J\boldsymbol{u} = \int_{\mathcal{M}} \boldsymbol{H}^s(\cdot, \boldsymbol{y})(J\boldsymbol{u})(\boldsymbol{y}) \, \mathrm{d}s(\boldsymbol{y}).$$

So, we find for $\boldsymbol{u}, \boldsymbol{v} \in \mathbb{C}^{3n^2}$ that

$$\begin{aligned} \boldsymbol{v} \cdot \overline{J^* G_\delta J \boldsymbol{u}} &= \int_{\mathcal{M}} (J\boldsymbol{v})(\boldsymbol{x}) \cdot \overline{(G_\delta J\boldsymbol{u})(\boldsymbol{x})} \, \mathrm{d}s(\boldsymbol{x}) \\ &= \int_{\mathcal{M}} \boldsymbol{V}(\boldsymbol{x}) \cdot \overline{\int_{\mathcal{M}} \boldsymbol{H}^s(\boldsymbol{x}, \boldsymbol{y})(J\boldsymbol{u})(\boldsymbol{y}) \, \mathrm{d}s(\boldsymbol{y})} \, \mathrm{d}s(\boldsymbol{x}) \\ &\approx (D_h^2 \boldsymbol{v}) \cdot \overline{G_{\delta,h} D_h^2 \boldsymbol{u}} = \boldsymbol{v} \cdot \overline{D_h^2 G_{\delta,h} D_h^2 \boldsymbol{u}}, \end{aligned}$$

where D_h denotes the diagonal matrix, whose entries are the square roots of the weights of the tensor trapezoidal quadrature rule for the integral over $\mathcal{M}$, given the function values on $\mathcal{M}_h$. Therefore,

$$J^* G_\delta J \approx D_h^2 G_{\delta,h} D_h^2,$$

and we have constructed a finite dimensional approximation of the measurement operator G_δ as required in (4.15). We can now proceed as in the previous section to obtain approximations of the singular values and the singular vectors of G_δ. If $\boldsymbol{U} \in \boldsymbol{L}^2(\mathcal{M})$ is a (sufficiently smooth) function and $\boldsymbol{u} \in \mathbb{C}^{3n^2}$ is the vector that consists of the values of $\boldsymbol{U}$ on $\mathcal{M}_h$, then for all $\boldsymbol{v} \in \mathbb{C}^{3n^2}$,

$$(J^* \boldsymbol{U}) \cdot \overline{\boldsymbol{v}} = \int_{\mathcal{M}} \boldsymbol{U} \cdot \overline{\boldsymbol{V}} \, \mathrm{d}s \approx (D_h^2 \boldsymbol{u}) \cdot \overline{\boldsymbol{v}}.$$

So,

$$J^* J\boldsymbol{u} = J^* \boldsymbol{U} \approx D_h^2 \boldsymbol{u},$$

which means that $Q := (J^*J)^{-1/2}$ corresponds to D_h^{-1}. Let $(\sigma_{h,l}^\delta)_{l=1}^{3n^2}$, $(\boldsymbol{v}_{h,l}^\delta)_{l=1}^{3n^2}$, and $(\boldsymbol{u}_{h,l}^\delta)_{l=1}^{3n^2}$ be the singular values and singular vectors of

$$QJ^* G_{\delta,h} JQ = D_h G_{\delta,h} D_h.$$

Then, as seen before, $(\sigma_{h,l}^\delta)_{l=1}^{3n^2}$, $(JQ\boldsymbol{v}_{h,l}^\delta)_{l=1}^{3n^2}$, and $(JQ\boldsymbol{u}_{h,l}^\delta)_{l=1}^{3n^2}$ are approximations of the singular values and singular vectors of the Galerkin projection of G_δ on $\mathcal{R}(J)$. Therefore, we will use $(\sigma_{h,l}^\delta)_{l=1}^{3n^2}$, $(D_h^{-1}\boldsymbol{v}_{h,l}^\delta)_{l=1}^{3n^2}$, and $(D_h^{-1}\boldsymbol{u}_{h,l}^\delta)_{l=1}^{3n^2}$ as finite dimensional approximations of the singular values and singular vectors of G_δ on $\mathcal{M}_h$ in the numerical implementation of Algorithm 4.2.

Remark 4.11. Kirsch proved in [73, Theorem 2.1] (see also [4, Proposition 6.3]) that for any number m of buried scatterers there exists a lower bound for number of grid points n^2 of the discretized measurement device $\mathcal{M}_h$ such that for this and all finer grids the range criterion from Proposition 4.4 also holds for the discretized measurement setup. But no explicit lower bound for the number of grid points on the measurement device that is sufficient to recover a given number of scatterers is provided. Our numerical experience indicates that n^2 is a relatively small number, e.g. $n^2 = 9$ in case of $m = 2$ scatterers. Therefore the singular value decomposition of $D_h G_{\delta,h} D_h$ is rather cheap to compute.

However, this singular value decomposition usually only approximates the dominant singular values and the corresponding singular vectors of $D_h G_{\delta,h} D_h$. Of course, the situation gets worse, if the data contain errors, which will always be the case in practise. To estimate the error contained in simulated or measured data for $D_h G_{\delta,h} D_h$, we measure the non–symmetric part of this matrix, i.e.,

$$\tilde{e} := \left\| D_h \big(G_{\delta,h} - G_{\delta,h}^\top \big) D_h \right\|_2,$$

because this should be zero for exact data and of order of the data error otherwise. By the Bauer–Fike Theorem (cf. Golub and Van Loan [55, Theorem 7.2.2]), the singular values of $D_h G_{\delta,h} D_h$ are perturbations of those of the corresponding unperturbed matrix and the perturbations are bounded by $\tilde{e}$. This means that the singular values of $D_h G_{\delta,h} D_h$, which are larger than $\tilde{e}$, will go through a comparatively small relative change. From [55, Corollary 8.1.11] we find that the same holds for orthogonal projections on subspaces spanned by the corresponding singular vectors.

On the other hand, it turns out that at least slightly more than $6m$ singular vectors are necessary to distinguish m buried scatterers, regardless of the noise level. So, in practise the number of scatterers that can be recovered with the reconstruction algorithm is restricted according to the number of singular values that can be approximated stably, i.e., according to the noise level. In our numerical experiments we work with $n^2 = 36$ grid points on the measurement device, which leads to a discrete measurement operator $G_{\delta,h} \in \mathbb{C}^{108\times 108}$. For the reconstruction of up to two buried scatterers we use only the first 20 singular vectors.

For our numerical examples, we simulate the discrete measurement operator $G_{\delta,h}$ numerically. For this purpose, we use a modified and extended version of a boundary element method with piecewise constant ansatz functions that was developed in the course of the BMBF–project [61] by Roland Potthast and his group in Göttingen; see also [46].

We implemented Algorithm 4.2 by modifying and extending the code for the Linear Sampling Method from [52], which was developed by Christoph Schneider.

4.4 Numerical Results

In this section, we present our numerical results for the following experimental setup: The measurement device operates on a square $\mathcal{M}$ of size 50×50 cm^2 parallel to the surface of ground, centered at $(0, 0, 10)$ cm. We discretize $\mathcal{M}$ using an equidistant rectangular 6×6 grid $\mathcal{M}_h \subset \mathcal{M}$ with step size $h = 10$ cm. The incident fields imposed on $\mathcal{M}_h$ have a frequency of 20 kHz, which corresponds to an angular velocity of $\omega = 1.26 \cdot 10^5$ s^{-1}.

We consider two different types of background media.

Homogeneous background medium: The whole $\mathbb{R}^3$ is assumed to be empty, i.e., vacuum,

$$\varepsilon_+ = \varepsilon_- = \varepsilon_0 = 8.85 \cdot 10^{-12} \text{ Fm}^{-1},$$
$$\mu_+ = \mu_- = \mu_0 = 1.26 \cdot 10^{-6} \text{ Hm}^{-1}.$$

Accordingly, $k_+ = k_- = 4.22 \cdot 10^{-4}$ m^{-1}, and the corresponding wavelength is $\lambda_+ = \lambda_- = 14.9$ km.

Two–layered background medium: The upper halfspace is supposed to be empty,

$$\varepsilon_+ = \varepsilon_0 = 8.85 \cdot 10^{-12} \text{ Fm}^{-1},$$
$$\mu_+ = \mu_0 = 1.26 \cdot 10^{-6} \text{ Hm}^{-1},$$

while the lower halfspace is assumed to be filled with soil,

$$\varepsilon_- = \varepsilon_0 \Big(\varepsilon_r + \mathrm{i} \, \frac{\sigma}{\omega \varepsilon_0} \Big) = 8.67 \cdot 10^{-11} + \mathrm{i}\, 5.95 \cdot 10^{-9} \text{ Fm}^{-1},$$
$$\mu_- = (1 + \chi)\mu_0 = 1.26 \cdot 10^{-6} \text{ Hm}^{-1},$$

where

$$\sigma = 7.5 \cdot 10^{-4} \text{ Sm}^{-1}, \quad \chi = 1.9 \cdot 10^{-5}, \quad \varepsilon_r = 9.8.$$

The electromagnetic parameters for the lower halfspace are measurement data for a soil consisting of a poor clay sand (St2) taken by Igel and Preetz [63] in course of the project [61]. Accordingly, $k_+ = 4.22 \cdot 10^{-4}$ m^{-1} and $k_- = (7.77 + \mathrm{i}\, 7.66) \cdot 10^{-3}$ m^{-1}. So the wavelengths in the two halfspaces are $\lambda_+ = 14.9$ km and $\lambda_- = 0.81$ km, respectively. This setup is meant to represent a realistic test case for subsurface exploration using commercial off–the–shelf metal detectors.

4.4.1 Asymptotic Behavior of the Singular Values

First, we illustrate the asymptotic behavior of the singular values from (4.12). For this purpose, we consider a perfectly conducting small scatterer

$D_\delta = \boldsymbol{z} + \delta B$, $0 < \delta \leq 1$, with $\boldsymbol{z} = (0, 0, -20)$ cm, where B is an ellipsoid with semi axes of length $(9, 7, 5)$ cm (aligned with the coordinate axes) centered at the origin. We simulate the corresponding discrete measurement operator $G_{\delta,h} \in \mathbb{C}^{108\times 108}$ for the homogeneous background medium using the boundary element method mentioned above with 1216 triangles on the boundary of the scatterer for $\delta = 1$, $\delta = 10^{-1}$, and $\delta = 10^{-2}$. Then, we calculate the singular values $(\sigma_{h,l}^{\delta})_{l=1}^{108}$ of $D_h G_{\delta,h} D_h$, which are approximations of the singular values of the measurement operator G_δ, and plot the first 20 of them for $\delta = 1$, $\delta = 10^{-1}$, and $\delta = 10^{-2}$ on the left hand side of Figure 4.1. According to (4.12) and Proposition 4.3, we expect to see 6 singular values of order $\mathcal{O}(\delta^3)$, while the remaining singular values should be of order $\mathcal{O}(\delta^4)$. This qualitative behavior is indeed verified by the numerical simulations. Observe that the first 6 singular values appear in two close triples. This is a typical feature we found in many of our numerical simulations for single scatterers. By Proposition 4.3, the range of the leading order term T of the asymptotic expansion of G_δ is spanned by the columns of the 3×3 tensors $\mathbb{G}^m(\cdot, \boldsymbol{z})$ and $\mathbf{curl}_x\, \mathbb{G}^e(\cdot, \boldsymbol{z})$. This may explain this triplet structure.

Next, we consider tangential and normal excitations and measurements as studied in Section 4.1.2 and Section 4.1.3, respectively. We visualize the approximations of the first 20 singular values of the tangential measurement operator $G_{\delta,t} = P_t G_\delta P_t^\top$ and of the normal measurement operator $G_{\delta,n} = P_n G_\delta P_n^\top$ for $\delta = 1$, $\delta = 10^{-1}$, and $\delta = 10^{-2}$ on the right–hand side of Figure 4.1. In case of tangential excitations and measurements, according to (4.7) and Proposition 4.5, we also expect 6 singular values of order $\mathcal{O}(\delta^3)$, while the remaining singular values should be of order $\mathcal{O}(\delta^4)$. But for normal excitations and measurements, recalling (4.8) and Proposition 4.8, we anticipate only 5 singular values of order $\mathcal{O}(\delta^3)$ and the remaining singular values should have smaller magnitude. Again, this qualitative behavior is verified by the numerical example.

In a second example, we do the same simulations for the two–layered background medium. The corresponding approximations of the first 20 singular values of the full measurement operator G_δ, the tangential measurement operator $G_{\delta,t}$, and the normal measurement operator $G_{\delta,n}$ for $\delta = 1$, $\delta = 10^{-1}$, $\delta = 10^{-2}$, and $\delta = 10^{-3}$ can be found in Figure 4.2. Although the theoretical predictions are also fulfilled by these simulations, the gap between the first 6 (resp. 5) singular values and the singular values corresponding to higher order terms in the asymptotic expansion is not as distinct as for the homogeneous background medium.

For further studies of the eigenvalue structure of the discrete measurement operator $G_{\delta,h}$ we refer to [4], Chambers and Berryman [31,32], and to [62]. Our results are in accordance with these investigations.

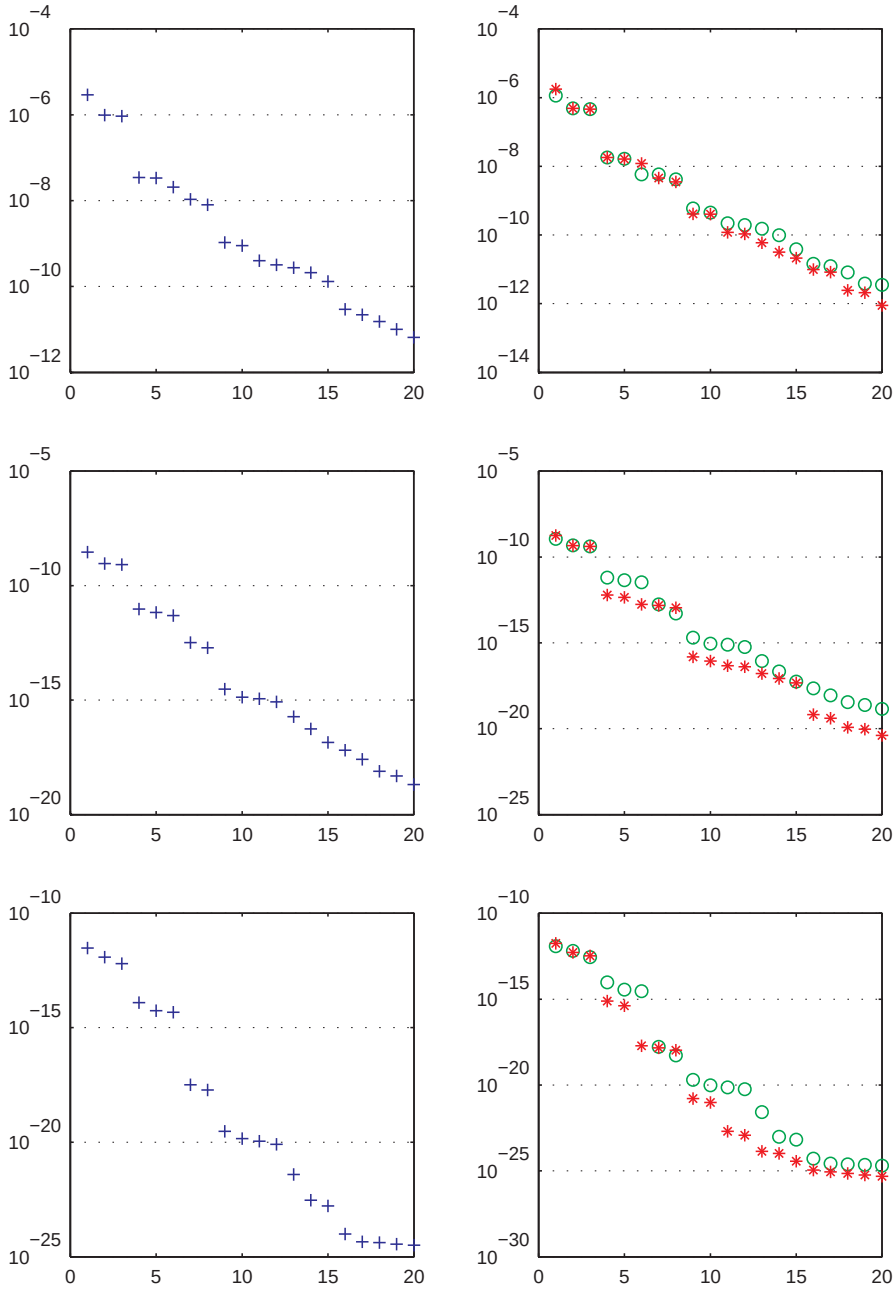

Figure 4.1: Singular values of the measurement operators G_δ (left), $G_{\delta,t}$, and $G_{\delta,n}$ (right) for $\delta = 1$, $\delta = 10^{-1}$, and $\delta = 10^{-2}$ (top down) in homogeneous background medium ($+$... full excitations and measurements, $\circ$... tangential excitations and measurements, $*$... normal excitations and measurements).

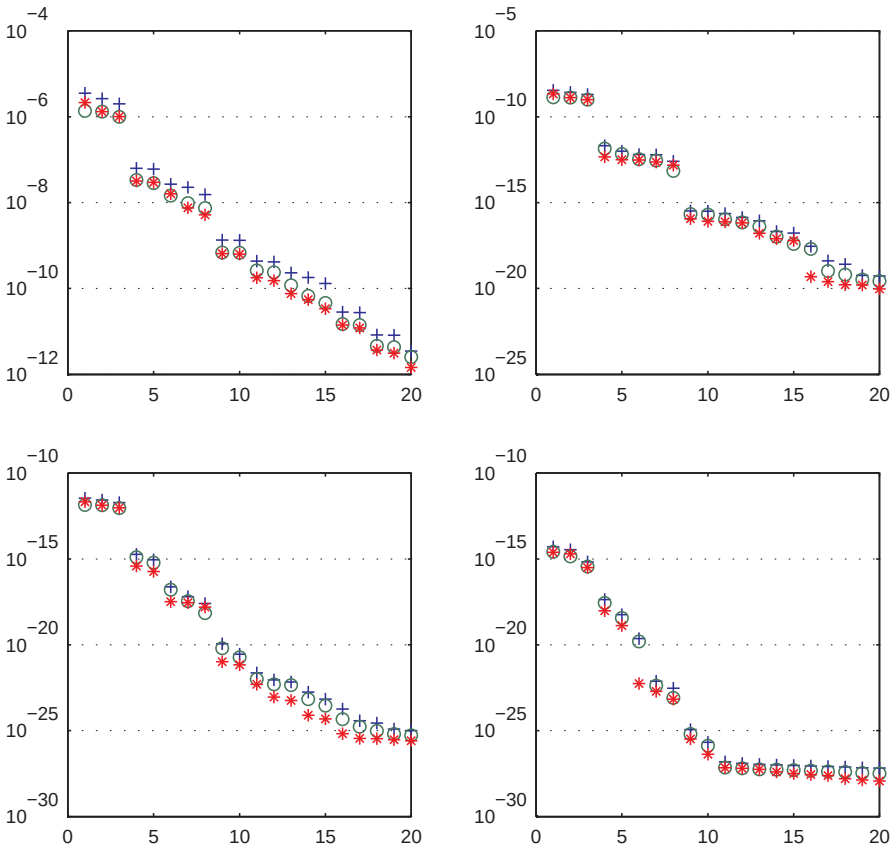

Figure 4.2: Singular values of the measurement operators G_δ, $G_{\delta,t}$, and $G_{\delta,n}$ for $\delta = 1$, $\delta = 10^{-1}$, $\delta = 10^{-2}$, and $\delta = 10^{-3}$ (from left to right and top down) in two–layered background medium ($+$ . . . full excitations and measurements, $\circ$ . . . tangential excitations and measurements, $*$ . . . normal excitations and measurements).

4.4.2 Choosing the Test Dipole Direction

In this and the following example, we apply Algorithm 4.2 to reconstruct the location of two small perfectly conducting ellipsoids with semi axes of length $(0.1, 0.2, 0.3)$ cm and $(2, 3, 1)$ cm (aligned with the coordinate axes) buried in the lower halfspace of the two–layered background medium at position $\boldsymbol{z}_1 := (-15, 15, -10)$ cm and $\boldsymbol{z}_2 := (15, -15, -40)$ cm, respectively. We consider three–dimensional excitations and measurements, where the simulated forward data have been obtained using the boundary element method with 612 triangles per scatterer and contain an estimated numerical error of 3%. Additionally, we perturb these data by a uniformly distributed relative error of 1%.

Figure 4.3 shows approximations of the first 20 singular values of the measurement operator G_δ. Note that in contrast to (4.12) and Proposi-

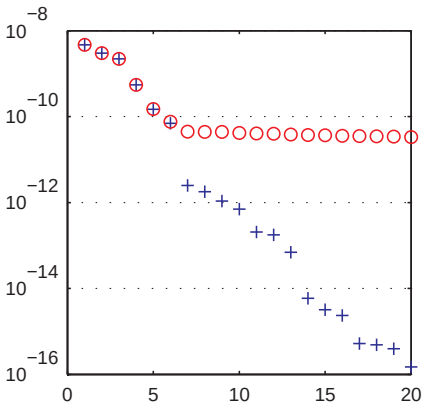

Figure 4.3: Singular values of the measurement operators G_δ (+ . . . without additional noise, ∘ . . . with 1% uniformly distributed noise).

tion 4.3 there is no distinct gap after the first 12 singular value. One reason for this may be the (numerical) error contained in the forward data. On the other hand, recalling the singular value decompositions in Figure 4.2, the scatterers seem not to be small enough to lead to the perfect asymptotic behavior for this background medium. However, here the iterative procedure described in Algorithm 4.2 can be used to estimate the number of scatterers.

We study the influence of the polarization vector $\boldsymbol{d} \in (\mathbb{C}^3 \times \mathbb{C}^3) \setminus \{(0,0)\}$ of the test function $\boldsymbol{g}_{y,d}$ (cf. Proposition 4.4) on the performance of the reconstruction method. For this purpose, we consider four different *polarization vectors*: $\boldsymbol{d} = (\boldsymbol{e}_1, 0)$, $\boldsymbol{d} = (\boldsymbol{e}_3, 0)$, $\boldsymbol{d} = (0, \boldsymbol{e}_1)$, and $\boldsymbol{d} = (0, \boldsymbol{e}_3)$. The first two polarizations correspond to test functions that are magnetic dipoles (singularity of order 3), while the latter two polarizations correspond to test functions that are curls of electric dipoles (singularity of order 2). The values of $\cot \tilde{\beta}^\delta_{12}$ (with $N_0 = 20$) corresponding to these test functions are used to visualize the location of the scatterers on a three–dimensional equidistant rectangular *sampling grid* with step size 0.5 cm on the *search domain* $[-25, 25]^2 \times [-50, 0]$ cm^3.

We start by studying the test function $\boldsymbol{g}_{y,d}$ with polarization vector $\boldsymbol{d} = (\boldsymbol{e}_1, 0)$. Figure 4.4 shows horizontal cross sections of $\cot \tilde{\beta}^\delta_{12}(\boldsymbol{y})$ corresponding to this test function for $y_3 = -10$ cm and $y_3 = -40$ cm. The position of the lower scatterer is well reconstructed, but the position of the upper scatterer can hardly be estimated from these visualizations. Note that away from buried scatterers these visualizations should be close to white (depending on the noise level). This was the case in all our numerical examples. It turned out to be better not to use automatic scaling for the coloraxis in these cross sectional plots but the same coloraxis throughout the search

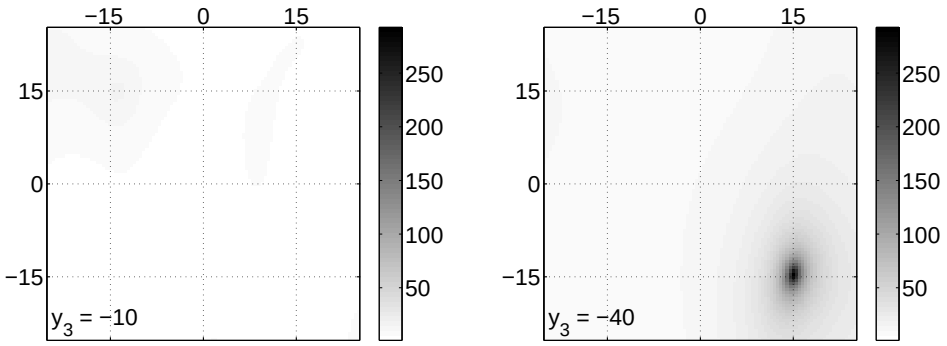

Figure 4.4: Cross–sectional plots of $\cot \tilde{\beta}_{12}^{\delta}(\boldsymbol{y})$ with polarization vector $\boldsymbol{d} = (\boldsymbol{e}_1, 0)$ for $y_3 = -10$ cm and $y_3 = -40$ cm with 1% noise.

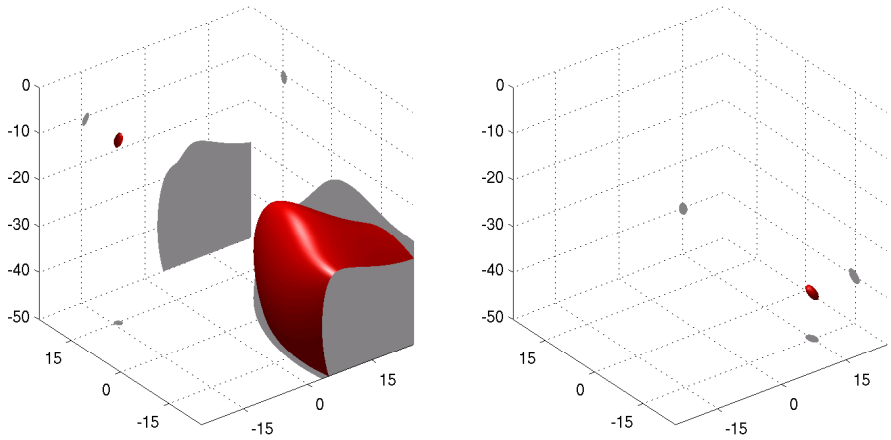

Figure 4.5: Isosurface plots $\cot \tilde{\beta}_{12}^{\delta} = 15$ and $\cot \tilde{\beta}_{12}^{\delta} = 175$ with polarization vector $\boldsymbol{d} = (\boldsymbol{e}_1, 0)$ and with 1% noise.

domain. Figure 4.5 shows isosurface plots $\cot \tilde{\beta}_{12}^{\delta} = 15$ and $\cot \tilde{\beta}_{12}^{\delta} = 175$. From these visualizations the positions of both scatterers can be estimated. The gray areas on the coordinate planes are the orthogonal projections of the red surfaces on these planes. We emphasize that these plots should not be mistaken as reconstructions of the shape of the scatterers. They give just an idea of possible positions of buried objects; these can be expected to be inside the (red) surfaces. In contrast to the Factorization Method, our method does not allow a binary test for whether some point belongs to a scatterer or not.

Next, we consider the test function $\boldsymbol{g}_{y,d}$ with polarization $\boldsymbol{d} = (\boldsymbol{e}_3, 0)$. Figure 4.6 shows horizontal cross sections of $\cot \tilde{\beta}_{12}^{\delta}(\boldsymbol{y})$ for $y_3 = -10$ cm and $y_3 = -40$ cm. Here, the position of both scatterers can be well estimated. Note that the values of the local maxima of $\cot \tilde{\beta}_{12}^{\delta}$ are larger for this choice

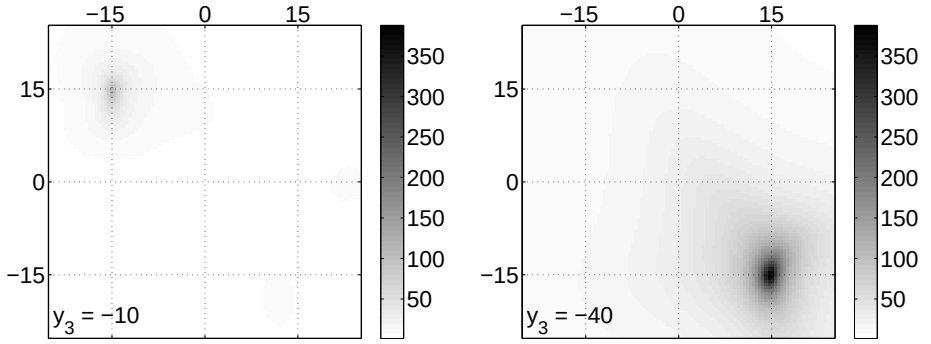

Figure 4.6: Cross–sectional plots of $\cot \tilde{\beta}_{12}^{\delta}(\boldsymbol{y})$ with polarization vector $\boldsymbol{d} = (\boldsymbol{e}_3, 0)$ for $y_3 = -10$ cm and $y_3 = -40$ cm with 1% noise.

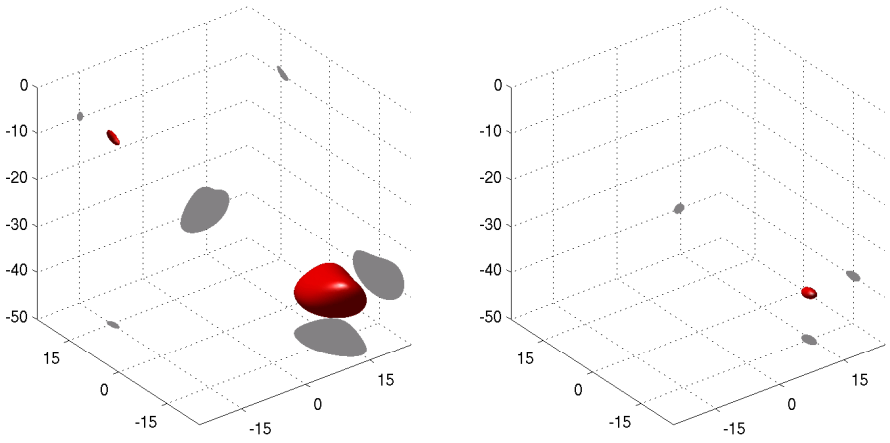

Figure 4.7: Isosurface plots $\cot \tilde{\beta}_{12}^{\delta} = 75$ and $\cot \tilde{\beta}_{12}^{\delta} = 250$ with polarization vector $\boldsymbol{d} = (\boldsymbol{e}_3, 0)$ and with 1% noise.

of the polarization vector. This is preferable, because it allows for a better identifiability of possible scatterers. Figure 4.7 shows isosurface plots $\cot \tilde{\beta}_{12}^{\delta} = 75$ and $\cot \tilde{\beta}_{12}^{\delta} = 250$.

Considering the test functions $\boldsymbol{g}_{y,d}$ with polarization vectors $\boldsymbol{d} = (0, \boldsymbol{e}_1)$ and $\boldsymbol{d} = (0, \boldsymbol{e}_3)$, we found from numerical experiments that the positions of the two scatterers cannot be reconstructed from visualizations of $\cot \tilde{\beta}_{12}^{\delta}$. For the present example the values of $\cot \tilde{\beta}_{12}^{\delta}$ in the search domain corresponding to these polarization vectors are between 0 and 3 and the function has no distinct local maxima, which would indicate scatterers. Recalling Proposition 4.3 and the singular value decomposition in Figure 4.3, this can be explained as follows: By Proposition 4.3, the range $\mathcal{R}(T)$ of the leading order term T of the asymptotic expansion (4.2) of the measurement operator G_δ is spanned by the columns of $\mathbb{G}^m(\cdot, \boldsymbol{z}_1)|_{\mathcal{M}}$, $\mathbb{G}^m(\cdot, \boldsymbol{z}_2)|_{\mathcal{M}}$, $\mathbf{curl}_x\, \mathbb{G}^e(\cdot, \boldsymbol{z}_1)|_{\mathcal{M}}$,

and $\mathbf{curl}_x\, \mathbb{G}^e(\cdot, \boldsymbol{z}_2)|_{\mathcal{M}}$, where $\boldsymbol{z}_1$ and $\boldsymbol{z}_2$ are the positions of the two scatterers. The reconstruction algorithm essentially checks, whether the function $\boldsymbol{g}_{y,d}$ belongs to this 12–dimensional range space or not. But in the singular value decomposition of G_δ in Figure 4.3 only two triples of singular values are separated from the others (which are smaller than the estimated numerical error in the simulated forward data). The numerical experiments indicate that the corresponding 6–dimensional subspace of $\mathcal{R}(T)$ is spanned by the columns of $\mathbb{G}^m(\cdot, \boldsymbol{z}_1)|_{\mathcal{M}}$ and $\mathbb{G}^m(\cdot, \boldsymbol{z}_2)|_{\mathcal{M}}$ — for the corresponding test functions the reconstruction algorithm works. On the other hand, the subspace spanned by the following 6 singular vectors seems not to be spanned by the columns of $\mathbf{curl}_x\, \mathbb{G}^e(\cdot, \boldsymbol{z}_1)|_{\mathcal{M}}$ and $\mathbf{curl}_x\, \mathbb{G}^e(\cdot, \boldsymbol{z}_2)|_{\mathcal{M}}$ — for the corresponding test functions the reconstruction method fails. Figure 4.3 indicates that this is due to the numerical error contained in the forward data.

So, for this particular example the test function $\boldsymbol{g}_{y,d}$ with $\boldsymbol{d} = (\boldsymbol{e}_3, 0)$ would be an appropriate choice for the reconstruction algorithm. However, it is not clear that the field due to the magnetic dipoles in the asymptotic expansion of the scattered field (3.71) always dominates the field due to the corresponding electric dipoles, as it does in this example. In the following examples, we use the test function $\boldsymbol{g}_{y,d}$ with polarization vector $\boldsymbol{d} = (\boldsymbol{e}_3, \boldsymbol{e}_3)$, which is a combination of an electric and a magnetic dipole and thus works irrespective of which part of the field dominates. With this test function we obtained good reconstructions for a varietey of numerical examples. (We mention that for normal excitations and measurements a test function $\boldsymbol{g}_{y,d}$ with polarization vector $\boldsymbol{d} = (\boldsymbol{e}_3, \boldsymbol{e}_1)$ or $\boldsymbol{d} = (\boldsymbol{e}_3, \boldsymbol{e}_2)$ would be more appropriate.)

4.4.3 Three–Dimensional, Tangential, and Normal Excitations and Measurements

In this example, we compare numerical results for the three measurement setups considered in Section 4.1. For this purpose, we reconstruct the two perfectly conducting ellipsoidal scatterers described in Section 4.4.2 using three–dimensional, tangential, and normal excitations and measurements. The forward data used in these experiments have been obtained as in the previous example, but here we perturb these data by a uniformly distributed relative error of 3% (instead of 1% before).

We start with three–dimensional excitations and measurements. The values of $\cot \tilde{\beta}^\delta_{12}$ for the test function $\boldsymbol{g}_{y,d}$ with polarization vector $\boldsymbol{d} = (\boldsymbol{e}_3, \boldsymbol{e}_3)$ are used to visualize the location of the scatterers on a three–dimensional equidistant rectangular sampling grid with step size 0.5 cm on the search domain $[-25, 25]^2 \times [-50, 0]$ cm^3. Figure 4.8 shows horizontal cross sections of $\cot \tilde{\beta}^\delta_{12}(\boldsymbol{y})$ for $y_3 = -10$ cm and $y_3 = -40$ cm. Isosurface plots $\cot \tilde{\beta}^\delta_{12} = 25$

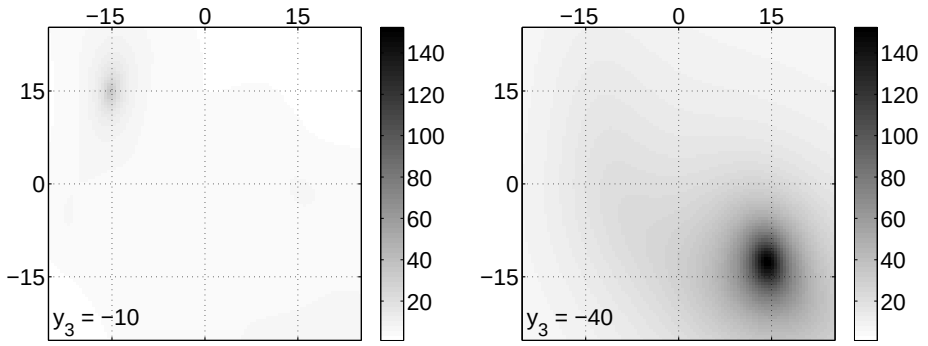

Figure 4.8: Cross–sectional plots of $\cot \tilde{\beta}_{12}^{\delta}(\boldsymbol{y})$ for three–dimensional excitations and measurements with 3% noise at $y_3 = -10$ cm and $y_3 = -40$ cm.

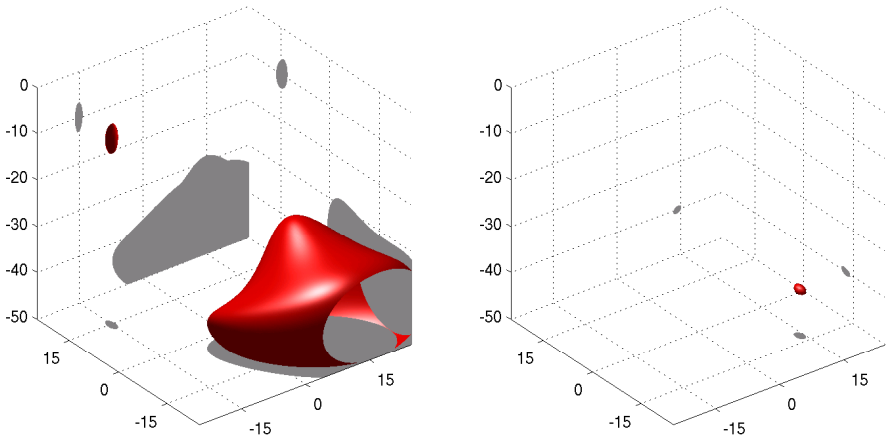

Figure 4.9: Isosurface plots $\cot \tilde{\beta}_{12}^{\delta} = 25$ and $\cot \tilde{\beta}_{12}^{\delta} = 140$ for three–dimensional excitations and measurements with 3% noise.

and $\cot \tilde{\beta}_{12}^{\delta} = 140$ can be found in Figure 4.9. The positions of both scatterers can be estimated from these visualizations. Due to the higher amount of noise contained in the forward data for this example, the local maxima of $\cot \tilde{\beta}_{12}^{\delta}$ are not as distinct as in Section 4.4.2 (cf. Figure 4.6). If we perturb the simulated forward data by a uniformly distributed relative error of 5%, the reconstructions of the positions of the scatterers get worse, but still two scatterers are reconstructed. For higher amounts of noise the method no longer recovers both scatterers.

Comparing the MUSIC–type reconstruction method proposed here with the Linear Sampling Method from [52], using amongst others this example, we found that the Linear Sampling Method is more sensitive to uncorrelated noise. Using forward data containing 1% uniformly distributed relative error the position of both scatterers has also been reconstructed by the linear

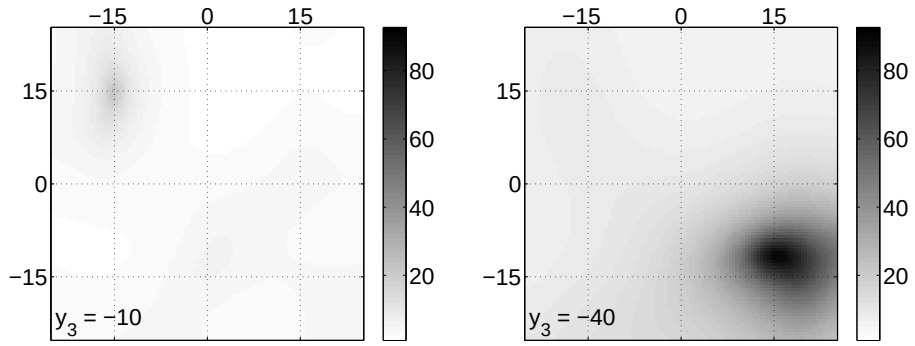

Figure 4.10: Cross–sectional plots of $\cot \tilde{\beta}_{12}^{\delta}(\boldsymbol{y})$ for tangential excitations and measurements with 3% noise at $y_3 = -10$ cm and $y_3 = -40$ cm.

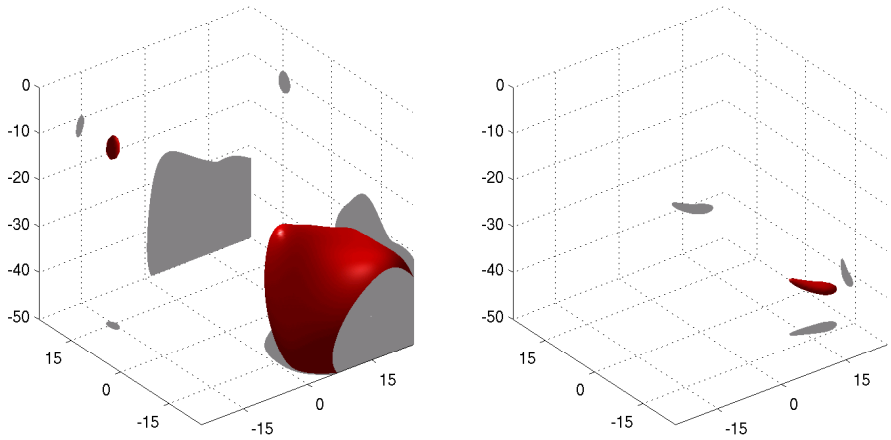

Figure 4.11: Isosurface plots $\cot \tilde{\beta}_{12}^{\delta} = 20$ and $\cot \tilde{\beta}_{12}^{\delta} = 85$ for tangential excitations and measurements with 3% noise.

sampling method. But with 3% noise (or more) in the data the Linear Sampling Method failed to reconstruct both scatterers. Similar observations were made by Hanke and Brühl [59] for inverse conductivity problems.

Next we consider tangential excitations and measurements as introduced in Section 4.1.2. We use the modified test function $\boldsymbol{g}_{y,d}^{t}$ with polarization vector $\boldsymbol{d} = (\boldsymbol{e}_3, \boldsymbol{e}_3)$ (cf. Proposition 4.6) and compute the values of $\cot \tilde{\beta}_{12}^{\delta}$ corresponding to the tangential measurement operator $G_{\delta,t} = P_t G_\delta P_t^\top$ on the sampling grid as used before to visualize the location of the scatterers. Figure 4.10 shows horizontal cross sections of $\cot \tilde{\beta}_{12}^{\delta}(\boldsymbol{y})$ for $y_3 = -10$ cm and $y_3 = -40$ cm. Isosurface plots $\cot \tilde{\beta}_{12}^{\delta} = 85$ and $\cot \tilde{\beta}_{12}^{\delta} = 20$ can be found in Figure 4.11. Expectedly, the reconstructions for tangential excitations and measurements are worse than for fully three–dimensional excitations and

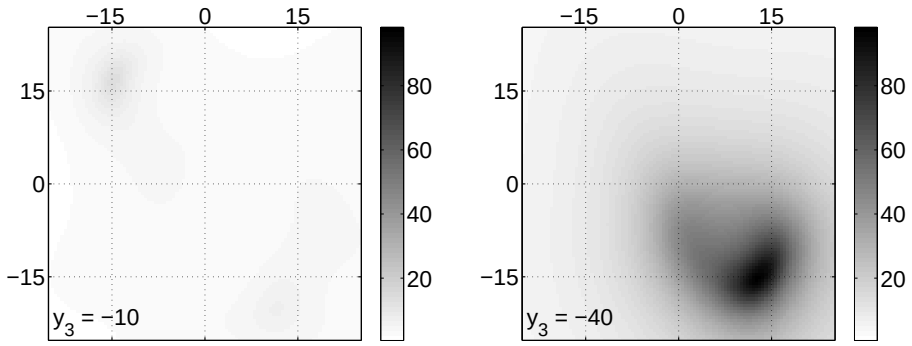

Figure 4.12: Cross–sectional plots of $\cot \tilde{\beta}_{10}^{\delta}(\boldsymbol{y})$ for normal excitations and measurements with 3% noise at $y_3 = -10$ cm and $y_3 = -40$ cm.

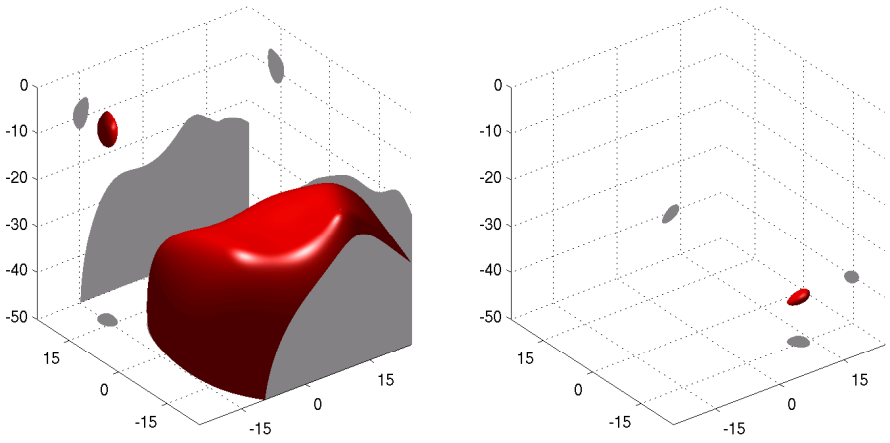

Figure 4.13: Isosurface plots $\cot \tilde{\beta}_{10}^{\delta} = 10$ and $\cot \tilde{\beta}_{10}^{\delta} = 85$ for normal excitations and measurements with 3% noise.

measurements, but the approximate positions of both scatterers can still be estimated.

For normal excitations and measurements (cf. Section 4.1.3) we use the modified test function $\boldsymbol{g}_{y,d}^{n}$ with polarization vector $\boldsymbol{d} = (\boldsymbol{e}_3, \boldsymbol{e}_3)$ (cf. Proposition 4.9) and compute the values of $\cot \tilde{\beta}_{10}^{\delta}$ corresponding to the normal measurement operator $G_{\delta,n} = P_n G_\delta P_n^\top$ on the sampling grid as used before to visualize the location of the scatterers. Figure 4.12 shows horizontal cross sections of $\cot \tilde{\beta}_{10}^{\delta}(\boldsymbol{y})$ for $y_3 = -10$ cm and $y_3 = -40$ cm. Isosurface plots $\cot \tilde{\beta}_{10}^{\delta} = 10$ and $\cot \tilde{\beta}_{10}^{\delta} = 85$ can be found in Figure 4.13. The positions of both scatterers can be estimated from these visualizations. The reconstructions are not as sharp as for fully three–dimensional excitations and measurements but comparable or even a bit better than for tangential

excitations and measurements.

4.4.4 Two Examples where the Method Fails

In this section, we point out some limitations of the MUSIC–type reconstruction method. For this purpose, we slightly modify the geometrical setup considered in the previous two examples such that the reconstruction algorithm no longer recovers the positions of both scatterers and explain this behavior theoretically.

First, we try to reconstruct the positions of two small perfectly conducting ellipsoids with semi axes of length $(1, 2, 3)$ cm and $(2, 3, 1)$ cm (aligned with the coordinate axes) buried in the lower halfspace of the two–layered background medium at position $(-15, 15, -10)$ cm and $(15, -15, -40)$ cm, respectively. Note that this is the same geometry as studied in Section 4.4.2 and Section 4.4.3, but here the diameter of the upper scatterer is 10 times larger than before. We consider three–dimensional excitations and measurements, where the forward data have been obtained using the boundary element method with 612 triangles per scatterer and contain an estimated numerical error of 2%. Additionally, we perturb these data by a uniformly distributed relative error of 3%.

We use the test function $\boldsymbol{g}_{y,d}$ with polarization vector $\boldsymbol{d} = (\boldsymbol{e}_3, \boldsymbol{e}_3)$ and compute the values of $\cot \tilde{\beta}_{12}^{\delta}$ on the same sampling grid as used in the previous examples to visualize the location of the scatterers. Figure 4.14 shows horizontal cross sections of $\cot \tilde{\beta}_{12}^{\delta}(\boldsymbol{y})$ for $y_3 = -10$ cm and $y_3 = -40$ cm. Note that only the position of the upper scatterer can be estimated from these plots. Approximations of the first 20 singular values of the measurement operator G_δ and an isosurface plot $\cot \tilde{\beta}_{12}^{\delta} = 100$ can be found in Figure 4.15.

Recalling the asymptotic formula (3.71), we find that the magnitude of the scattered field due to the upper scatterer in this example is approximately 1000 times larger than in the previous two examples, because the diameter of this scatterer is 10 times larger than before. On the other hand, the magnitude of the scattered field due to the lower scatterer remains unchanged. Comparing the singular value decompositions in Figure 4.3 and Figure 4.15, in particular the first two triples of singular values, this behavior can indeed be observed in the numerical simulations. Due to the larger scattered field also the absolute error contained in the forward data increases dramatically. This noise largely dominates the information on the lower scatterer contained in the forward data and thus only the upper scatterer is recovered by the reconstruction algorithm.

Next, we try to reconstruct the positions of two perfectly conducting ellipsoids with semi axes of length $(0.1, 0.2, 0.3)$ cm and $(2, 3, 1)$ cm (aligned

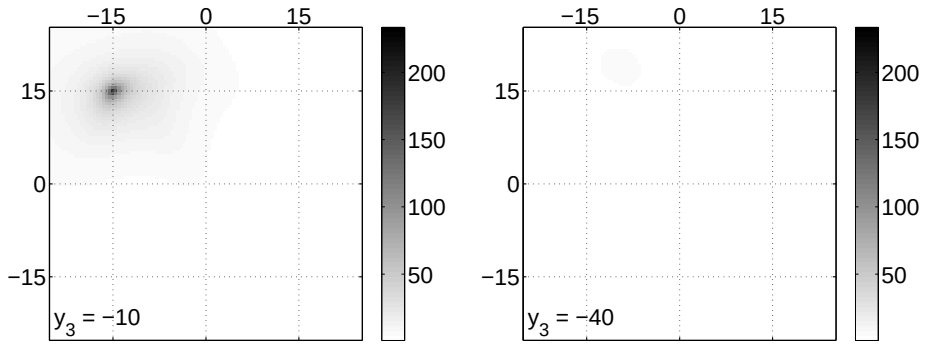

Figure 4.14: Cross–sectional plots of $\cot \tilde{\beta}_{12}^{\delta}(\boldsymbol{y})$ at $y_3 = -10$ cm and $y_3 = -40$ cm with 3% noise.

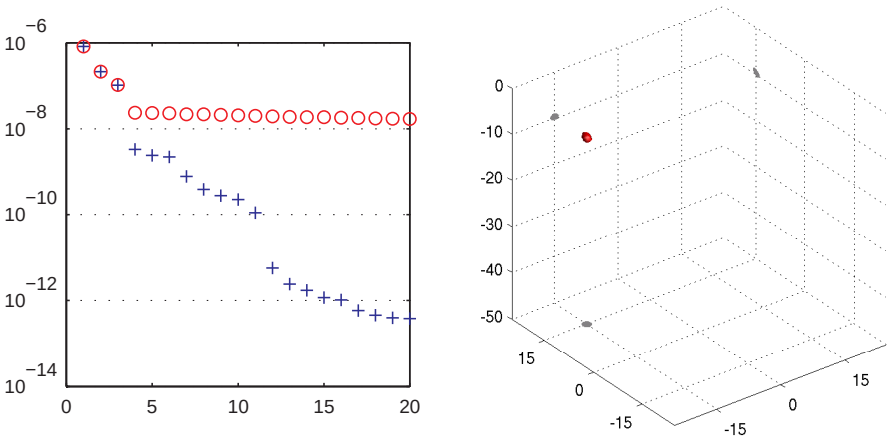

Figure 4.15: Singular values of the measurement operators G_δ ($+\ldots$ without additional noise, $\circ\ldots$ with 3% uniformly distributed noise) and isosurface plot $\cot \tilde{\beta}_{12}^{\delta} = 100$ with 3% noise.

with the coordinate axes) buried in the lower halfspace of the two–layered background medium at position $(-40, 40, -10)$ cm and $(40, -40, -40)$ cm, respectively. Note that these are the same ellipsoids as studied in the Sections 4.4.2 and 4.4.3, but here they are no longer buried directly underneath the measurement device. We consider three–dimensional excitations and measurements, where the forward data have been obtained using the boundary element method with 612 triangles per scatterer and contain an estimated numerical error of 1%. Additionally, we perturb these data by a uniformly distributed relative error of 3%.

We use the test function $\boldsymbol{g}_{y,d}$ with $\boldsymbol{d} = (\boldsymbol{e}_3, \boldsymbol{e}_3)$ and compute the values of $\cot \tilde{\beta}_{12}^{\delta}$ on a three–dimensional equidistant rectangular sampling grid with step size 0.5 cm on the search domain $[-50, 50]^2 \times [-50, 0]$ cm^3 to

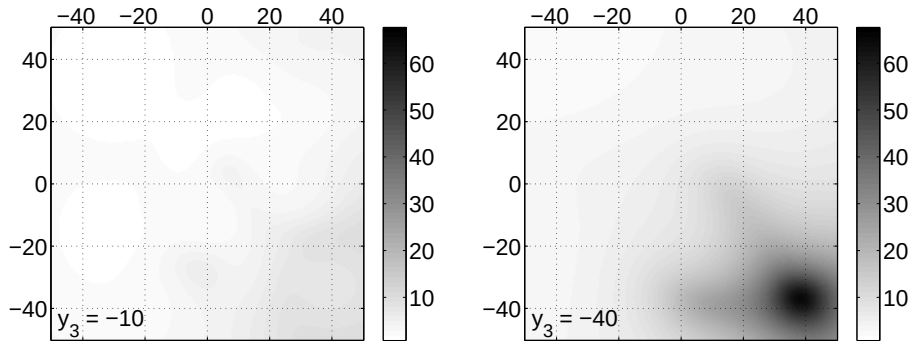

Figure 4.16: Cross–sectional plots of $\cot \tilde{\beta}_{12}^{\delta}(\boldsymbol{y})$ at $y_3 = -10$ cm and $y_3 = -40$ cm with 3% noise.

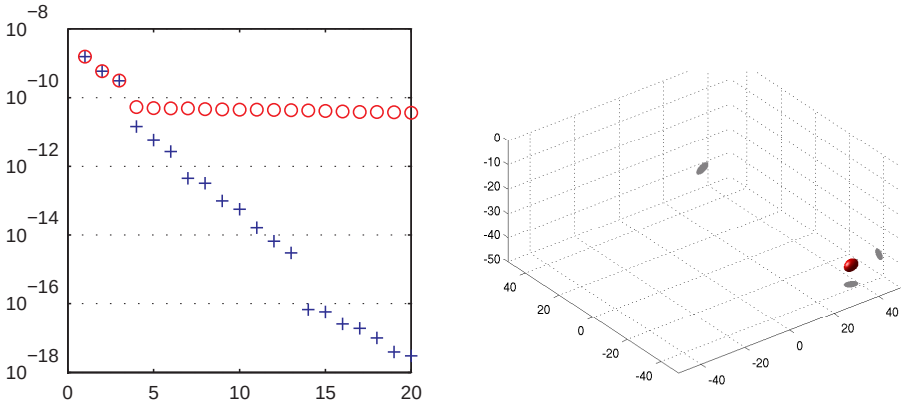

Figure 4.17: Singular values of the measurement operators G_δ ($+\ldots$ without additional noise, $\circ\ldots$ with 3% uniformly distributed noise) and isosurface plot $\cot \tilde{\beta}_{12}^{\delta} = 65$ with 3% noise.

visualize the location of the scatterers. Figure 4.16 shows horizontal cross sections of $\cot \tilde{\beta}_{12}^{\delta}(\boldsymbol{y})$ for $y_3 = -10$ cm and $y_3 = -40$ cm. Only the position of the lower scatterer can be estimated from these plots. Approximations of the first 20 singular values of the measurement operator G_δ and an isosurface plot $\cot \tilde{\beta}_{12}^{\delta} = 100$ can be found in Figure 4.17. As can be seen from the singular value decomposition, the singular values corresponding to the upper scatterer are below the noise level and thus this scatterer is not reconstructed.

However, it is a success that the reconstruction method recovers the lower scatterer, even though it is not buried directly underneath the measurement device. In practise it is typically possible to move the measurement device around while searching for buried objects.

4.4.5 Test Functions for Homogeneous Background Media

For two–layered background media, evaluating the test functions $\boldsymbol{g}_{y,d}$ on the discrete measurement device $\mathcal{M}_h$ for each sampling point $\boldsymbol{y}$ in the search domain (cf. Algorithm 4.2) is computationally very expensive. These test functions are superpositions of magnetic dyadic Green's functions and the curl of electric dyadic Green's functions (cf. Proposition 4.4), which are not known in closed form for two–layered background media, but only via Hankel transforms of their matrix elements. So, evaluating test functions $\boldsymbol{g}_{y,d}$ on the measurement device means to evaluate these Hankel transforms.

On the other hand, the dyadic Green's function for homogeneous background media is known explicitly (cf. (3.7)) and can be evaluated very efficiently. Numerical experiments show that for low frequencies as considered here the Green's functions for two–layered media do not differ very much from the Green's functions for homogeneous media. Thus, we apply in this example the test function $\boldsymbol{g}_{y,d}$ for the homogeneous background medium to reconstruct two small scatterers buried in the lower halfspace of the two–layered background medium.

For this purpose, we consider the same example as studied in Section 4.4.2 and Section 4.4.3: Two perfectly conducting ellipsoids with semi axes of length $(0.1, 0.2, 0.3)$ cm and $(2, 3, 1)$ cm (aligned with the coordinate axes) are buried in the lower halfspace of the two–layered background medium at position $(-15, 15, -10)$ cm and $(15, -15, -40)$ cm, respectively. We consider three–dimensional excitations and measurements, where the forward data have been obtained using the boundary element method (for the two–layered background medium) with 612 triangles per scatterer and contain an estimated numerical error of 3%. Additionally we perturb these data by a uniformly distributed relative error of 3%.

The values of $\cot \tilde{\beta}_{12}^{\delta}$ on a three–dimensional equidistant rectangular sampling grid with step size 0.5 cm on the search domain $[-25, 25]^2 \times [-50, 0]$ cm^3 corresponding to the test function $\boldsymbol{g}_{y,d}$ for the homogeneous background medium with polarization vector $\boldsymbol{d} = (\boldsymbol{e}_3, \boldsymbol{e}_3)$ are used to visualize the location of the scatterers. Figure 4.18 shows horizontal cross sections of $\cot \tilde{\beta}_{12}^{\delta}(\boldsymbol{y})$ for $y_3 = -10$ cm and $y_3 = -40$ cm. Isosurface plots $\cot \tilde{\beta}_{12}^{\delta} = 20$ and $\cot \tilde{\beta}_{12}^{\delta} = 85$ can be found in Figure 4.19. The reconstructions are slightly worse than the ones obtained in Section 4.4.3 with the test function for two–layered background medium (cf. Figure 4.8 and Figure 4.9), but the approximate position of both scatterers can be estimated.

The reconstruction applying the test function for homogeneous background medium in this section was 85 times faster than the reconstruction using the test function for the two–layered background medium in Section 4.4.3.

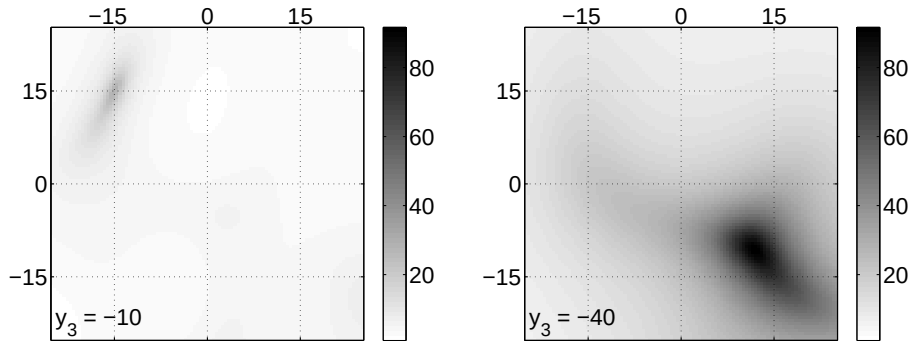

Figure 4.18: Cross–sectional plots of $\cot \tilde{\beta}_{12}^{\delta}(\boldsymbol{y})$ corresponding to a test function for the homogeneous background medium at $y_3 = -10$ cm and $y_3 = -40$ cm with 3% noise.

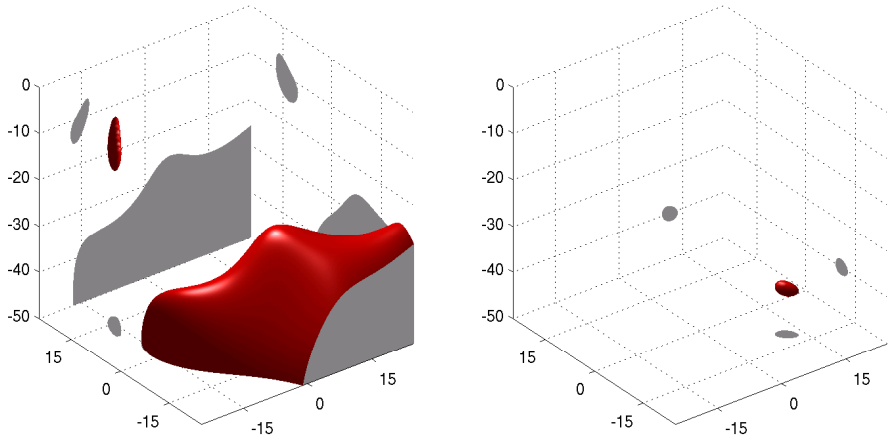

Figure 4.19: Isosurface plots $\cot \tilde{\beta}_{12}^{\delta} = 20$ and $\cot \tilde{\beta}_{12}^{\delta} = 85$ corresponding to a test function for the homogeneous background medium with 3% noise.

4.4.6 Spatial Resolution of the Reconstruction Algorithm

Finally, we investigate the spatial resolution of the MUSIC–type reconstruction algorithm for the measurement setup as introduced at the beginning of Section 4.4 working at a frequency of 20 kHz. For simplicity, we consider the homogeneous background medium and assume that two perfectly conducting spheres with radius 1 cm are buried underneath the measurement device at position $(-a/2, 0, -10)$ cm and $(a/2, 0, -10)$ cm, respectively, with $a \in \{5, 7.5, 10, 12.5, 15, 20\}$ cm.

We consider three–dimensional excitations and measurements, where the forward data have been obtained using the boundary element method with 616 triangles per scatterer and contain an estimated numerical error of 1.3%. Additionally, we perturb these data by a uniformly distributed relative error of 1%.

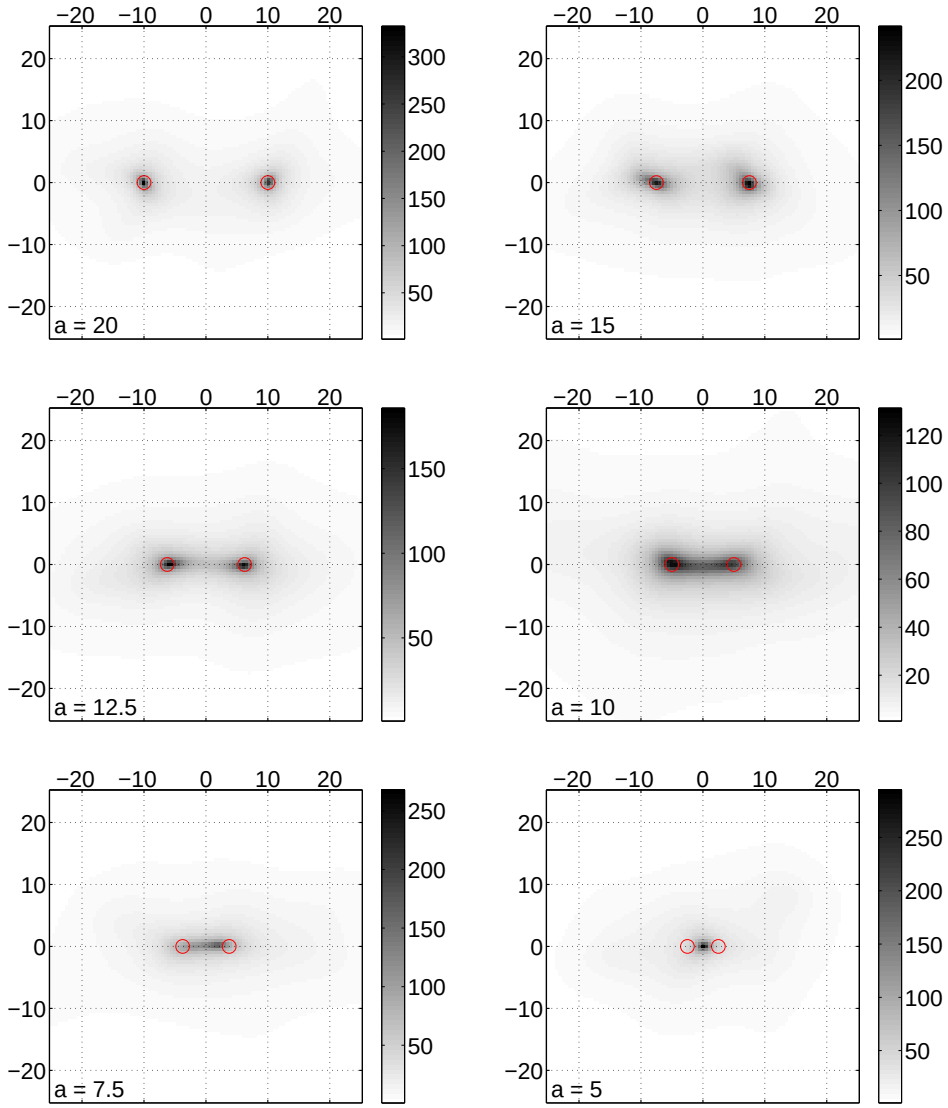

Figure 4.20: Cross–sectional plots of $\cot \tilde{\beta}^{\delta}_{12}(\boldsymbol{y})$ for $y_3 = -10$ cm with 1% noise.

The values of $\cot \tilde{\beta}^{\delta}_{12}$ on a three–dimensional equidistant rectangular sampling grid with step size 0.5 cm on the search domain $[-25, 25]^2 \times [-50, 0]$ cm^3 corresponding to the test function $\boldsymbol{g}_{y,d}$ for the homogeneous background medium with polarization vector $\boldsymbol{d} = (\boldsymbol{e}_3, \boldsymbol{e}_3)$ are used to visualize the location of the scatterers. Figure 4.20 shows horizontal cross sections of $\cot \tilde{\beta}^{\delta}_{12}(\boldsymbol{y})$ for $y_3 = -10$ cm and $a \in \{5, 7.5, 10, 12.5, 15, 20\}$ cm. Here, the red circles indicate the position and the size of the two scatterers. Note that for $a \geq 12.5$ cm the two scatterers can be perfectly distinguished

in the reconstructions. For $a = 10$ cm and even more for $a = 7.5$ cm the visualization starts smearing out the two scatterers to one. But for $a = 5$ cm (and also for smaller values of a) the reconstruction method determines only a single object positioned in the center of mass of both scatterers. This means that the two scatterers are no longer reconstructed as two individual small objects but as one small object consisting of two components.

Figure 4.21 shows approximations of the first 20 singular values of the measurement operator G_δ for $a \in \{5, 7.5, 10, 12.5, 15, 20\}$ cm and for different noise levels. For $a = 20$ cm, the first 6 singular values are clearly distinguished from the others, and the numerical results in Figure 4.20 indicate that the corresponding 6 singular vectors contain information on the positions of both scatterers. But the smaller the distance a between the two scatterers is, the smaller becomes the gap after the first 6 singular values and the bigger becomes the gap between the first and the second triple of singular values. For distances a such that the order of magnitude of the second triple of singular values is close to the noise level of 1%, the reconstructions in Figure 4.20 show just one object, that must be characterized by the first three singular vectors.

Not surprisingly, we found that the resolution of the reconstruction algorithm, i.e., the minimal value of the distance a such that both scatterers are reconstructed independently, strongly depends on the amount of noise, which we add to the forward data. Figure 4.22 shows horizontal cross sections of $\cot \tilde{\beta}_{12}^{\delta}(\boldsymbol{y})$ for $y_3 = -10$ cm corresponding to forward data which have only been perturbed by 0.3% uniformly distributed noise. In these visualizations the resolution is significantly better than in Figure 4.20. For $a \geq 7.5$ cm both scatterers are reconstructed separately. For $a = 5$ cm the visualization smears out but still information on both scatterers is recovered. Note that for $a = 5$ cm the second triple of singular values in Figure 4.21 is still above but close to the noise level of 0.3%. On the other hand, horizontal cross sections of $\cot \tilde{\beta}_{12}^{\delta}(\boldsymbol{y})$ for $y_3 = -10$ cm corresponding to forward data, which have been perturbed by 3% uniformly distributed noise, can be found in Figure 4.23. Only for $a \geq 15$ cm both scatterers are reconstructed seperatedly. Note that already for $a = 7.5$ cm the two scatterers are reconstructed as one scatterer located in their center of mass. Recalling Figure 4.21, we find that for $a \leq 12.5$ the second triple of singular values is close to or below the noise level of 3%.

Next, we analyzed whether the number of grid points of the discretized measurement device $\mathcal{M}_h$, in particular the step size h of this measurement grid, has an influence on the resolution of the reconstruction algorithm. For this purpose, we repeated the previous numerical experiments for an equidistant 11×11 grid $\mathcal{M}_h \subset \mathcal{M}$ with step size $h = 5$ cm (instead of a 6×6 grid with $h = 10$ cm in the previous example). The reconstructions do not change significantly, and the resolution does not improve for this finer measurement grid. Further experiments with a 3×3 measurement grid

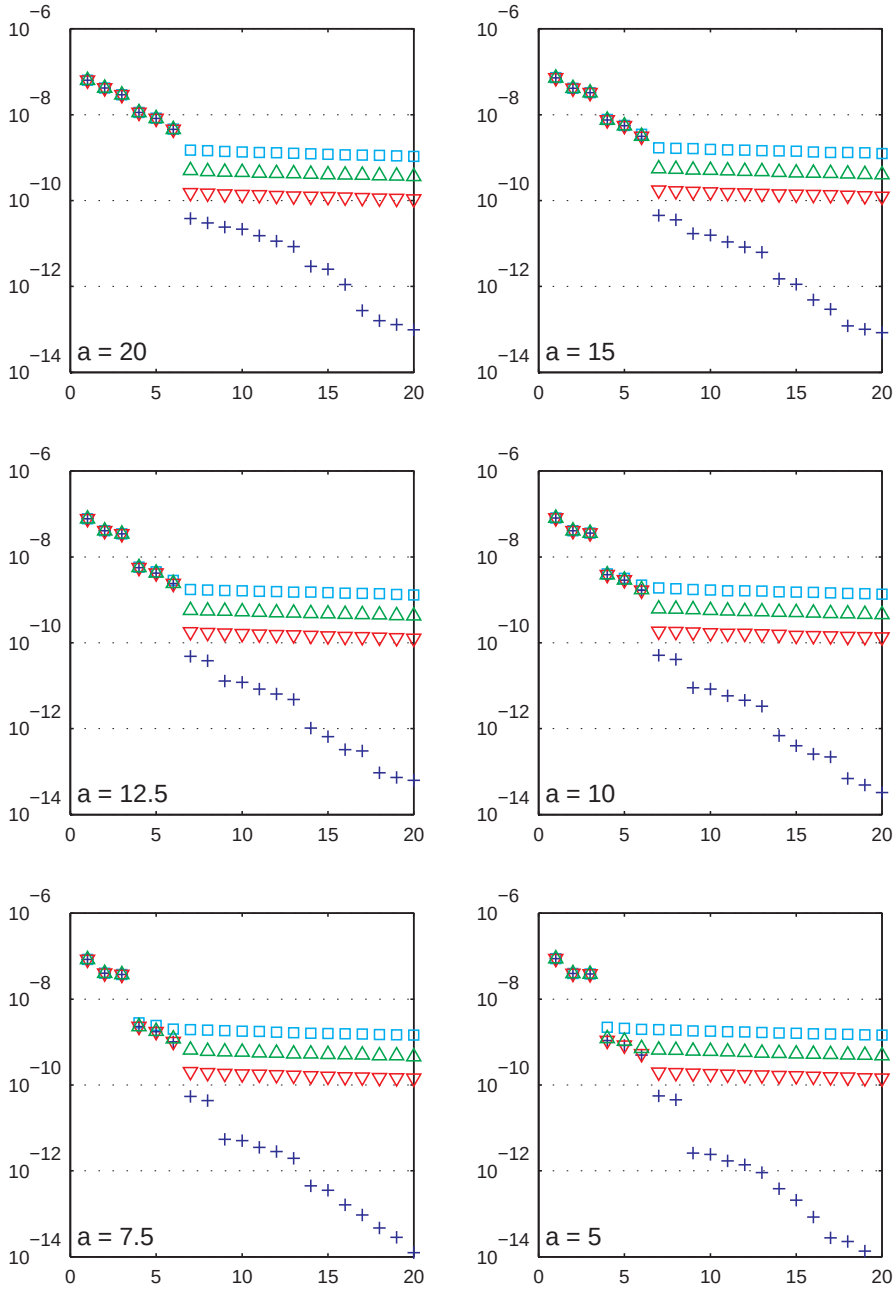

Figure 4.21: Singular values of the measurement operators G_δ (+ ... without additional noise, ▽ ... with 0.3% uniformly distributed noise, △ ... with 1% uniformly distributed noise, □ ... with 3% uniformly distributed noise).

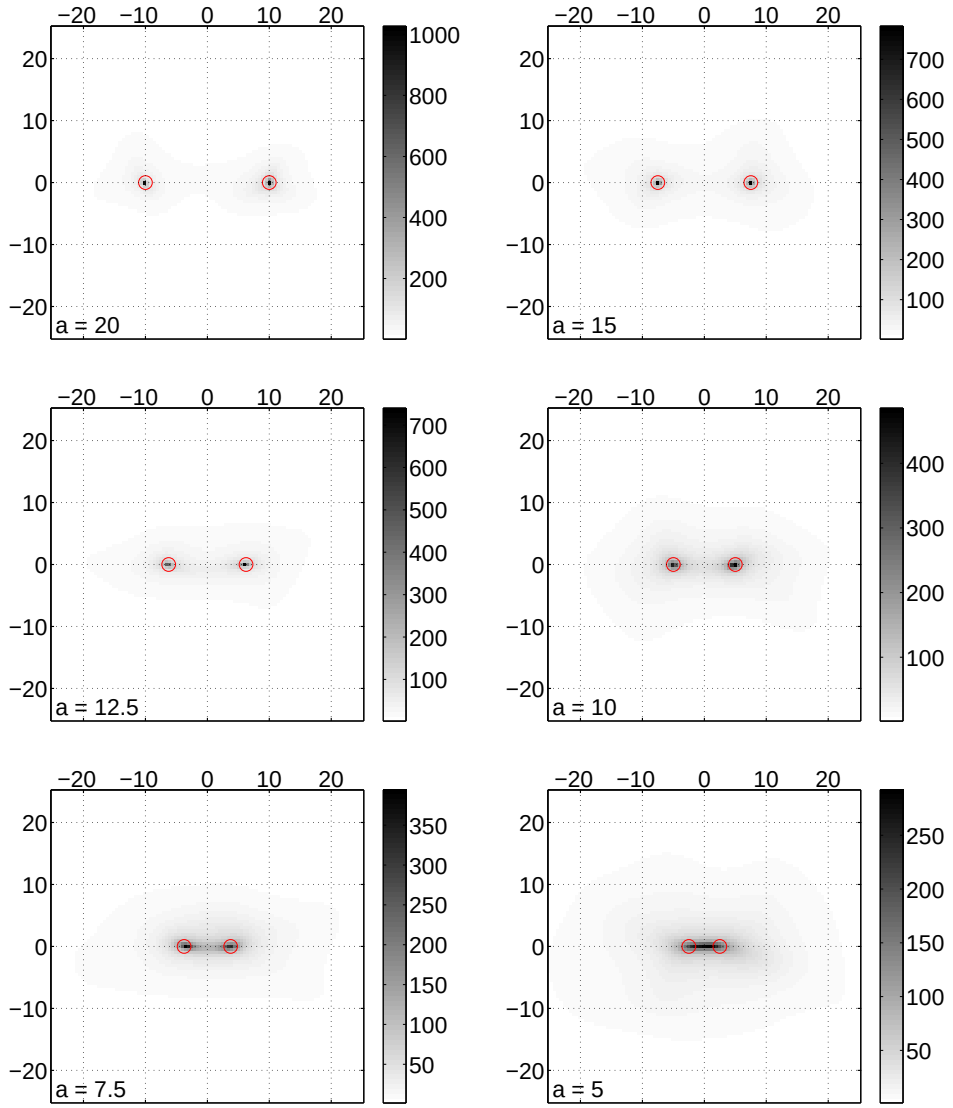

Figure 4.22: Cross–sectional plots of $\cot \tilde{\beta}_{12}^{\delta}(\boldsymbol{y})$ for $y_3 = -10$ cm with 0.3% noise.

(step size $h = 25$ cm) and a 21×21 measurement grid (step size $h = 2.5$ cm) confirmed that the resolution of the reconstruction algorithm is independent of the number of grid points and the step size of the measurement grid. (Of course there must be sufficiently many grid points to obtain enough data to compute the number of singular vectors required for the reconstruction of two scatterers; cf. Remark 4.11.)

To explain this behavior theoretically, we recall Corollary 3.25 and assume for a moment that the scattered field on the measurement device due

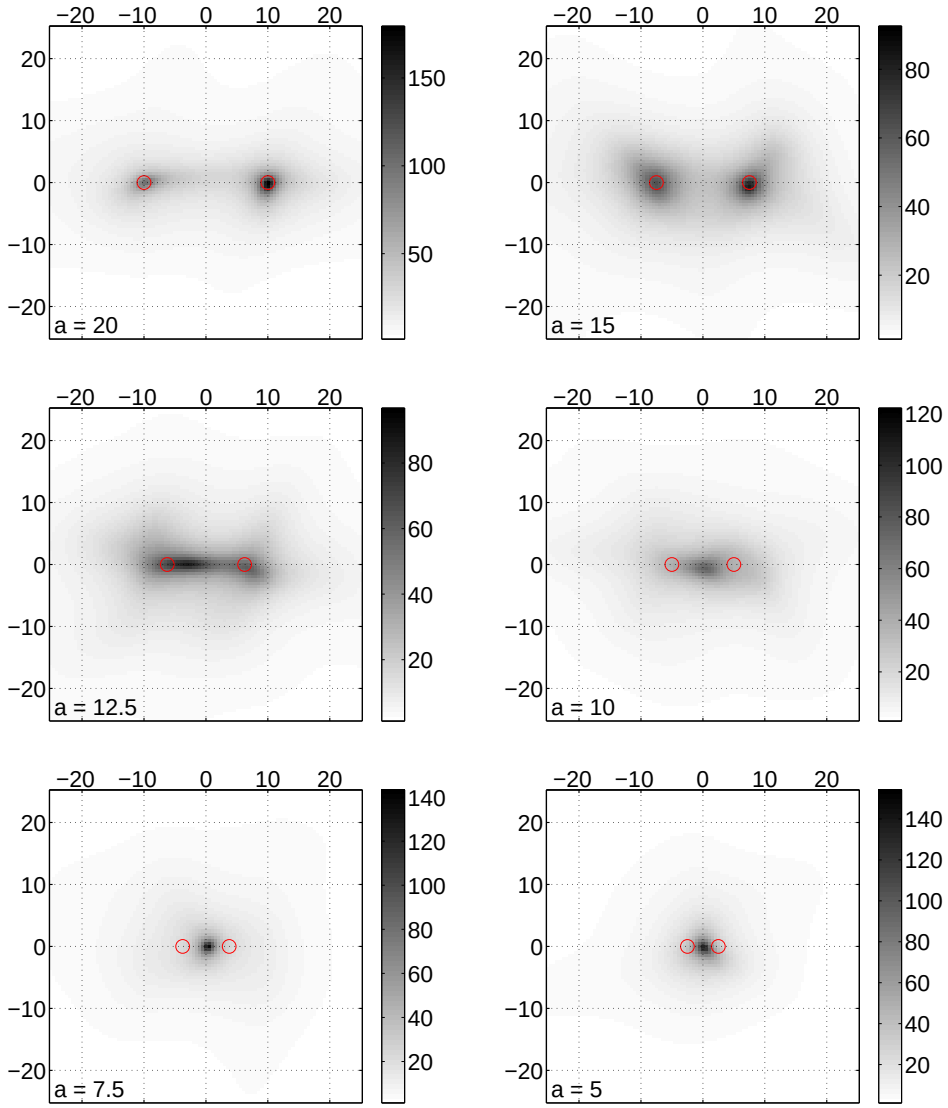

Figure 4.23: Cross–sectional plots of $\cot \tilde{\beta}_{12}^{\delta}(\boldsymbol{y})$ for $y_3 = -10$ cm with 3% noise.

to two small scatterers located at $\boldsymbol{z}_1, \boldsymbol{z}_2 \subset \mathbb{R}^3_-$ is exactly described by the leading order term in the asymptotic expansion (3.71), i.e., as a superposition of fields due to electric and magnetic dipoles located at $\boldsymbol{z}_1$ and $\boldsymbol{z}_2$. The MUSIC–type reconstruction algorithm computes for each sampling point $\boldsymbol{y}$ in the search domain a test function $\boldsymbol{g}_{y,d}$, which is a superposition of an electric and a magnetic dipole in $\boldsymbol{y}$, and compares its values on the measurement device with the measurement data to check whether such a test dipole pattern is contained in these data or not. So, according to Proposi-

tion 4.4, it suffices to distinguish the values of two test functions $\boldsymbol{g}_{z_1,d}$ and $\boldsymbol{g}_{z_2,d}$ on the measurement device $\mathcal{M}$ in order to distinguish the corresponding two small scatterers located at $\boldsymbol{z}_1$ and $\boldsymbol{z}_2$ by means of the reconstruction method. Recalling the result due to Kirsch [73, Theorem 2.1] (see also [4, Proposition 6.3]) mentioned in Remark 4.11, the same is true for the discrete measurement device $\mathcal{M}_h$, provided the number of grid points is large enough, which we assume henceforth. Thus, under the assumption that the leading order term in the asymptotic expansion (3.71) is sufficient to describe the scattering process and in absence of noise and numerical errors, the resolution of the reconstruction algorithm is theoretically arbitrarily fine.

Now, we consider the exact model: By Corollary 3.25, the scattered field due to two small scatterers is well approximated by the field due to appropriate superpositions of electric and magnetic dipoles located near these scatterers. However, if the scatterers are very close to each other, their scattered field is also well approximated by the field due to an appropriate superposition of electric and magnetic dipoles located near the center of mass of both scatterers, because the two scatterers can be interpreted as one small scatterer consisting of two components. The MUSIC–type reconstruction algorithm marks sampling points in the search domain in accordance with the quality of the approximations of parts of the measurement data by the test dipole fields with singularities in these sampling points. The better this approximation is, the larger is the value of $\cot \tilde{\beta}_{12}^{\delta}$ in the visualizations. This explains that the visualizations smear out the two scatterers to one if they get close to each other and finally show just one object located in the center of mass of both scatterers, because the closer the two scatterers are to each other, the better the corresponding scattered field is approximated by the field due to an appropriate dipole source located in the center of mass of these scatterers.

It is also clear that if the forward data contain noise, the reconstructions are less sharp, because then more dipole patterns due to test dipoles near the scatterers approximate parts of the measurement data at comparable but lower quality.

What remains to explain is why with increasing noise level closely spaced scatterers are reconstructed as one object for increasing distances: As already mentioned, two closely spaced small scatterers can on the one hand approximately be considered as two dipole sources that can in this example be acribed to the singular vectors corresponding to the first 6 singular values of the measurement operator. On the other hand, they can be considered as one dipole corresponding to the 3 dominating singular vectors. Recalling Figure 4.21, in presence of noise the 3 dominant singular vectors can be approximated more stably than the others. Thus, closely spaced scatterers are reconstructed as one object located in the center of mass of these scatterers also for larger distances, because the information that there are two objects is more sensitive to noise than the information on the approximate position

of the center of mass of both objects.

Note that, in order to investigate the resolution of the reconstruction algorithm, we studied just one particular example that does not cover all possible situations of interest. If for instance the two scatterers are not of equal size, the situation changes significantly; cf. Section 4.4.4. Finally, we mention that the reconstruction of closely spaced scatterers has recently also been studied in the context of inverse conductivity problems by Ammari et al. [9] (see also [4]).

Appendix A

Polarizability Tensors

In this chapter, we recall the definition and some important properties of *electric* and *magnetic polarizability tensors*. These tensors are essential components of the asymptotic formulas developed in Chapter 2 and Chapter 3, but they also occur in various other contexts such as for instance Rayleigh approximations of acoustic scattering, electromagnetic scattering, and elasticity (see Dassios and Kleinman [44] and Keller, Kleinman, and Senior [69]) or hydrodynamics of irrotational flows of incompressible inviscid fluids past rigid surfaces (see Schiffer and Szegö [98]).

The definition of polarizability tensors is not consistent in the literature. Here, we give a definition involving boundary integral operators similar to the one by Ammari and Kang [7, p. 45], but with a different sign for the magnetic polarizability tensor. Then, we show that this definition is equivalent to the one given in [44], by Friedman and Vogelius in [49], and in [69]. Note that recently polarizability tensors are often just called *polarization tensors*, but historically these were different quantities; cf. [44, pp. 163-169] and [69, p. 17].

Definition A.1. For a bounded open set $B \subset \mathbb{R}^n$ of class $C^{2,\alpha}$, we define the *magnetic polarizability tensor* $\mathbb{M}_B^0 \in \mathbb{R}^{n\times n}$ by $\mathbb{M}_B^0 := (m_{jl}^0)_{j,l=1}^n$ with

$$m_{jl}^0 := -\int_{\partial B} y_l \Big(\Big(-\frac{1}{2} I + {K_B^0}^\top \Big)^{-1} \nu_j \Big)(\boldsymbol{y})\, \mathrm{d}s(\boldsymbol{y}), \qquad 1 \le j,l \le n.$$

Furthermore, we define the *electric polarizability tensor* $\mathbb{M}_B^\infty \in \mathbb{R}^{n\times n}$ by $\mathbb{M}_B^\infty := (m_{jl}^\infty)_{j,l=1}^n$ with

$$m_{jl}^\infty := \int_{\partial B} y_l \Big(\Big(\frac{1}{2} I + {K_B^0}^\top \Big)^{-1} \nu_j \Big)(\boldsymbol{y})\, \mathrm{d}s(\boldsymbol{y}), \qquad 1 \le j,l \le n.$$

Next, we show that this definition is equivalent to the ones given in [49], [44, p. 166], and [69]. We start with the magnetic polarizability tensor and

introduce the functions v_l, $1 \leq l \leq n$, which solve the exterior boundary value problem

$$\Delta v_l = 0 \qquad \text{in } \mathbb{R}^n \setminus \overline{B}, \tag{A.1a}$$

$$\frac{\partial v_l}{\partial \boldsymbol{\nu}} = \nu_l \qquad \text{on } \partial B, \tag{A.1b}$$

$$v_l(\boldsymbol{y}) = o(1) \qquad \text{as } |\boldsymbol{y}| \to \infty. \tag{A.1c}$$

Such functions v_l exist and are unique; cf. Kress [79, Theorem 6.28]. For $n = 2$ the necessary condition $\int_{\partial B} \nu_l(\boldsymbol{y})\, \mathrm{d}s(\boldsymbol{y}) = 0$, $1 \leq l \leq n$, follows from the Divergence Theorem (cf. Monk [88, Theorem 3.19]).

Lemma A.2. *For $1 \leq j, l \leq n$ the elements m^0_{jl} of the magnetic polarizability tensor $\mathbb{M}^0_B$ satisfy*

$$m^0_{jl} = \int_{\partial B} \nu_j(\boldsymbol{y})\big(y_l - v_l(\boldsymbol{y})\big)\, \mathrm{d}s(\boldsymbol{y}).$$

Proof. Let $1 \leq j, l \leq n$. We define $\phi_l := \big(-\frac{1}{2}I + K^0_B\big)^{-1} y_l$ and $u_l := \mathcal{D}_B \phi_l$. Then, we obtain from the jump relations (2.4) that $u_l|^-_{\partial B} = y_l$, and so $u_l|_B$ is the unique solution to

$$\Delta u_l = 0 \quad \text{in } B, \qquad u_l|^-_{\partial B} = y_l.$$

Therefore, $u_l|_B = y_l$, and we have $\frac{\partial u_l}{\partial \boldsymbol{\nu}}\big|^+_{\partial B} = \frac{\partial u_l}{\partial \boldsymbol{\nu}}\big|^-_{\partial B} = \nu_l$ on ∂B. Thus, $u_l\big|_{\mathbb{R}^n \setminus \overline{B}}$ solves (A.1), and from the uniqueness of solutions to (A.1) we get $u_l\big|_{\mathbb{R}^n \setminus \overline{B}} = v_l$. Again from (2.4), we obtain that

$$\phi_l = u_l|^+_{\partial B} - u_l|^-_{\partial B} = v_l|_{\partial B} - y_l.$$

This gives

$$\begin{aligned} m^0_{jl} &= -\int_{\partial B} y_l \Big(\Big(-\frac{1}{2}I + {K^0_B}^{\top}\Big)^{-1} \nu_j\Big)(\boldsymbol{y})\, \mathrm{d}s(\boldsymbol{y}) \\ &= -\int_{\partial B} \nu_j(\boldsymbol{x}) \Big(\Big(-\frac{1}{2}I + K^0_B\Big)^{-1} y_l\Big)(\boldsymbol{x})\, \mathrm{d}s(\boldsymbol{x}) \\ &= -\int_{\partial B} \nu_j(\boldsymbol{x}) \phi_l(\boldsymbol{x})\, \mathrm{d}s(\boldsymbol{x}) \\ &= \int_{\partial B} \nu_j(\boldsymbol{x})\big(x_l - v_l(\boldsymbol{x})\big)\, \mathrm{d}s(\boldsymbol{x}). \end{aligned}$$

□

Remark A.3. Closely related to the magnetic polarizability tensor $\mathbb{M}^0_B$ is the *virtual mass tensor* $\mathbb{W}_B := (W_{jl})_{j,l=1}^n$ with

$$W_{jl} := -\int_{\partial B} \nu_j(\boldsymbol{y}) v_l(\boldsymbol{y})\, \mathrm{d}s(\boldsymbol{y}), \qquad 1 \leq j, l \leq n;$$

cf. [44, p. 166], [69], and [98].

To show the equivalence for the electric polarizability tensor, we introduce the functions w_j, $1 \le j, l \le n$, which solve the exterior boundary value problem

$$\begin{aligned} \Delta w_j &= 0 && \text{in } \mathbb{R}^n \setminus \overline{B}, \\ w_j &= y_j && \text{on } \partial B, \\ w_j(\boldsymbol{y}) &= \mathcal{O}(1) && \text{as } |\boldsymbol{y}| \to \infty,\ n = 2, \\ w_j(\boldsymbol{y}) &= o(1) && \text{as } |\boldsymbol{y}| \to \infty,\ n \ge 3. \end{aligned}$$

Such w_j exist and are unique; cf. [79, Theorem 6.24]. We also need a function ϑ that satisfies

$$\begin{aligned} \Delta \vartheta &= 0 && \text{in } \mathbb{R}^n \setminus \overline{B}, \\ \vartheta &= 1 && \text{on } \partial B, \\ \vartheta(\boldsymbol{y}) &= \mathcal{O}(1) && \text{as } |\boldsymbol{y}| \to \infty,\ n = 2, \\ \vartheta(\boldsymbol{y}) &= o(1) && \text{as } |\boldsymbol{y}| \to \infty,\ n \ge 3. \end{aligned}$$

Lemma A.4. *For $1 \le j, l \le n$, the elements m_{jl}^{∞} of the electric polarizability tensor $\mathbb{M}_B^{\infty}$ satisfy*

$$\begin{aligned} m_{jl}^{\infty} &= \int_{\partial B} y_l \Big(\nu_j(\boldsymbol{y}) - \frac{\partial w_j}{\partial \boldsymbol{\nu}}(\boldsymbol{y}) \Big) \, \mathrm{d}s(\boldsymbol{y}), && n = 2, \\ m_{jl}^{\infty} &= \int_{\partial B} y_l \Big(\nu_j(\boldsymbol{y}) - \frac{\partial w_j}{\partial \boldsymbol{\nu}}(\boldsymbol{y}) \Big) \, \mathrm{d}s(\boldsymbol{y}) \\ &\quad + \Big(\int_{\partial B} \frac{\partial \vartheta}{\partial \boldsymbol{\nu}} \, \mathrm{d}s \Big)^{-1} \Big(\int_{\partial B} \frac{\partial w_j}{\partial \boldsymbol{\nu}} \, \mathrm{d}s \Big) \Big(\int_{\partial B} \frac{\partial w_l}{\partial \boldsymbol{\nu}} \, \mathrm{d}s \Big), && n \ge 3. \end{aligned}$$

Proof. Let $1 \le j, l \le n$. We define $\psi_j := \big(\frac{1}{2} I + K_B^{0\,\top} \big)^{-1} \nu_j$ and $u_j := \mathcal{S}_B \psi_j$. Then, we obtain from the jump relations (2.4) that $\frac{\partial u_j}{\partial \boldsymbol{\nu}} \big|_{\partial B}^{-} = \nu_j$, and so $u_j|_B$ solves

$$\Delta u_j = 0 \quad \text{in } B, \qquad \frac{\partial u_j}{\partial \boldsymbol{\nu}} \Big|_{\partial B}^{-} = \nu_j.$$

Therefore, $u_j|_B = y_j + c_j$ for some constant $c_j \in \mathbb{R}$, and we find that $u_j|_{\partial B}^{+} = u_j|_{\partial B}^{-} = y_j + c_j$. So, $u_j|_{\mathbb{R}^n \setminus \overline{B}}$ solves the exterior boundary value problem

$$\begin{aligned} \Delta u_j &= 0 && \text{in } \mathbb{R}^n \setminus \overline{B}, \\ u_j &= y_j + c_j && \text{on } \partial B, \\ u_j(\boldsymbol{y}) &= o(1) && \text{as } |\boldsymbol{y}| \to \infty. \end{aligned}$$

Note that for $n = 2$ the last equation follows from the fact that

$$\int_{\partial B} \psi_j(\boldsymbol{y}) \, \mathrm{d}s(\boldsymbol{y}) = 0;$$

cf. [79, p. 86]. So, we can write

$$u_j = w_j + c_j\vartheta.$$

Observe that

$$\psi_j = \frac{\partial u_j}{\partial \boldsymbol{\nu}}\Big|_{\partial B}^{-} - \frac{\partial u_j}{\partial \boldsymbol{\nu}}\Big|_{\partial B}^{+} = \nu_j - \frac{\partial w_j}{\partial \boldsymbol{\nu}}\Big|_{\partial B} - c_j \frac{\partial \vartheta}{\partial \boldsymbol{\nu}}\Big|_{\partial B}.$$

For $n = 2$, it is clear that $\vartheta \equiv 1$. Therefore, $\frac{\partial \vartheta}{\partial \boldsymbol{\nu}}\big|_{\partial B} = 0$, and we obtain

$$\begin{aligned} m_{jl}^{\infty} &= \int_{\partial B} y_l \Big(\Big(\frac{1}{2} I + {K_B^0}^{\top} \Big)^{-1} \nu_j \Big)(\boldsymbol{y}) \, \mathrm{d}s(\boldsymbol{y}) \\ &= \int_{\partial B} y_l \psi_j(\boldsymbol{y}) \, \mathrm{d}s(\boldsymbol{y}) \\ &= \int_{\partial B} y_l \Big(\nu_j(\boldsymbol{y}) - \frac{\partial w_j}{\partial \boldsymbol{\nu}}(\boldsymbol{y}) \Big) \, \mathrm{d}s(\boldsymbol{y}). \end{aligned}$$

For $n \geq 3$, the function ϑ is nontrivial, and from the maximum principle (cf. [79, Corollary 6.9]) we find that $\frac{\partial \vartheta}{\partial \boldsymbol{\nu}}\big|_{\partial B} < 0$. Because

$$0 = \int_{\partial B} \psi_j(\boldsymbol{y}) \, \mathrm{d}s(\boldsymbol{y}) = \int_{\partial B} \Big(\nu_i(\boldsymbol{y}) - \frac{\partial w_j}{\partial \boldsymbol{\nu}}(\boldsymbol{y}) - c_j \frac{\partial \vartheta}{\partial \boldsymbol{\nu}}(\boldsymbol{y}) \Big) \, \mathrm{d}s(\boldsymbol{y}),$$

we obtain that

$$c_j = \left(\int_{\partial B} \frac{\partial \vartheta}{\partial \boldsymbol{\nu}}(\boldsymbol{y}) \, \mathrm{d}s(\boldsymbol{y}) \right)^{-1} \int_{\partial B} \frac{\partial w_j}{\partial \boldsymbol{\nu}}(\boldsymbol{y}) \, \mathrm{d}s(\boldsymbol{y}). \tag{A.2}$$

As above,

$$\begin{aligned} m_{jl}^{\infty} &= \int_{\partial B} y_l \Big(\Big(\frac{1}{2} I + {K_B^0}^{\top} \Big)^{-1} \nu_j \Big)(\boldsymbol{y}) \, \mathrm{d}s(\boldsymbol{y}) \\ &= \int_{\partial B} y_l \psi_j(\boldsymbol{y}) \, \mathrm{d}s(\boldsymbol{y}) \\ &= \int_{\partial B} y_l \Big(\nu_j(\boldsymbol{y}) - \frac{\partial w_j}{\partial \boldsymbol{\nu}}(\boldsymbol{y}) - c_j \frac{\partial \vartheta}{\partial \boldsymbol{\nu}}(\boldsymbol{y}) \Big) \, \mathrm{d}s(\boldsymbol{y}). \end{aligned} \tag{A.3}$$

Inserting (A.2) into (A.3) and applying Green's Theorem (cf. [79, Theorem 6.3]) yields the assertion. Here, we used that bounded harmonic functions U in an exterior domain satisfy

$$U(\boldsymbol{x}) = U_{\infty} + \mathcal{O}\Big(\frac{1}{|\boldsymbol{x}|} \Big), \quad \nabla U(\boldsymbol{x}) = \mathcal{O}\Big(\frac{1}{|\boldsymbol{x}|^{n-1}} \Big), \quad |\boldsymbol{x}| \to \infty, \tag{A.4}$$

uniformly for all directions, where U_{∞} is some constant; cf. [79, p. 74]. □

Remark A.5. Closely related to the electric polarizability tensor $\mathbb{M}_B^\infty$ is the *polarization tensor* $\mathbb{Q}_B := (Q_{jl})_{j,l=1}^n$ with

$$Q_{jl} = -\int_{\partial B} y_l \frac{\partial w_j}{\partial \boldsymbol{\nu}}(\boldsymbol{y})\, \mathrm{d}s(\boldsymbol{y}), \qquad 1 \le j,l \le n,\ n = 2,$$

$$Q_{jl} = -\int_{\partial B} y_l \frac{\partial w_j}{\partial \boldsymbol{\nu}}(\boldsymbol{y})\, \mathrm{d}s(\boldsymbol{y}) + \Big(\int_{\partial B} \frac{\partial \vartheta}{\partial \boldsymbol{\nu}}\, \mathrm{d}s\Big)^{-1} \Big(\int_{\partial B} \frac{\partial w_j}{\partial \boldsymbol{\nu}}\, \mathrm{d}s\Big)\Big(\int_{\partial B} \frac{\partial w_l}{\partial \boldsymbol{\nu}}\, \mathrm{d}s\Big), \quad 1 \le j,l \le n,\ n \ge 3;$$

cf. [44, p. 165], [69], and [98].

Proposition A.6. *The magnetic and the electric polarizability tensor are symmetric and positive definite.*

Proof. Based on the representations of these tensors given in Lemma A.2 and Lemma A.4, this has been proven in [49]. We include the proof for the sake of completeness.

The fact that $\mathbb{M}_B^0$ and $\mathbb{M}_B^\infty$ are symmetric follows from Green's Theorem (cf. [79, Theorem 6.3]) and the decay condition (A.4). To verify that $\mathbb{M}_B^0$ is positive definite we compute for $\boldsymbol{x} \in \mathbb{R}^n$ through integration by parts and use of (A.4) that

$$\begin{aligned}\sum_{j,l=1}^n m_{jl}^0 x_j x_l &= \sum_{j,l=1}^n x_j x_l \int_B \nabla_y y_j \cdot \nabla_y y_l \, \mathrm{d}\boldsymbol{y} \\ &\quad + \sum_{j,l=1}^n x_j x_l \int_{\mathbb{R}^3 \setminus \overline{B}} \nabla_y v_j(\boldsymbol{y}) \cdot \nabla_y v_l(\boldsymbol{y})\, \mathrm{d}\boldsymbol{y} \\ &= |B||\boldsymbol{x}|^2 + \int_{\mathbb{R}^3 \setminus \overline{B}} \Big|\nabla_y \Big(\sum_{j=1}^n x_j v_j(\boldsymbol{y})\Big)\Big|^2 \, \mathrm{d}\boldsymbol{y} \ge |B||\boldsymbol{x}|^2,\end{aligned}$$

where $|B|$ denotes the measure of B. Analogously, we obtain for $\mathbb{M}_B^\infty$, $n = 2$ and $\boldsymbol{x} \in \mathbb{R}^n$ that

$$\sum_{j,l=1}^n m_{jl}^\infty x_j x_l = |B||\boldsymbol{x}|^2 + \int_{\mathbb{R}^3 \setminus \overline{B}} \Big|\nabla_y \Big(\sum_{j=1}^n x_j w_j(\boldsymbol{y})\Big)\Big|^2 \, \mathrm{d}\boldsymbol{y} \ge |B||\boldsymbol{x}|^2.$$

Finally, for $n \ge 3$ and $\boldsymbol{x} \in \mathbb{R}^n$,

$$\begin{aligned}\sum_{j,l=1}^n m_{jl}^\infty x_j x_l &= |B||\boldsymbol{x}|^2 + \int_{\mathbb{R}^3 \setminus \overline{B}} \Big|\nabla_y \Big(\sum_{j=1}^n x_j w_j(\boldsymbol{y})\Big)\Big|^2 \, \mathrm{d}\boldsymbol{y} \\ &\quad - \Big(\int_{\mathbb{R}^3 \setminus \overline{B}} |\nabla_y \vartheta(\boldsymbol{y})|^2 \, \mathrm{d}\boldsymbol{y}\Big)^{-1} \Big(\int_{\mathbb{R}^3 \setminus \overline{B}} \nabla_y \Big(\sum_{j=1}^n x_j w_j(\boldsymbol{y})\Big) \cdot \nabla_y \vartheta(\boldsymbol{y})\, \mathrm{d}\boldsymbol{y}\Big)^2 \\ &\ge |B||\boldsymbol{x}|^2,\end{aligned}$$

by Cauchy–Schwarz's inequality. □

We mention that over the past years several generalizations of polarizability tensors have been introduced and collect some of them in the following:

- The consideration of transmission problems instead of boundary value problems, i.e., penetrable inhomogeneities instead of insulating or perfectly conducting inhomogeneities, leads to so–called *general polarizability tensors*; cf. Cedio–Fengya, Moskow, and Vogelius [29] and [44, pp. 167-168].

- In the course of justifying asymptotic expansions of boundary voltage potentials in presence of small penetrable inhomogeneities including higher order terms Ammari and Kang [5] introduced *generalized polarization tensors*, which are extensions of general polarizability tensors. The properties of these tensors have been studied by Ammari and Kang [6–8]. Electric and magnetic polarizability tensors can be generalized in the same way; cf. [7, p. 45].

- Developing a representation formula for boundary voltage perturbations caused by internal conductivity inhomogeneities of low volume fraction that requires minimal regularity from the boundaries of these inhomogeneities, Capdeboscq and Vogelius [26] extended general polarizability tensors in the sense of measure theory. The elements of these tensors are regular Borel measures. Their properties have been studied by Capdeboscq and Vogelius [27, 28].

Appendix B

Representation Theorem and Reciprocity Relations

B.1 Representation Theorem

In this section, we consider representation formulas for electric and magnetic fields in two–layered background media. For this purpose, we study the mathematical setting as introduced in Section 3.4. In addition, let the bounded set $D \subset \mathbb{R}^3_0$ be the open complement of an unbounded domain of class $C^{2,\alpha}$, $0 < \alpha < 1$, such that D is compactly contained in $\mathbb{R}^3_0$, and denote by $\boldsymbol{\nu}$ the unit outward normal to ∂D relative to D.

We mention that the formulas (B.3) and (B.5), which we are going to prove, have already been stated without proof by Cutzach and Hazard [43]. Our proof roughly follows Colton and Kress [38, pp. 110–116] and Ammari and Latiri–Grouz [11].

Theorem B.1. *Let* $\boldsymbol{E}, \boldsymbol{H} \in \boldsymbol{H}_{\mathrm{loc}}(\mathbf{curl}, \mathbb{R}^3 \setminus \overline{D})$ *be a solution to Maxwell's equations*

$$\mathbf{curl}\boldsymbol{H} + \mathrm{i}\,\omega\varepsilon\boldsymbol{E} = 0, \quad \mathbf{curl}\boldsymbol{E} - \mathrm{i}\,\omega\mu\boldsymbol{H} = 0 \qquad \text{in } \mathbb{R}^3 \setminus \overline{D}, \tag{B.1}$$

satisfying the Silver-Müller radiation condition

$$\int_{\partial B_R(0)} \left| \frac{\boldsymbol{x}}{R} \times \boldsymbol{H}(\boldsymbol{x}) + \left(\frac{\varepsilon(\boldsymbol{x})}{\mu(\boldsymbol{x})}\right)^{1/2} \boldsymbol{E}(\boldsymbol{x}) \right|^2 \mathrm{d}s(\boldsymbol{x}) = o(1) \qquad \text{as } R \to \infty. \tag{B.2}$$

Then, we have for any $\boldsymbol{y} \in \mathbb{R}^3_0 \setminus \overline{D}$ *the* Stratton–Chu formula

$$\boldsymbol{H}(\boldsymbol{y}) = \int_{\partial D} \frac{\varepsilon(\boldsymbol{y})}{\varepsilon(\boldsymbol{x})} \Big(\mathbb{G}^{m\top}(\boldsymbol{x}, \boldsymbol{y})(\boldsymbol{\nu} \times \mathbf{curl}\boldsymbol{H})(\boldsymbol{x}) + (\mathbf{curl}_x\, \mathbb{G}^m)^\top(\boldsymbol{x}, \boldsymbol{y})(\boldsymbol{\nu} \times \boldsymbol{H})(\boldsymbol{x}) \Big)\, \mathrm{d}s(\boldsymbol{x}). \tag{B.3}$$

Remark B.2. A similar representation formula holds for the electric field $\boldsymbol{E}$: Let $\boldsymbol{E}, \boldsymbol{H} \in \boldsymbol{H}_{\mathrm{loc}}(\mathbf{curl}, \mathbb{R}^3 \setminus \overline{D})$ be a solution to Maxwell's equations (B.1) satisfying the Silver-Müller radiation condition

$$\int_{\partial B_R(0)} \left| \frac{\boldsymbol{x}}{R} \times \boldsymbol{E}(\boldsymbol{x}) - \Big(\frac{\mu(\boldsymbol{x})}{\varepsilon(\boldsymbol{x})}\Big)^{1/2} \boldsymbol{H}(\boldsymbol{x}) \right|^2 \mathrm{d}s(\boldsymbol{x}) = o(1) \qquad \text{as } R \to \infty. \tag{B.4}$$

Then, we have for any $\boldsymbol{y} \in \mathbb{R}^3_0 \setminus \overline{D}$ the *Stratton–Chu formula*

$$\boldsymbol{E}(\boldsymbol{y}) = \int_{\partial D} \frac{\mu(\boldsymbol{y})}{\mu(\boldsymbol{x})} \Big(\mathbb{G}^{e\top}(\boldsymbol{x}, \boldsymbol{y})(\boldsymbol{\nu} \times \mathbf{curl}\boldsymbol{E})(\boldsymbol{x}) + (\mathbf{curl}_x \mathbb{G}^e)^\top(\boldsymbol{x}, \boldsymbol{y})(\boldsymbol{\nu} \times \boldsymbol{E})(\boldsymbol{x}) \Big) \mathrm{d}s(\boldsymbol{x}). \tag{B.5}$$

This formula can be proven in the same way as Theorem B.1.

Proof of Theorem B.1. First, we observe that as a consequence of the radiation condition (B.2),

$$\int_{\partial B_R} |\boldsymbol{\nu} \times \boldsymbol{H}|^2 \, \mathrm{d}s = \mathcal{O}(1) \qquad \text{and} \qquad \int_{\partial B_R} |\boldsymbol{E}|^2 \, \mathrm{d}s = \mathcal{O}(1) \tag{B.6}$$

as $R \to \infty$. This can be proven in the same way as done by Monk [88, p. 231] for homogeneous background medium.

Let $\boldsymbol{y} \in \mathbb{R}^3_0 \setminus \overline{D}$ and choose $R > 0$ large enough so that $B_R(0)$ contains $\boldsymbol{y}$. Moreover, let $r > 0$ be small enough such that $B_r(\boldsymbol{y})$ is contained in $B_R(0)$. From Maxwell's equations for $\boldsymbol{E}$ and $\boldsymbol{H}$ we obtain

$$\mathbf{curl} \frac{1}{\varepsilon} \mathbf{curl} \boldsymbol{H} = \omega^2 \mu \boldsymbol{H} \qquad \text{in } \mathbb{R}^3 \setminus \overline{D}.$$

So, we see from (3.11) for $\boldsymbol{x} \in B_R(0) \setminus \overline{B_r(\boldsymbol{y})}$ that

$$\begin{aligned} 0 &= \Big(\mathbf{curl}_x \frac{1}{\varepsilon(\boldsymbol{x})} \mathbf{curl}_x \mathbb{G}^m(\boldsymbol{x}, \boldsymbol{y}) \Big)^\top \boldsymbol{H}(\boldsymbol{x}) - \omega^2 \mu(\boldsymbol{x}) \, \mathbb{G}^{m\top}(\boldsymbol{x}, \boldsymbol{y}) \boldsymbol{H}(\boldsymbol{x}) \\ &= \Big(\mathbf{curl}_x \frac{1}{\varepsilon(\boldsymbol{x})} \mathbf{curl}_x \mathbb{G}^m(\boldsymbol{x}, \boldsymbol{y}) \Big)^\top \boldsymbol{H}(\boldsymbol{x}) - \mathbb{G}^{m\top}(\boldsymbol{x}, \boldsymbol{y}) \mathbf{curl} \frac{1}{\varepsilon(\boldsymbol{x})} \mathbf{curl} \boldsymbol{H}(\boldsymbol{x}). \end{aligned}$$

Integration by parts (3.1) yields

$$
\begin{aligned}
0 = \int_{B_R(0)\setminus\overline{B_r(\boldsymbol{y})\cup D}} \Bigg(& \Big(\mathbf{curl}_x \frac{1}{\varepsilon(\boldsymbol{x})} \mathbf{curl}_x \, \mathbb{G}^m(\boldsymbol{x},\boldsymbol{y})\Big)^\top \boldsymbol{H}(\boldsymbol{x}) \\
& - \mathbb{G}^{m\top}(\boldsymbol{x},\boldsymbol{y}) \mathbf{curl} \frac{1}{\varepsilon(\boldsymbol{x})} \mathbf{curl} \boldsymbol{H}(\boldsymbol{x}) \Bigg) \, \mathrm{d}\boldsymbol{x} \\
= \int_{\partial B_R(0)} \frac{1}{\varepsilon(\boldsymbol{x})} \Bigg(& \big(\boldsymbol{\nu}(\boldsymbol{x}) \times \mathbf{curl}_x \, \mathbb{G}^m(\boldsymbol{x},\boldsymbol{y})\big)^\top \boldsymbol{H}(\boldsymbol{x}) \\
& - \mathbb{G}^{m\top}(\boldsymbol{x},\boldsymbol{y}) (\boldsymbol{\nu} \times \mathbf{curl} \boldsymbol{H})(\boldsymbol{x}) \Bigg) \, \mathrm{d}s(\boldsymbol{x}) \\
- \int_{\partial B_r(\boldsymbol{y})\cup\partial D} \frac{1}{\varepsilon(\boldsymbol{x})} \Bigg(& \big(\boldsymbol{\nu}(\boldsymbol{x}) \times \mathbf{curl}_x \, \mathbb{G}^m(\boldsymbol{x},\boldsymbol{y})\big)^\top \boldsymbol{H}(\boldsymbol{x}) \\
& - \mathbb{G}^{m\top}(\boldsymbol{x},\boldsymbol{y}) (\boldsymbol{\nu} \times \mathbf{curl} \boldsymbol{H})(\boldsymbol{x}) \Bigg) \, \mathrm{d}s(\boldsymbol{x}) \\
=: I_{\partial B_R(0)} + I_{\partial B_r(\boldsymbol{y})} + I_{\partial D}.
\end{aligned}
$$

For the first integral $I_{\partial B_R(0)}$ on the right–hand side we get

$$
\begin{aligned}
& I_{\partial B_R(0)} \\
& = - \int_{\partial B_R(0)} \frac{1}{\varepsilon(\boldsymbol{x})} \Bigg(\big(\mathbf{curl}_x \, \mathbb{G}^m(\boldsymbol{x},\boldsymbol{y})\big)^\top \Big(\frac{\boldsymbol{x}}{R} \times \boldsymbol{H}(\boldsymbol{x}) + \frac{\mathrm{i}}{k(\boldsymbol{x})} \mathbf{curl} \boldsymbol{H}(\boldsymbol{x}) \Big) \\
& \quad - \Big(\frac{\boldsymbol{x}}{R} \times \mathbb{G}^m(\boldsymbol{x},\boldsymbol{y}) + \frac{\mathrm{i}}{k(\boldsymbol{x})} \mathbf{curl}_x \, \mathbb{G}^m(\boldsymbol{x},\boldsymbol{y}) \Big)^\top \mathbf{curl} \boldsymbol{H}(\boldsymbol{x}) \Bigg) \, \mathrm{d}s(\boldsymbol{x}).
\end{aligned}
$$

From (B.6) and the radiation conditions (3.12) and (B.2), we obtain that $I_{\partial B_R(0)}$ vanishes as $R \to \infty$.

Applying (3.13), we obtain that

$$
\begin{aligned}
I_{\partial B_r(\boldsymbol{y})} = \int_{\partial B_r(\boldsymbol{y})} \frac{1}{\varepsilon(\boldsymbol{x})} \Bigg(& \big(\mathbf{curl}_x \Pi^m(\boldsymbol{x},\boldsymbol{y})\big)^\top (\boldsymbol{\nu} \times \boldsymbol{H})(\boldsymbol{x}) \\
& + \Big(\Pi^m(\boldsymbol{x},\boldsymbol{y}) + \frac{1}{k(\boldsymbol{x})^2} \nabla_x \operatorname{div}_x \Pi^m(\boldsymbol{x},\boldsymbol{y}) \Big)^\top (\boldsymbol{\nu} \times \mathbf{curl} \boldsymbol{H})(\boldsymbol{x}) \Bigg) \, \mathrm{d}s(\boldsymbol{x}).
\end{aligned}
$$

Because $\Pi^m(\boldsymbol{x},\boldsymbol{y}) = \Phi_{k(\boldsymbol{x})}(\boldsymbol{x}-\boldsymbol{y}) \, \mathbb{I}_3 + \mathcal{O}(1)$ on $\partial B_r(\boldsymbol{y})$ as $r \to 0$, this yields

$$
\begin{aligned}
& \lim_{r\to 0} I_{\partial B_r(\boldsymbol{y})} \\
& = \frac{1}{\varepsilon(\boldsymbol{y})} \lim_{r\to 0} \Bigg(\int_{\partial B_r(\boldsymbol{y})} \big(\mathbf{curl}_x (\Phi_{k(\boldsymbol{x})}(\boldsymbol{x}-\boldsymbol{y}) \, \mathbb{I}_3)\big)^\top (\boldsymbol{\nu} \times \boldsymbol{H})(\boldsymbol{x}) \, \mathrm{d}s(\boldsymbol{x}) \\
& \qquad - \int_{\partial B_r(\boldsymbol{y})} \mathrm{i}\,\omega\varepsilon(\boldsymbol{x}) \Phi_{k(\boldsymbol{x})}(\boldsymbol{x}-\boldsymbol{y}) (\boldsymbol{\nu} \times \boldsymbol{E})(\boldsymbol{x}) \, \mathrm{d}s(\boldsymbol{x}) \\
& \quad + \int_{\partial B_r(\boldsymbol{y})} \frac{1}{\mathrm{i}\,\omega\mu(\boldsymbol{x})} \big(\nabla_x \operatorname{div}_x (\Phi_{k(\boldsymbol{x})}(\boldsymbol{x}-\boldsymbol{y}) \, \mathbb{I}_3)\big)^\top (\boldsymbol{\nu} \times \boldsymbol{E})(\boldsymbol{x}) \, \mathrm{d}s(\boldsymbol{x}) \Bigg).
\end{aligned}
$$

Using Stoke's theorem (cf. [38, p. 61]), we find that

$$\begin{aligned}0 &= \int_{\partial B_r(\boldsymbol{y})} \boldsymbol{\nu}(\boldsymbol{x}) \cdot \mathbf{curl}_x\big(\boldsymbol{E}(\boldsymbol{x}) \operatorname{div}_x(\Phi_{k(\boldsymbol{x})}(\boldsymbol{x}-\boldsymbol{y})\,\mathbb{I}_3)\big)\,\mathrm{d}s(\boldsymbol{y}) \\ &= \int_{\partial B_r(\boldsymbol{y})} \boldsymbol{\nu}(\boldsymbol{x}) \cdot \Big(\mathrm{i}\,\omega\mu(\boldsymbol{x})\boldsymbol{H}(\boldsymbol{x}) \operatorname{div}_x(\Phi_{k(\boldsymbol{x})}(\boldsymbol{x}-\boldsymbol{y})\,\mathbb{I}_3) \\ &\qquad\qquad - \boldsymbol{E}(\boldsymbol{x}) \times \nabla_x \operatorname{div}_x(\Phi_{k(\boldsymbol{x})}(\boldsymbol{x}-\boldsymbol{y})\,\mathbb{I}_3)\Big)\,\mathrm{d}s(\boldsymbol{y}).\end{aligned}$$

Thus,

$$\begin{aligned}&\lim_{r\to 0} \int_{\partial B_r(\boldsymbol{y})} \frac{1}{\mathrm{i}\,\omega\mu(\boldsymbol{x})}\big(\nabla_x \operatorname{div}_x(\Phi_{k(\boldsymbol{x})}(\boldsymbol{x}-\boldsymbol{y})\,\mathbb{I}_3)\big)^\top (\boldsymbol{\nu}\times\boldsymbol{E})(\boldsymbol{x})\,\mathrm{d}s(\boldsymbol{x}) \\ &\qquad = \lim_{r\to 0} \int_{\partial B_r(\boldsymbol{y})} (\boldsymbol{\nu}\cdot\boldsymbol{H})(\boldsymbol{x}) \operatorname{div}_x(\Phi_{k(\boldsymbol{x})}(\boldsymbol{x}-\boldsymbol{y})\,\mathbb{I}_3)\,\mathrm{d}s(\boldsymbol{x}).\end{aligned}$$

Then, because on $B_r(\boldsymbol{y})$ holds that $\Phi_{k(\boldsymbol{x})}(\boldsymbol{x}-\boldsymbol{y}) = \mathcal{O}(\frac{1}{r})$ and

$$\begin{aligned}\operatorname{div}_x(\Phi_{k(\boldsymbol{x})}(\boldsymbol{x}-\boldsymbol{y})\,\mathbb{I}_3) &= \frac{1}{4\pi r^2}\boldsymbol{\nu}(\boldsymbol{x})\cdot\mathbb{I}_3 + \mathcal{O}\Big(\frac{1}{r}\Big), \\ \mathbf{curl}_x(\Phi_{k(\boldsymbol{x})}(\boldsymbol{x}-\boldsymbol{y})\,\mathbb{I}_3) &= \frac{1}{4\pi r^2}\boldsymbol{\nu}(\boldsymbol{x})\times\mathbb{I}_3 + \mathcal{O}\Big(\frac{1}{r}\Big),\end{aligned}$$

we obtain

$$\begin{aligned}\lim_{r\to 0} I_{\partial B_r(\boldsymbol{y})} &= \frac{1}{\varepsilon(\boldsymbol{y})} \lim_{r\to 0} \frac{1}{4\pi r^2}\bigg(\int_{\partial B_r(\boldsymbol{y})} (\boldsymbol{\nu}(\boldsymbol{x})\times\mathbb{I}_3)^\top(\boldsymbol{\nu}\times\boldsymbol{H})(\boldsymbol{x})\,\mathrm{d}s(\boldsymbol{x}) \\ &\qquad + \int_{\partial B_r(\boldsymbol{y})} (\boldsymbol{\nu}\cdot\boldsymbol{H})(\boldsymbol{x})(\boldsymbol{\nu}(\boldsymbol{x})\cdot\mathbb{I}_3)\,\mathrm{d}s(\boldsymbol{x})\bigg) \\ &= \frac{1}{\varepsilon(\boldsymbol{y})} \lim_{r\to 0} \frac{1}{4\pi r^2} \int_{\partial B_r(\boldsymbol{y})} \boldsymbol{H}(\boldsymbol{x})\,\mathrm{d}s(\boldsymbol{x}) = \frac{1}{\varepsilon(\boldsymbol{y})}\boldsymbol{H}(\boldsymbol{y}).\end{aligned}$$

This yields the desired result. □

B.2 Reciprocity Relations

In this section, we prove reciprocity relations for the electric and magnetic dyadic Green's functions $\mathbb{G}^e$ and $\mathbb{G}^m$ defined in Section 3.2. We mention that these formulas have been previously stated without proof by Chew [35, p. 411], in [43], and by Iakovleva et al. [62].

Lemma B.3. *Let $\boldsymbol{x}, \boldsymbol{y} \in \mathbb{R}^3_0$ with $\boldsymbol{x} \neq \boldsymbol{y}$. Then,*

$$\mu(\boldsymbol{y})\,\mathbb{G}^e(\boldsymbol{x},\boldsymbol{y}) = \mu(\boldsymbol{x})\,\mathbb{G}^{e\top}(\boldsymbol{y},\boldsymbol{x}), \tag{B.7a}$$

$$\varepsilon(\boldsymbol{y})\,\mathbb{G}^m(\boldsymbol{x},\boldsymbol{y}) = \varepsilon(\boldsymbol{x})\,\mathbb{G}^{m\top}(\boldsymbol{y},\boldsymbol{x}). \tag{B.7b}$$

Remark B.4. Throughout, we denote by $\mathbf{curl}_x\,\mathbb{G}^{e/m}$ the curl of $\mathbb{G}^{e/m}$ with respect to the first variable and by $\mathbf{curl}_y\,\mathbb{G}^{e/m}$ the curl of $\mathbb{G}^{e/m}$ with respect to the second variable.

Proof of Lemma B.3. Let $\boldsymbol{x}, \boldsymbol{y} \in \mathbb{R}^3_0$ with $\boldsymbol{x} \neq \boldsymbol{y}$ and choose $R > 0$ large enough so that $B_R(0)$ contains $\boldsymbol{x}$ and $\boldsymbol{y}$. Moreover, let $r > 0$ be small enough such that $B_r(\boldsymbol{x})$ and $B_r(\boldsymbol{y})$ are disjoint subsets of $B_R(0)$, which do not intersect the interface Σ_0. From (3.9) and an integration by parts (3.1), we obtain

$$\begin{aligned}
0 &= \int_{B_R(0)\setminus\overline{B_r(\boldsymbol{x})\cup B_r(\boldsymbol{y})}} \Big(\mathbf{curl}_x \frac{1}{\mu(\boldsymbol{z})} \mathbf{curl}_x\, \mathbb{G}^e(\boldsymbol{z},\boldsymbol{x}) \\
&\qquad\qquad - \omega^2 \varepsilon(\boldsymbol{z})\, \mathbb{G}^e(\boldsymbol{z},\boldsymbol{x})\Big)^\top \mathbb{G}^e(\boldsymbol{z},\boldsymbol{y})\, \mathrm{d}\boldsymbol{z} \\
&= \int_{B_R(0)\setminus\overline{B_r(\boldsymbol{x})\cup B_r(\boldsymbol{y})}} \Big(\frac{1}{\mu(\boldsymbol{z})} (\mathbf{curl}_x\, \mathbb{G}^e)^\top(\boldsymbol{z},\boldsymbol{x}) \mathbf{curl}_x\, \mathbb{G}^e(\boldsymbol{z},\boldsymbol{y}) \\
&\qquad\qquad - \omega^2 \varepsilon(\boldsymbol{z})\, \mathbb{G}^{e\top}(\boldsymbol{z},\boldsymbol{x})\, \mathbb{G}^e(\boldsymbol{z},\boldsymbol{y})\Big)\, \mathrm{d}\boldsymbol{z} \\
&\quad + \int_{\partial B_R(0)} \frac{1}{\mu(\boldsymbol{z})} \big(\boldsymbol{\nu}(\boldsymbol{z}) \times \mathbf{curl}_x\, \mathbb{G}^e(\boldsymbol{z},\boldsymbol{x})\big)^\top \mathbb{G}^e(\boldsymbol{z},\boldsymbol{y})\, \mathrm{d}s(\boldsymbol{z}) \\
&\quad - \int_{\partial(B_r(\boldsymbol{x})\cup B_r(\boldsymbol{y}))} \frac{1}{\mu(\boldsymbol{z})} \big(\boldsymbol{\nu}(\boldsymbol{z}) \times \mathbf{curl}_x\, \mathbb{G}^e(\boldsymbol{z},\boldsymbol{x})\big)^\top \mathbb{G}^e(\boldsymbol{z},\boldsymbol{y})\, \mathrm{d}s(\boldsymbol{z}).
\end{aligned}$$

Another integration by parts and applying (3.9) yields

$$\begin{aligned}
0 &= \int_{\partial B_R(0)} \frac{1}{\mu(\boldsymbol{z})} \Big(\big(\boldsymbol{\nu}(\boldsymbol{z}) \times \mathbf{curl}_x\, \mathbb{G}^e(\boldsymbol{z},\boldsymbol{x})\big)^\top \mathbb{G}^e(\boldsymbol{z},\boldsymbol{y}) \\
&\qquad\qquad + \big(\boldsymbol{\nu}(\boldsymbol{z}) \times \mathbb{G}^e(\boldsymbol{z},\boldsymbol{x})\big)^\top \mathbf{curl}_x\, \mathbb{G}^e(\boldsymbol{z},\boldsymbol{y})\Big)\, \mathrm{d}s(\boldsymbol{z}) \\
&\quad - \int_{\partial(B_r(\boldsymbol{x})\cup B_r(\boldsymbol{y}))} \frac{1}{\mu(\boldsymbol{z})} \Big(\big(\boldsymbol{\nu}(\boldsymbol{z}) \times \mathbf{curl}_x\, \mathbb{G}^e(\boldsymbol{z},\boldsymbol{x})\big)^\top \mathbb{G}^e(\boldsymbol{z},\boldsymbol{y}) \\
&\qquad\qquad + \big(\boldsymbol{\nu}(\boldsymbol{z}) \times \mathbb{G}^e(\boldsymbol{z},\boldsymbol{x})\big)^\top \mathbf{curl}_x\, \mathbb{G}^e(\boldsymbol{z},\boldsymbol{y})\Big)\, \mathrm{d}s(\boldsymbol{z}).
\end{aligned}$$

From the radiation condition (3.10), we find as in the proof of Theorem B.1 that the integral over $\partial B_R(0)$ vanishes as $R \to \infty$. Therefore,

$$\begin{aligned}
&\int_{\partial B_r(\boldsymbol{x})} \frac{1}{\mu(\boldsymbol{z})} \Big(\big(\boldsymbol{\nu}(\boldsymbol{z}) \times \mathbf{curl}_x\, \mathbb{G}^e(\boldsymbol{z},\boldsymbol{x})\big)^\top \mathbb{G}^e(\boldsymbol{z},\boldsymbol{y}) \\
&\qquad\qquad + \big(\boldsymbol{\nu}(\boldsymbol{z}) \times \mathbb{G}^e(\boldsymbol{z},\boldsymbol{x})\big)^\top \mathbf{curl}_x\, \mathbb{G}^e(\boldsymbol{z},\boldsymbol{y})\Big)\, \mathrm{d}s(\boldsymbol{z}) \\
&= -\int_{\partial B_r(\boldsymbol{y})} \frac{1}{\mu(\boldsymbol{z})} \Big(\big(\boldsymbol{\nu}(\boldsymbol{z}) \times \mathbf{curl}_x\, \mathbb{G}^e(\boldsymbol{z},\boldsymbol{x})\big)^\top \mathbb{G}^e(\boldsymbol{z},\boldsymbol{y}) \\
&\qquad\qquad + \big(\boldsymbol{\nu}(\boldsymbol{z}) \times \mathbb{G}^e(\boldsymbol{z},\boldsymbol{x})\big)^\top \mathbf{curl}_x\, \mathbb{G}^e(\boldsymbol{z},\boldsymbol{y})\Big)\, \mathrm{d}s(\boldsymbol{z}),
\end{aligned}$$

and so,

$$\begin{aligned}
&\frac{1}{\mu(\boldsymbol{y})}\Big(\int_{\partial B_r(\boldsymbol{x})}\frac{\mu(\boldsymbol{y})}{\mu(\boldsymbol{z})}\Big(\,\mathbb{G}^{e\top}(\boldsymbol{z},\boldsymbol{y})\big(\boldsymbol{\nu}(\boldsymbol{z})\times\mathbf{curl}_x\,\mathbb{G}^e(\boldsymbol{z},\boldsymbol{x})\big)\\
&\qquad\qquad+(\mathbf{curl}_x\,\mathbb{G}^e)^\top(\boldsymbol{z},\boldsymbol{y})\big(\boldsymbol{\nu}(\boldsymbol{z})\times\,\mathbb{G}^e(\boldsymbol{z},\boldsymbol{x})\big)\Big)\,\mathrm{d}s(\boldsymbol{z})\Big)^\top\\
&=\frac{1}{\mu(\boldsymbol{x})}\int_{\partial B_r(\boldsymbol{y})}\frac{\mu(\boldsymbol{x})}{\mu(\boldsymbol{z})}\Big(\,\mathbb{G}^{e\top}(\boldsymbol{z},\boldsymbol{x})\big(\boldsymbol{\nu}(\boldsymbol{z})\times\mathbf{curl}_x\,\mathbb{G}^e(\boldsymbol{z},\boldsymbol{y})\big)\\
&\qquad\qquad+(\mathbf{curl}_x\,\mathbb{G}^e)^\top(\boldsymbol{z},\boldsymbol{x})\big(\boldsymbol{\nu}(\boldsymbol{z})\times\,\mathbb{G}^e(\boldsymbol{z},\boldsymbol{y})\big)\Big)\,\mathrm{d}s(\boldsymbol{z}).
\end{aligned}$$

Now, (B.7a) follows from the representation formula (B.5).

Formula (B.7b) can be proven in the same way. □

Lemma B.5. *Let $\boldsymbol{x},\boldsymbol{y}\in\mathbb{R}^3_0$ with $\boldsymbol{x}\neq\boldsymbol{y}$. Then,*

$$k^2(\boldsymbol{y})\mathbf{curl}_x\,\mathbb{G}^e(\boldsymbol{x},\boldsymbol{y})=k^2(\boldsymbol{x})(\mathbf{curl}_x\,\mathbb{G}^m)^\top(\boldsymbol{y},\boldsymbol{x}).\tag{B.8}$$

Proof. Let $\boldsymbol{x},\boldsymbol{y}\in\mathbb{R}^3_0$ with $\boldsymbol{x}\neq\boldsymbol{y}$ and choose $R>0$ large enough so that $B_R(0)$ contains $\boldsymbol{x}$ and $\boldsymbol{y}$. Moreover, let $r>0$ be small enough such that $B_r(\boldsymbol{x})$ and $B_r(\boldsymbol{y})$ are disjoint subsets of $B_R(0)$, which do not intersect the interface Σ_0. As in the proof of Lemma B.3, applying two times integration by parts, we obtain that

$$\begin{aligned}
0&=\int_{B_R(0)\setminus\overline{B_r(\boldsymbol{x})\cup B_r(\boldsymbol{y})}}\Big(\mathbf{curl}_x\frac{1}{\mu(\boldsymbol{z})}\mathbf{curl}_x\,\mathbb{G}^e(\boldsymbol{z},\boldsymbol{x})\\
&\qquad\qquad-\omega^2\varepsilon(\boldsymbol{z})\,\mathbb{G}^e(\boldsymbol{z},\boldsymbol{x})\Big)^\top\frac{1}{\omega^2\varepsilon(\boldsymbol{z})}\mathbf{curl}_x\,\mathbb{G}^m(\boldsymbol{z},\boldsymbol{y})\,\mathrm{d}\boldsymbol{z}\\
&=-\int_{\partial(B_r(\boldsymbol{x})\cup B_r(\boldsymbol{y}))}\frac{1}{k(\boldsymbol{z})^2}\Big(\big(\boldsymbol{\nu}(\boldsymbol{z})\times\mathbf{curl}_x\,\mathbb{G}^e(\boldsymbol{z},\boldsymbol{x})\big)^\top\mathbf{curl}_x\,\mathbb{G}^m(\boldsymbol{z},\boldsymbol{y})\\
&\qquad\qquad-\,\mathbb{G}^{e\top}(\boldsymbol{z},\boldsymbol{x})\big(k(\boldsymbol{z})^2\boldsymbol{\nu}(\boldsymbol{z})\times\,\mathbb{G}^m(\boldsymbol{z},\boldsymbol{y})\big)\Big)\,\mathrm{d}s(\boldsymbol{z})\\
&=-\frac{1}{k(\boldsymbol{x})^2}\int_{\partial B_r(\boldsymbol{x})}\Big(\,\mathbb{G}^{m\top}(\boldsymbol{z},\boldsymbol{y})\big(\boldsymbol{\nu}(\boldsymbol{z})\times(k(\boldsymbol{z})^2\,\mathbb{G}^e(\boldsymbol{z},\boldsymbol{x}))\big)\\
&\qquad\qquad+(\mathbf{curl}_x\,\mathbb{G}^m)^\top(\boldsymbol{z},\boldsymbol{y})\big(\boldsymbol{\nu}(\boldsymbol{z})\times\mathbf{curl}_x\,\mathbb{G}^e(\boldsymbol{z},\boldsymbol{x})\big)\Big)^\top\,\mathrm{d}s(\boldsymbol{z})\\
&\quad+\frac{1}{k(\boldsymbol{y})^2}\int_{\partial B_r(\boldsymbol{y})}\Big(\,\mathbb{G}^{e\top}(\boldsymbol{z},\boldsymbol{x})\big(\boldsymbol{\nu}(\boldsymbol{z})\times(k(\boldsymbol{z})^2\,\mathbb{G}^m(\boldsymbol{z},\boldsymbol{y}))\big)\\
&\qquad\qquad+(\mathbf{curl}_x\,\mathbb{G}^e)^\top(\boldsymbol{z},\boldsymbol{x})\big(\boldsymbol{\nu}(\boldsymbol{z})\times\mathbf{curl}_x\,\mathbb{G}^m(\boldsymbol{z},\boldsymbol{y})\big)\Big)\,\mathrm{d}s(\boldsymbol{z}).
\end{aligned}$$

Applying (3.9), (3.11), (B.3), and (B.5) we obtain (B.8). □

Remark B.6. We assumed in Section 3.2.2 that the electric and magnetic dyadic Green's functions $\mathbb{G}^e$ and $\mathbb{G}^m$ satisfy the radiation conditions (3.10) and (3.12), respectively. From the representation formulas (B.3) and (B.5) and from Lemma B.3 we can deduce that the radiation condition (B.2) implies (B.4) and vice versa. Moreover, recalling the beginning of the proof of Theorem B.1, we obtain that radiating solutions of Maxwell's equations in two–layered background media as introduced in Section 3.2.2 automatically satisfy the finiteness conditions

$$\int_{\partial B_R} |\boldsymbol{H}|^2 \, \mathrm{d}s = \mathcal{O}(1) \qquad \text{and} \qquad \int_{\partial B_R} |\boldsymbol{E}|^2 \, \mathrm{d}s = \mathcal{O}(1); \tag{B.9}$$

see also Colton and Kress [39, p. 162] for a similar result for homogeneous background media.

B.3 Singularities of the Dyadic Green's Functions

We study the nature of the singularities of the electric and magnetic dyadic Green's function $\mathbb{G}^{e/m}(\cdot, \boldsymbol{y})$ (cf. Section 3.2) and of $\mathbf{curl}_x \, \mathbb{G}^{e/m}(\cdot, \boldsymbol{y})$ in a point $\boldsymbol{y} \in \mathbb{R}^3_-$ with $\operatorname{dist}(\boldsymbol{y}, \Sigma_0) > d_0$ for some constant $d_0 > 0$. Because the matrix valued function $\mathbb{G}^{e/m}(\cdot, \boldsymbol{y})$ differs from the dyadic Green's function $\mathbb{G}(\cdot, \boldsymbol{y})$ for homogeneous background medium with constant wavenumber k_- in a neighborhood of $\boldsymbol{y}$ only by a smooth matrix valued function (cf. Section 3.2.2), it is sufficient to consider the singularities of $\mathbb{G}(\cdot, \boldsymbol{y})$ and $\mathbf{curl}_x \, \mathbb{G}(\cdot, \boldsymbol{y})$ in $\boldsymbol{y}$. Moreover, recalling (3.6) and (3.7), we find that we can analyze without loss of generality the singularities of $\mathbb{G}(\cdot, 0)$ and $\mathbf{curl}_x \, \mathbb{G}(\cdot, 0)$ in 0.

From (3.46), we see that

$$\begin{aligned} \mathbf{curl}_x \, \mathbb{G}(\boldsymbol{x}, 0) &= \nabla_x \Phi_{k_-}(\boldsymbol{x}) \times \mathbb{I}_3 \\ &= \Big(\mathrm{i}\, k_- - \frac{1}{|\boldsymbol{x}|} \Big) \Phi_{k_-}(\boldsymbol{x}) \frac{1}{|\boldsymbol{x}|} \begin{pmatrix} 0 & -x_3 & x_2 \\ x_3 & 0 & -x_1 \\ -x_2 & x_1 & 0 \end{pmatrix}, \end{aligned} \tag{B.10}$$

$\boldsymbol{x} \neq 0$, has a singularity of order 2 in $\boldsymbol{x} = 0$. Furthermore, because for $1 \leq j, l \leq 3$,

$$\begin{aligned} &\big(\nabla_x \operatorname{div}_x (\Phi_{k_-} \, \mathbb{I}_3) \big)_{jl}(\boldsymbol{x}) \\ &\qquad = -k_-^2 \Phi_{k_-}(\boldsymbol{x}) \frac{x_j x_l}{|\boldsymbol{x}|^2} + \frac{1}{|\boldsymbol{x}|} \Big(\mathrm{i}\, k_- - \frac{1}{|\boldsymbol{x}|} \Big) \Phi_{k_-}(\boldsymbol{x}) \Big(\delta_{jl} - \frac{3 x_j x_l}{|\boldsymbol{x}|^2} \Big), \end{aligned}$$

$\boldsymbol{x} \neq 0$, where δ_{jl} denotes the Kronecker–delta, we find that $\mathbb{G}(\boldsymbol{x}, 0)$ has a singularity of order 3 in $\boldsymbol{x} = 0$. Recalling (3.7), the corresponding term of

order -3 is given by

$$\frac{1}{k_-^2}\frac{1}{|\boldsymbol{x}|^2}\Phi_{k_-}(\boldsymbol{x})\frac{1}{|\boldsymbol{x}|^2}\begin{pmatrix} |\boldsymbol{x}|^2-3x_1^2 & -3x_1x_2 & -3x_1x_3 \\ -3x_1x_2 & |\boldsymbol{x}|^2-3x_2^2 & -3x_2x_3 \\ -3x_1x_3 & -3x_2x_3 & |\boldsymbol{x}|^2-3x_3^2 \end{pmatrix}. \tag{B.11}$$

Appendix C

Uniqueness Theorems

In this chapter, we comment on uniqueness of solutions to the *exterior Maxwell problem* and to the *Maxwell transmission problem* in two–layered background media as introduced in Section 3.4, which are given as follows.

Assume that the bounded set $D \subset \mathbb{R}^3_-$ is the open complement of an unbounded domain of class $C^{2,\alpha}$, $0 < \alpha < 1$, such that D is compactly contained in $\mathbb{R}^3_-$ and denote by $\boldsymbol{\nu}$ the unit outward normal to ∂D relative to D.

Exterior Maxwell problem:
Find $\boldsymbol{E}, \boldsymbol{H} \in \boldsymbol{H}_{\rm loc}(\mathbf{curl}, \mathbb{R}^3 \setminus \overline{D})$ satisfying Maxwell's equations (3.32) in $\mathbb{R}^3 \setminus \overline{D}$, the Silver-Müller radiation condition (3.33), and the boundary condition

$$\boldsymbol{\nu} \times \boldsymbol{E} = \boldsymbol{\psi} \qquad \text{on } \partial D,$$

where $\boldsymbol{\psi} \in \boldsymbol{H}^{-1/2}_{\rm div}(\partial D)$ is a given tangential vector field.

Maxwell transmission problem:
Find $\boldsymbol{E}$ and $\boldsymbol{H}$ with $\boldsymbol{E}|_D, \boldsymbol{H}|_D \in \boldsymbol{H}(\mathbf{curl}, D)$ and $\boldsymbol{E}|_{\mathbb{R}^3\setminus\overline{D}}, \boldsymbol{H}|_{\mathbb{R}^3\setminus\overline{D}} \in \boldsymbol{H}_{\rm loc}(\mathbf{curl}, \mathbb{R}^3 \setminus \overline{D})$ satisfying Maxwell's equations (3.32) in $\mathbb{R}^3 \setminus \partial D$, the Silver-Müller radiation condition (3.33), and the transmission conditions

$$[(\boldsymbol{\nu} \times \boldsymbol{H}) \times \boldsymbol{\nu}]_{\partial D} = \boldsymbol{\chi}, \qquad [\boldsymbol{\nu} \times \boldsymbol{E}]_{\partial D} = \boldsymbol{\phi} \qquad \text{on } \partial D,$$

where $\boldsymbol{\chi} \in \boldsymbol{H}^{-1/2}_{\rm curl}(\partial D)$ and $\boldsymbol{\phi} \in \boldsymbol{H}^{-1/2}_{\rm div}(\partial D)$ are given tangential vector fields.

In order to prove uniqueness of solutions to these problems we have to distinguish two cases: If the electric permeability ε_- is real, i.e., the medium in the lower halfspace is nondissipative, uniqueness of solutions of the exterior Maxwell problem and the Maxwell transmission problem has been shown by Cutzach and Hazard [43] and by Kirsch [75], respectively.

For $\operatorname{Im}\varepsilon_- > 0$, we will prove uniqueness of solutions of these problems by similar arguments as used by Petry [92, pp. 61–63] for a uniqueness result for transmission problems in a multiply layered background medium under more restrictive assumptions. We mention that a similar uniqueness proof for the exterior Maxwell problem (with a slightly different decay condition for the lower halfspace) has recently been given by Delbary et al. [46].

Proposition C.1. *Let* $\operatorname{Im}\varepsilon_- = 0$*. Then, the exterior Maxwell problem and the Maxwell transmission problem have at most one solution.*

Proof. Uniqueness of solutions to the exterior Maxwell problem in nondissipative media has been shown in [43, Proposition 2.5]. For the Maxwell transmission problem this has been proven in [75, Theorem 3.4]. □

Proposition C.2. *Let* $\operatorname{Im}\varepsilon_- > 0$*. Then, the exterior Maxwell problem has at most one solution.*

For the proof of this proposition we need the following two technical lemmas.

Lemma C.3. *Suppose* $\operatorname{Im}\varepsilon_- > 0$ *and let* $(\boldsymbol{E}, \boldsymbol{H})$ *be a solution of the exterior Maxwell problem with* $\boldsymbol{\psi} = 0$*. Then, for any* $R > 0$ *such that* $\overline{D} \subset B_R(0)$*,*

$$\omega \int_{B_R(0)\cap\mathbb{R}^3_+} (\mu_+|\boldsymbol{H}|^2 - \overline{\varepsilon_+}|\boldsymbol{E}|^2)\,\mathrm{d}\boldsymbol{x} = \mathrm{i}\int_{\partial(B_R(0)\cap\mathbb{R}^3_+)} \boldsymbol{\nu}\times\overline{\boldsymbol{H}}\cdot\boldsymbol{E}\,\mathrm{d}s,$$

$$\omega \int_{(B_R(0)\cap\mathbb{R}^3_-)\setminus\overline{D}} (\mu_-|\boldsymbol{H}|^2 - \overline{\varepsilon_-}|\boldsymbol{E}|^2)\,\mathrm{d}\boldsymbol{x} = \mathrm{i}\int_{\partial(B_R(0)\cap\mathbb{R}^3_-)} \boldsymbol{\nu}\times\overline{\boldsymbol{H}}\cdot\boldsymbol{E}\,\mathrm{d}s.$$

Proof. Using

$$\operatorname{div}(\overline{\boldsymbol{H}}\times\boldsymbol{E}) = \mathbf{curl}\overline{\boldsymbol{H}}\cdot\boldsymbol{E} - \overline{\boldsymbol{H}}\cdot\mathbf{curl}\boldsymbol{E} = \mathrm{i}\,\omega\overline{\varepsilon}|\boldsymbol{E}|^2 - \mathrm{i}\,\omega\mu|\boldsymbol{H}|^2,$$

we find that

$$\mathrm{i}\operatorname{div}(\overline{\boldsymbol{H}}\times\boldsymbol{E}) = \omega\mu|\boldsymbol{H}|^2 - \omega\overline{\varepsilon}|\boldsymbol{E}|^2.$$

Let $R > 0$ such that $\overline{D} \subset B_R(0)$. Then, applying the Divergence Theorem (cf. Monk [88, Theorem 3.24]), we obtain

$$\begin{aligned}\omega \int_{B_R(0)\cap\mathbb{R}^3_+} (\mu_+|\boldsymbol{H}|^2 - \overline{\varepsilon_+}|\boldsymbol{E}|^2)\,\mathrm{d}\boldsymbol{x} &= \mathrm{i}\int_{B_R(0)\cap\mathbb{R}^3_+} \operatorname{div}(\overline{\boldsymbol{H}}\times\boldsymbol{E})\,\mathrm{d}\boldsymbol{x}\\ &= \mathrm{i}\int_{\partial(B_R(0)\cap\mathbb{R}^3_+)} \boldsymbol{\nu}\cdot\overline{\boldsymbol{H}}\times\boldsymbol{E}\,\mathrm{d}s = \mathrm{i}\int_{\partial(B_R(0)\cap\mathbb{R}^3_+)} \boldsymbol{\nu}\times\overline{\boldsymbol{H}}\cdot\boldsymbol{E}\,\mathrm{d}s.\end{aligned}$$

Recalling that $\boldsymbol{\nu}\times\boldsymbol{E}|_{\partial D} = 0$, the second equation follows analogously. □

Lemma C.4. *Suppose* $\operatorname{Im}\varepsilon_- > 0$ *and let* $(\boldsymbol{E}, \boldsymbol{H})$ *be a solution of the exterior Maxwell problem with* $\boldsymbol{\psi} = 0$*. Then,*

$$\operatorname{Re}\int_{\partial B_R(0)} \boldsymbol{\nu}\times\overline{\boldsymbol{H}}\cdot\boldsymbol{E}\,\mathrm{d}s = o(1) \qquad \text{as } R\to\infty.$$

Proof. From Lemma C.3 and the continuity of the tangential components of $\boldsymbol{E}$ and $\boldsymbol{H}$ across Σ_0, we find that

$$\mathrm{i}\int_{\partial B_R(0)} \boldsymbol{\nu}\times\overline{\boldsymbol{H}}\cdot\boldsymbol{E}\,\mathrm{d}s = \omega\int_{B_R(0)\cap\mathbb{R}^3_+}(\mu_+|\boldsymbol{H}|^2-\overline{\varepsilon_+}|\boldsymbol{E}|^2)\,\mathrm{d}\boldsymbol{x} + \omega\int_{(B_R(0)\cap\mathbb{R}^3_-)\setminus\overline{D}}(\mu_-|\boldsymbol{H}|^2-\overline{\varepsilon_-}|\boldsymbol{E}|^2)\,\mathrm{d}\boldsymbol{x}.$$

Because $\operatorname{Im}\varepsilon_+ = 0$, taking the imaginary part yields

$$\operatorname{Re}\int_{\partial B_R(0)} \boldsymbol{\nu}\times\overline{\boldsymbol{H}}\cdot\boldsymbol{E}\,\mathrm{d}s = \omega\operatorname{Im}\varepsilon_-\int_{(B_R(0)\cap\mathbb{R}^3_-)\setminus\overline{D}}|\boldsymbol{E}|^2\,\mathrm{d}\boldsymbol{x}. \tag{C.1}$$

So,

$$\liminf_{R\to\infty}\Big(\operatorname{Re}\int_{\partial B_R(0)}\boldsymbol{\nu}\times\overline{\boldsymbol{H}}\cdot\boldsymbol{E}\,\mathrm{d}s\Big)\geq 0. \tag{C.2}$$

The radiation condition (3.33) and the decay condition (B.9) give

$$\int_{\partial B_R(0)}\Big|\boldsymbol{\nu}\times\overline{\boldsymbol{H}}\cdot\boldsymbol{E}+\Big(\frac{\varepsilon}{\mu}\Big)^{1/2}\overline{\boldsymbol{E}}\cdot\boldsymbol{E}\Big|\,\mathrm{d}s = o(1)\qquad\text{as } R\to\infty.$$

Thus,

$$\int_{\partial B_R(0)}\boldsymbol{\nu}\times\overline{\boldsymbol{H}}\cdot\boldsymbol{E}\,\mathrm{d}s+\int_{\partial B_R(0)}\Big(\frac{\varepsilon}{\mu}\Big)^{1/2}|\boldsymbol{E}|^2\,\mathrm{d}s = o(1)\qquad\text{as } R\to\infty,$$

and therefore

$$\limsup_{R\to\infty}\Big(\operatorname{Re}\int_{\partial B_R(0)}\boldsymbol{\nu}\times\overline{\boldsymbol{H}}\cdot\boldsymbol{E}\,\mathrm{d}s\Big)\leq 0. \tag{C.3}$$

The statement now follows from (C.2) and (C.3). □

Proof of Proposition C.2. From Lemma C.4 and (C.1), we obtain that

$$0 = \lim_{R\to\infty}\Big(\omega\operatorname{Im}\varepsilon_-\int_{(B_R(0)\cap\mathbb{R}^3_-)\setminus\overline{D}}|\boldsymbol{E}|^2\,\mathrm{d}\boldsymbol{x}\Big).$$

Therefore, $\boldsymbol{E}=\boldsymbol{H}=0$ in $\mathbb{R}^3_-\setminus\overline{D}$. In particular, $\boldsymbol{E}$ and $\boldsymbol{H}$ have vanishing tangential components on Σ_0. As they are continuous across Σ_0, it now follows from Holmgren's theorem (cf. [80, Theorem 2.4, p. 179]) that $(\boldsymbol{E},\boldsymbol{H})$ is zero in a neighborhood of Σ_0 in $\mathbb{R}^3_+$, because it is a solution of the homogeneous Maxwell system with constant coefficients ε_+ and μ_+. Accordingly, $\boldsymbol{E}=\boldsymbol{H}=0$ in $\mathbb{R}^3_+$ because of its analyticity. □

Proposition C.5. *Let* $\operatorname{Im}\varepsilon_->0$. *Then, the Maxwell transmission problem has at most one solution.*

Again, we need two technical lemmas for the proof of this result.

Lemma C.6. *Suppose* $\operatorname{Im}\varepsilon_- > 0$ *and let* $(\boldsymbol{E},\boldsymbol{H})$ *be a solution of the Maxwell transmission problem with* $\boldsymbol{\chi} = \boldsymbol{\phi} = 0$. *Then, for any* $R > 0$ *such that* $\overline{D} \subset B_R(0)$,

$$\begin{aligned}
\omega \int_D (\mu_- |\boldsymbol{H}|^2 - \overline{\varepsilon_-}|\boldsymbol{E}|^2)\, \mathrm{d}\boldsymbol{x} &= \mathrm{i} \int_{\partial D} \boldsymbol{\nu} \times \overline{\boldsymbol{H}} \cdot \boldsymbol{E}\, \mathrm{d}s, \\
\omega \int_{B_R(0)\cap\mathbb{R}^3_+} (\mu_+ |\boldsymbol{H}|^2 - \overline{\varepsilon_+}|\boldsymbol{E}|^2)\, \mathrm{d}\boldsymbol{x} &= \mathrm{i} \int_{\partial(B_R(0)\cap\mathbb{R}^3_+)} \boldsymbol{\nu} \times \overline{\boldsymbol{H}} \cdot \boldsymbol{E}\, \mathrm{d}s, \\
\omega \int_{(B_R(0)\cap\mathbb{R}^3_-)\setminus\overline{D}} (\mu_- |\boldsymbol{H}|^2 - \overline{\varepsilon_-}|\boldsymbol{E}|^2)\, \mathrm{d}\boldsymbol{x} &= \mathrm{i} \int_{\partial(B_R(0)\cap\mathbb{R}^3_-)} \boldsymbol{\nu} \times \overline{\boldsymbol{H}} \cdot \boldsymbol{E}\, \mathrm{d}s \\
&\quad - \mathrm{i} \int_{\partial D} \boldsymbol{\nu} \times \overline{\boldsymbol{H}} \cdot \boldsymbol{E}\, \mathrm{d}s.
\end{aligned}$$

Proof. These formulas can be proven in the same manner as the formulas in Lemma C.3. □

Lemma C.7. *Suppose* $\operatorname{Im}\varepsilon_- > 0$ *and let* $(\boldsymbol{E},\boldsymbol{H})$ *be a solution of the Maxwell transmission problem with* $\boldsymbol{\chi} = \boldsymbol{\phi} = 0$. *Then,*

$$\operatorname{Re} \int_{\partial B_R(0)} \boldsymbol{\nu} \times \overline{\boldsymbol{H}} \cdot \boldsymbol{E}\, \mathrm{d}s = o(1) \qquad \text{as } R \to \infty.$$

Proof. From Lemma C.6 and the continuity of the tangential components of $\boldsymbol{E}$ and $\boldsymbol{H}$ across ∂D and Σ_0, we find that

$$\begin{aligned}
\mathrm{i} \int_{\partial B_R(0)} \boldsymbol{\nu} \times \overline{\boldsymbol{H}} \cdot \boldsymbol{E}\, \mathrm{d}s &= \omega \int_{B_R(0)\cap\mathbb{R}^3_+} (\mu_+ |\boldsymbol{H}|^2 - \overline{\varepsilon_+}|\boldsymbol{E}|^2)\, \mathrm{d}\boldsymbol{x} \\
&\quad + \omega \int_{B_R(0)\cap\mathbb{R}^3_-} (\mu_- |\boldsymbol{H}|^2 - \overline{\varepsilon_-}|\boldsymbol{E}|^2)\, \mathrm{d}\boldsymbol{x}.
\end{aligned}$$

Because $\operatorname{Im}\varepsilon_+ = 0$, taking the imaginary part yields

$$\operatorname{Re} \int_{\partial B_R(0)} \boldsymbol{\nu} \times \overline{\boldsymbol{H}} \cdot \boldsymbol{E}\, \mathrm{d}s = \omega \operatorname{Im}\varepsilon_- \int_{B_R(0)\cap\mathbb{R}^3_-} |\boldsymbol{E}|^2\, \mathrm{d}\boldsymbol{x}. \tag{C.4}$$

So,

$$\liminf_{R\to\infty} \Big(\operatorname{Re} \int_{\partial B_R(0)} \boldsymbol{\nu} \times \overline{\boldsymbol{H}} \cdot \boldsymbol{E}\, \mathrm{d}s \Big) \geq 0.$$

From the radiation condition (3.33) and the decay condition (B.9) we find as in the proof of Lemma C.4 that

$$\limsup_{R\to\infty} \Big(\operatorname{Re} \int_{\partial B_R(0)} \boldsymbol{\nu} \times \overline{\boldsymbol{H}} \cdot \boldsymbol{E}\, \mathrm{d}s \Big) \leq 0.$$

This yields the assertion. □

Proof of Proposition C.5. From Lemma C.7 and (C.4), we obtain that

$$0 = \lim_{R\to\infty}\Big(\omega \operatorname{Im}\varepsilon_- \int_{B_R(0)\cap\mathbb{R}^3_-} |\boldsymbol{E}|^2 \,\mathrm{d}\boldsymbol{x}\Big).$$

Therefore, $\boldsymbol{E} = \boldsymbol{H} = 0$ in $\mathbb{R}^3_-$ and as in the proof of Proposition C.2 we find from Holmgren's theorem that $\boldsymbol{E} = \boldsymbol{H} = 0$ in $\mathbb{R}^3_+$. □

Bibliography

[1] S. Agmon, *Lectures on Elliptic Boundary Value Problems*, Van Nostrand Mathematical Studies, vol. 2, D. Van Nostrand, Princeton, N.J.–Toronto–London, 1965.

[2] G. Alessandrini, *Examples of instability in inverse boundary–value problems*, Inverse Problems **13** (1997), no. 4, 887–897.

[3] H. Ammari, R. Griesmaier, and M. Hanke, *Identification of small inhomogeneities: asymptotic factorization*, Math. Comput. **76** (2007), no. 259, 1425–1448.

[4] H. Ammari, E. Iakovleva, D. Lesselier, and G. Perrusson, *MUSIC–type electromagnetic imaging of a collection of small three–dimensional bounded inclusions*, SIAM J. Sci. Comput. **29** (2007), no. 2, 674–709.

[5] H. Ammari and H. Kang, *High–order terms in the asymptotic expansions of the steady–state voltage potentials in the presence of conductivity inhomogeneities of small diameter*, SIAM J. Math. Anal. **34** (2003), no. 5, 1152–1166.

[6] ———, *Properties of the generalized polarization tensors*, Multiscale Model. Simul. **1** (2003), no. 2, 335–348.

[7] ———, *Reconstruction of Small Inhomogeneities from Boundary Measurements*, Lecture Notes in Math., vol. 1846, Springer–Verlag, Berlin, 2004.

[8] ———, *Polarization and Moment Tensors with Applications to Inverse Problems and Effective Medium Theory*, Appl. Math. Sci., vol. 162, Springer–Verlag, Berlin, 2007.

[9] H. Ammari, H. Kang, E. Kim, and M. Lim, *Reconstruction of closely spaced small inclusions*, SIAM J. Numer. Anal. **42** (2005), no. 6, 2408–2428.

[10] H. Ammari and A. Khelifi, *Electromagnetic scattering by small dielectric inhomogeneities*, J. Math. Pures Appl. **82** (2003), no. 7, 749–842.

[11] H. Ammari and C. Latiri–Grouz, *An integral equation method for the electromagnetic scattering from a scatterer on an absorbing plane*, Integral Equations Operator Theory **39** (2001), no. 2, 159–181.

[12] H. Ammari, S. Moskow, and M. S. Vogelius, *Boundary integral formulae for the reconstruction of electric and electromagnetic inhomogeneities of small volume*, ESAIM Control Optim. Calc. Var. **9** (2003), 49–66.

[13] H. Ammari and J. K. Seo, *An accurate formula for the reconstruction of conductivity inhomogeneities*, Adv. in Appl. Math. **30** (2003), no. 4, 679–705.

[14] H. Ammari, M. S. Vogelius, and D. Volkov, *Asymptotic formulas for perturbations in the electromagnetic fields due to the presence of inhomogeneities of small diameter II. The full Maxwell equations*, J. Math. Pures Appl. **80** (2001), 769–814.

[15] H. Ammari and D. Volkov, *The leading order term in the asymptotic expansion of the scattering amplitude of a collection of finite number of dielectric inhomogeneities of small diameter*, International Journal for Multiscale Computational Engineering **3** (2005), no. 3, 149–160.

[16] E. Beretta, A. Mukherjee, and M. S. Vogelius, *Asymptotic formulas for steady state voltage potentials in the presence of conductivity imperfections of small area*, Z. Angew. Math. Phys. **52** (2001), no. 4, 543–572.

[17] E. Beretta, E. Francini, and M. S. Vogelius, *Asymptotic formulas for steady state voltage potentials in the presence of thin inhomogeneities. A rigorous error analysis.*, J. Math. Pures Appl. **82** (2003), no. 10, 1277–1301.

[18] L. Borcea, *Electrical impedance tomography*, Inverse Problems **18** (2002), no. 6, R99–R136.

[19] ———, *Addendum to: "Electrical impedance tomography" [Inverse Problems 18 (2002), no. 6, R99–R136; 1955896]*, Inverse Problems **19** (2003), no. 4, 997–998.

[20] M. Brühl and M. Hanke, *Numerical implementation of two noniterative methods for locating inclusions by impedance tomography*, Inverse Problems **16** (2000), no. 4, 1029–1042.

[21] M. Brühl, *Explicit characterization of inclusions in electrical impedance tomography*, SIAM J. Math. Anal. **32** (2001), no. 6, 1327–1341.

[22] M. Brühl, M. Hanke, and M. S. Vogelius, *A direct impedance tomography algorithm for locating small inhomogeneities*, Numer. Math. **93** (2003), 635–654.

[23] A. Buffa, M. Costabel, and D. Sheen, *On traces of $H(\mathrm{curl}, \Omega)$ in Lipschitz domains*, J. Math. Anal. Appl. **276** (2002), no. 2, 845–867.

[24] F. Cakoni and D. Colton, *Qualitative Methods in Inverse Scattering Theory. An Introduction*, Interact. Mech. Math., Springer–Verlag, Berlin, 2006.

[25] F. Cakoni, M'B. Fares, and H. Haddar, *Analysis of two linear sampling methods applied to electromagnetic imaging of buried objects*, Inverse Problems **22** (2006), no. 3, 845–867.

[26] Y. Capdeboscq and M. S. Vogelius, *A general representation formula for boundary voltage perturbations caused by internal conductivity inhomogeneities of low volume fraction*, Math. Model. Numer. Anal. **37** (2003), no. 1, 159–173.

[27] ———, *Optimal asymptotic estimates for the volume of internal inhomogeneities in terms of multiple boundary measurements*, Math. Model. Numer. Anal. **37** (2003), no. 2, 227–240.

[28] ———, *A review of some recent work on impedance imaging for inhomogeneities of low volume fraction* (C. Conca, R. Manasevich, G. Uhlmann, and M. S. Vogelius, eds.), Contemp. Math., vol. 362, Amer. Math. Soc., Providence, 2004.

[29] D. Cedio–Fengya, S. Moskow, and M. S. Vogelius, *Identification of conductivity imperfections of small diameter by boundary measurements. Continuous dependence and computational reconstruction*, Inverse Problems **14** (1998), no. 3, 553–595.

[30] M. Cessenat, *Mathematical Methods in Electromagnetism. Linear Theory and Applications*, Ser. Adv. Math. Appl. Sci., vol. 41, World Scientific Publishing, River Edge, NJ, 1996.

[31] D. H. Chambers and J. G. Berryman, *Analysis of the time–reversal operator for a small scatterer in an electromagnetic field*, IEEE Trans. Antennas Propagat. **52** (2004), no. 7, 1729–1738.

[32] ———, *Target characterization using decomposition of the time–reversal operator: electromagnetic scattering from small ellipsoids*, Inverse Problems **22** (2006), no. 6, 2145–2163.

[33] M. Cheney, D. Isaacson, and J. C. Newell, *Electrical impedance tomography*, SIAM Rev. **41** (1999), no. 1, 85–101.

[34] M. Cheney, *The linear sampling method and the MUSIC algorithm*, Inverse Problems **17** (2001), no. 4, 591–595.

[35] W. C. Chew, *Waves and Fields in Inhomogeneous Media*, Van Nostrand Reinhold, New York, 1990.

[36] D. Colton, J. Coyle, and P. Monk, *Recent developments in inverse acoustic scattering theory*, SIAM Rev. **42** (2000), no. 3, 369–414.

[37] D. Colton and A. Kirsch, *A simple method for solving inverse scattering problems in the resonance region*, Inverse Problems **12** (1996), no. 4, 383–393.

[38] D. Colton and R. Kress, *Integral Equation Methods in Scattering Theory*, John Wiley & Sons, New York, 1983.

[39] ———, *Inverse Acoustic and Electromagnetic Scattering Theory*, 2nd ed., Appl. Math. Sci., vol. 93, Springer–Verlag, Berlin, 1998.

[40] ———, *Using fundamental solutions in inverse scattering*, Inverse Problems **22** (2006), no. 3, R49–R66.

[41] D. Colton and P. Monk, *A novel method for solving the inverse scattering problem for time–harmonic acoustic waves in the resonance region*, SIAM J. Appl. Math. **45** (1985), no. 6, 1039–1053.

[42] ———, *A novel method for solving the inverse scattering problem for time–harmonic acoustic waves in the resonance region II*, SIAM J. Appl. Math. **46** (1986), no. 3, 506–523.

[43] P.-M. Cutzach and C. Hazard, *Existence, uniqueness and analyticity properties for electromagnetic scattering in a two–layered medium*, Math. Methods Appl. Sci. **21** (1998), no. 5, 433–461.

[44] G. Dassios and R. Kleinman, *Low Frequency Scattering*, Oxford Math. Monogr., Oxford University Press, New York, 2000.

[45] R. Dautray and J. L. Lions, *Mathematical Analysis and Numerical Methods for Science and Technology. Vol. 1. Physical Origins and Classical Methods*, Springer–Verlag, Berlin, 1990.

[46] F. Delbary, K. Erhard, R. Kress, R. Potthast, and J. Schulz, *Inverse electromagnetic scattering in a two–layered medium with an application to mine detection*, Inverse Problems **24** (2008), no. 1, 015002 (18 pp.)

[47] A. J. Devaney, *Super–resolution processing of multi–static data using time reversal and MUSIC*, Preprint, Department of Electrical Engineering, Northeastern University, Boston, MA (1999).

[48] H. W. Engl, M. Hanke, and A. Neubauer, *Regularization of Inverse Problems*, Mathematics and its Applications, vol. 375, Kluwer Academic Publishers Group, Dordrecht, 1996.

[49] A. Friedman and M. S. Vogelius, *Identification of small inhomogeneities of extreme conductivity by boundary measurements: a theorem on continuous dependence*, Arch. Rational Mech. Anal. **105** (1989), no. 4, 299–326.

[50] B. Gebauer, *The factorization method for real elliptic problems*, Z. Anal. Anwend. **25** (2006), no. 1, 81–102.

[51] ———, *Gebietserkennung mit der Faktorisierungsmethode*, Ph.D. thesis, Johannes Gutenberg–Universität, Mainz, 2006.

[52] B. Gebauer, M. Hanke, A. Kirsch, W. Muniz, and C. Schneider, *A sampling method for detecting buried objects using electromagnetic scattering*, Inverse Problems **21** (2005), no. 6, 2035–2050.

[53] B. Gebauer, M. Hanke, and C. Schneider, *Sampling methods for low–frequency electromagnetic imaging*, Inverse Problems **24** (2008), no. 1, 015007 (18pp).

[54] V. Girault and P.-A. Raviart, *Finite Element Methods for Navier–Stokes Equations. Theory and Algorithms*, Springer Ser. Comput. Math., vol. 5, Springer–Verlag, Berlin, 1986.

[55] G. H. Golub and Ch. F. Van Loan, *Matrix Computations*, 3rd ed., Johns Hopkins Studies in the Mathematical Sciences, Johns Hopkins University Press, Baltimore, MD, 1996.

[56] R. Griesmaier, *An asymptotic factorization method for inverse electromagnetic scattering in layered media*, SIAM J. Appl. Math. **68** (2008), no. 5, 1378–1403.

[57] D. Guelle, A. Smith, A. Lewis, and T. Bloodworth, *EUR 20837 Metal Detector Handbook for Humanitarian Demining*, Office for Official Publications of the European Communities, Luxembourg, 2003.

[58] P. Hähner, *An inverse problem in electrostatics*, Inverse Problems **15** (1999), no. 4, 961–975.

[59] M. Hanke and M. Brühl, *Recent progress in electrical impedance tomography*, Inverse Problems **19** (2003), no. 6, S65–S90.

[60] M. Hanke and B. Schappel, *The factorization method for electrical impedance tomography in the half space*, SIAM J. Appl. Math. **68** (2007), no. 4, 907–924.

[61] *HuMin/MD — Metal detectors for humanitarian demining — Development potentials in data analysis methodology and measurement,* Project Network, `http://www.humin-md.de/`.

[62] E. Iakovleva, S. Gdoura, D. Lesselier, and G. Perrusson, *Multi–static response matrix of a 3–D inclusion in half space and MUSIC imaging*, IEEE Trans. Antennas Propagat. **55** (2007), no. 9, 2598–2609.

[63] J. Igel and H. Preetz, *Elektromagnetische Bodenparameter und ihre Abhängigkeit von den Bodeneigenschaften. — Zwischenbericht Projektverbund Humanitäres Minenräumen*, Technical Report, Leibniz Institute of Applied Geosciences, Hannover (2005).

[64] M. Ikehata, *Reconstruction of the shape of the inclusion by boundary measurements*, Comm. Partial Differential Equations **23** (1998), no. 7–8, 1459–1474.

[65] V. Isakov, *On uniqueness of recovery of a discontinuous conductivity coefficient*, Comm. Pure Appl. Math. **41** (1988), no. 7, 865–877.

[66] ———, *Inverse Problems for Partial Differential Equations*, 2nd ed., Appl. Math. Sci., vol. 127, Springer–Verlag, New York, 2006.

[67] H. Kang and H. Lee, *Identification of simple poles via boundary measurements and an application of EIT*, Inverse Problems **20** (2004), no. 6, 1853–1863.

[68] T. Kato, *Perturbation Theory for Linear Operators*, Grundlehren Math. Wiss., vol. 132, Springer–Verlag, Berlin, 1966.

[69] J. B. Keller, R. E. Kleinman, and T. B. A. Senior, *Dipole moments in Rayleigh scattering*, J. Inst. Math. Appl. **9** (1972), no. 1, 14–22.

[70] A. Kirsch, *Surface gradients and continuity properties for some integral operators in classical scattering theory*, Math. Methods Appl. Sci. **11** (1989), no. 6, 789–804.

[71] ———, *An Introduction to the Mathematical Theory of Inverse Problems*, Appl. Math. Sci., vol. 120, Springer–Verlag, New York, 1996.

[72] ———, *Characterization of the shape of a scattering obstacle using the spectral data of the far field operator*, Inverse Problems **14** (1998), no. 6, 1489–1512.

[73] ———, *The MUSIC algorithm and the factorization method in inverse scattering theory for inhomogeneous media*, Inverse Problems **18** (2002), no. 4, 1025–1040.

[74] ———, *The factorization method for a class of inverse elliptic problems*, Math. Nachr. **278** (2005), no. 3, 258–277.

[75] ———, *An integral equation for Maxwell's equations in a layered medium with an application to the factorization method*, J. Integral Equations Appl. **19** (2007), no. 3, 333–359.

[76] A. Kirsch and N. Grinberg, *The Factorization Method for Inverse Problems*, Oxford Lecture Ser. Math. Appl., vol. 36, Oxford University Press, New York, 2008.

[77] A. Kirsch and R. Kress, *An optimization method in inverse acoustic scattering*, Boundary elements IX, Vol. 3: Fluid Flow and Potential Applicatoins (1987), 3–18.

[78] R. V. Kohn and M. S. Vogelius, *Determining conductivity by boundary measurements. II. Interior results*, Comm. Pure Appl. Math. **38** (1985), no. 5, 643–667.

[79] R. Kress, *Linear Integral Equations*, 2nd ed., Appl. Math. Sci., vol. 82, Springer–Verlag, New York, 1999.

[80] ———, *Electromagnetic waves scattering: Specific theoretical tools,* in: Scattering. Scattering and Inverse Scattering in Pure and Applied Science (E. R. Pike and P. C. Sabatier, eds.), Academic Press, San Diego, 2002.

[81] ———, *Acoustic scattering: Specific theoretical tools,* in: Scattering. Scattering and Inverse Scattering in Pure and Applied Science (E. R. Pike and P. C. Sabatier, eds.), Academic Press, San Diego, 2002.

[82] R. Kress and L. Kühn, *Linear sampling methods for inverse boundary value problems in potential theory*, Appl. Numer. Math. **43** (2002), no. 1–2, 161–173.

[83] G. Kristensson, *A uniqueness theorem for Helmholtz' equation: penetrable media with an infinite interface*, SIAM J. Math. Anal. **11** (1980), no. 6, 1104–1117.

[84] S. Kusiak and J. Sylvester, *The scattering support*, Comm. Pure Appl. Math. **56** (2003), no. 11, 1525–1548.

[85] D. R. Luke and R. Potthast, *The no response test—a sampling method for inverse scattering problems*, SIAM J. Appl. Math. **63** (2003), no. 4, 1292–1312.

[86] W. McLean, *Strongly Elliptic Systems and Boundary Integral Equations*, Cambridge University Press, Cambridge, 2000.

[87] D. Mitrea, M. Mitrea, and J. Pipher, *Vector potential theory on nonsmooth domains in R^3 and applications to electromagnetic scattering*, J. Fourier Anal. Appl. **3** (1997), no. 2, 131–192.

[88] P. Monk, *Finite Element Methods for Maxwell's Equations*, Numer. Math. Sci. Comput., Oxford University Press, New York, 2003.

[89] W. Muniz, *Dipole sources and Green's dyadics*, Unpublished Notes, Fakultät für Mathematik, Universität Karlsruhe, Karlsruhe (2005).

[90] A. I. Nachman, L. Päivärinta, and A. Teirilä, *On imaging obstacles inside inhomogeneous media*, J. Funct. Anal. **252** (2007), no. 2, 490–516.

[91] J.-C. Nédélec, *Acoustic and Electromagnetic Equations. Integral Representations for Harmonic Problems*, Appl. Math. Sci., vol. 144, Springer–Verlag, New York, 2001.

[92] M. Petry, *Über die Streuung zeitharmonischer Wellen im geschichteten Raum*, Ph.D. thesis, Georg–August–Universität zu Göttingen, Göttingen, 1993.

[93] E. R. Pike and P. C. Sabatier (eds.), *Scattering. Scattering and Inverse Scattering in Pure and Applied Science*, Academic Press, San Diego, 2002.

[94] R. Potthast, *Stability estimates and reconstructions in inverse acoustic scattering using singular sources*, J. Comput. Appl. Math. **114** (2000), no. 2, 247–274.

[95] ———, *A survey on sampling and probe methods for inverse problems*, Inverse Problems **22** (2006), no. 2, R1–R47.

[96] R. Potthast, J. Sylvester, and S. Kusiak, *A 'range test' for determining scatterers with unknown physical properties*, Inverse Problems **19** (2003), no. 3, 533–547.

[97] Lord Rayleigh, *On the incidence of aerial and electric waves upon small obstacles in the form of ellipsoids or elliptic cylinders, and on the passage of electric waves through a circular aperture in a conducting screen*, Phil. Mag. **44** (1897), no. 5, 28–52.

[98] M. Schiffer and G. Szegö, *Virtual mass and polarization*, Trans. Amer. Math. Soc. **67** (1949), no. 1, 130–205.

[99] A. Sommerfeld, *Partial Differential Equations in Physics*, Academic Press, New York, 1949.

[100] C. Weber, *Regularity theorems for Maxwell's equations*, Math. Methods Appl. Sci. **3** (1981), no. 4, 523–536.

Notation

Symbol	*Explanation*	*Ref., p.*
Vectors, matrices, and sets		
$\mathbb{R}^n$	n–dimensional real Euclidean space	
$\mathbb{C}^n$	n–dimensional complex Euclidean space	
$(\boldsymbol{e}_1, \ldots, \boldsymbol{e}_n)$	standard basis of $\mathbb{R}^n$	
$\boldsymbol{x} = (x_1, \ldots, x_n)$	generic point in $\mathbb{R}^n$ or $\mathbb{C}^n$	
$\boldsymbol{x} \cdot \boldsymbol{y}$	standard scalar product on $\mathbb{R}^n$, also used on $\mathbb{C}^n$ (bilinear)	
$\overline{\boldsymbol{x}}$	componentwise complex conjugate on $\mathbb{C}^n$	
$\lvert\boldsymbol{x}\rvert$	Euclidean norm on $\mathbb{R}^n$ and $\mathbb{C}^n$	
$(\cdot)^\top$	transpose of a vector or matrix	
$\mathbb{I}_3$	3×3 identity matrix	
$B_r(\boldsymbol{x})$	ball of radius r centered at $\boldsymbol{x}$	
D	bounded open set	
∂D	boundary of D	
$\lvert\partial D\rvert$	area of ∂D	
$\operatorname{dist}(x, D)$	distance from point $\boldsymbol{x}$ to set D	15
$\boldsymbol{\nu}$	unit outward normal vector	
$D_{\delta,l}$, D_δ	scalable inclusion or scatterer	15, 50
B_l, B	shape of scalable inclusion or scatterer	15, 50
$\boldsymbol{z}_l$, $\boldsymbol{z}$	position of scalable inclusion or scatterer	15, 50
δ	scaling parameter	15, 50
$\mathbb{M}_B^0$	magnetic polarizability tensor	113
$\mathbb{M}_B^\infty$	electric polarizability tensor	113
Σ_0	surface of ground	39
$\mathbb{R}^3_+$	upper half space	39
$\mathbb{R}^3_-$	lower half space	39
$\mathbb{R}^3_0$	$\mathbb{R}^3 \setminus \Sigma_0$	39
$\mathcal{M}$	measurement device	49

$\mathcal{M}_h$	discrete measurement device	87

Function spaces

$C^\infty(\overline{D})$	space of restrictions to D of infinitely differentiable functions on $\mathbb{R}^n$, real valued	
$L^2(D)$	space of square integrable functions on D, real valued	
$H^r(D)$	Sobolev space on D, real valued	9
$H^r_{\mathrm{loc}}(\mathbb{R}^n)$	Sobolev space on $\mathbb{R}^n$, real valued	9
$H^r_{\mathrm{loc}}(\mathbb{R}^n \setminus \overline{D})$	Sobolev space on $\mathbb{R}^n \setminus \overline{D}$, real valued	9
$L^2(\partial D)$	space of square integrable functions on ∂D, real valued	
$H^s(\partial D)$	Sobolev space on ∂D, real valued	9
$\|\cdot\|_{H^{\pm 1/2}(\partial D)}$	norm on $H^{\pm 1/2}(\partial D)$	19
$\langle\cdot,\cdot\rangle_{\partial D}$	dual pairing between $H^{1/2}(\partial D)$ and $H^{-1/2}(\partial D)$	19
$H^1_\diamond(D)$	Sobolev space on D, real valued	16
$H^1_{\diamond,\partial\Omega}(\Omega \setminus \overline{D})$	Sobolev space on $\Omega \setminus \overline{D}$, real valued	15
$H^{\pm 1/2}_\diamond(\partial D)$	Sobolev space on ∂D, real valued	12, 14
$C^\infty(\overline{D};\mathbb{C})$	space of restrictions to D of infinitely differentiable functions on $\mathbb{R}^n$, complex valued	
$L^2(D;\mathbb{C})$	space of square integrable functions on D, complex valued	
$H^r(D;\mathbb{C})$	Sobolev space on D, complex valued	36
$H^r_{\mathrm{loc}}(\mathbb{R}^n;\mathbb{C})$	Sobolev space on $\mathbb{R}^n$, complex valued	36
$H^r_{\mathrm{loc}}(\mathbb{R}^n \setminus \overline{D};\mathbb{C})$	Sobolev space on $\mathbb{R}^n \setminus \overline{D}$, complex valued	36
$L^2(\partial D;\mathbb{C})$	space of square integrable functions on ∂D, complex valued	
$H^s(\partial D;\mathbb{C})$	Sobolev space on ∂D, complex valued	36
$\boldsymbol{H}(\mathrm{div}, D)$	Sobolev space on D, complex valued	37
$\boldsymbol{H}(\mathbf{curl}, D)$	Sobolev space on D, complex valued	37
$\boldsymbol{H}_{\mathrm{loc}}(\mathrm{div}, \mathbb{R}^3 \setminus \overline{D})$	Sobolev space, complex valued	37
$\boldsymbol{H}_{\mathrm{loc}}(\mathbf{curl}, \mathbb{R}^3 \setminus \overline{D})$	Sobolev space, complex valued	37
$\boldsymbol{L}^2_t(\partial D)$	tangential square integrable vector fields on ∂D, complex valued	37
$\boldsymbol{H}^s_t(\partial D)$	Sobolev space on ∂D, complex valued	37
$\boldsymbol{H}^{-1/2}_{\mathrm{div}}(\partial D)$	Sobolev space on ∂D, complex valued	37
$\boldsymbol{H}^{-1/2}_{\mathrm{curl}}(\partial D)$	Sobolev space on ∂D, complex valued	37

$\|\cdot\|_{\boldsymbol{H}_{\mathrm{div}}^{-1/2}(\partial D)}$	norm on $\boldsymbol{H}_{\mathrm{div}}^{-1/2}(\partial D)$	54
$\|\cdot\|_{\boldsymbol{H}_{\mathrm{curl}}^{-1/2}(\partial D)}$	norm on $\boldsymbol{H}_{\mathrm{curl}}^{-1/2}(\partial D)$	54
$\langle\cdot,\cdot\rangle_{\partial D}$	dual pairing between $\boldsymbol{H}_{\mathrm{curl}}^{-1/2}(\partial D)$ and $\boldsymbol{H}_{\mathrm{div}}^{-1/2}(\partial D)$	38
$\boldsymbol{L}^2(\mathcal{M})$	square integrable vector fields on $\mathcal{M}$, complex valued	49
$\langle\cdot,\cdot\rangle_{\mathcal{M}}$	bilinear form on $\boldsymbol{L}^2(\mathcal{M})$	51
$(\cdot,\cdot)_{\mathcal{M}}$	complex scalar product on $\boldsymbol{L}^2(\mathcal{M})$	
$\mathcal{L}(X,Y)$	bounded linear operators on X to Y	
$\mathcal{L}(X)$	$\mathcal{L}(X,X)$, bounded linear operators on X	
$\|\cdot\|$	operator norm on $\mathcal{L}(X,Y)$	

Functional notation

γ_0	standard trace operator	9, 36
γ_n	normal trace	9, 37
γ_t	tangential trace	37
π_t	projection on the tangent plane	37
n	normal component operator	37
r	rotation operator	37
$\|^{\pm}_{\partial D}$	trace from outside or inside	
$[\,\cdot\,]_{\partial D}$	jump of the trace across ∂D, inwards	
$\nabla_{\partial D}$	surface gradient	37
$\mathbf{curl}_{\partial D}$	surface vector curl	37
$\mathrm{div}_{\partial D}$	surface divergence	37
$\mathrm{curl}_{\partial D}$	surface scalar curl	37
$\mathcal{R}(A)$	range (image) of linear operator A	
$\mathcal{N}(A)$	null space (kernel) of linear operator A	
$A^{\top}$	transpose of an operator A, dual operator	
I	identity operator	
δ	Dirac–delta distribution	
Λ_0, Λ_δ	Neumann–to–Dirichlet operator	16
G_δ	measurement operator	50
$G_{\delta,t}$	measurement operator, tangential	78
$G_{\delta,n}$	measurement operator, normal	79
$G_{\delta,h}$	discrete measurement operator	87
L_δ	operator, factorization	17, 51
F_δ	operator, factorization	18, 53
L	operator, asymptotic factorization	23
F	operator, asymptotic factorization	26

L_0, L_1	operator, asymptotic factorization	59
F_0, F_1	operator, asymptotic factorization	62
T	operator, characterization	75
R	operator, characterization	33, 75
M	operator, characterization	77
$\boldsymbol{g}_{y,d}$	test function	77
$\boldsymbol{g}^t_{y,d}$	test function, tangential	79
$\boldsymbol{g}^n_{y,d}$	test function, normal	82
β_p	angle, reconstruction method	84
β^δ_p	angle, reconstruction method	85
$\tilde{\beta}^\delta_p$	angle, reconstruction method	86

Fundamental solutions and Green's functions

Φ_0	fundamental solution, Laplace equation	10
N	Neumann function, Laplace equation	10
p_N	kernel function	11
Φ_k	fundamental solution, Helmholtz equation	38
$\mathbb{G}$	dyadic Green's function, homogeneous medium	39
$\mathbb{G}^e$	electric dyadic Green's function, two–layered medium	39
$\mathbb{G}^m$	magnetic dyadic Green's function, two–layered medium	40
$\Pi^{e/m}$	Hertz vector	40
$F^{e/m}$	kernel function	40

Integral operators

$\mathcal{S}^0_D$	single layer potential, Laplace equation	11
$\mathcal{D}^0_D$	double layer potential, Laplace equation	11
K^0_D	double layer operator, Laplace equation	11
$\mathcal{S}^N_D$	modified single layer potential	12
$\mathcal{D}^N_D$	modified double layer potential	12
K^N_D	modified double layer operator	13
P^N_D	boundary integral operator	13
$\mathcal{S}^k_D$	single layer potential	41
$\mathcal{A}^k_D$	vector potential	42
M^k_D	boundary integral operator	42
N^k_D	boundary integral operator	42
$\mathcal{A}^0_D$	vector potential, zero frequency	45

M_D^0	boundary integral operator, zero frequency	45
N_D^0	boundary integral operator, zero frequency	45
$\mathcal{A}_D^{e/m}$	modified vector potential	47
$M_D^{e/m}$	boundary integral operator	47
$R_D^{e/m}$	boundary integral operator	47

Physical notation

σ_δ, σ_0	electric conductivity	15
ε, ε_+, ε_-	electric permittivity	39
μ, μ_+, μ_-	magnetic permeability	39
k, k_+, k_-	wave number	39
ω	angular velocity	39

Other notation

C	generic positive constant	
ω_n	area of the $(n-1)$–dimensional unit sphere	
$\hat{\varphi}$, $(\varphi)^\wedge$	change of coordinates	18
$\check{\varphi}$, $(\varphi)^\vee$	change of coordinates	18
$\mathcal{O}$	Landau symbol	
o	Landau symbol	

Index